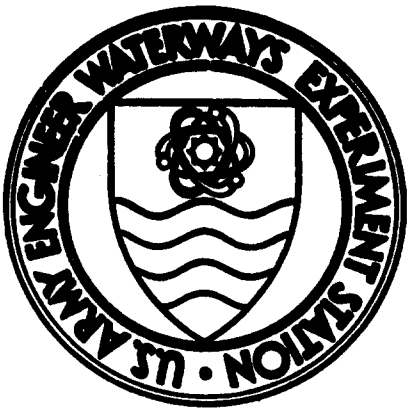

CONTRACT REPORT N-69-1

GEOMECHANICAL MODEL STUDY OF THE BEHAVIOR OF UNDERGROUND OPENINGS IN ROCK SUBJECTED TO STATIC LOADS

Report 3

TESTS ON LINED OPENINGS IN JOINTED AND INTACT ROCK

by

A. J. Hendron, Jr., Paul Engeling, A. K. Aiyer

with Appendix by S. L. Paul

June 1972

Sponsored by Defense Nuclear Agency

Conducted for U. S. Army Engineer Waterways Experiment Station
Weapons Effects Laboratory
Vicksburg, Mississippi

Under Contract No. DACA 39-67-C-0009

by Department of Civil Engineering, University of Illinois, Urbana, Illinois

ARMY-MRC VICKSBURG, MISS.

Unclassified

Security Classification

DOCUMENT CONTROL DATA - R & D

(Security classification of title, body of abstract and indexing annotation must be entered when the overall report is classified)

1. ORIGINATING ACTIVITY (Corporate author)	2a. REPORT SECURITY CLASSIFICATION
Department of Civil Engineering University of Illinois Urbana, Illinois	Unclassified
	2b. GROUP

3. REPORT TITLE

GEOMECHANICAL MODEL STUDY OF THE BEHAVIOR OF UNDERGROUND OPENINGS IN ROCK SUBJECTED TO STATIC LOADS; Report 3, TESTS ON LINED OPENINGS IN JOINTED AND INTACT ROCK

4. DESCRIPTIVE NOTES (Type of report and inclusive dates)

Report 3 of a series

5. AUTHOR(S) (First name, middle initial, last name)

A. J. Hendron, Jr. A. K. Aiyer
Paul Engeling S. L. Paul
A. K. Aiyer

6. REPORT DATE	7a. TOTAL NO. OF PAGES	7b. NO. OF REFS
June 1972	188	2

8a. CONTRACT OR GRANT NO. DACA 39-67-C-0009	9a. ORIGINATOR'S REPORT NUMBER(S)
b. PROJECT NO.	
c.	9b. OTHER REPORT NO(S) (Any other numbers that may be assigned this report) U. S. Army Engineer Waterways Experiment Station Contract Report N-69-1, Report 3
d.	

10. DISTRIBUTION STATEMENT

Approved for public release; distribution unlimited.

11. SUPPLEMENTARY NOTES	12. SPONSORING MILITARY ACTIVITY
Prepared under contract for U. S. Army Engineer Waterways Experiment Station, Vicksburg, Mississippi	Defense Nuclear Agency Washington, D. C.

13. ABSTRACT

The results of eleven geomechanical model tests are presented and discussed in this report. Six of these tests were on lined tunnels in solid test blocks and the remaining five tests were on lined tunnels in jointed test blocks. The size of the models tested was 24" x 24" x 8". Uniformly distributed loads up to 134 tons were applied to the 24" x 8" faces of the models. To maintain a plane-strain condition in the models, loads of up to 160 tons were applied to the top 24" x 24" face of the model to null strains parallel to the 8 in. dimension. Friction along the loading faces was controlled with sheets of teflon. The developments of jointed models and the instrumentation necessary for maintaining the jointed models are described. The behavior of the tunnel was measured by diametrical extensometers inside the tunnel liners and strain gages mounted on the tunnel liner. Strain measurements of the solid model blocks were made by the use of strain gages mounted on the model material. Average strain measurements of the jointed models were made by the use of buried extensometers. For models tested at a principal stress ratio of 1.0, the observed behavior was analyzed and compared to theoretical predictions. For models tested at a principal stress ratio of 2/3, the data was plotted in dimensionless form and a relation was shown to exist between the ratio of liner to the jointed model stiffness and the ratio of liner to free-field model strain.

DD FORM 1 NOV 68 1473 REPLACES DD FORM 1473, 1 JAN 64, WHICH IS OBSOLETE FOR ARMY USE.

Unclassified

Security Classification

14. KEY WORDS	LINK A		LINK B		LINK C	
	ROLE	WT	ROLE	WT	ROLE	WT
Geomechanical models						
Models						
Rock mechanics						
Rock properties						
Static loads						
Tunnels						
Underground openings						

CONTRACT REPORT N-69-1

GEOMECHANICAL MODEL STUDY OF THE BEHAVIOR OF UNDERGROUND OPENINGS IN ROCK SUBJECTED TO STATIC LOADS

Rep 3

TESTS ON LINED OPENINGS IN JOINTED AND INTACT ROCK

by

A. J. Hendron, Jr., Paul Engeling, A. K. Aiyer

with Appendix by S. L. Paul

June 1972

Sponsored by Defense Nuclear Agency

Conducted for U. S. Army Engineer Waterways Experiment Station
Weapons Effects Laboratory
Vicksburg, Mississippi

Under Contract No. DACA 39-67-C-0009

By Department of Civil Engineering, University of Illinois, Urbana, Illinois

ARMY-MRC VICKSBURG, MISS.

ACKNOWLEDGEMENTS

The work described in this report was accomplished in the Department of Civil Engineering at the University of Illinois under contract No. DACA 39-67-C-0009 for the U. S. Army Engineer Waterways Experiment Station (WES). The work was sponsored by the Defense Nuclear Agency. Mr. Paul Engeling, Research Assistant in Civil Engineering, was directly responsible for the laboratory work reported in the main body of this report, under the direct supervision of Dr. A. J. Hendron, Jr., Professor of Civil Engineering. Mr. J. F. Thibeaux, Research Assistant in Civil Engineering, was directly responsible for the laboratory work reported in Appendix A, under the direct supervision of Dr. S. L. Paul, Professor of Civil Engineering.

The contract was under the general supervision of Mr. G. L. Arbuthnot, Jr., Chief, Weapons Effects Laboratory, WES. Contracting officer was Col. E. D. Peixotto, Director, WES.

TABLE OF CONTENTS

Chapter 1

INTRODUCTION

1.1 General

The study described in this report is a continuation of the study reported by Heuer and Hendron (1969) and Heuer and Hendron (1971). In the earlier phases of this study the similitude requirements for model tests of tunnels in rock were set forth which required that a special model material be developed in order to conduct tests at reduced stresses in the laboratory. A material with the desired characteristics was developed on this study (Heuer and Hendron 1969, 1971) and represents a significant step forward in the elimination of a factor which had violated similitude conditions in model tests of previous investigators. After the strength and stress-strain properties of the model material were fully documented under various states of stress, techniques were then developed for constructing solid models which contained unlined tunnels. Concurrent with the development of techniques for constructing the model, methods for instrumenting the models were developed to measure the strains and displacements in the model as it was loaded in a plane strain loading frame developed on this study (Heuer and Hendron, 1971). After the required techniques were developed for constructing and testing these models, a series of model tests was conducted on lined and unlined tunnels in solid models of the artificially prepared model rock material. The behavior of the unlined tunnels is reported by Heuer and Hendron (1971). The test variables investigated in this study include the principal stress ratio and the liner stiffness. A summary of all tests conducted on solid blocks is shown in Table I.

After the tests on solid models were completed a considerable effort on this study was directed toward the construction of jointed models containing lined tunnels. Successful techniques were eventually developed for constructing jointed

models and a test series was conducted where the liner stiffness, the ratio of joint spacing to tunnel diameter, and the direction of the applied principal stresses with respect to the joint pattern were varied. A list of the tests conducted on jointed models is given in Table 2.

1.2 Scope

In this report an analysis and comparison of the tests on lined tunnels in solid blocks is given in Chapter 2.

The techniques for constructing and instrumenting jointed models is given in Chapter 3.

The results of initial tests on lined tunnels in jointed models are presented and discussed in Chapter 4.

In Appendix I a series of special tests on model silos in solid rock modeling material is presented and discussed.

Table 1

Tests on Solid Blocks

Test Block Number	Tunnel Diameter	Liner	$N=\sigma_h/\sigma_v$	Maximum Pressure psi
TB #1	No tunnel	--	1	1000
TB #2	No tunnel	--	1	1000
TB #3	4"	unlined	1	1000
TB #4	4"	unlined	1/4	1000
TB #5	4"	unlined	1/4	1000
TB #6	4"	unlined	2/3	1000
* TB #7	4"	steel t = 0.065" EI/R^3 = 86 psi Et/R = 975,000 psi	1/4	1000
TB #8	2 1/2"	unlined	1/4	1000
* TB #9	4"	steel t = 0.120" EI/R^3 = 540 psi Et/R = 1,800,000 psi	1	1000
* TB #10	4"	steel t = 0.065" EI/R^3 = 86 psi Et/R = 975,000 psi	1	1000
* TB #11	4"	steel t = 0.065" EI/R^3 = 86 psi Et/R = 975,000 psi	2/3	1000
* TB #12	4"	aluminum t = 0.035" EI/R^3 = 5 psi Et/R = 175,000 psi	1	1000
* TB #13	4"	aluminum t = 0.035" EI/R^3 = 5 psi Et/R = 175,000 psi	2/3	1300

* Tests conducted for this report.

Table 2

Tests on Jointed Blocks

Test Block Number	Tunnel Diameter	Liner	Joints		$N=\sigma_h/\sigma_v$	Maximum Pressure (psi)	Model Stiffness E_m (psi)
			Spacing	Orientation			
JB #1	4"	steel $t = 0.065"$ $EI/R^3 = 86$ psi $Et/R = 975,000$ psi	2"	parallel to applied stresses	2/3	1000	80,000
JB #2	4"	aluminum $t = 0.035"$ $EI/R^3 = 5$ psi $Et/R = 175,000$ psi	2"	parallel to applied stresses	2/3	1000	84,000
JB #3	4"	aluminum $t = 0.035"$ $EI/R^3 = 5$ psi $Et/R = 175,000$ psi	2"	45° to applied stresses	2/3	1000	65,000
JB #4	4"	aluminum $t = 0.035"$ $EI/R^3 = 5$ psi $Et/R = 175,000$ psi	2"	45° to applied stresses	2/3	1300	62,000
JB #5	4"	aluminum $t = 0.035"$ $EI/R^3 = 5$ psi $Et/R = 175,000$ psi	1"	45° to applied stresses	2/3	1300	38,500

CHAPTER 2

RESULTS OF SMALL SCALE MODEL TESTS OF LINED TUNNELS IN INTACT ROCK

2.1 General

During this study 6 tests were conducted with lined openings of varying stiffness in intact model rock material. The models were prepared in exactly the same manner as the intact models described by Heuer and Hendron, 1971, except that an instrumented tunnel liner was inserted and grouted with sulfaset as described in Chapter three. In these tests (tests 7, 9, 10, 11, 12, and 13) both the liner stiffness and the ratio of the applied principal stresses were varied as shown in Table 1. In the following sections a detailed discussion is given of the measurements made in some of the tests and comparisons are made which reflect the influence of the liner stiffness and the principal stress ratio on the behavior. Comparisons are also made between the observed diameter changes and the diameter changes calculated from both elastic and elasto-plastic calculations in section 2.

2.2 Results of Typical Tests on Lined Openings in Solid Test Blocks

Test Block #11

TB#11 was tested with a steel liner of thickness 0.065" at a principal stress ratio ($N = \sigma_h/\sigma_v$) of 2/3. The EI/R^3 value of the liner was 86 psi per lineal inch of liner and the Et/R value was 1×10^6 psi. In this test the liner was instrumented with twenty-four SR-4 strain gages, twelve on the inside and twelve on the outside of the tunnel liner. Sixteen of these gages were located at Section I and the remaining eight were located at Section II. At Section I the

gages were spaced 45° apart on the circumference whereas at Section II they were spaced at 90° as shown in Fig. 1. Sections I and II were spaced 2" apart at the midlength of the tunnel (Fig. 2). Each gage was identified by specifying the section and location at which it was placed. These gages were used to estimate the moments and thrusts induced in the liner as it was loaded by the medium during the test. The changes in the diameter of the tunnel liner were also measured during the test using berrylium-copper clip gages located at the springline, crown-invert section and at the 45° lines, as shown in Fig. 1a. These clip gages have been described previously (Heuer and Hendron, 1969). The model medium was not instrumented to measure free-field strains. An estimate of the free-field strains was made using the data from TB#6 which was tested at the same N value with an unlined opening.

The diametrical movements observed in TB#11, are presented as plots of dimaterical strain, $\Delta D/D$, versus applied vertical stress, σ_v, in Fig. 3. The crown-invert diameter shortens throughout the test, as it should, under the influence of the applied loading. At lower levels of applied stress, the springline diameter also decreases, but as the loading is increased, the springline diameter starts to elongate. At high stresses, the springline diameter is considerably lengthened. It is also seen that in contrast to the crown-invert and springline diameters, the two 45° diameters experience considerably smaller amounts of strain. Even though diametrical extensometers #3 and #5 should theoretically give the same relationship, there is a small amount of scatter in the test results obtained. But the degree of scatter is

well within the range that is usual in model tests of this type.

Thrusts and Moments in the Liner

Thrusts, T, and Moments, M, in the liner were calculated from the strain readings of the gages placed on the inside and outside of the liner, using the following equations:

$$T = (\varepsilon_0 + \varepsilon_i)\ \frac{Et}{2} \qquad (1)$$

$$M = (\varepsilon_0 - \varepsilon_i)\ \frac{Et^2}{12} \qquad (2)$$

where ε_i and ε_0 are the circumferential strains at the 'inner' and 'outer' fibers of the liner, E is the modulus of elasticity of the liner material and t is the liner thickness. The modulus of elasticity of the steel liner was assumed to be 30×10^6 psi. The maximum measured fiber strain did not at any time exceed the yield strain of the liner material, indicating that the liner remained completely elastic throughout the test. The thrusts and moments calculated for the different gage locations were then plotted in dimensionless form as $\frac{T}{\sigma_v \cdot R}$ and $\frac{T}{\sigma_v \cdot R^2}$ versus the applied pressure, σ_v. Compressive thrusts were considered to be positive. Moments were considered positive when they produce compression in the outer fibers.

The variations of thrusts with applied pressure at different positions of the liner of TB#11 are shown in Figs. 4 through 7. At most of the gage locations the average dimensionless thrust increased approximately linearly with increasing stress level. Ninety percent of the thrust measurements fell into a relatively small band as shown in Fig. 7. The average dimensionless thrusts varied from approximately 0.5 at σ_v = 100 psi to approximately 0.8 at σ_v = 1000 psi. This means that the liner was not as stiff as the model rock mass adjacent to it so

that a portion of the load applied over the tunnel was arched around the liner. At lower stress levels approximately 50% of the load was arched around the liner. As the free-field stress level increased, the stiffness of the model rock material decreased and therefore the liner picked up an increasing percentage of the load applied on the tunnel. At the highest free-field stress level tested (σ_v = 1000 psi), the liner carried about 80% of the applied load on the tunnel.

The variations of dimensionless moments at different gage locations for TB#11 are shown in Figs. 8 through 11. Dimensionless moments at the crown and invert remained almost constant throughout the loading at an average value of 0.05×10^{-2}. At the springline also, the dimensionless moments remained almost constant throughout the test and had an average value of about $.025 \times 10^{-2}$. At the 45° sections, the dimensionless moment values increased almost linearly with increasing stress level from approximately 0.05×10^{-2} at σ_v = 100 psi to about 0.15×10^{-2} at σ_v = 1000 psi. Ninety-five percent of all the moment measurements fell within a horizontal band as shown in Fig. 11 with an average value of about 0.05×10^{-2}.

Heretofore (Tests 7, 9, and 10) all the liners tested had about the same or a higher stiffness than the medium. It was considered desirable to conduct tests with liners having a circumferential stiffness less than that of the medium. Accordingly, two tests (TB#12 and 13) were conducted on solid test blocks with aluminum liners having an Et/R value of about 1/5 of the modulus of the medium.

Test Block #12

TB#12 was tested with an aluminum liner of thickness 0.035" at a

principal stress ratio of 1. The EI/R^3 value of the liner was 5 psi per lineal inch of liner and the Et/R value was 175,000 psi. Radial displacements and strains were measured by means of buried extensometers and strain gages as had been done in the earlier tests. The diametrical changes and circumferential strains in the liner were measured by means of strain gages and diametrical extensometers located as shown in Figs. 1 and 2. The performance of all the strain gages and extensometers was quite satisfactory.

For TB#12 the free-field strains were estimated from three independent monitoring systems: (1) using internal rosette strain gages located within the block (Heuer and Hendron, 1971); (2) using an extensometer which was positioned within the tunnel and which measured the distance between two 5/32" diameter drill rods extending back through the tunnel and anchored into the test block; and (3) having two extensometers located outside the block to measure the relative movements of two points located in the medium. Figure 12 shows the arrangement of the extensometers for measuring free-field strains. The extensometers were positioned along the crown and invert of the tunnel.

The diametrical movements observed in TB#12 are presented as plots of diametrical strain, $\Delta D/D$, versus applied stress, σ_v, (Fig. 13). Since the loading is hydrostatic, theoretically the diameter changes along the crown-invert, springline and the 45^o lines should be equal. But the test data show some scatter, especially at higher levels of loading. The exact reason for this scatter is not known; however, the degree of scatter is not very large and the average of the four diametrical extensometer readings may be taken as the most probable value

of the diametrical strain of the liner. This average value of diametrical strain is plotted against applied vertical stress in Fig. 14. The average diametrical strain of the tunnel liner can also be plotted against the vertical free-field strain, ϵ_{vff} in the medium, a. shown in Fig. 15. The solid line showing the relationship obtained from test measurements is essentially linear, thus suggesting an essentially elastic behavior of the lined openings. An elastic analysis of the lined opening has been made using Savin's elastic solution and the results are shown by the dotted line in Fig. 15. It is clearly apparent that the actual measurements are very nearly the same as those predicted by theory.

The plots of dimensionless quantities $T/\sigma_v \cdot R$ and $M/\sigma_v \cdot R^2$ against the average model pressure have been presented in Figs. 16 through 18. At all gage locations the average dimensionless thrust increased approximately linearly with increasing stress level, from approximately 0.28 at σ_v = 100 psi to approximately 0.62 at σ_v = 1000 psi. This may again be explained by the fact that the stiffness of the liner relative to that of the model rock material increased with increasing free-field stress level because of the nonlinear stress-strain properties of the model rock material. Since the loading was hydrostatic (N = 1) the average dimensionless thrust values should be about the same at crown and invert, springline and 45° sections. This was found to be true. Similarly a hydrostatic loading should theoretically produce no bending moments in the liner, and this situation was approximated very closely. The dimensionless moment values at all gage locations were very small. At the springline, crown, and invert, the observed moments

were negative.

Test Block #13

TB#13 was tested with an aluminum liner having a thickness of 0.035" at a principal stress ratio of 2/3. The diameter of the tunnel was 4". The El/R^3 value of the liner was 5 psi per lineal inch of liner and the Et/R value was 175,000 psi.

The diametrical changes and the circumferential strains in the liner were measured, as in the previous tests, by means of diametrical extensometers and strain gages located as shown in Figs. 1 and 2. The free-field strains were measured by means of external extensometers located in the test block as shown in Fig. 19. A total of sixteen extensometers were used: eight were placed in the simulated vertical stress direction and the other eight, in the simulated horizontal stress direction. The free-field strains were estimated by measuring the changes in length of two sets of lines having gage lengths of 14" and 18" respectively. There were eight measurements of free field strains, four in the vertical direction and four in the horizontal direction.

The diametrical strains measured in TB#13 are plotted versus the applied vertical pressure as shown in Fig. 20. This is the first test in the series where the applied vertical pressure was increased to 1300 psi before unloading. Figure 20 shows that the tunnel liner undergoes a decrease in the diameter at all sections. The diameter decrease is a maximum at the crown and invert section and is a minimum at the springlines. The diameter decrease along the 45° sections is intermediate between those two extreme values.

Figure 21 shows a plot of diametrical strain versus vertical free-field strain. This plot also illustrates that the decrease in diameter is a maximum at the crown-invert section, a minimum at the springlines and an intermediate value at the 45° sections. Figures 20 and 21 also indicate that the diametrical strains are almost proportional to the applied pressure at low levels of loading and that with increasing stress level the behavior becomes more and more nonlinear. For the given test conditions the rate of decrease of diameter is a maximum at the crown-invert and a minimum at the springline.

The plots of dimsionless thrusts $T/\sigma_{v \cdot R}$ against the average vertical model pressure σ_v, have been presented in Figs. 22 through 24. These plots show that the dimensionless thrusts at all sections of the liner increased almost linearly with increasing model pressure. The dimensionless thrusts are much lower for TB#13 than they were for TB#11 (Fig. 4 through Fig. 7) which was also tested at a principal stress ratio of N = 2/3. The thrusts in the liner in TB#13 were lower than for TB#11 because the circumferential stiffness of the liner (Et/R = 175,000 psi) was lower than the circumferential stiffness of the liner in TB#11 (Et/R = 975,000 psi). Comparisons between Figs. 22 through 24 show that the highest thrusts are at the springline and the lowest thrusts are at the crown and invert with intermediate thrust values at the 45° sections. Test block #12 had an aluminum liner of the same stiffness as TB#13; the only difference between the two tests was that TB#12 was tested at N = 1 and TB#13 was tested at N = 2/3. The dimensionless thrusts in TB#12 increased linearly with loading from about 0.25 at 50 psi model pressure to 0.6 at 1000 psi model pressure

(Figs. 16 through 18); whereas, the dimensionless thrusts in TB#13 increased from only about 0.15 to 0.3 over the same range of vertical model pressure. Thus, it appears that the ovaling due to bending stresses in the liner tested at N = 2/3 (TB#13) resulted in some arching which tended to reduce the thrusts in the liner to values below the case for N = 1 (TB#12).

2.3 Behavior of Lined Openings

Based on the results of tests on lined openings it is possible to make some comparisons and to draw a few pertinent conclusions regarding the behavior of lined openings, under plane strain conditions.

2.4 Diameter Changes

A liner generally increases the stability of an opening and the diameter changes of a lined opening are less than those of an unlined opening under the same loading conditions. For loadings at a principal stress ratio N = 1 the liner is in compression without significant bending and the liner in turn exerts a compressive radial pressure on the medium surrounding the tunnel. This causes an increase in the radial stresses throughout the medium and a decrease in the circumferential stresses near the tunnel. Thus the principal stress difference is lowered (especially near the tunnel) and thereby the severe stress condition which would have developed in the unlined case, is eliminated. In general, the stiffer the liner, the smaller is the diametrical strain of the liner as shown in Fig. 25. The curves for TB#3 (unlined tunnel) and TB#12 (EI/R^3 = 5 psi) almost coincide until σ_v = 600 psi; thereafter they diverge. Thus, it appears that the aluminum liner in TB#12 was

not effective in reducing the diametrical strain until a stress level of 600 psi was reached. Above this stress level the diameter changes in the unlined opening increased at an increasing rate with pressure because of the dilatancy associated with local failure of the material at shallow depths behind the tunnel wall. The confining pressure provided by the liner apparently was sufficient to considerably reduce the depth to which the material was failing and thus reduce the diameter changes due to the dilatancy of the failed rock material around the opening. Below 600 psi both the liner and rock were behaving almost elastically and the liner in TB#12 was not stiff enough to reduce the diameter changes to values below those measured in the unlined tunnel (TB#3) at pressure levels below 600 psi. This behavior is very reasonable because the circumferential stiffness of the aluminum liner in TB#12 was only 175,000 psi while the stiffness of the model was about 625,000 psi.

The diameter changes shown in Fig. 25 for TB#10 definitely show the effect of a stiffer liner in reducing the deformations. For TB#10 the value of Et/R of the liner was 975,000 psi (Table 1) as compared to the stiffness of the model of about 625,000 psi.

For a loading at $N \neq 1$, the liner deforms into an elliptical shape where the diameter parallel to the maximum free-field stress shortens. The change in the diameter at right angles to the maximum free-field stress depends on the value of the principal stress ratio, N, and the stiffness of the liner used. In general the lower the value of N, the greater is the tendency for the springline diameter to increase in length as illustrated in Fig. 26. Figure 26 shows the relationship

between diametrical strain at springline and the applied vertical pressure, for three different tests (TB#10, #11, and #7) conducted at N-values of 1, 2/3 and 1/4 respectively. The characteristics of the liners used in all these three tests were the same (Table 1). The springline diameter for the hydrostatic case (TB#10) continued to decrease in length with increasing stress level. On the other hand, for TB#7 (N = 1/4), the springline diameter lengthened throughout the test. The increase in the length of the springline diameter was also much more for TB#7 with N = 1/4 than for TB#10 with N = 1. For the intermediate case of TB#11 with N = 2/3, the springline diameter decreased in length at low stress levels but at high stress levels the trend reversed and the springline diameter increased. At a pressure level of 1000 psi on TB#11, the diametrical strain at the springline was of the order of 2000 μ-in/in.

Figure 27 shows the variation of diametrical strain between the crown and the invert, for the three tests discussed above (TB#7, TB#10, TB#11), with increasing stress level for three values of N (N = 1, 2/3, and 1/4). In the case of hydrostatic loading (N = 1) the diametrical movement is minimal. At any given pressure, as the value of N decreases, the shortening of the crown-invert diameter becomes greater. The diametrical strain at the crown-invert section for TB#7 with N = 1/4 was found to be about 27 times greater than that for TB#10 with N = 1. The corresponding diametrical strain for TB#11 with N = 2/3 was approximately 5 times as great as that for TB#10 with N = 1.

The variation of diametrical strains at 45° sections is shown in

Fig. 28 for TB#10 (N = 1), TB#11 (N = 2/3) and TB#7 (N = 1/4). In general, the diametrical strains at 45° sections remain smaller than those on the crown-invert and springline diameters for the same liner stiffnesses and loading conditions. In TB#7 with N = 1/4, the 45° sections showed an increase in diameter at all pressures while in TB#10 with N = 1, the 45° diameters decreased during the entire loading from 0 to 1000 psi. In TB#11 with N = 2/3, the 45° diameters increased at low free-field stress levels but decreased in diameter as the stress level was increased. In Figs. 29 through 31 are shown the comparisons of the model pressure-diametrical strain relationships at N = 2/3 for different values of the liner stiffness. The data for these plots have been obtained from test results of TB#11 and TB#13 which have been tested at N = 2/3, with liners having stiffness values (EI/R^3) of 86 psi and 5 psi respectively. The results of the test at N = 2/3 on TB#6 with an unlined tunnel have also been plotted in these figures for comparison.

These plots in general show the considerable reduction in diametrical strains due to the provision of a liner. When the tunnel tends to close in due to the applied free-field pressure, the liner is strained and the liner in turn exerts a radial pressure on the medium which increases its strength. This changes the pressure distribution around the tunnel toward a more stable distribution. The resulting diametrical strains are considerably smaller than those of an unlined tunnel.

In Fig. 30 it is shown that TB#11 increases in diameter at the springline (after an initial decrease) whereas TB#13 with a thinner liner decreases in diameter at the springline throughout the loading.

springline diameter but the magnitude of the deformation is much smaller because of the higher bending stiffness of the liner.

On Fig. 32 the diametrical changes along the crown-invert diameter are plotted for the same three tests (TB#5, 7 and 9). All tests show a decrease of the crown-invert diameter for the N = 1/4 loading. As would be expected, the stiff liner in TB#9 deformed much less along the vertical diameter than did the more flexible liner in TB#7. However, the unlined opening did not strain as much along the crown-invert diameter as the flexible liner (EI/R^3 = 86 psi) in TB#7. This behavior probably results at lower pressures because the circumferential stresses around an unlined opening at the crown and invert are small for a loading ratio of N = 1/4. At higher pressures the unlined tunnel should deform more than the lined tunnel in TB#7 (EI/R^3 = 86 psi). It appears from the increasing rate of change of diameter with increases in vertical model pressure shown in Fig. 32 for the unlined tunnel at a stress level of 800 psi that the unlined tunnel (TB#5) would have experienced larger diameter changes than the flexible tunnel liner in TB#7 (EI/R^3 = 86 psi) if the test on TB#5 had been conducted to higher pressures.

The magnitude of the diametrical strains along 45° sections is much smaller than those at the crown-invert or springline (Fig. 34). For the unlined opening the 45° diameter decreases in length while that of the lined openings (TB#7 and TB#9) increase in length. As can be expected, the stiffer liner (TB#9) results in a smaller amount of diametrical strain at the 45° sections.

It has been observed that the stress-strain relationship of the model material is nonlinear, and that the effective modulus of the

This is because the stiffer liner under vertical loading has a large enough bending stiffness to push the medium outward at the springline. The thinner liner has a small flexural stiffness and thus all diameters decreased in length as dictated by the movements of the surrounding medium. In Fig. 29 it has been observed that the diametrical strain at the crown-invert section for the stiff liner is slightly greater than that for the thinner liner. This results primarily because the thinner liner is subjected to more uniform pressures and both the vertical and horizontal diameters show a decrease in diameter rather than the ovalling experienced by the stiffer liner which apparently is subjected to more nonuniform pressure.

At the 45^{o} sections (Fig. 31), the diametrical strains of the lined tunnels are also considerably smaller than those of the unlined tunnel. The tunnel opening with the thin liner, (TB#13) experiences slightly greater diametrical strains at the 45^{o} lines, when compared to a tunnel with a stiffer liner (TB#11).

Figures 32 through 34 also show comparisons similar to those of Figs 29 through 31 for models tested at an N value of 1/4. The test data shown in these figures are for tests TB#5 (unlined), TB#7 (EI/R^3 = 86 psi) and TB#9 (EI/R^3 = 540 psi).

As shown in Fig. 33 the springline diameter of the unlined opening in TB#5 continued to decrease in length throughout the loading. The steel liner (EI/R^3 = 86 psi) tested in TB#7 however showed an increase in length of the springline diameter with increasing pressure as would be expected for a loading applied with N = 1/4. The data shown for the stiff liner in TB#9 (EI/R^3 = 540 psi) also show a lengthening of the

material decreases throughout the test. Therefore a more meaningful comparison of the behavior of the lined openings can be made by plotting the diametrical strains against the vertical free-field strains in the medium, rather than against the vertical model pressure. Thus the variation of the modulus of the medium with pressure level is indirectly taken into account and the resulting plots are dimensionless.

Figure 35 shows such a plot of diametrical strain against vertical free-field strain for tests of TB#3, TB#10 and TB#12. TB#3 contained an unlined tunnel whereas TB#10 and TB#12 contained lined tunnels with EI/R^3 values of 86 psi and 5 psi respectively. All three tests were conducted at a principal stress ratio of N = 1. The solid lines in these plots denote the observed relationship between the free-field strain in the model and the diametrical strain of the tunnel. Since the loading is hydrostatic, the diametrical strains at the various locations in the tunnel liner should theoretically be the same. However in actual measurement a small amount of scatter was observed; therefore, the average value of the diametrical strains have been used in preparing these plots. Figure 35 shows that the measured diametrical strains for the unlined opening are much more than those predicted by using an elastic theory. The behavior of the unlined opening is obviously inelastic especially at higher levels of loading and thus the use of an elastic theory to predict the diametrical strains in such a case would be grossly in error. In comparison, it is seen from Fig. 35 that the observed and theoretical relationships (based on elastic theory) between diametrical strain and free-field strain in the model for TB#10 and TB#12, in general show very good agreement. This indicates

that the lined openings in TB#10 and TB#12 were behaving almost elastically. The difference between the observed behavior and the theoretical behavior is well within the range of scatter in these tests. This figure also illustrates the reduction in diametrical strain as a function of lining stiffness.

An analytical investigation has been carried out in an attempt to correlate the non-linear behavior observed in these model tests on unlined tunnels with existing methods for analyzing inelastic behavior around tunnels. Newmark (1969) has given an elasto-plastic solution to determine the stresses and strains around tunnels subjected to a hydrostatic free-field loading under plane strain conditions. The diametrical strains as predicted by his solution, are plotted against the estimated vertical free-field strains as shown in Fig. 36. In these calculations the stress-strain properties of the intact model material were taken as $E = 1 \times 10^6$ psi and $\nu = 0.25$. The angle of internal friction was taken as 30^0 and the unconfined compressive strength used was 550 psi. The measured diametrical strains and those computed using an elastic theory are also plotted on Fig. 36 for purposes of comparison. Newmark's solution gives a closer fit to the measured data than the elastic solution. In Newmark's solution, the dilatancy effects in the plastic zone are assumed to be zero; in other words the plastic zone is assumed to deform without any change in volume. In most practical cases, this assumption is not valid. Invariably there is a certain amount of increase in the volume (dilatancy) of the medium around the opening. Recently a solution was developed (Hendron and Aiyer, 1971) which takes into account the effects of dilatancy in

the plastic zone. The diametrical strain-free-field strain relationship, predicted by this elasto-plastic solution with dilatancy is also presented in Fig. 36, and it is easily seen that the agreement with the observed behavior is better than that of Newmark's solution or the elastic solution.

Figures 37 and 38 show the diametrical strain versus vertical free-field strain relationships at the crown-invert and springline sections for models loaded with a principal stress ratio of N = 1/4. These plots have been prepared from the test data from TB#7 (EI/R^3 = 86 psi) and TB#9 (EI/R^3 = 540 psi). The corresponding relationship for an unlined tunnel (TB#5) loaded at N = 1/4 is also shown for purposes of comparison. Figures 37 and 38 indicate that the behavior of the unlined tunnel is considerably nonlinear and inelastic. For the unlined tunnel the diametrical strain remains positive (indicating a decrease in the length of the diameter) at both the springline and the crown-invert sections. But for the lined tunnels, the diameter at the springline increases in length whereas the crown-invert diameter undergoes a decrease in length. The percentage increase in length of the springline diameter for TB#7 with a liner stiffness of 86 psi was greater than that for TB#9 with a liner stiffness of about 540 psi. For TB#7 (EI/R^3 = 86 psi) the diametrical strains at the springline and between the crown and invert were about ten times the vertical free-field strains in the model. The diametrical strains at the springline and crown-invert sections of TB#9 (EI/R^3 = 540 psi) were about four times the vertical free-field strains.

A comparison of the diametrical strain versus vertical free-field

strain relationships for tests conducted at a principal stress loading ratio of N = 2/3 is presented in Figs. 39 and 40. Figure 39 shows that the diameter between the crown and the invert shortens for the unlined tunnel and the tunnel liners with bending stiffnesses of 86 psi and 5 psi. At a vertical free-field strain of 3000 μ in/in the diametrical strain of the unlined opening is about six times the free-field strain whereas the lined openings show a diametrical strain of about one and two-thirds times the free-field strain.

In Fig. 40 the model test data show that both the unlined tunnel and TB#13 with the flexible liner (EI/R^3 = 5 psi) decrease in diameter at the springline. But the stiffer liner (EI/R^3 = 86 psi) in TB#11 increased in diameter at the springline. At a vertical free-field strain of about 3000 μ in/in the diametrical strain at the springline of the stiff liner was about equal to the free-field strain whereas the unlined tunnel showed a diametrical strain of about six times the free-field strain. These data definitely show that when the bending stiffness of a liner gets sufficiently low and the circumferential strains in the rock medium approach failure the liner will decrease in length on all diameters for a loading at N = 2/3. A stiffer liner however will decrease in length along a vertical diameter and increase in length along the springline diameter.

In Fig. 41 the diametrical strain between the crown and invert for TB#11 is shown plotted versus the vertical free-field strain at a loading ratio of N = 2/3. For this test the liner had a bending stiffness (EI/R^3) of 86 psi. The elastic solution for this case is shown by the dashed line (Fig. 41) which was calculated from the

solution given by Savin (1960). The experimental data agree well with the elastic calculations for TB#11 even up to strains as large as 4000 μ in/in which is well beyond elastic behavior for the rock model materials.

Chapter 3

GEOMECHANICAL MODELING TECHNIQUES FOR CONSTRUCTION OF JOINTED MODELS

3.1 General

The same loading frame was used to test jointed models which was designed to test 24" x 24" x 8" solid models in plane strain (no strain along the axis of the tunnel). The model tunnels tested on this study were all 4 inches in diameter and were drilled through the center of the 24" x 24" faces. Thus, the model tunnel simulates a section of a long horizontal tunnel where the tunnel experiences no strain in the axial direction. All of the jointed models were constructed to have two sets of mutually perpendicular joints oriented parallel to the tunnel axis. Figs. 42, 43 and 44 show the joint configurations used in the models tested in this study. The models were tested with the 24" x 24" faces horizontal, and thus the longitudinal direction is vertical in the model whereas it would generally be the horizontal direction in the field. The models were tested in this orientation because it greatly simplified the design of the loading apparatus.

3.2 Development of Jointed Models

Fig. 42, 43 and 44 show that there was a large number of joint blocks required for the construction of a single model. There were two possible methods which could conceivably be used to manufacture such a large number of joint blocks. They could either be cast in a mold to the proper shape, or they could be sawed out of larger blocks of model material. Because of the large amount of time consuming work anticipated in a sawing process, it was first decided to try molding the blocks by vibrating a sand-water-plaster mix in a mold.

The anticipated model blocks would be required to have a low cohesion, c, so that inelastic action could be observed within the capacity of the loading frame. In addition a high angle of shearing resistance, ϕ, would be required to accurately simulate the properties of rock. It was necessary for the blocks to have a very dense packing of sand grains to prevent collapse of their structure at high confining pressures (Heuer and Hendron, 1971). It was also desired to use the same kind of sand and plaster in the vibrated model material as had been used in the compacted model material (Heuer and Hendron, 1969) used in the solid model blocks.

Attempts to make joint blocks by vibrating material in a mold proved to be futile because the blocks were too fragile to be removed from the mold. These blocks were 2" x 2" x 8" blocks which were the largest size contemplated for use on this study. The failure to successfully extrude the vibrated joint blocks was due largely to the very low cohesive strength of the material.

After attempts at molding joint blocks failed it was decided to make joint blocks by sawing them out of larger compacted blocks. Steel molds 20" x 20" x 6" were used to compact 20" x 20" x 3" blocks using the same compaction procedure and the same mix proportions as used by Heuer and Hendron (1969) on 24" x 24" x 8" solid model blocks (Fig. 45). A decided advantage of this procedure is that the intact material of the joint blocks would be essentially identical to the intact material composing the solid models tested previously by Heuer and Hendron (1971). This model material is probably the best model material which has been reported to date for modeling the properties of rock.

After compaction, these blocks are allowed to air dry for three days after which time they are put in an overn to dry at 105°F for about a week. When the 20" x 20" x 3" blocks are properly cured, they are strong enough to be easily

handled without breaking. They also saw very easily. A metal surface grinder with a moving table has been converted into a saw for accurately cutting joint blocks (Fig. 46). Diamond blades are used quite successfully for sawing joint blocks with this machine. It has been possible to saw blocks as small as 1/2" x 1/2" x 8" without excessive breakage. A jig has also been made to fit the saw for cutting triangular cross-section blocks for use around the edges of models which have joints oriented at 45° to the principal directions of loading.

Since exactly the same material is used in the joint blocks as was used by Heuer and Hendron (1969) in the solid blocks, a new series of material properties tests was not necessary. The standard mix is made in the ratio of 1.2/1/9/.01 (water/plaster/sand/retarder) by weight. The plaster used is White Molding Plaster. The sand used is the fine fraction of a Pleistocene sand deposit obtained from the Sangamon River valley near Mahomet, Illinois. The grain size distribution of the fine Sangamon River sand is shown in Fig. 47. The retarder used is Sodium Phosphate (Na_2HPO_4) in the dibasic anhydrous powder form.

The material is mixed in a Lancaster concrete mixer with a 300 lb capacity. The sand, plaster and retarder are mixed together dry for about 5 minutes, the plaster being periodically removed from the bowl and blades by the use of a stiff brush. When the dry mixture is homogeneous, the water is added while the mixer is running and the batch is mixed wet for about 5 minutes. The lumps are removed by cutting with trowels and crushing with hands while the mixer is running. When the wet mix is homogeneous, it is placed in the mold in about 1/2" thick layers and compacted with a pneumatic tamper by the same method used by Heuer and Hendron (1969).

The intact shear strength properties of the model material are shown in Fig. 48. The angle of internal friction is $\phi = 33°$ and the unconfined compressive strength is $q_u \cong 555$ psi.

The Mohr failure envelope for the intact material in Fig. 48 is essentially a straight line up to confining pressures as high as 1000 psi. This is in marked contrast to the behavior of most previous model materials which approach $\phi = 0°$ behavior at high pressure. Since a high frictional shearing resistance is one of the most important properties of jointed rock masses, it is essential that a model rock material have high frictional resistance.

A series of three direct shear tests were run on 2" x 6" sawed joint surfaces of the model material. These tests were conducted in the direct shear machine in the University of Illinois rock mechanics laboratory. Tests were run at normal stresses of 50 psi, 150 psi, and 400 psi. The measured maximum shear strength in each case respectively was 33.3 psi, 97.5 psi, and 230 psi. These three points are plotted in Fig. 49 which shows that the effective angle of shearing resistance on the joint surfaces decreases from 33° to 29° with increasing normal pressures. All three direct shear specimens had flat-top shear-strength vs. deformation curves for a given normal pressure. In all three cases, the residual shear strength after 3 cm of slip along the joint was essentially the same as the peak shear strength. These tests indicate that a value of the angle of shearing resistance for use in an analysis of the jointed models should be slightly lower than the value obtained in the triaxial tests of intact samples shown in Fig. 46. For any theoretical elasto-plastic analysis of a jointed mass, the appropriate angle of frictional resistance should be taken as the angle of frictional resistance along the joints not the angle of internal friction derived from triaxial tests on intact samples of the model material, Hendron and Aiyer (1971).

The sawing tolerance on the blocks is about $\pm$ .01". This means that in a model with 2" joint spacing, if all of the blocks on one row are 0.01" too thin and on the next row they are all 0.01" too thick, the maximum offset of the joints could accumulate across the model to as much as 0.24" which is intoler-

able. The test blocks must therefore be constructed by selecting the blocks such that they fit together to make straight joint lines with minimum offsets in both directions (Fig. 50). The blocks are constructed on a table and then moved block by block into the testing machine. Each of the external faces of the constructed model block is flattened by grinding and is thoroughly cleaned of dust with compressed air before placing it in the testing machine.

The solid test blocks were placed in the testing machine on a 1/4" thick aluminum plate which was the base of the mold in which the model block was compacted. There were 2 layers of wax paper between the model and the aluminum plate and the aluminum plate was seated in the machine with a layer of plaster. This procedure was used because the model could not be molded to exactly fit the shape of the base plate in the testing machine and because the aluminum plate was necessary to lift the model into the testing machine with a crane. The aluminum plate and plaster were not used for the jointed blocks because a jointed model can easily fit the shape of the base plate in the testing machine and because the separate joint blocks can be easily handled without a crane. The jointed models are placed in the testing machine on two sheets of 4 mil polyethylene plastic placed directly on the base plate of the testing machine. The polyethylene sheets are used to reduce friction between the model and the base plate of the testing machine.

When the model is constructed in the testing machine, the loading elements are put in place and a small seating load of about 25 psi is applied in both the horizontal and vertical directions. With the seating load held constant, the 4" diameter tunnel is cored and cleaned out thoroughly with a vacuum cleaner. The joints intersecting the tunnel are then sealed with a small bead of silastic caulking compound which is allowed to cure for two days. The tunnel wall is then

painted with SR-4 strain gage cement for water proofing purposes and the cement is allowed to cure for one day. The instrumented tunnel liner is then installed in the tunnel and the base of the liner is sealed with silastic. When the silastic has cured, the liner is grouted in place using a liquid grout consisting of one part water to one part sulfaset rock bolt cement by weight. The grout is cured for one day and then the loading head is placed on top of the model using two layers of 4 mil polyethylene sheet and a layer of plaster to get close contact between the model and the testing head. This procedure for placement of the loading head is the same as that used by Heuer and Hendron (1969).

Free Field Strain Measurement

In the solid blocks, the strains in the block were measured with foil strain gages mounted directly on the model material at the midplane of the block. In the jointed blocks, strain gage measurements on the intact blocks are not a good measure of freefield strain in the model due to slippage and closure along the joints. Thus, buried extensometers were used in the jointed models to measure the average relative displacements of two points across the block. Average strains of the block were obtained by dividing the relative displacement between the points by the distance between the points, ($\varepsilon = \Delta L/L$).

The buried extensometers are simply metal rods grouted with epoxy into holes drilled into the model to the specified depth. The extensometer holes are drilled with a masonry bit. Plastic tubing is used to contain the epoxy until it is extruded by pushing the extensometer into position in the model. Fig. 53 shows a series of extensometers ready to be filled with epoxy and installed. The extensometers are composed of a piece of 1/4" diameter metal rod with a seating hole drilled in the end and three pieces of flexible plastic tubing. Two

pieces of the plastic tubing are used to make a cup to contain the epoxy on one end of the extensometer (Fig. 51) and another piece is used as a spacer to center the rod in the hole near the face of the model (Fig. 51). A typical overall installation of two buried extensometers is shown in Fig. 52. The epoxy is very viscous and will not flow out when the extensometers are held in a horizontal position. Fig. 54 shows an extensometer as it was exposed after a test. The model must be under a seating load when the extensometer holes are drilled and when the extensometers are grouted in place.

The movements of the extensometers are measured with the use of beryllium-copper clip gages like those which have been used to measure diameter changes in the tunnels of the previous tests (Heuer and Hendron, 1971). These gages consist of curved strips of beryllium-copper five inches long with seating points on the ends. Each strip is gaged with four strain gages wired in a four arm bridge. These clip gages can be accurately calibrated with a standard strain indicator and they have a linear calibration curve over a range of about 1" deflection. Fig. 52 is a detail showing the apparatus used to measure the movements of the buried extensometers.

Each of the clip gages is calibrated before and after each test while wired to the same terminals as used during the test. There are small changes in the calibration of the gages from test to test and the continual recalibration is necessary to know the changes and to detect any possible faults in the system before running a test.

CHAPTER 4

TEST RESULTS OF LINED TUNNELS IN JOINTED MODELS

4.1 General

Five jointed model blocks were constructed and tested in this model study. These five models are designated JB #1 through JB #5. The basic parameters which distinguish the separate jointed models are presented in Table 2. All of the jointed models were constructed with two sets of mutually perpendicular joints and 4" diameter tunnels. The variables considered in this study were liner stiffness, joint spacing and joint orientation. Figures 42 through 44 illustrate the joint configurations used in this study.

All previous models tested on this study (TB #1 through TB #13) were solid model blocks. Real rock masses are always dissected by fractures of some nature, and thus jointed models are necessary to more closely simulate field conditions. Joints reduce the strength and increase the compressibility and permeability of rock masses; therefore, they significantly affect the behavior of any structure in rock.

The joints in the models tested in this study were smooth, plane surfaces and were all oriented in two sets striking parallel to the tunnel axis. This is the most unfavorable arrangement of joints possible with respect to loading of the tunnel liner because the joints cannot interlock at the tunnel wall.

As shown in Fig. 49, the effective angle of shearing resistance along the joints is about 30° and tends to decrease with increasing normal pressure. The shearing resistance along joints in the field could be either higher or lower than 30° depending on the degree of interlock of irregularities along the joints and the amount and nature of filling in the joints. These models simulate rock masses with clean, smooth unfilled joints.

The remainder of this chapter consists of a systematic presentation and discussion of the data obtained in the testing of JB#1 through JB#5. A series of plots comparing the results of the tests is presented at the end of this chapter.

4.2 Presentation of Test Results

Joint Block #1.

The first jointed model (JB#1) was constructed and tested with a 2 in. joint spacing in two mutually perpendicular directions with the joints oriented parallel to the principal loading directions (Fig. 42). The joint configuration was symmetrical about the tunnel. The tunnel was 4 in. in diameter and was lined with a steel liner (t = 0.065", Et/R = 975,000 psi) which had a circumferential stiffness (Et/R) higher than the overall stiffness, Em, of the model (Em = 78,000 psi). JB#1 was tested with a principal stress ratio $N = \sigma_h/\sigma_v = 2/3$. JB#1 contained buried extensometers to measure the stiffness of the jointed mass (Fig. 52).

Fig. 55 is a plot of vertical free-field strain of the model (ε_{vff}) as a function of the vertical model pressure (σ_v). The stress axis of Fig. 55 was shifted 3000 μ in/in to the right to account for the initial seating or slack between the joint blocks. In this first test on a jointed model a seating load was not applied and released before the test readings were made. This procedure was followed on all subsequent tests however, and eliminated much of the initial seating deformation. The slope of the initial linear portion of this model stress-strain curve is about 80,000 psi. For an intact block of the same model material (TB#13), the slope of the vertical free-field stress-strain curve was about 625,000 psi. Thus, the stiffness of the block was reduced to a value of one-eighth the stiffness of the solid material due to the presence of the joints.

Fig. 56 is a plot of diametrical strain of the liner as a function of vertical model pressure for the crown and invert (0°), springline (90°), and the two 45° diameters. Since the joint spacing is symmetrical about the liner, the two 45° diametrical strains should theoretically be identical. The minor variation shown in Fig. 56 is due to experimental error mainly in constructing the model. As shown in Fig. 56, the crown and invert diameter shortened throughout the test while the springline diameter and one of the 45° diameters expanded throughout the test. The other 45° diameter first expanded and then began to compress above a vertical stress, σ_v, of 600 psi. The divergence between the crown - invert diametrical strain and the springline diametrical strain with increasing stress level in Fig. 56 indicates a considerable amount of bending of the liner. The liner ovalled in this fashion because it attracted large vertical loads due to the fact that the circumferential stiffness of the liner Et/R was much greater than the stiffness, Em, of the model and because the model was loaded with a principal stress ratio less than one ($N = \sigma_h/\sigma_v = 2/3$). In this test, the diametrical strains of the liner were due almost entirely to bending; the maximum average circumferential strain of the liner being only about 1000 μ in/in compression while the total crown - invert diametrical compressive strain was 14,000 μ in/in.

Fig. 57 is a dimensionless plot of the diametrical strain of the liner on four different diameters as a function of the vertical free-field strain of the model. In this plot, the stress-strain curve for the model given in Fig. 55 was used as the free-field stress-strain curve. Presentation of the data in this manner is helpful for an immediate comparison between the diametrical strain of the liner, $\Delta D/D$, and the vertical free-field strain of the model. Also, since such a plot is dimensionless, it is useful for comparisons of data from different test blocks

with different model stiffnesses. From this plot it is clear that the tunnel liner was much stiffer than the model medium since the diametrical strains, $\Delta D/D$, measured in all cases were less than the vertical free-field strain of the model at free-field strains below 12,000 μ in./in.

Joint Block #2.

The second jointed model (JB#2) was constructed and tested with a 2 in. joint spacing in two mutually perpendicular directions with the joints parallel to the principal loading directions (Fig. 42). The tunnel was 4 in. in diameter and was lined with an aluminum liner (t = 0.035", Et/R = 175,000 psi, with a circumferential stiffness, Et/R, greater than twice the stiffness of the jointed model block (Em = 84,000 psi). This thin aluminum liner was much more susceptible to buckling (EI/R^3 = 5 psi) than the steel liner used in JB#1 (EI/R^3 = 86 psi). JB#2 was tested with a principal stress ratio $N = \sigma_H/\sigma_v = 2/3$ and contained four pairs of buried extensometers which worked well throughout the test. The model was loaded to a peak vertical pressure of 1000 psi with no visible failure of either the tunnel or the block except at the corners of the model where the material spalled out from behind the loading elements (Fig. 58). The ovaling of the tunnel liner was not apparent by visual inspection, but it could be clearly measured with a caliper and the caliper measurements agreed with the diametrical extensometer measurements taken during the test. No shearing displacement along the joint planes was visually apparent (Fig. 58). Careful examination of the liner after completion of the test revealed no indications of buckling.

JB#2 was instrumented with four pairs of buried extensometers grouted 3" deep into the faces of the model and thus are designated shallow according to Fig. 19. These extensometers are designated as vertical, horizontal, on the centerline, or offset as shown on Fig. 19. The tunnel liner was instrumented with

four diametrical extensometers located at the crown and invert, springline and two 45° diameters. The springline diametrical extensometer failed to give readings because of a bad switch. The data obtained from the buried extensometers and the diametrical extensometers in the tunnel are presented in Fig. 59 through Fig. 61.

The displacement data from the external extensometers were converted to model strains ($\varepsilon = \Delta L/L$) by dividing the displacements, ΔL, by the gage length, L, and the calculated strains were plotted as a function of vertical model pressure, σ_v, in Fig. 59. Thus these curves are average stress-strain curves of the jointed model. The curves for the vertical direction are actual stress-strain curves while the curves for the horizontal direction are pseudo stress-strain curves since the horizontal strains are also plotted versus the vertical model pressure. The vertical stress-strain curves of the model are concave upward from 0-200 psi, linear with a slope of about 100,000 psi from 200-800 psi and concave downward above 800 psi. Thus the model strains were affected by seating of open joints from 0-200 psi. The linear portion of the curve from 200-800 psi indicates essentially elastic action, and the final concave downward section of the curve shows increasing inelastic action probably caused by shearing deformations along the joints. The horizontal strain in the model was less than the vertical strain, as would be expected for a loading at N = 2/3. The centerline stress-strain curves show smaller strains than the offset stress-strain curves in both the horizontal and in the vertical directions. Such a result would be expected if the tunnel liner were stiffer than the model block. The block had an average stiffness of about 100,000 psi in the elastic range of behavior while the liner had a calculated elastic circumferential stiffness of 175, 000 psi. Relatively stiff behavior of the tunnel liner is illustrated in Fig. 61 by the dimensionless diametrical strain curves for the 45° diameters of the liner. At the 45° diameters,

the diametrical strain was consistently less than the vertical free-field strain. The diametrical strains of the liner are plotted versus vertical model pressure in Fig. 60. The aluminum liners used have a yield strain of about 4000 μ in./in. and thus the liner yielded generallyat about 800 psi vertical model pressure where the 45° diametrical strain became about 4000 μ in./in. Local yielding of the liner probably occurred at lower model stresses due to the ovaling of the liner illustrated by the large diametrical strains at the crown and invert with respect to the 45° diametrical strains (Fig. 60).

Figure 61 is a plot of the diametrical strain of the tunnel liner on three different diameters as a function of the vertical free-field strain of the model. The vertical-centerline stress-strain curve was used as the free-field strain of the model. For the entire range of loading of the model, the diametrical strains at the crown and invert diameter are approximately double the vertical free-field strains while the diametrical strains at the 45° diameters are less than half of the vertical free-field strains at pressure levels below general yield of the liner (800 psi.).

The small strains at the 45° diameters indicate that the circumferential stiffness, Et/R, of the liner was stiff compared to the medium; but, the large difference between the strains between the vertical diameter and the 45° diameter shown in Fig. 61 is the result of the ovaling of the liner because the bending stiffness, EI/R^3, of the liner was small.

Joint Block #3

The third jointed model (JB#3) was constructed and tested with two sets of mutually perpendicular joints spaced at 2 in. and oriented at 45° to the principal loading directions (Fig. 43). As shown in Fig. 43, the joints were not spaced symmetrically about the tunnel. The tunnel was 4 in. in diameter and was lined

with an aluminum liner which had a circumferential stiffness (Et/R = 175,000 psi) about three times as large as the stiffness of the model block (Em = 65,500 psi). The bending stiffness of this liner (EI/R^3 = 5 psi) was very low, and thus the liner would be expected to bend freely with any shearing distortions of the model caused by the principal stress ratio of N = 2/3 used in loading the model. Eight pairs of extensometers were used to measure the overall strains of the model. The extensometers were located and are designated as shown in Fig. 19.

JB#3 was loaded to a peak model pressure of 1000 psi in the vertical direction with no visible failure of the tunnel or the block except at the corners of the model where the model material spalled out from behind the loading elements. Visual inspection of the model after the test revealed no visible ovaling of the liner and no visible shearing displacements along the joints. Careful examination of the tunnel liner revealed absolutely no indication of buckling.

JB#3 was instrumented with eight pairs of buried extensometers, four pairs grouted 3 in. deep and four pairs grouted 5 in. deep into the face of the model. Seven of the eight pairs of extensometers worked throughout the loading of the model. The data obtained from these extensometers are presented in Fig. 62. The curves plotted in Fig. 62 are clearly separated into a group of four vertical stress-strain curves and three horizontal pseudo stress-strain curves. The scatter of the data from the average is minimal considering that the various extensometers were located at different depths and at different locations with respect to the tunnel. After seating movements up to a vertical model pressure of about 125 psi, all of the model stress-strain curves in Fig. 62 are essentially straight lines to the peak load. The seating strains are not shown. In this test, the average model stress-strain curve designated on Fig. 62 as vertical - centerline - shallow, according to Fig. 19, was used as the free-field stress-strain curve of the model. The slope of the linear portion of this stress-strain

curve is 65,500 psi as compared to a model stiffness, Em, of 80,000 psi for JB#1 and 84,000 psi for JB#2. This reduction in model stiffness was due to the 45° orientation of the joints because the vertical deformations measured by the extensometers in JB#3 included the shear deformations along the joint planes. In JB#1 and JB#2, the joints were parallel to the principal loading directions, and there were no significant shear stresses along the joints. In JB#3, however, the maximum shear stresses acted along the joint planes. Thus, in JB#3 the maximum shear stresses acted along the planes of minimum shear strength and larger shearing displacements would be expected.

The tunnel liner in JB#3 was instrumented with four diametrical extensometers located at the crown and invert (0°), springline (90°), and two 45° diameters. The data obtained from the tunnel diametrical extensometers are presented in Fig. 63. The liner deformations in this test were also due mainly to bending as is shown by the large expansion of the springline diameter, the large compression of the crown and invert diameter and the relatively small compression of the 45° diameters. No buckling of the liner occurred during this test which was stopped at a maximum vertical model pressure σ_v = 1000 psi. The two 45° diametrical strain curves show a much wider separation than in previous tests. In previous tests, the joint spacing about the liner was symmetrical. But in JB#3 the joint spacing about the liner was not symmetrical as shown in Fig. 43 and the two 45° diameters were not subjected to the same external conditions. The 45° extensometer which recorded the smaller strain was located along the centerplane of a row of blocks while the one which recorded largerstrain was along a joint plane. Thus it appears that the shearing displacements along the joint planes caused the asymmetrical distortion of the tunnel liner.

A dimensionless plot of the diametrical strain of the tunnel liner as a function of the vertical model free-field strain is presented in Fig. 64. It is shown in Fig. 64 that the liner was stiffer than the average model stiffness as the diametrical strains at the 45° diameters was less than half of the model free-field strain throughout most of the loading range. The average diametrical strain at the springline was about two thirds of the free-field strain and the diametrical strain between the crown and the invert was about one and one-third times the free-field strain.

Joint Block #4.

The fourth jointed model (JB#4) was constructed and tested with a 2 in. joint spacing in two mutually perpendicular directions at 45° to the principal loading directions (Fig. 65). The tunnel was 4 in. in diameter and was lined with a .035 in. thick aluminum liner with an elastic circumferential stiffness of 175,000 psi. The average measured vertical stiffness of the model was 62,500 psi. JB#4 was tested at a principal stress ratio $N = \sigma_H/\sigma_V = 2/3$ to a maximum vertical model pressure of 1300 psi in an attempt to fail the liner. The model was instrumented with eight pairs of buried extensometers as shown in Fig. 19, and six diametrical extensometers in the tunnel liner. The two additional diametrical extensometers were placed in the liner at points where the joints intersected the liner (Fig. 65).

The data obtained from the six pairs of buried extensometers which worked during the test are presented as stress-strain curves of the model in Fig. 66. Buckling of the liner did occur in this test at a pressure level of about 1100 psi. The buckling of the liner is reflected in the average stress-strain curves of the block as a distinct deviation from linearity at a pressure of about 1100 psi. The vertical stress-strain curve showed a distinct increase in compression above 1100

psi while the horizontal pseudo stress-strain curves showed a sudden distinct bulging of the model in the horizontal direction. The probable physical cause of this behavior is a wedging action caused by shearing displacements along the joint planes whereby loads were concentrated at the crown and enhanced a buckling failure. In JB#4, the buckling of the liner probably affected the measurements of the model strain at high pressures. Therefore at stresses above 1100 psi the measured model strain is not the true free-field strain of the medium. A larger model would have been necessary to measure true free-field strains of the model after the liner buckled.

Six diametrical extensometers were used in the tunnel liner of JB#4 instead of the usual four. The two additional extensometers were placed at points where joints intersected the liner. These points occurred on diameters located at 20° and 70° from the crown-invert diameter. The other four diametrical extensometers were at the crown-invert (0°), the springline (90°) and the two 45° diameters as in previous model tests. Note in Fig. 65 that one of the 45° diameters falls along a joint plane while the other 45° diameter falls along the midplane of a row of joint blocks. In JB#3, which was the same as JB#4 except that JB#4 was loaded to a higher model pressure, larger diametrical strain was observed along the 45° diameter at the intersection of the liner and a joint plane than for the 45° diameter which lined up with the midplane of a row of joint blocks. It was because of this apparent strain concentration along the joint planes that the two additional diametrical extensometers were placed at 20° and 70° in JB#4.

The data obtained from the six diametrical extensometers is plotted in Fig. 67 as a function of the vertical model pressure. Buckling of the liner is clearly shown at a vertical model pressure of about 1100 psi. The actual buckling occurred as a pair of buckles located along the 45° diametrical plane which coincided with

the intersection of a joint plane with the tunnel liner. The 45° diametrical extensometer designated as #2 on Fig. 67 was actually located on the buckle. The other 45° diametrical extensometer, #4, showed considerably different behavior than #2. The crown and invert (0°) and the 20° diameter showed about the same diametrical strains throughout the test as would be expected for approximately homogeneous behavior of the model. The movements of the other four extensometers were strongly affected by the movements along the joint planes.

The diametrical strain measurements of the tunnel liner are plotted as a function of the vertical free-field strain of the model in Fig. 68. These curves show clearly that the liner behaved stiff in comparison to the model until yield of the liner was reached. Buckling of the liner is clearly shown above a vertical free-field strain of about 18,000 μ in./in.

Joint Block #5.

The fifth jointed model (JB#5) was constructed and tested with a 1 in. joint spacing in two mutually perpendicular directions at 45° to the principal loading directions (Fig. 44). The joint spacing was symmetrical about the tunnel in this test. The tunnel had a 4 in. diameter and was lined with an aluminum liner (t = 0.035") which had a circumferential stiffness (Et/R = 175,000 psi) greater than four times the stiffness of the model (Em = 38,500 psi). JB#5 was tested at a principal stress ratio $N = \sigma_H/\sigma_v = 2/3$ to a maximum vertical model pressure of $\sigma_v = 1445$ psi. The maximum vertical model pressure of 1445 psi was reached and held constant for an hour with no further diametrical strains of the liner and no further model strains even though the liner was severely buckled (Fig. 70). JB#5 contained four pairs of buried extensometers to measure the free-field strains.

Joint Block #5 contained only four pairs of buried extensometers at the centerlines because the holes for the offset pairs could not be drilled with the loading elements in place. In the models with 2 in. joint blocks, the drilling could be done without a seating load. But the 1 in. joint blocks were too fragile to drill except with the model under a seating load. The data obtained from the four pairs of extensometers used in JB #5 are plotted in Fig. 71. The two horizontal pseudo stress-strain curves are essentially identical, with very small strains all the way to the maximum model pressure. The two vertical stress-strain curves are linear above a vertical model pressure of 150 psi. The stress-strain curve designated "deep" shows greater strain than the stress-strain curve designated "shallow." Thus it appears that the movements of the "vertical-deep" pair of extensometers were affected by the deformation of the tunnel liner. The average slope of the "vertical-shallow" stress-strain curve is about 38,500 psi as compared to 65,500 psi for JB#3 and 62,500 psi for JB#4. Thus reducing the joint spacing from 2 in. to 1 in. and retaining the 45° orientation of the joints caused about a 40% reduction in the overall stiffness of the model.

Six diametrical extensometers were used to measure the diametrical strain of the liner in JB#5. The two additional extensometers were placed at the two 30° diameters because joints intersected the liner at these locations. The data obtained from the six diametrical extensometers are plotted in Fig. 72. Note in Fig. 72 that the diametrical strains of the liner are due mainly to bending, and that the liner buckled at a vertical model pressure of about 700 psi. The springline diameter expanded almost linearly with pressure until buckling of the liner occurred. The largest buckle in the liner (Fig. 70) occurred near the springline. Thus, above 700 psi, the curve for the springline diametrical strain in Fig. 72 includes the buckling movements.

A dimensionless plot of the diametrical strain of the tunnel liner at these six different diameters as a function of the vertical free-field strain of the model is presented in Fig. 73. Each of the six curves is approximately bilinear. Each linear branch of the bilinear curves corresponds to a separate mode of behavior of the liner. The first linear branch from 0-22,000 μ in./in. vertical free-field strain corresponds to the elastic behavior of the liner. The second linear branch above 22,000 μ in./in. vertical free-field strain corresponds to the behavior of the liner after buckling. The first regime of behavior illustrates stiff behavior of the liner while the second branch illustrates flexible behavior. Note that after buckling all diameters tended to decrease in length as an extremely flexible liner would behave whereas before buckling the springline diameter lengthened and the crown-invert diameter shortened.

4.3 Comparisons Between Data from Various Test Blocks

Average vertical free-field stress-strain curves for the five jointed blocks and one solid block are plotted in Fig. 74. Seating errors of the jointed blocks were removed graphically from the curves for JB#1, JB#2 and JB#3 by extending the straight line portions of the curves below 125 psi down to zero pressure and then shifting the pressure axis. This was done to make all of the curves pass through the origin. Such a graphical procedure was not used on JB#4 and JB#5; rather a seating pressure of 125 psi model pressure was applied and released before the test was started. A seating pressure of 125 psi was used because it appeared that all seating movements occurred below 125 psi in JB#1, JB#2 and JB#3. Fig. 74 shows that there were seating movements up to about 200 psi in JB#5 even after the seating pressure had been applied and released. The important part of the stress-strain curves for the model blocks is the approximately linear portion above the

seating pressure. The slope of the linear portion of the stress-strain curve is the effective stiffness of the block in the vertical direction. The reduction in stiffness of the models due to even rather widely spaced joints is very great. For the solid block, the stiffness was about 625,000 psi; the stiffness for 2 in. jointed blocks ranged from 62,000 psi to 84,000 psi depending on the joint orientation and the intact modulus of the joint blocks; the stiffness of the single block with a 1 in. joint spacing was about 38,500 psi. JB#1 and JB#2 should have had the same stiffness if properly constructed; their actual measured stiffnesses were 80,000 psi and 84,000 psi. JB#3 and JB#4 similarly should have had the same stiffness and their measured stiffnesses were 65,000 psi and 62,000 psi. Thus it appears that the models are adequately reproducible.

It is commonly believed that the modulus of a rock mass is reduced by jointing because of the separation of the joints before loading but that after the joints are closed the stiffness will again approach the intact stiffness. These model tests indicate that there is a permanent effect of jointing in drastically reducing the modulus of a rock mass even when it is loaded to very high compressive stresses. The stiffnesses of the jointed blocks never showed any tendency to increase and approach the stiffness of an intact block even when loaded to very high pressure. There were seating movements which took place in all of the jointed model tests, but these occurred only below about 125 psi for 2 in. joint spacing and below about 200 psi for 1 in. joint spacing.

Figures 75, 76 and 77 are plots of the diametrical strains of the liners at the crown-invert, springline, and average of the two 45° diameters as a function of vertical model pressure for the various test blocks. All of these plots include the effects of circumferential compression and bending of the liner. The principal stress ratio was constant, $N = \sigma_H/\sigma_V = 2/3$, for all of these tests. The shape of these curves depended primarily on the relative stiffness of the

liner and the model. Some of the curves were affected by the location of joints and by buckling of the liner.

Consider Fig. 75 which is the plot of diametrical strain of liner at the crown and invert as a function of vertical model pressure for the various test blocks. The curve for TB#13 shows the smallest diametrical strains because the model was very stiff (E_H = 625,000 psi, see Fig. 74). TB#13, JB#2, JB#3, JB#4 and JB#5 had thin aluminum liners, Et/R = 175,000 psi. JB#1 had a steel liner, Et/R = 975,000 psi. The curve for JB#5 had very large diametrical strain because the model stiffness was only about E_H = 38,500 psi. Considering JB#1 and JB#2, which both had the same joint configurations; JB#2 had a larger diametrical strain between the crown-invert than JB#1 because JB#1 had a much stiffer liner. The curves for JB#3 and JB#4 should be the same within experimental error since the models were constructed to be exactly the same. If the curve for JB#4 is shifted to pass through zero strain at 125 psi model pressure, then the two curves are in fact very close

Considering only the relative stiffnesses of the blocks it would be expected that the crown and invert diametrical strain (Fig. 75) would be greater for JB#3 and JB#4 than for JB#2. In fact, the crown and invert diametrical strain for JB#2 was significantly greater than that of JB#3 and JB#4. Since this behavior is not explained by the relative vertical stiffnesses of the models, it must be due to the orientation of the joints. The 2 in. joint blocks which had joints oriented at 45° to the principal loading directions (JB#3 and JB#4) had larger vertical deformations and smaller horizontal deformations than the 2 in. joint models which had joints oriented parallel to the principal loading directions (JB#2). These measured test results indicate that high shearing strains along the joints or joint slippage resulted in a more compressible model in the direction of the major principal free-field stress for those cases where the joints were oriented at 45° or in a direction which coincided with the maximum shearing stresses.

Fig. 76 is a plot of the diametrical strains of the liner at the springline as a function of vertical model pressure for the same model tests shown in Fig. 75. The tunnel liner expanded at the springline in all of the jointed models but compressed in the solid model. The springline diameter compressed in the solid model because the model stiffness, Em, (625,000 psi) was more than three times stiffer than the circumferential stiffness, Et/R, of the liner (175,000 psi). The curve for JB#5 shows large expansion of the springline diameter up to a model pressure of 700 psi, and then rapid compression above 700 psi. The tunnel liner buckled at a vertical model pressure of about 700 psi due to the low bending stiffness (EI/R^3 = 5 psi) of the lining. Note also that the springline deformations for JB#5 are much greater than those for JB#3 and JB#4 for pressure levels below the buckling failure. This is due to the fact that JB#5 is composed of 1 in. joint blocks and JB#3 and JB#4 are composed of 2 in. joint blocks because the tunnel liner was the same in all three of these tests. From Fig. 76 it can also be shown that the liner in JB#5 buckled at a vertical stress of 700 psi whereas an identical liner in JB#4 buckled at a vertical stress level of 1000 psi. The liner in JB#4 buckled at a higher stress because the JB#4, composed of 2 in. joint blocks, was stiffer than JB#5, composed of 1 in. joint blocks.

Fig. 77 is a plot of the average diametrical strain of the liner at the two 45° diameters for the various test blocks. The curve for JB#1 shows that the liner expanded at the 45° sections. This expansion occurred because the liner was over twelve times as stiff as the model in resisting thrusts and since the crown and invert compressed most of the rest of the liner expanded. The curve for TB#13 shows that the liner compressed at the 45° diameters. This compression occurred because the liner was less than one third as stiff as the model in resisting thrusts and thus the whole liner compressed. The remaining curves

for JB#2, JB#3, JB#4, and JB#5 all show compression of the 45° diameters and they all fall in a fairly narrow band.

Comparisons between model tests are much more meaningful if they are made in terms of dimensionless parameters. Figs. 78, 79 and 80 are dimensionless plots of the diametrical strains of the liners at the crown-invert, springline, and average of two 45° diameters as a function of the vertical free-field strain of the model. The ratio of the circumferential stiffness of the liner to the vertical model stiffness $(\frac{Et/R}{Em})$ is shown on each curve. Et/R is the circumferential stiffness of the liner assuming no bending and Em is the plane-strain stiffness of the model taken as the average slope of the vertical free-field stress-strain curve of the model.

Fig. 78 is the dimensionless plot of diametrical strain of the liner at the crown-invert as a function of the vertical free-field strain of the model for the various test blocks. Among the tests with similar joint orientation the ratio of the circumferential stiffness of the liner to the stiffness of the model seems to be a significant parameter to consider in explaining the relative position of the curves. In this plot, the curves for JB#3 and JB#4 (joints at 45° to principal directions) plot very closely and almost parallel. They are located in the proper relative positions according to the relative stiffness of the model and the liner. The curve for JB#5 falls below the curves for JB#3 and JB#4 as would be expected by the higher value of the ratio of the liner stiffness to the model stiffness. In the models with joints oriented parallel to the principal directions of loading (JB#1 and JB#2) the crown-invert section showed higher diametrical strains than the models with the joints at 45° for given values of the vertical free-field strain and ratio of liner to model stiffness $(\frac{Et/R}{Em})$. The results shown in Fig. 78 do illustrate quite well that the behavior of the model

tunnels falls into a pattern in which the diametrical strain of the liners decreases in relation to the vertical free field strain as the ratio of the liner to model stiffness $(\frac{Et/R}{Em})$ increases. Normalizing the data in this manner also consistently combines the data from test blocks with different joint spacings.

Fig. 79 is the dimensionless plot of the diametrical strain of the liner at the springline as a function of the vertical free-field strain. These data show that the diametrical strains at the springline are 1/2 to 1 times the free-field vertical strain for a loading ratio of N = 2/3 for the complete range of liner to model stiffness ratios investigated with the jointed block models ($Et/R/Em$ = 2.7 ~ 12.2).

Fig. 80 is a plot of the average of the diametrical strains of the two 45° diameters of the tunnel liner as a function of the vertical free-field strain of the model for the various test blocks. This is perhaps the most meaningful of the set of three dimensionless plots. The diametrical strains of the 45° diameters most nearly represent the circumferential strain of the liners since they are the least affected by bending. As shown in Fig. 80, the relative locations of these curves is very clearly influenced by the ratio of the tunnel liner to model stiffness $(\frac{Et/R}{E_M})$ regardless of the joint orientation or spacing. For low values of the stiffness ratio the diameters shorten and as the stiffness ratios increase the magnitude of the shortening decreases until the liners elongate on the 45° diameters at high values of the stiffness ratio. For a stiffness ratio of about 3 the diametrical strains are about 1/2 to 2/3 of the vertical free-field strain and for a stiffness ratio of 4.5 the diametrical strain is about 1/10 of the free-field vertical strain.

Chapter 5

SUMMARY AND CONCLUSIONS

5.1 Summary

The results of eleven geomechanical model tests are presented in this report. Six of these tests were lined tunnels in solid test blocks and five tests were lined tunnels in jointed test blocks. The tests of lined tunnels in solid test blocks, were conducted using, the model material, the testing machine and the same basic testing techniques and instrumentation used by Heuer and Hendron (1971).

The techniques for constructing and instrumenting jointed models were developed on this study. The jointed models were constructed of small blocks of the same model material used in the solid test blocks. The small blocks were made by sawing them out of larger compacted blocks with a diamond blade saw. The intact shear strength properties of this material can be described by

$$\sigma_1 = q_u + \sigma_3 \frac{1 + \sin \phi}{1 - \sin \phi} \qquad (3)$$

where σ_1 is the major principal stress at failure, σ_3 is the minor principal stress at failure, ϕ is the angle of shearing resistance, and q_u is the unconfined compressive strength of the model material. The angle of shearing resistance, ϕ, and the unconfined compressive strength, q_u, of the intact model material are 33° and 550 psi respectively. A series of direct shear tests conducted on joint block surfaces showed that the angle of shearing resistance along the joints decreased from about 33° to 28° as the normal pressure on the joint surface was increased from 50 psi to 400 psi. The

angle of shearing resistance in direct shear did not depend on the amount of displacement along the joint at constant normal pressure.

The deformations of the tunnel liners in the jointed models were measured with clip gauges identical to those used in the solid model tests. The free-field strains of the jointed models, however, could not be measured by the use of strain gages which were used for the solid model tests. Buried extensometers were therefore developed to measure average free-field strains in the jointed models. The results of the free-field strain measurements on the jointed blocks have shown that the vertical plane-strain stiffness of the jointed models tested at a principal stress ratio of 2/3 is about 40,000 to 80,000 psi in contrst to the 500,000 psi measured on solid blocks. Thus one of the major effects of jointing was to reduce the model stiffness by a factor of about 10. It was also found that the stiffness of models composed of 1" joint blocks was lower than the stiffness of models composed of 2" joint blocks. This behavior is similar to the observed field behavior of rock masses where the stiffness is very sensitive to the fracture frequency in the rock mass. It was also found that models were more compressible for joints oriented at 45° to the major and minor principal stresses than for joints coincident with the principal planes. This behavior was due to shearing displacements which occurred along the joints at 45° to the principal planes.

The tests on lined tunnels in solid model blocks have verified that a liner generally increases the overall stability of an opening. A liner which is stiff compared to the rock mass significantly decreases the diametrical strains of the tunnel throughout the loading range if it has adequate strength and ductility. A liner which is very flexible compared to the rock

mass has little effect on elastic deformations of the tunnel, but if it has adequate strength and ductility it greatly reduces plastic deformations. Comparisons of the test results of the tunnels in solid blocks with theoretical elastic predictions of the tunnel behavior showed that all of the lined tunnels behaved essentially elastically while the unlined tunnels showed much greater deformations than predicted by elastic theory. Two elasto-plastic theories are available for predicting the stresses and strains around a cylindrical tunnel in an elasto-plastic material which fails according to the Coulomb-Navier yield criterion. Newmark (1969) presents an elasto-plastic solution which assumes no dilatancy of the model material in the zone of failure. In other words, Newmark assumed that the plastic zone deforms without any change in volume of the model material by assuming the following relationship between the plastic strain components:

$$\varepsilon_{r(plastic)} = -\varepsilon_{\theta(plastic)} \tag{4}$$

In most practical cases this assumption is not valid. There is almost always a certain amount of increase in volume (dilatancy) of a dense frictional material during failure. Hendron and Aiyer (1971) have presented an elasto-plastic analysis similar to Newmark's, except that a condition of dilatancy was assumed in the failure zone. This was done by assuming the following relationship between the plastic strain components:

$$\varepsilon_{r(plastic)} = -N_{\phi}\, \varepsilon_{\theta(plastic)} \tag{5}$$

This relation gives an increase in volume of the model material during failure and the percentage volume change increases as N_{ϕ} increases. The

Newmark solution, assuming no dilatancy, gives a lower-bound estimate of the diametrical strains of a tunnel while the Hendron-Aiyer solution, assuming a dilatancy based on "normality" (Drucker and Prager, 1953), gives an upper bound estimate of the diametrical strains.

Calculations using these elasto-plastic theories have been used successfully to more closely fit the behavior of the unlined model tunnels in solid blocks. The results of the elasto-plastic calculations are compared with the actual model behavior and elastic theory in Fig. 36. It is clear from Fig. 36 that the Hendron-Aiyer analysis, which includes the effects of dilatancy during shear failure of the material, gives the closest fit to the actual model test data.

No tests were conducted on unlined tunnels in jointed rock masses. The assumption can, however, be made that the provision of a structural liner generally increases the overall stability of an opening in a jointed rock mass to an even greater extent than in a solid rock mass. This is because the liner prevents the loosening and subsequent loss of confinement of the jointed rock mass around the tunnel. A meaningful summary of the data from the jointed models reported here is presented in Figs. 78 and 80.

Figure 78 is a dimensionless plot of the diametrical strain at the crown-invert diameter as a function of the vertical free-field strain in the model for six models tested at a principal stress ratio of 2/3. Among the four tests on jointed models with aluminum liners of the same stiffness (JB #2 to JB #5), the ratio $\frac{Et/R}{E_m}$ is a significant parameter determining the relative position of the curves regardless of the joint orientation and spacing. The results shown in Fig. 78 for these four models illustrate that the ratio

of the diametrical strain of the liners to the vertical free-field strain decreases as the ratio of the liner to model stiffness ($\frac{Et/R}{E_m}$) increases. The data in Fig. 78, for the crown-invert diametrical strain of the tunnel, can be summarized as follows:

(1) For a liner to model stiffness ratio ($\frac{Et/R}{E_m}$) of about 2, the ratio of tunnel diametrical strain, $\Delta D/D$, to the free-field model strain was about 2.0 for the full range of free-field strain.

(2) For a liner to model stiffness ratio of about 3, the ratio of the diametrical strain to the free-field model strain was about 1.0 for model strains below 1% and about 1.5 for model strains above 1%.

(3) For a liner to model stiffness ratio of about 4, the ratio of tunnel diametrical strain to the free-field model strain was about 2/3 for model strains below 1% and about 1.0 for model strains above 1%.

The model with a steel liner (JB #1), however, did not fall into the pattern discussed above. This is because the ratio $\frac{Et/R}{E_m}$ describes only the circumferential stiffness of the liner and not the flexural stiffness (EI/R^3). The steel liner in JB #1 had such a high circumferential stiffness that essentially all of the deformation of the liner was due to ovaling (flexure) rather than overall circumferential compression (Fig. 56). To consistently combine the data from tunnels lined with different thickness liners and loaded at a principal stress ratio other than 1.0, the bending stiffness of the liner must be considered in addition to the circumferential stiffness. Thus an important parameter to consider in extrapoltaing test results is the ratio of the flexural to the circumferential stiffness of the liner ($\frac{EI/R^3}{Et/R}$).

Figure 80 is a dimensionless plot of the average diametrical strains of the two 45° diameters of the tunnels as a function of the vertical free-field strain of the models. The diametrical strains of the 45° diameters of the tunnel most nearly represent the circumferential strain of the liners since they are the least affected by ovaling. Thus the parameter $\frac{Et/R}{E_m}$ should more consistently control the relative positions of these curves for any type of liner. As shown in Fig. 80, the relative locations of the curves is very clearly controlled by the ratio $\frac{Et/R}{E_m}$ since the behavior of all of the model tunnels fall into a pattern in which the diametrical strain of the tunnel liners decreases with respect to the vertical free-field strain as the liner to model stiffness increases.

The bending stiffness (EI/R^3) of the aluminum liners used in the tests reported here was so small that two of them buckled under loading. In both cases, the buckles in the liners occurred at the intersection of a joint plane with the tunnel liner. Thus it appears that strain concentration due to slippage along the joint planes was the local cause of buckling of the liners. Even after buckling, the liners were able to support the tunnel opening with the full load still on the model.

5.2 Conclusions

On the basis of the model tests and analyses reported here, the following conclusions may be drawn:

(1) A structural liner generally increases the overall stability of an opening in both solid and jointed rock masses.

(2) A liner which is very flexible compared to the rock mass surrounding the tunnel has little effect on elastic deformation of the tunnel.

(3) Inelastic deformations of a tunnel are greatly reduced by a structural liner.

(4) Available elasto-plastic theory was used to closely estimate the deformations of an unlined tunnel in an intact model tested at a principal stress ratio of 1.0.

(5) One of the major effects of jointing was to reduce the model stiffnesses by a factor of about 10. The deformation moduli of models composed of 1 in. joint blocks were lower than the moduli of models composed of 2 in. joint blocks. Also, the deformation moduli of models with joints oriented at 45° to the principal stress directions were lower than the moduli of models with joints parallel to the principal stress directions.

(6) Comparison between model tests with varying parameters are most meaningful if they are made in terms of dimensionless parameters.

(7) The thrust stiffness ratio $\frac{Et/R}{E_m}$ is a significant parameter affecting the diametrical strains of tunnel liners. Disregarding the effects of ovaling, the diametrical strains of tunnel liners decrease with respect to model free-field strain as the liner to model stiffness ($\frac{Et/R}{E_m}$) increases.

(8) Buckling of the liners in the models reported here was clearly initiated by shearing deformations along joint planes in the models.

(9) The ratio of the circumferential stiffness of the liner to the flexural stiffness of the liner ($\frac{Et/R}{EI/R^3}$) must be reasonably constant between model and prototype or the model will be distorted. Thus the model test results presented herein apply only to prototype cases in the field where the ratio of circumferential to flexural stiffness is about the same. Thus these results would only apply to prototype integral liners of steel and aluminum. It has been found on another study (Hendron and Engeling, 1972) that plexiglas liners could be used in the 1 in. jointed models described herein to model the behavior of integral reinforced concrete liners in rock with very little distortion.

REFERENCES

Drucker, D. C., and Prager, W., 1953, "Limit Analysis of Two and Three-Dimensional Soil Mechanics Problems," J. Mech. and Phys. of Sol., Vol. 1, No. 4, pp. 217-226.

Hendron, A. J., Jr. and Aiyer, A. K. (1971), Stresses and Strains Around a Cylindrical Tunnel in an Elasto-Plastic Material with Dilatancy, Report on Contract No. DACA 45-69-C-0100, Omaha District, U. S. Army Corps of Engineers, January, 1971.

Hendron, A. J., Jr., and Paul Engeling, (1972), Model Tests on Lined Tunnels in a Jointed Rock Mass, Report on Contract No. DACA 23-70-C-0050, U. S. Army Engineer Construction Engineering Research Laboratory.

Heuer, R. E. and Hendron, A. J., Jr., (1969), Geomechanical Model Study of the Behavior of Underground Openings in Rock Subjected to Static Loads, Report 1, Development of Modeling Techniques, Contract Report N-69-1, October 1969, U. S. Army Engineer Waterways Experiment Station, Corps of Engineers, Vicksburg, Mississippi, 209 pp.

Heuer, R. E., and Hendron, A. J., Jr., (1971), Geomechanical Model Study of the Behavior of Underground Openings in Rock Subjected to Static Loads, Report 2, Tests on Unlined Openings in Intact Rock, Contract Report N-69-1, Corps of Engineers, Vicksburg, Mississippi, 370 pp.

Newmark, N. M., (1969), "Design of Rock Silo and Rock Cavity Linings," Technical Report to Space and Missiles Systems Organization, Air Force Systems Command, Norton Air Force Base, on Contract No. FO 4701-69-C-0155.

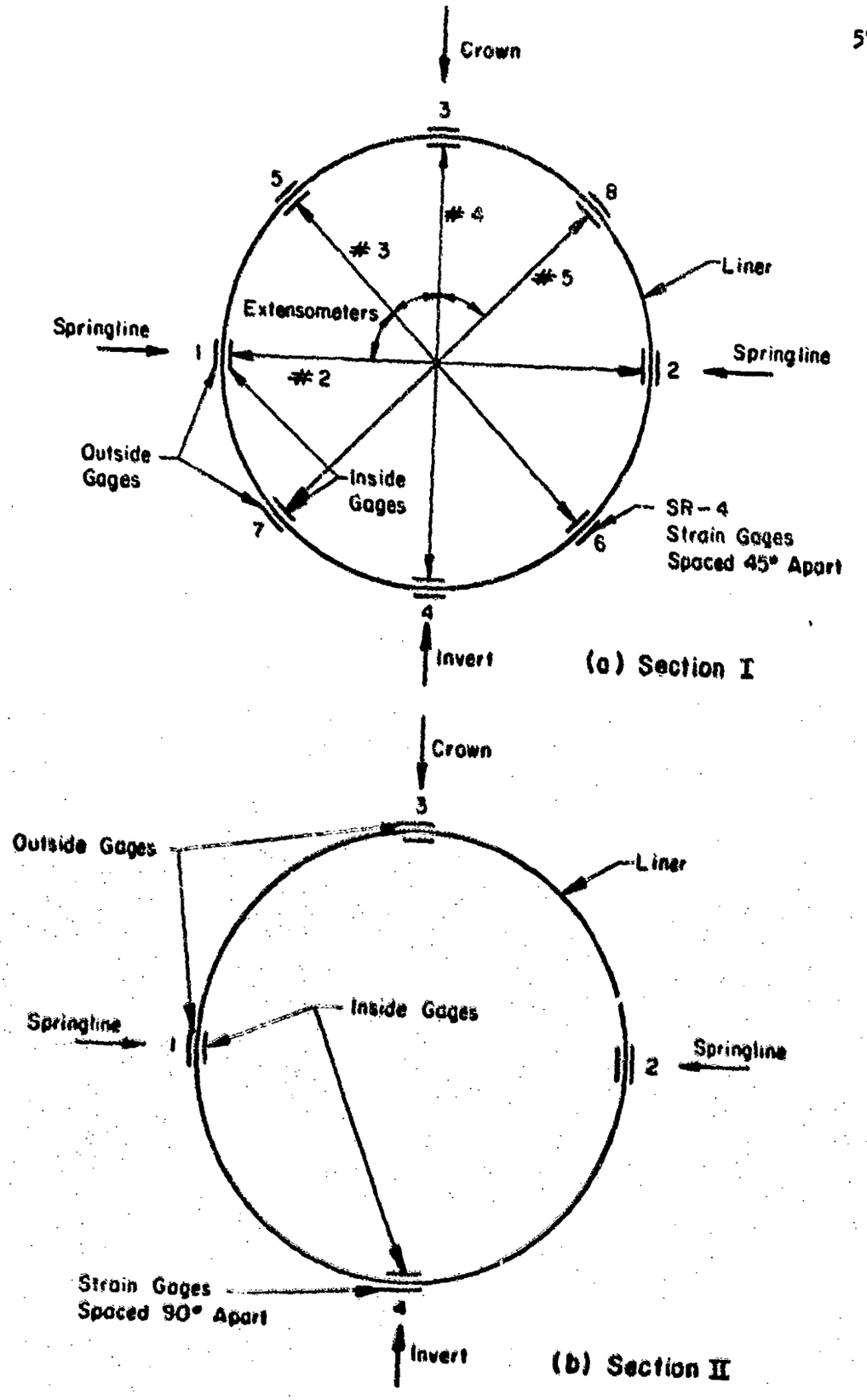

FIG. 1 LOCATION OF STRAIN GAGES AND DIAMETRICAL EXTENSOMETERS

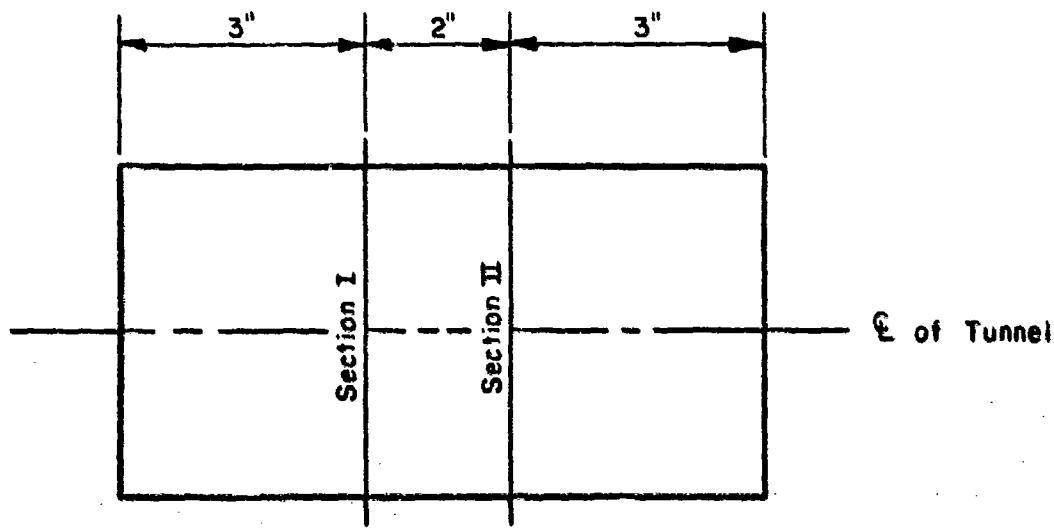

4" O.D. Steel Lined Tunnel, 8" Long

FIG. 2 LOCATION OF STRAIN GAGES AND DIAMETRICAL EXTENSOMETERS

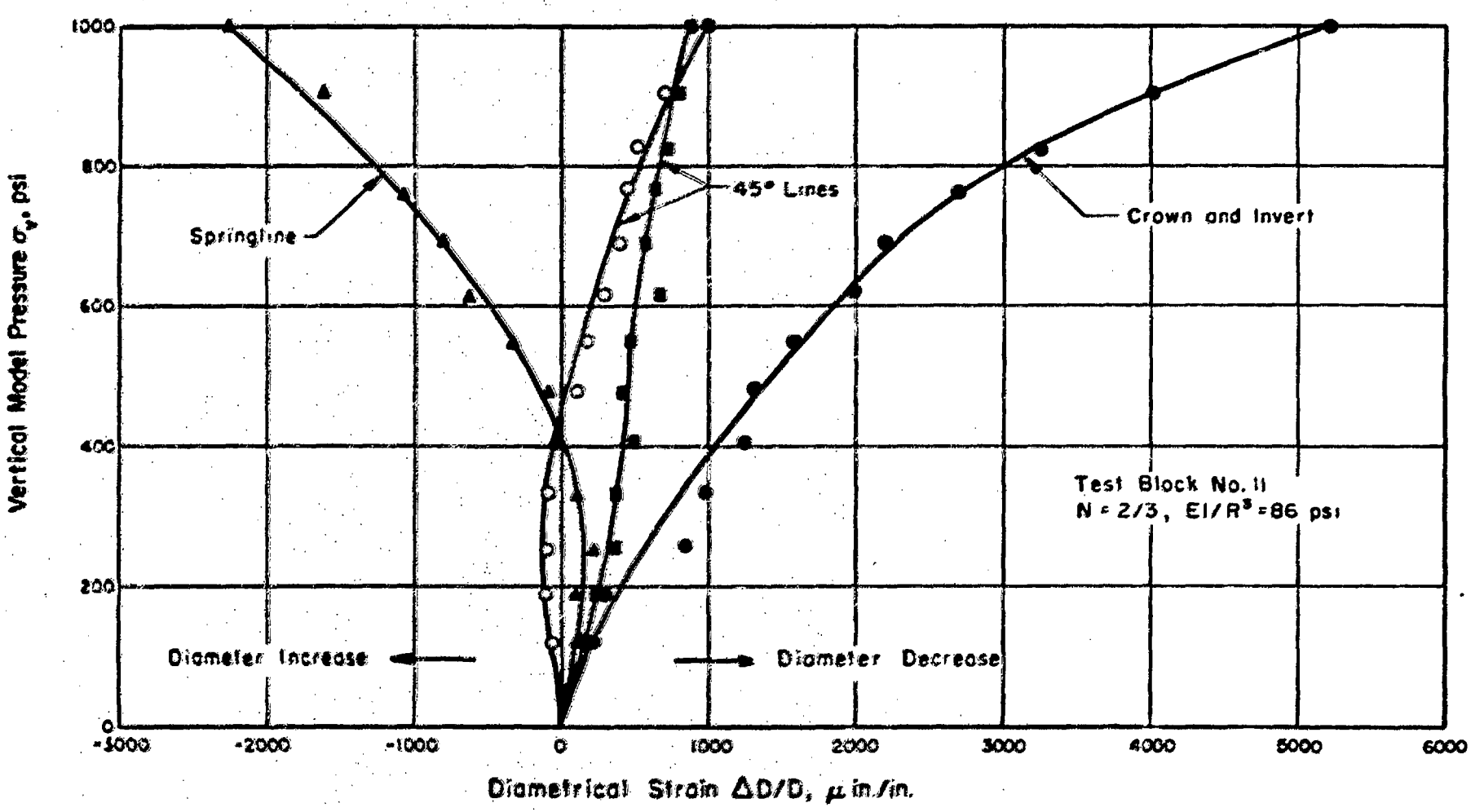

FIG. 3 DIAMETRICAL EXTENSOMETER DATA

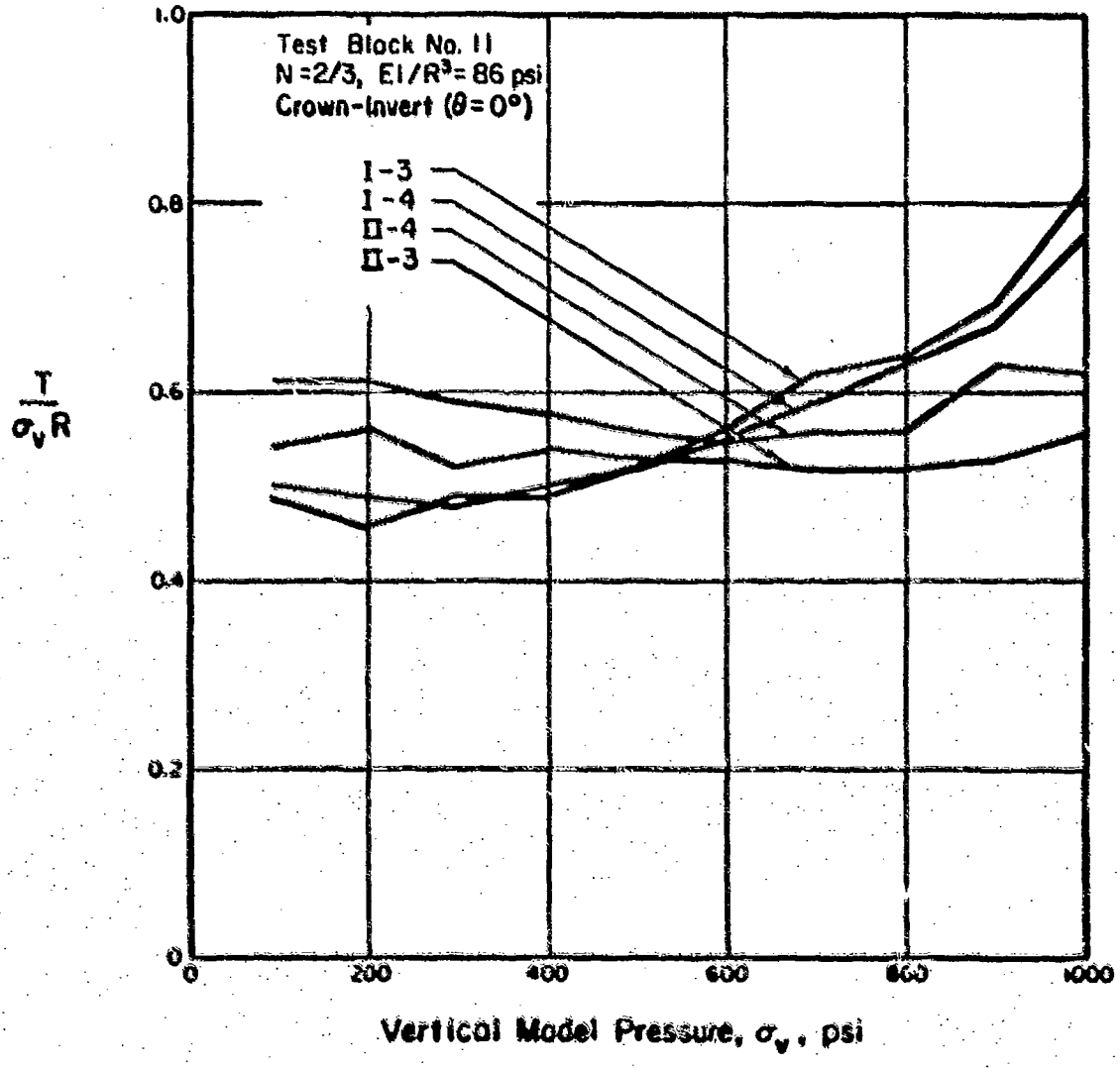

FIG. 4 PLOTS OF DIMENSIONLESS THRUST VERSUS VERTICAL MODEL PRESSURE

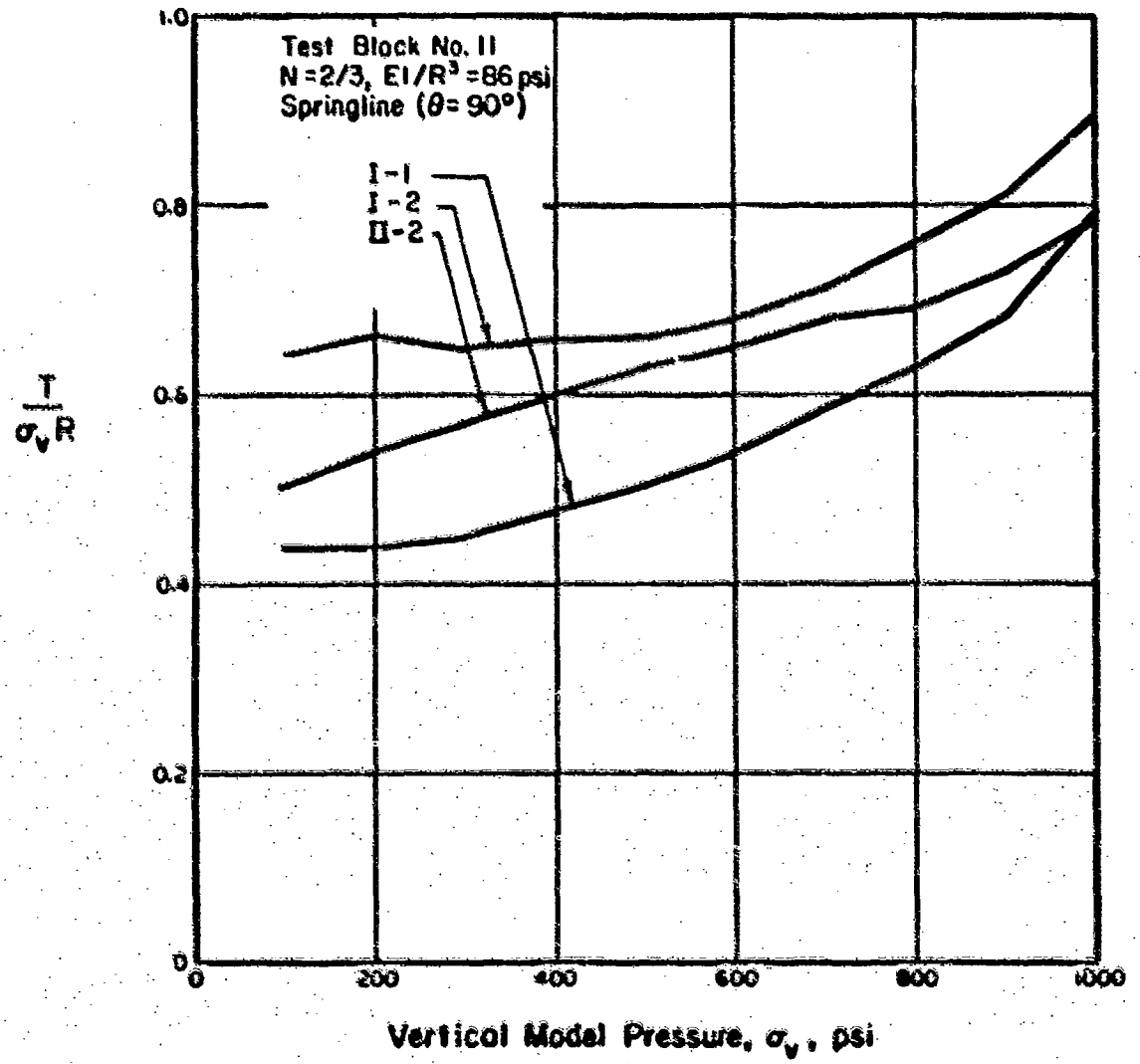

FIG. 5 PLOTS OF DIMENSIONLESS THRUST VERSUS VERTICAL MODEL PRESSURE

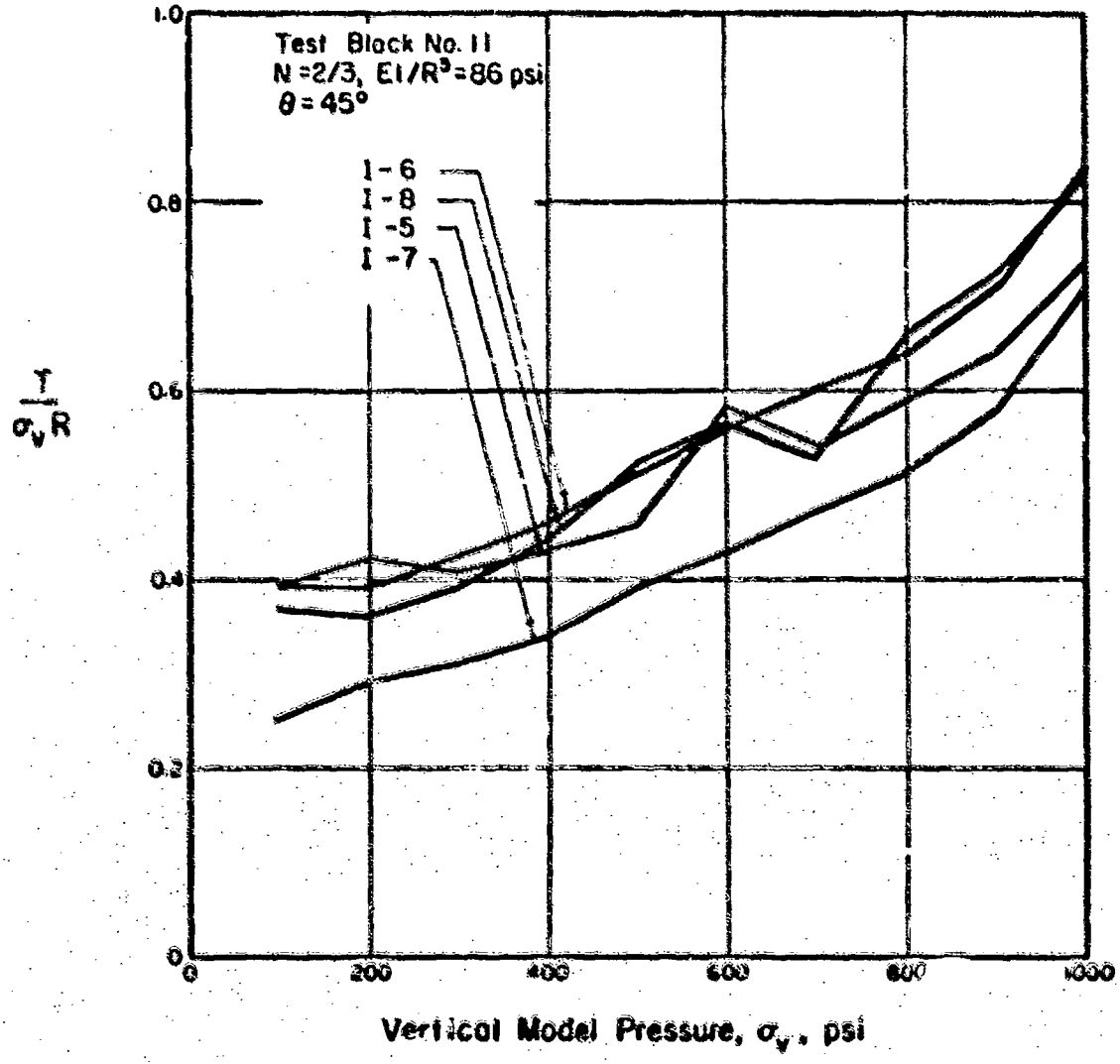

FIG. 6 PLOTS OF DIMENSIONLESS THRUST VERSUS VERTICAL MODEL PRESSURE

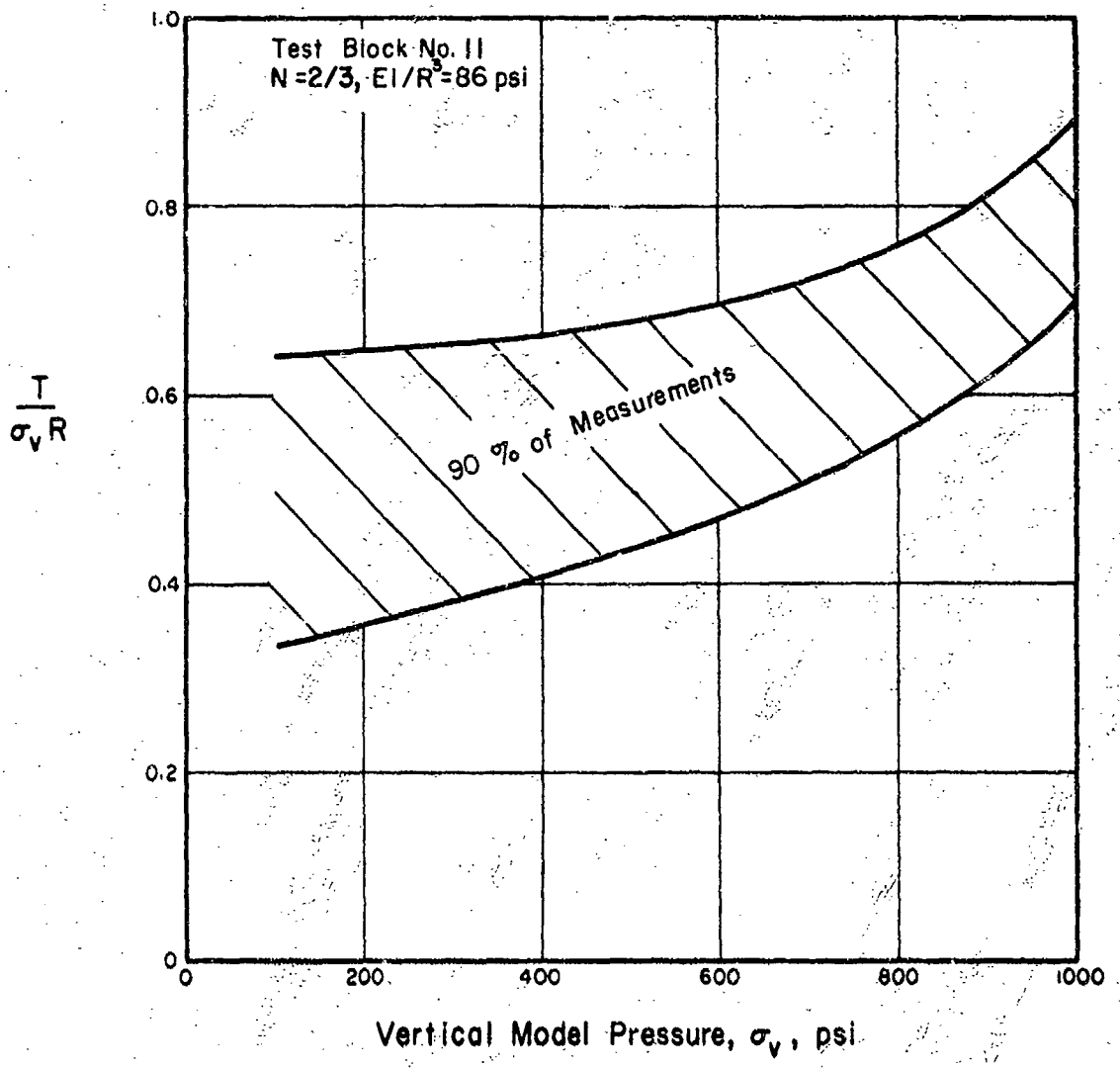

FIG. 7 PLOTS OF DIMENSIONLESS THRUST VERSUS VERTICAL MODEL PRESSURE

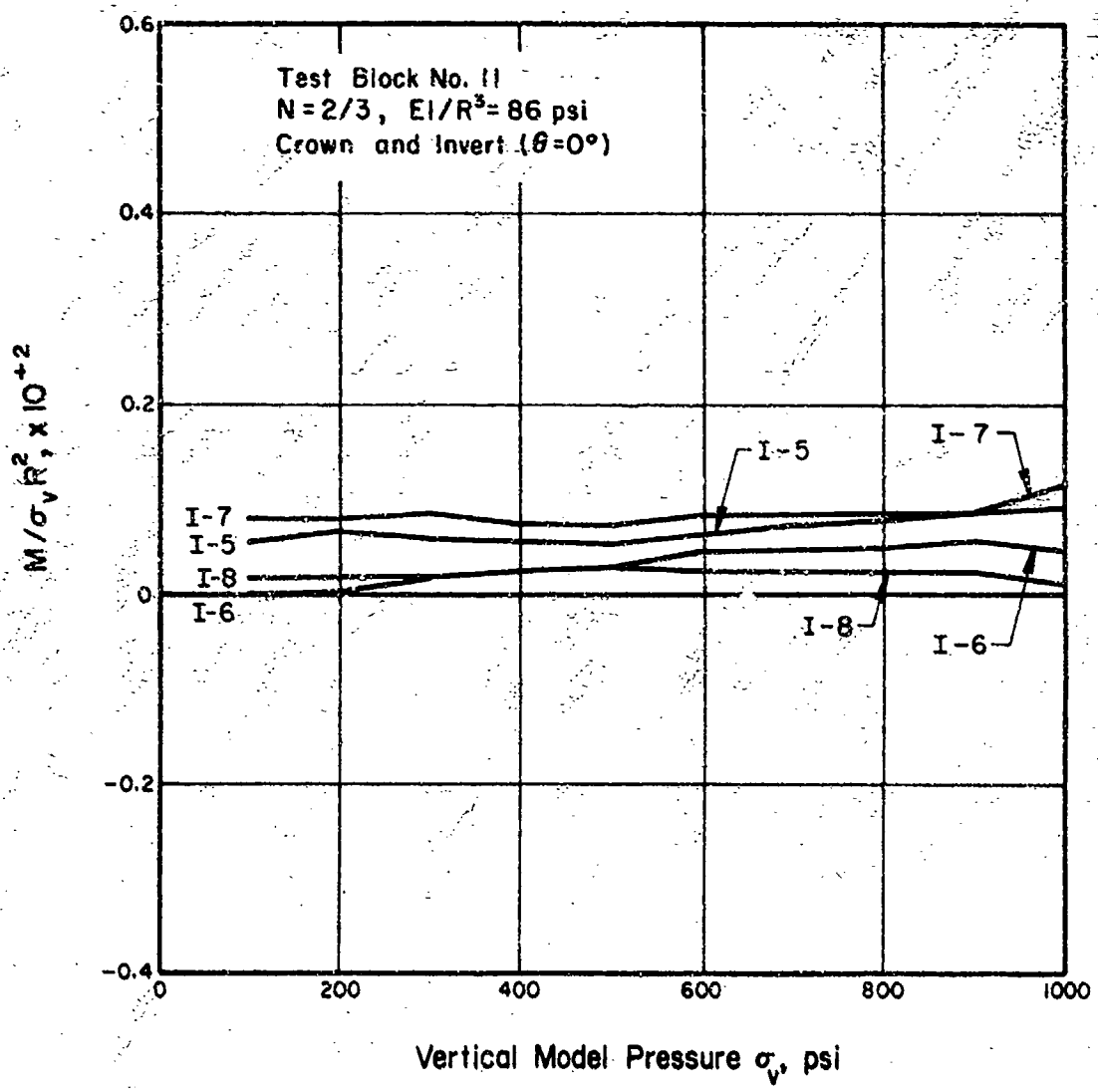

FIG. 8 PLOTS OF DIMENSIONLESS MOMENT VERSUS VERTICAL MODEL PRESSURE

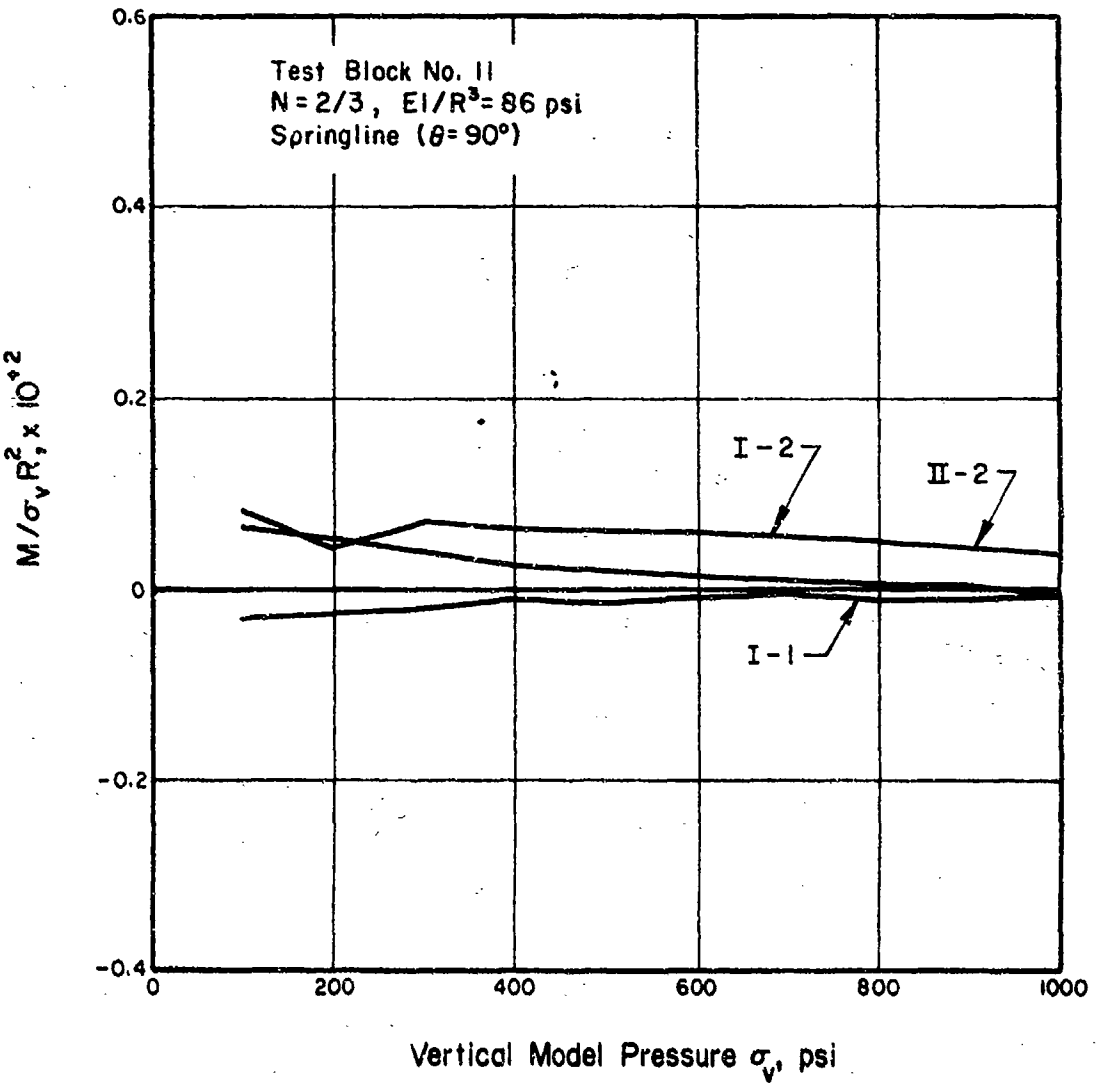

FIG. 9 PLOTS OF DIMENSIONLESS MOMENT VERSUS VERTICAL MODEL PRESSURE

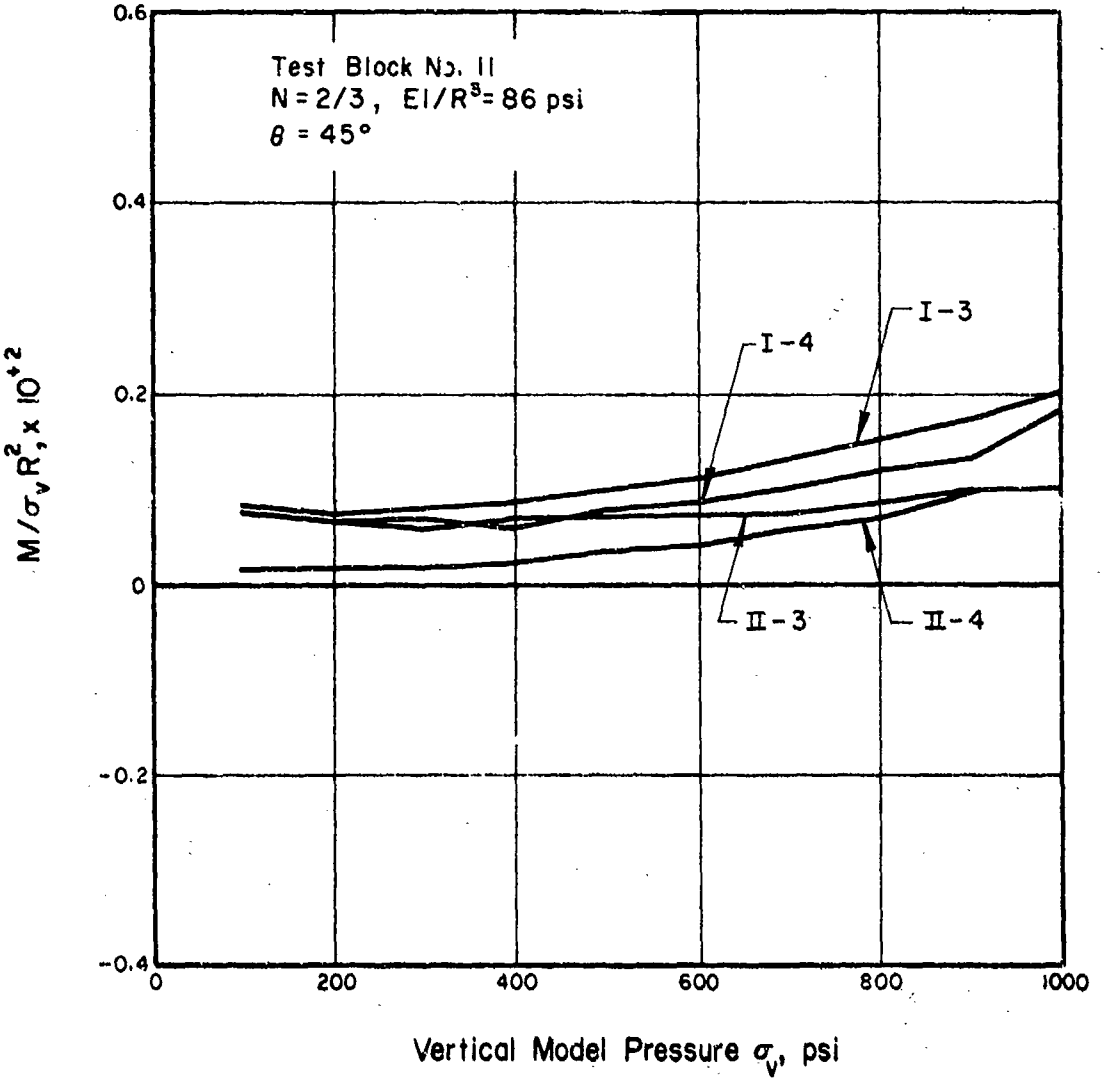

FIG. 10 PLOTS OF DIMENSIONLESS MOMENT VERSUS VERTICAL MODEL PRESSURE

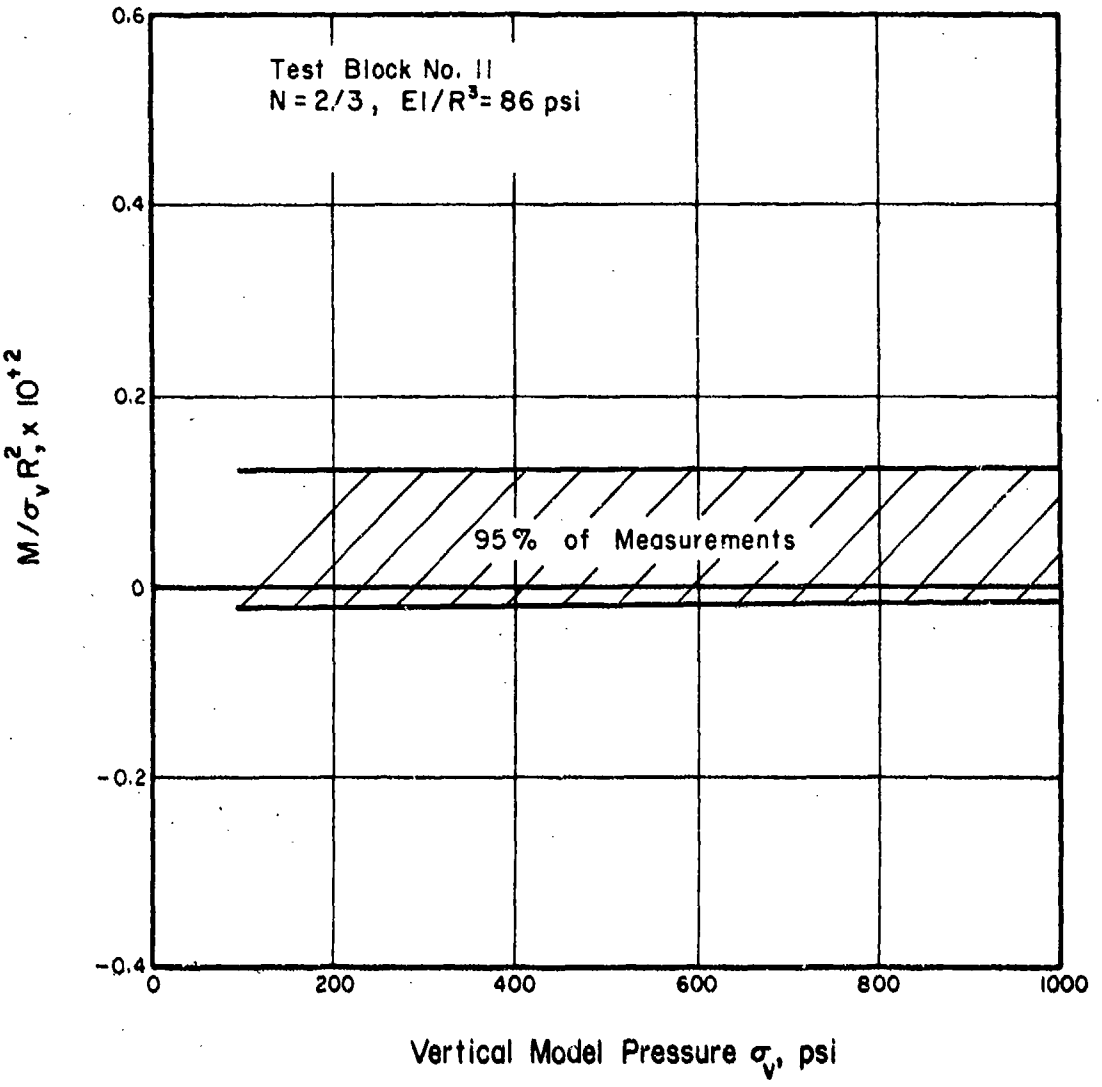

FIG. 11 PLOTS OF DIMENSIONLESS MOMENT VERSUS VERTICAL MODEL PRESSURE

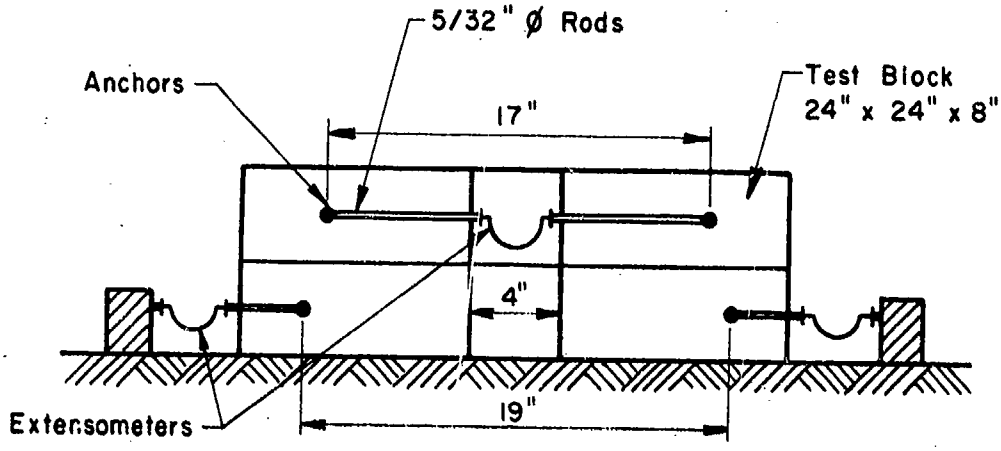

FIG. 12 MEASUREMENT OF FREE FIELD STRAIN

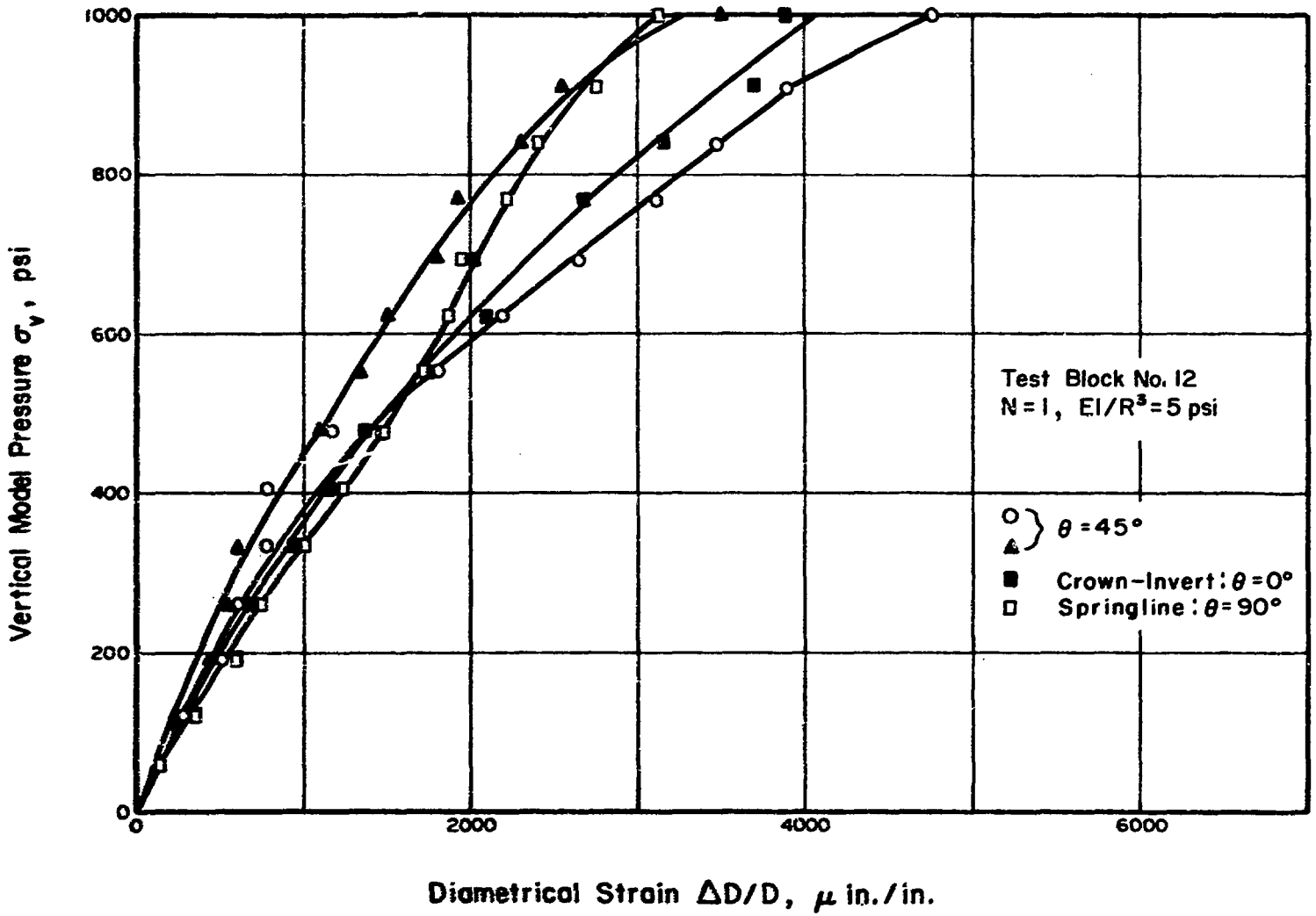

FIG. 13 DIAMETRICAL EXTENSOMETER DATA

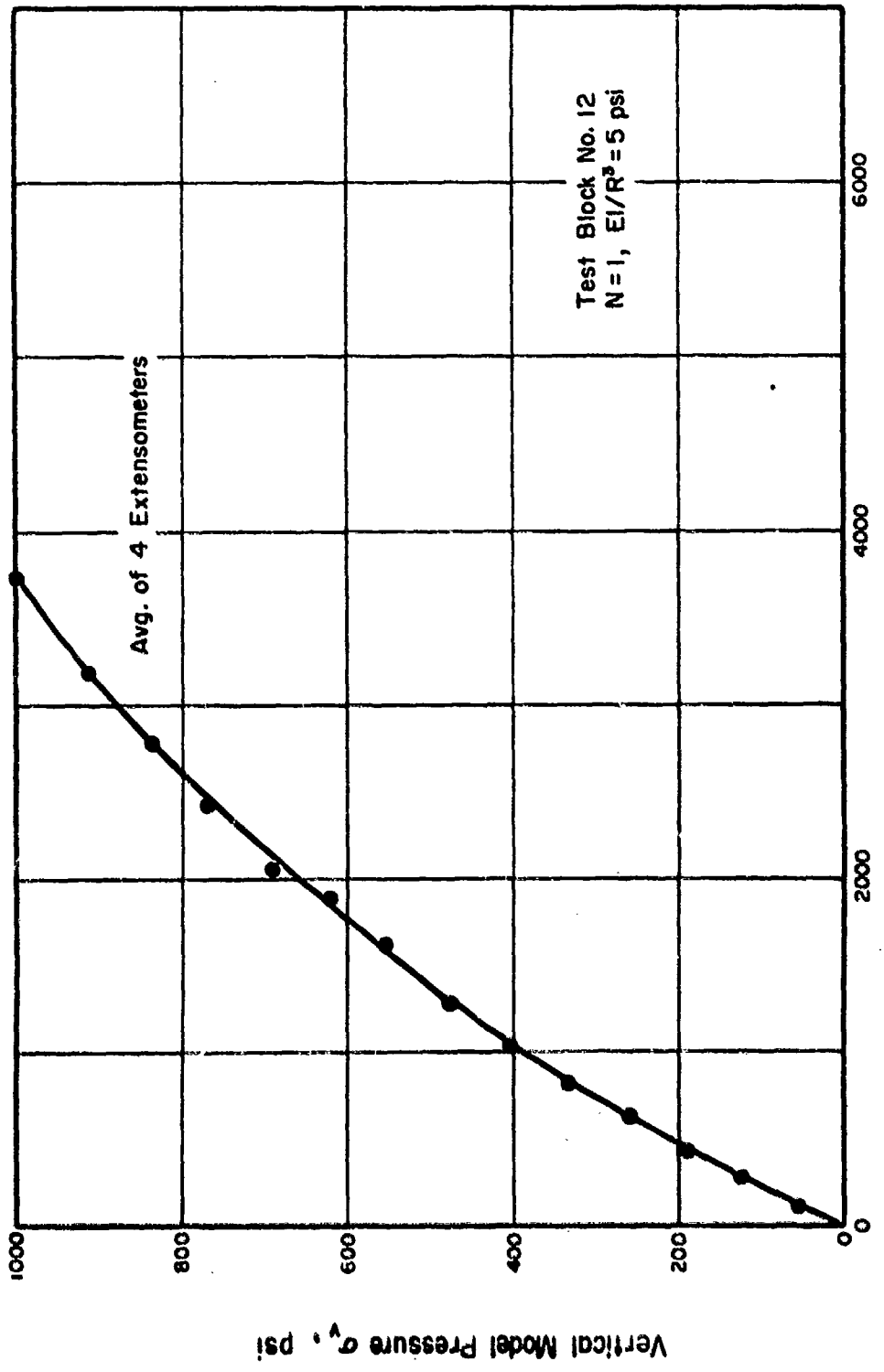

FIG. 14 DIAMETRICAL EXTENSOMETER DATA

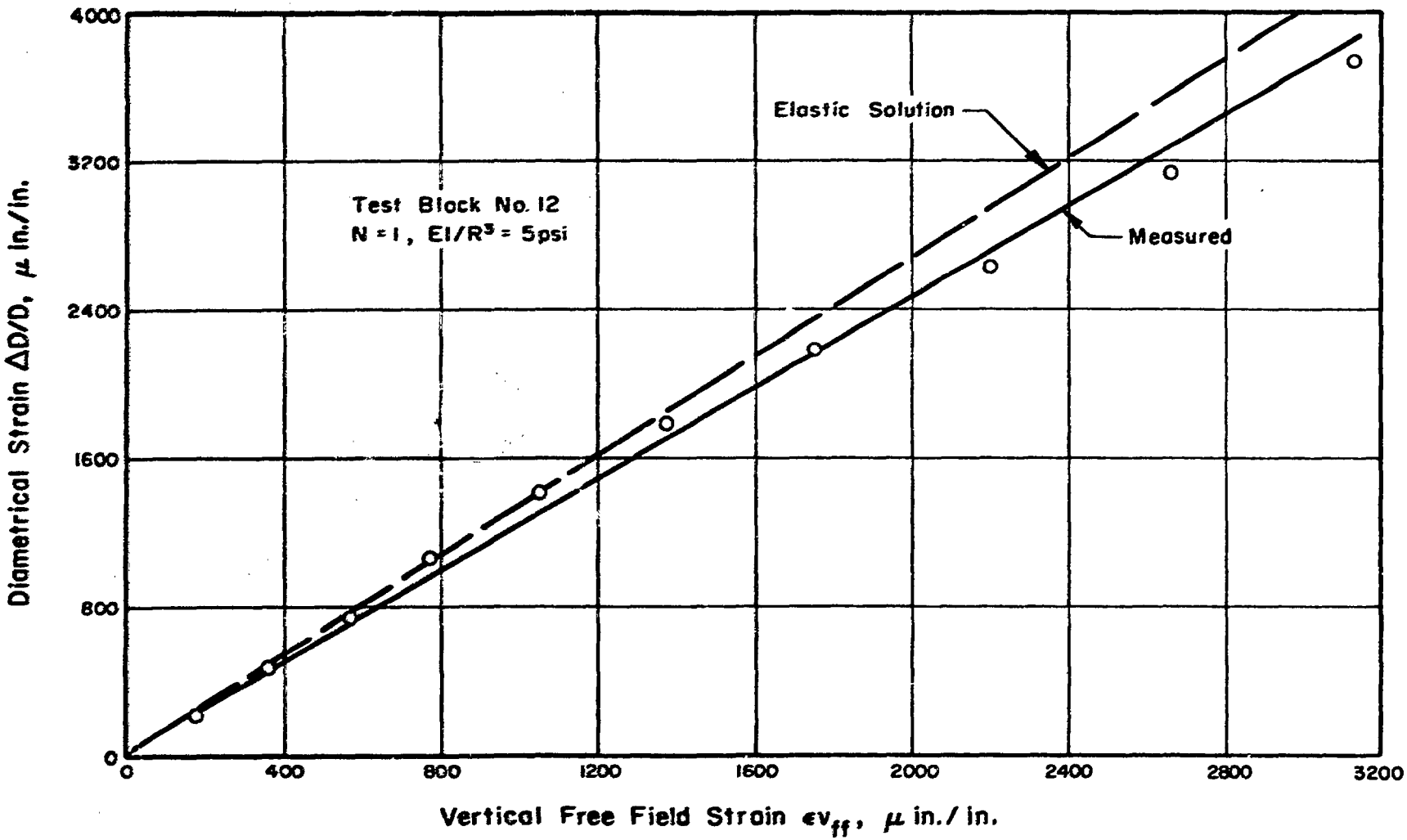

FIG. 15 DIAMETRICAL STRAIN OF LINER AS A FUNCTION OF VERTICAL FREE FIELD STRAIN

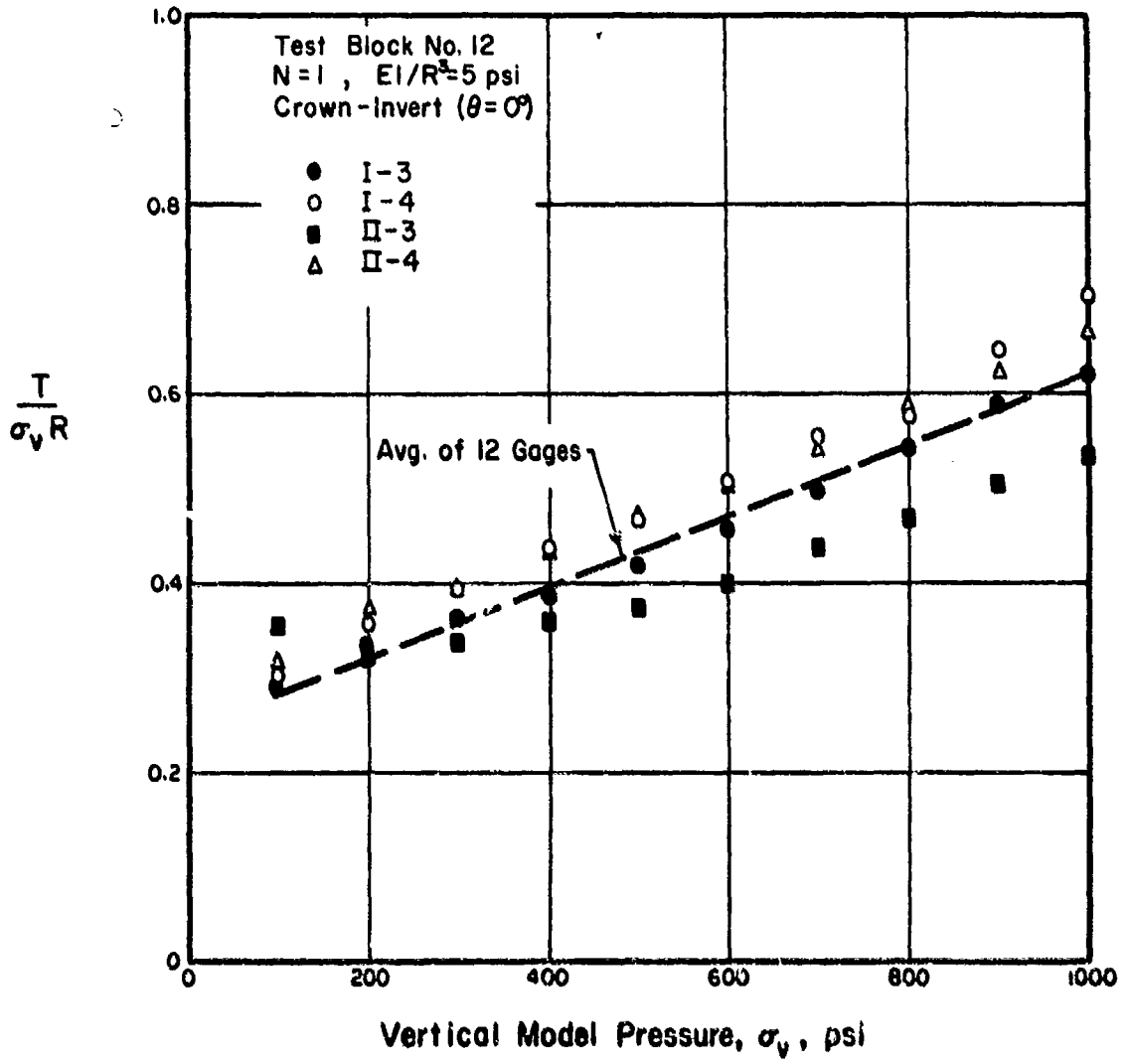

FIG. 16 PLOTS OF DIMENSIONLESS THRUST VERSUS VERTICAL MODEL PRESSURE

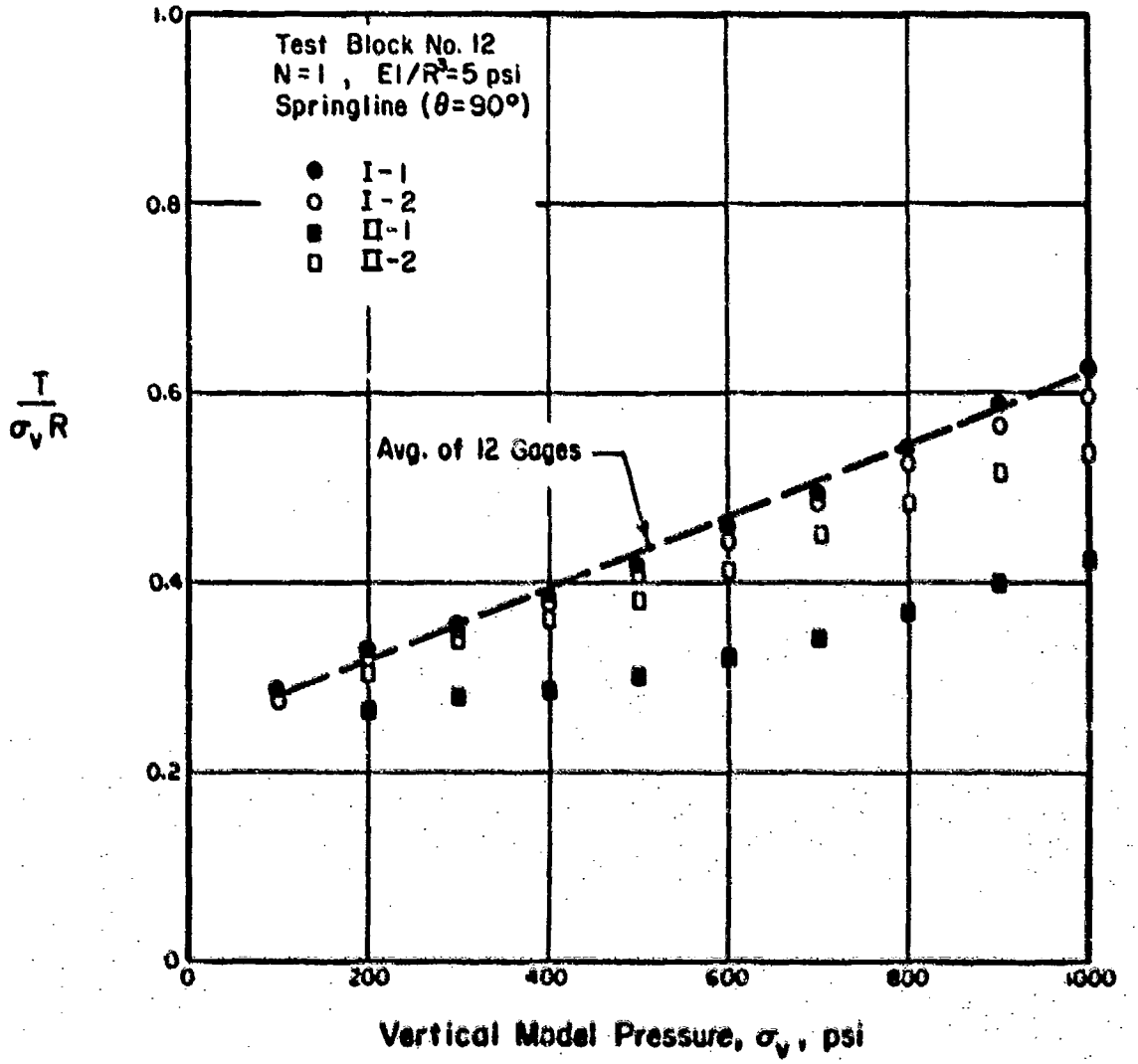

FIG. 17 PLOTS OF DIMENSIONLESS THRUST VERSUS VERTICAL MODEL PRESSURE

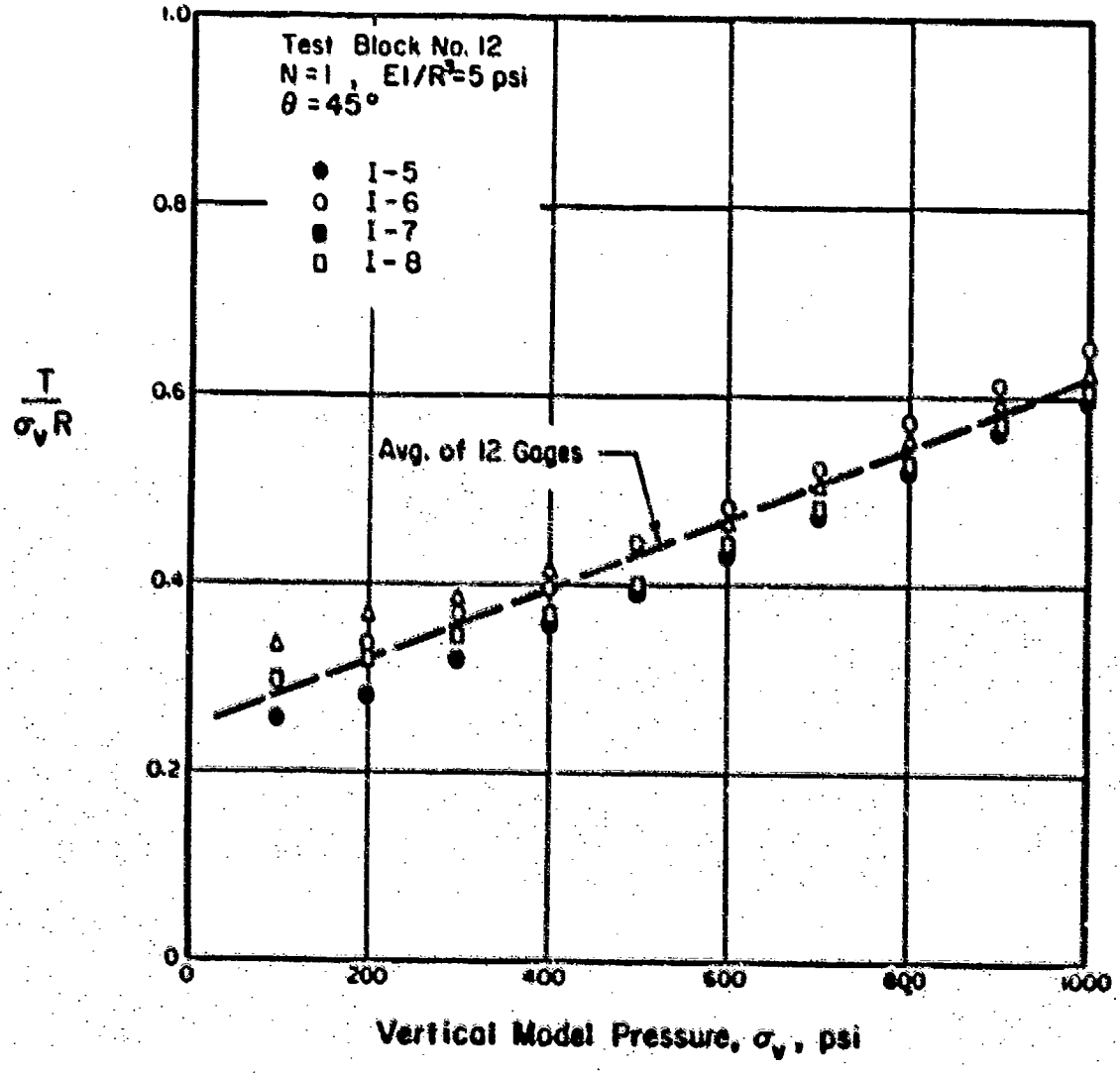

FIG. 18 PLOTS OF DIMENSIONLESS THRUST VERSUS VERTICAL MODEL PRESSURE

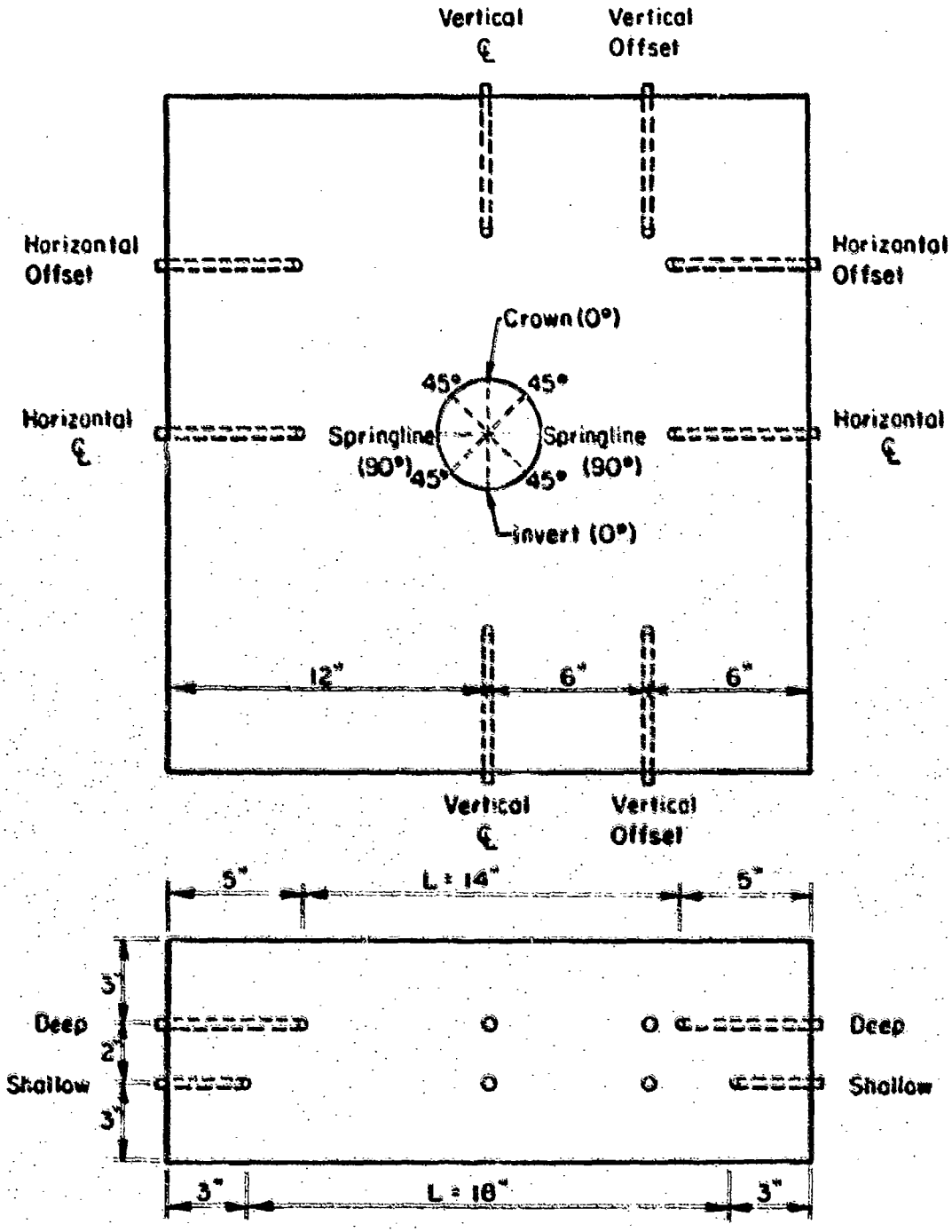

FIG. 19 LOCATIONS OF EXTENSOMETERS IN JOINTED TEST BLOCKS

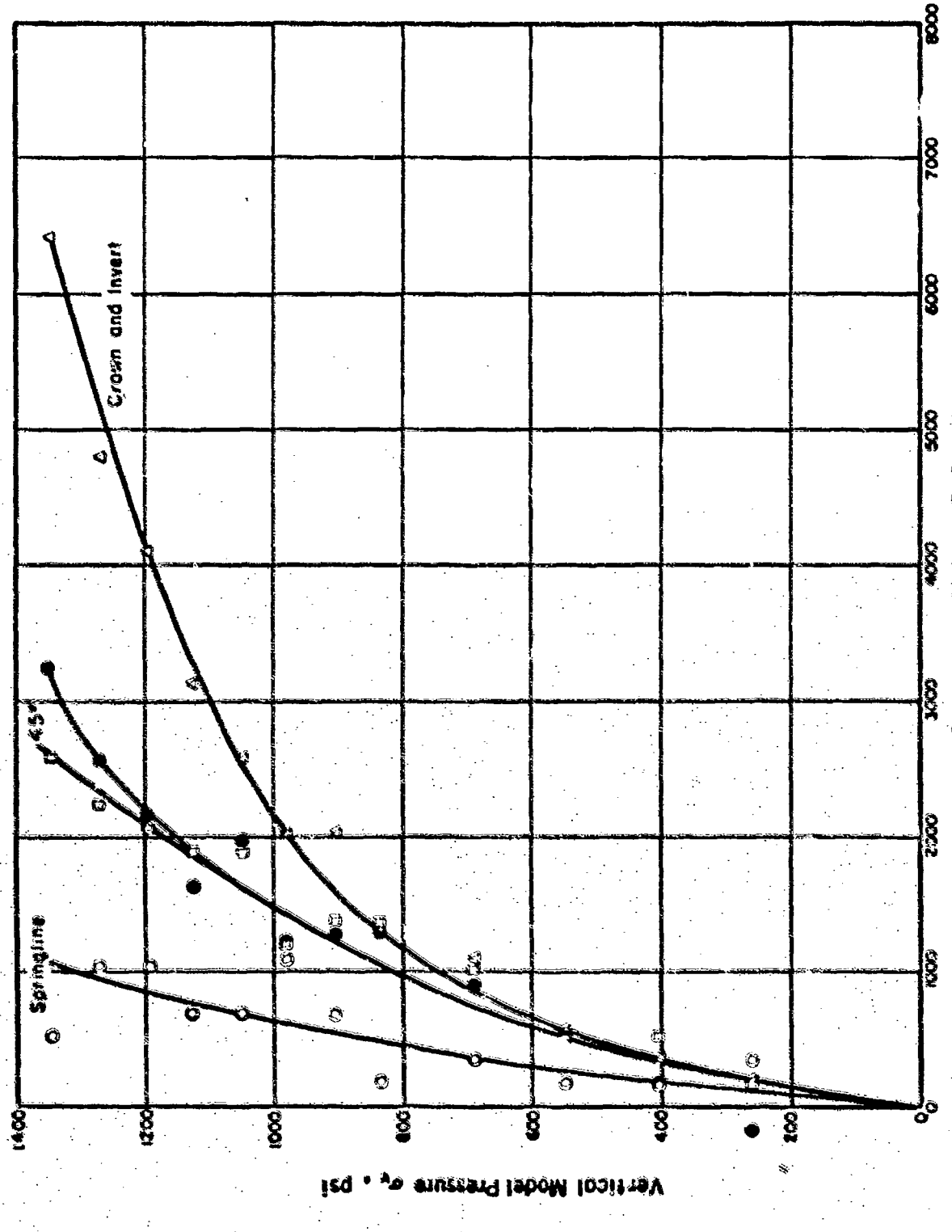

FIG. 20 DIAMETRICAL STRAIN OF TUNNEL LINER AS A FUNCTION OF VERTICAL MODEL PRESSURE FOR TEST BLOCK NO. 13

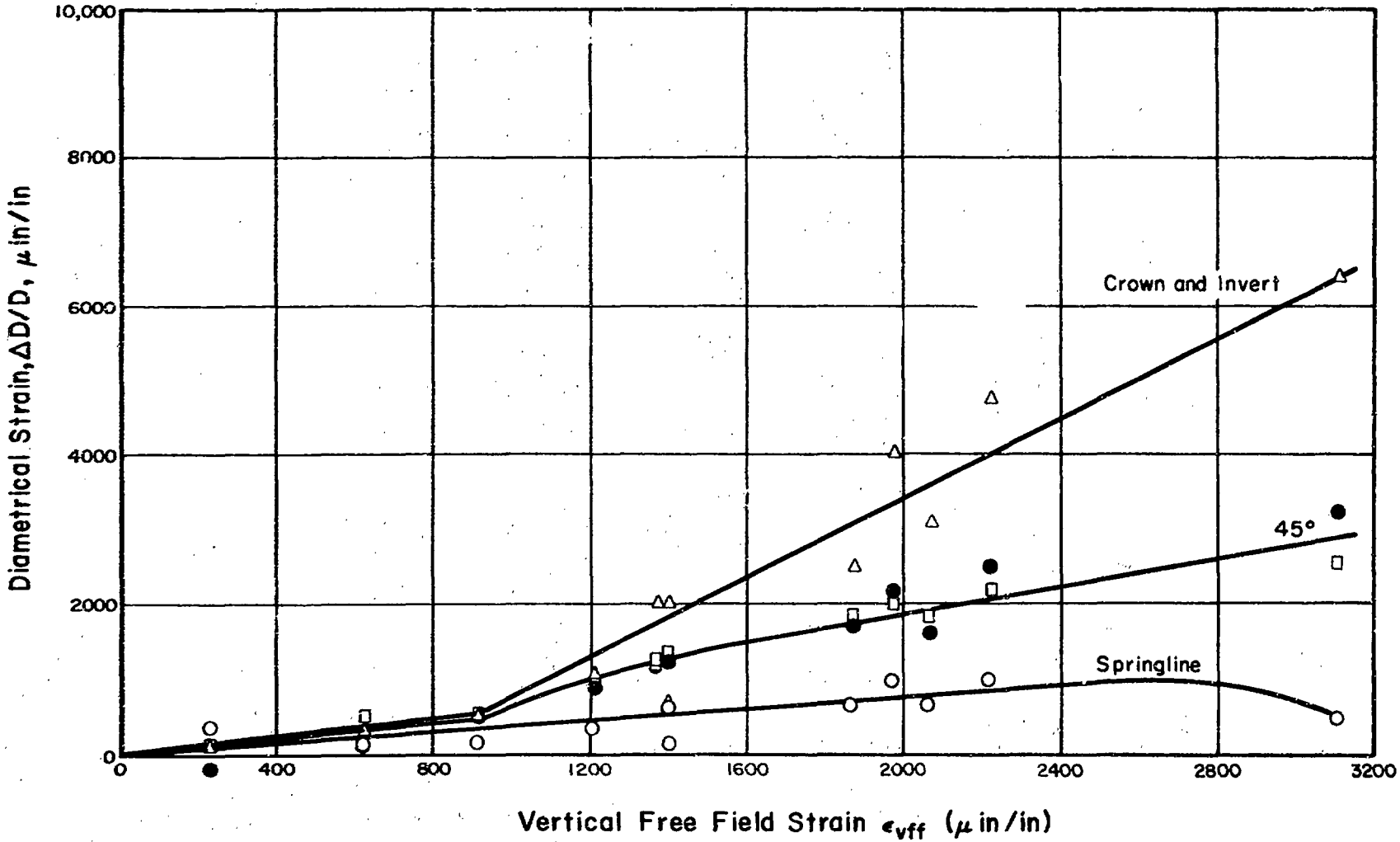

FIG. 21 DIAMETRICAL STRAIN OF TUNNEL LINER AS A FUNCTION OF FREE-FIELD STRAIN FOR TEST BLOCK NO. 13

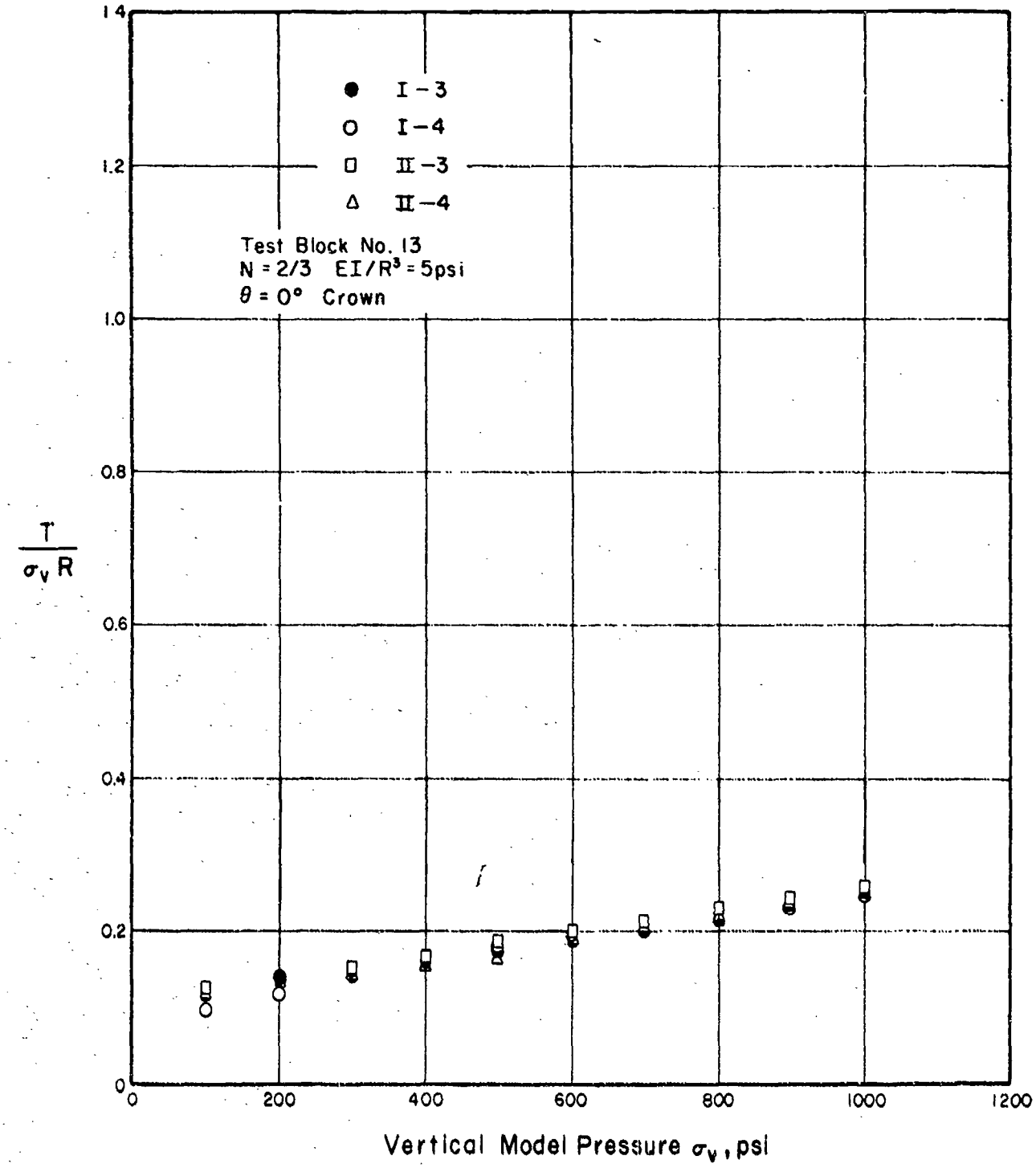

FIG. 22 PLOTS OF DIMENSIONLESS THRUST VERSUS VERTICAL MODEL PRESSURE

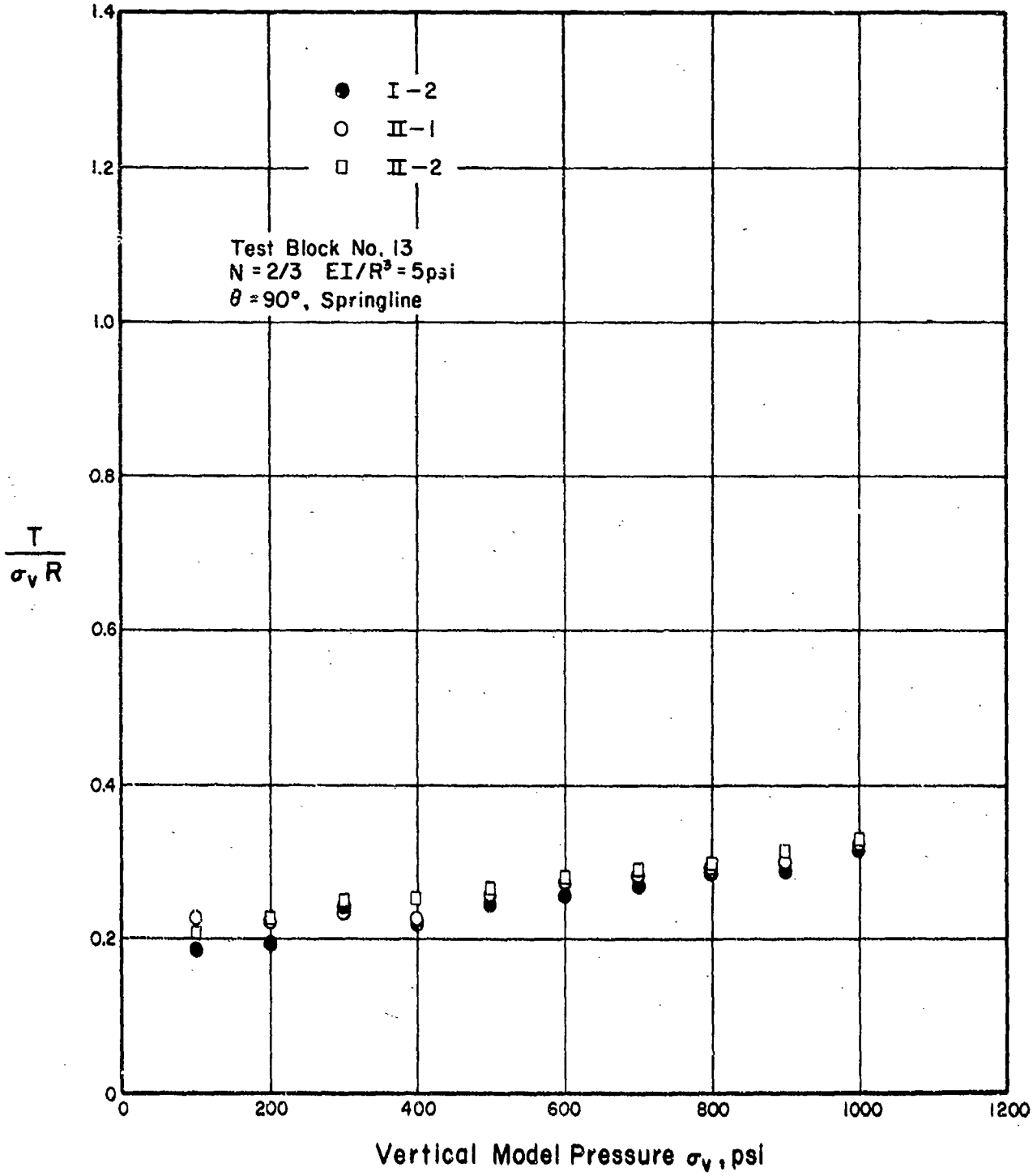

FIG. 23 PLOTS OF DIMENSIONLESS THRUST VERSUS VERTICAL MODEL PRESSURE

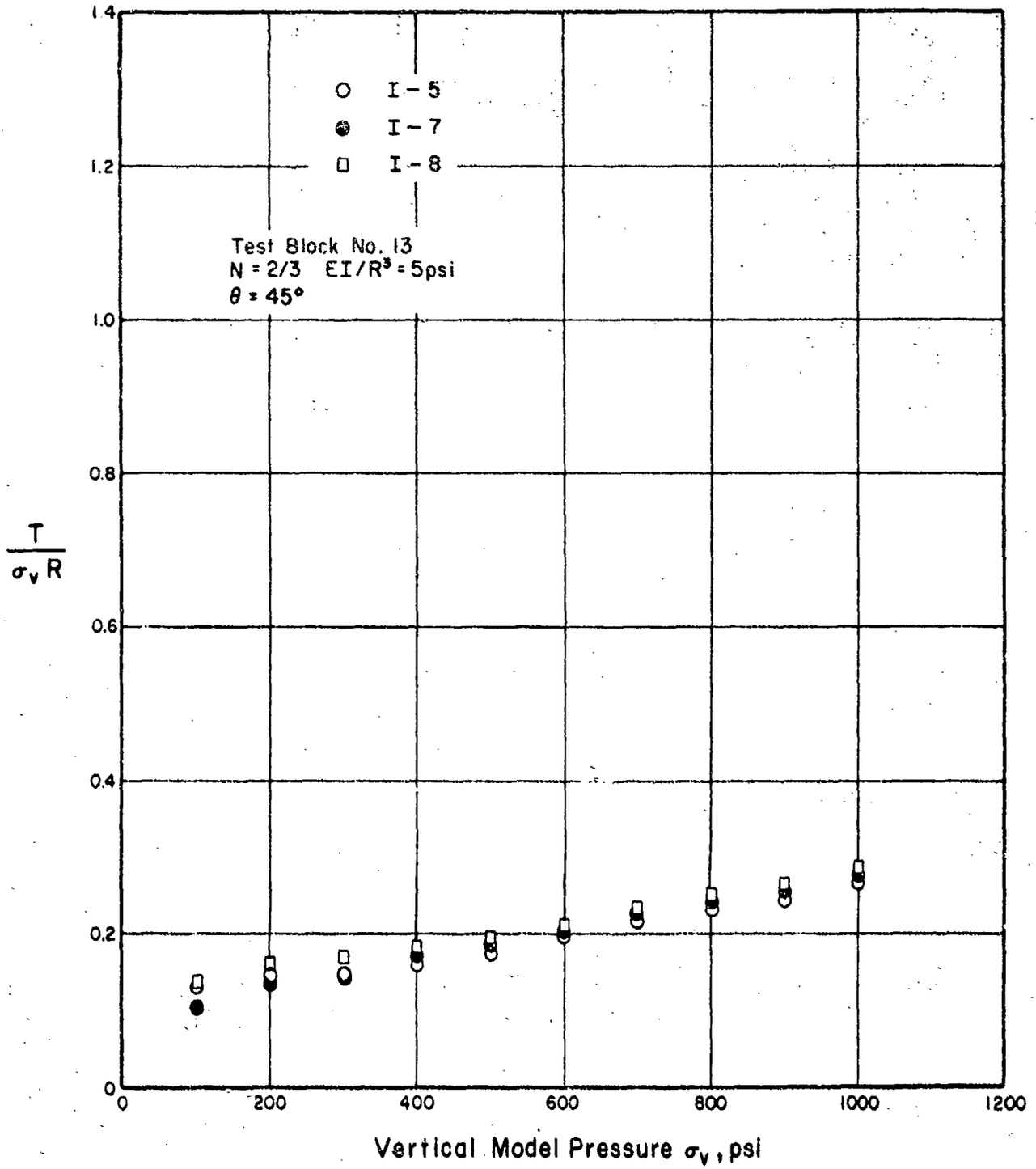

FIG. 24 PLOTS OF DIMENSIONLESS THRUST VERSUS VERTICAL MODEL PRESSURE

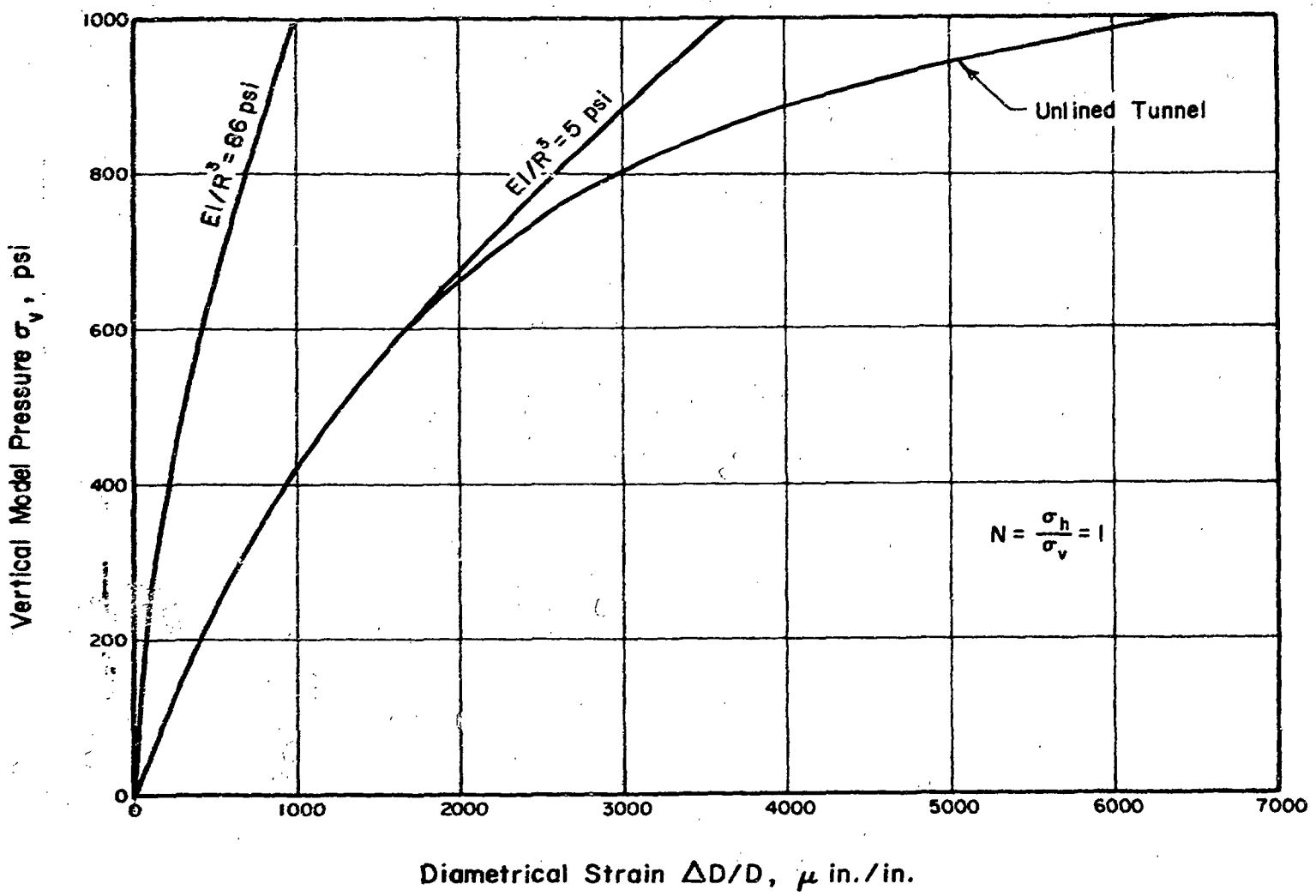

FIG. 25 COMPARISON OF DIAMETRICAL STRAINS FOR DIFFERENT VALUES OF LINER STIFFNESS

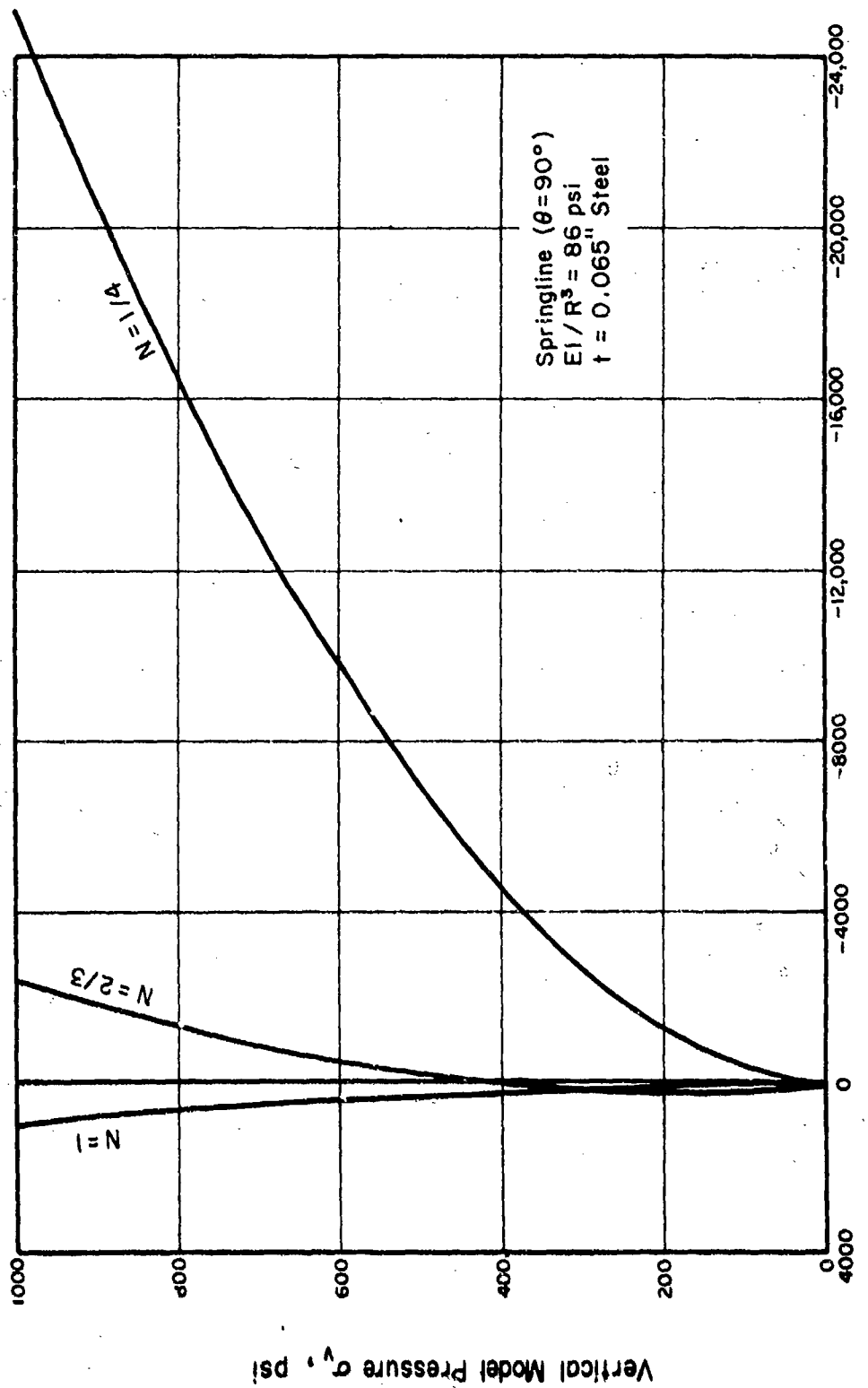

FIG. 26 COMPARISON OF DIAMETRICAL STRAIN AT SPRINGLINE FOR DIFFERENT VALUES OF N

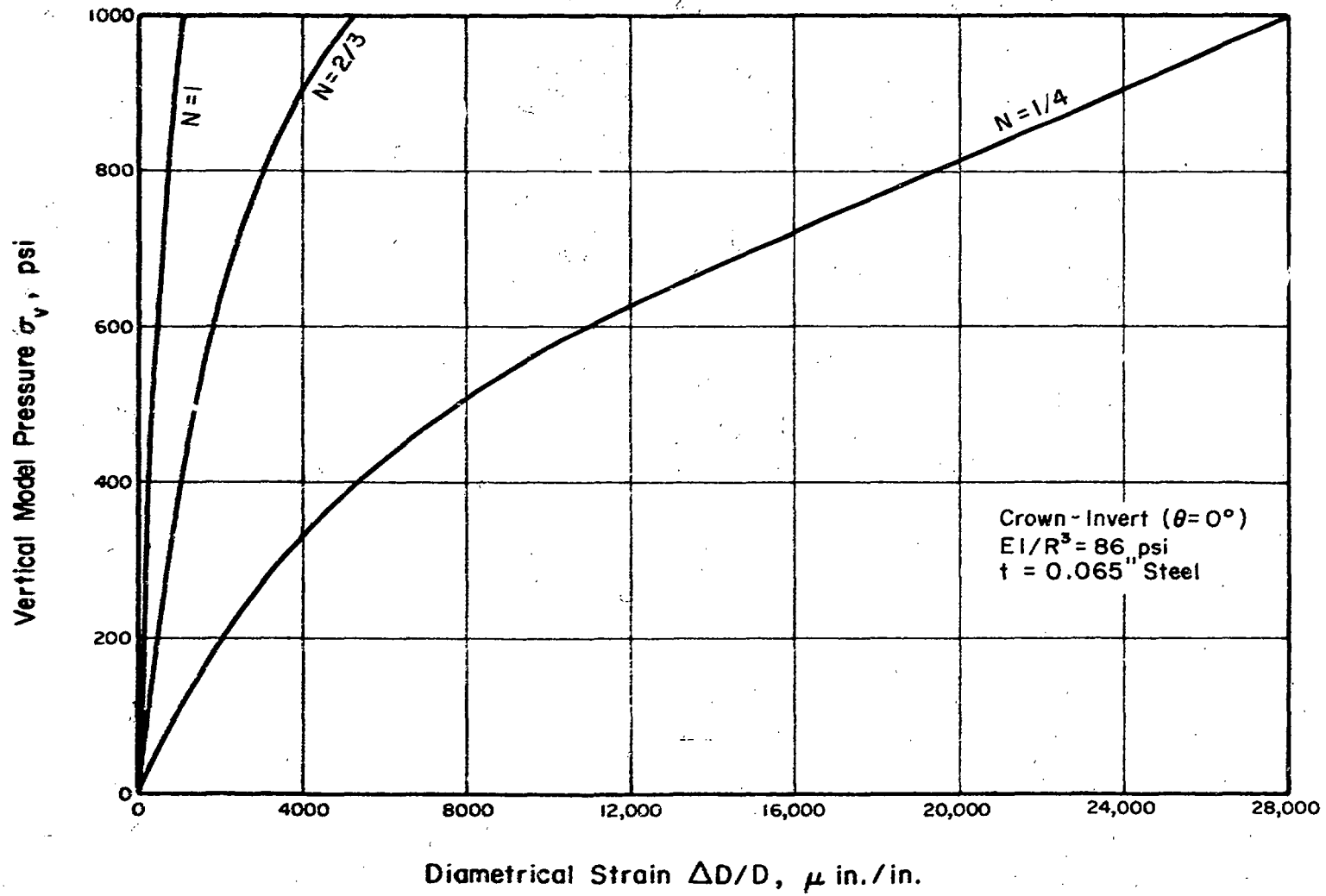

FIG. 27 COMPARISON OF DIAMETRICAL STRAIN AT CROWN-INVERT FOR DIFFERENT VALUES OF N

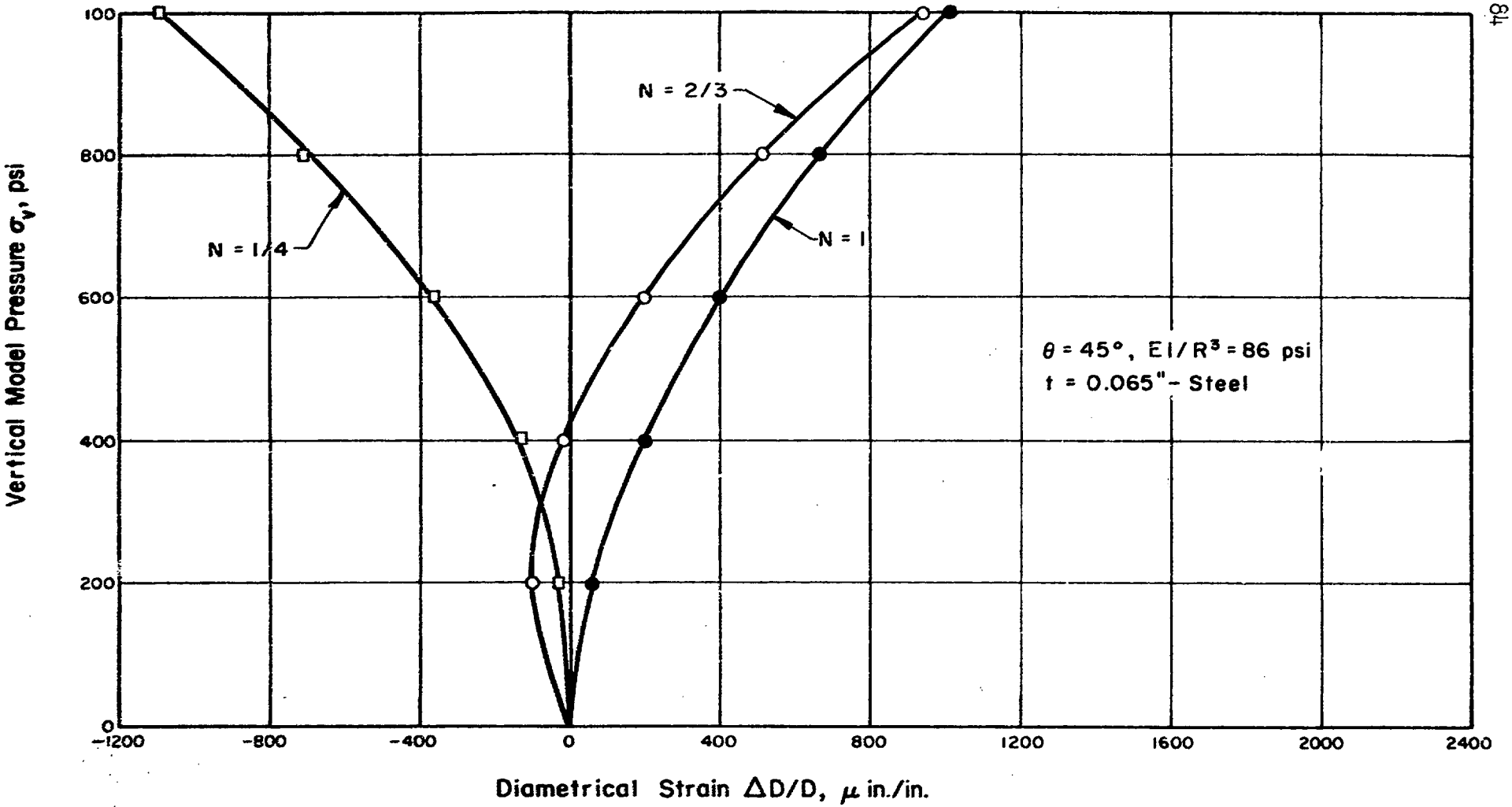

FIG. 28 COMPARISON OF DIAMETRICAL STRAIN AT 45° SECTIONS FOR DIFFERENT VALUES OF N

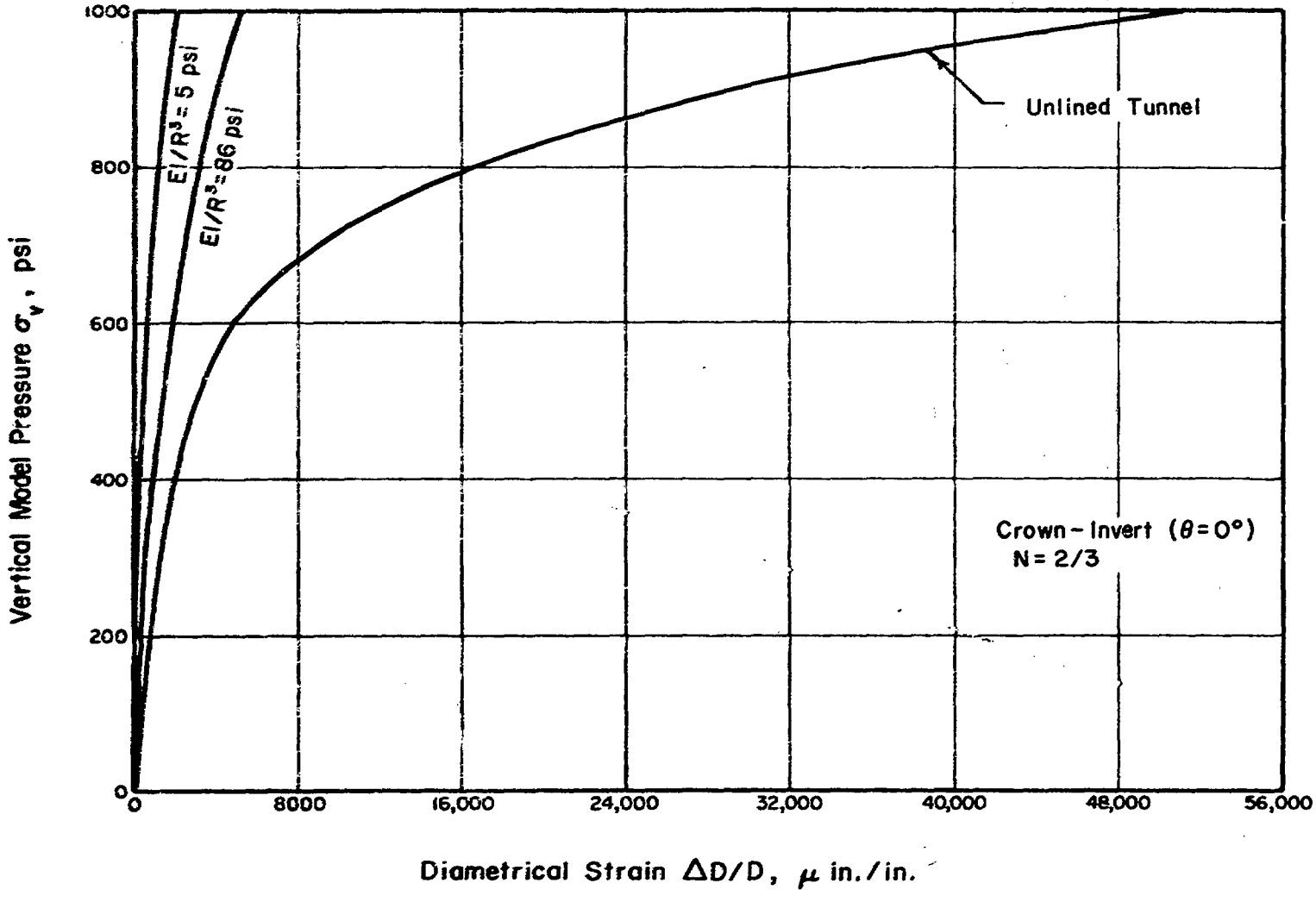

FIG. 29 COMPARISON OF DIAMETRICAL STRAINS AT CROWN-INVERT FOR DIFFERENT VALUES OF LINER STIFFNESS

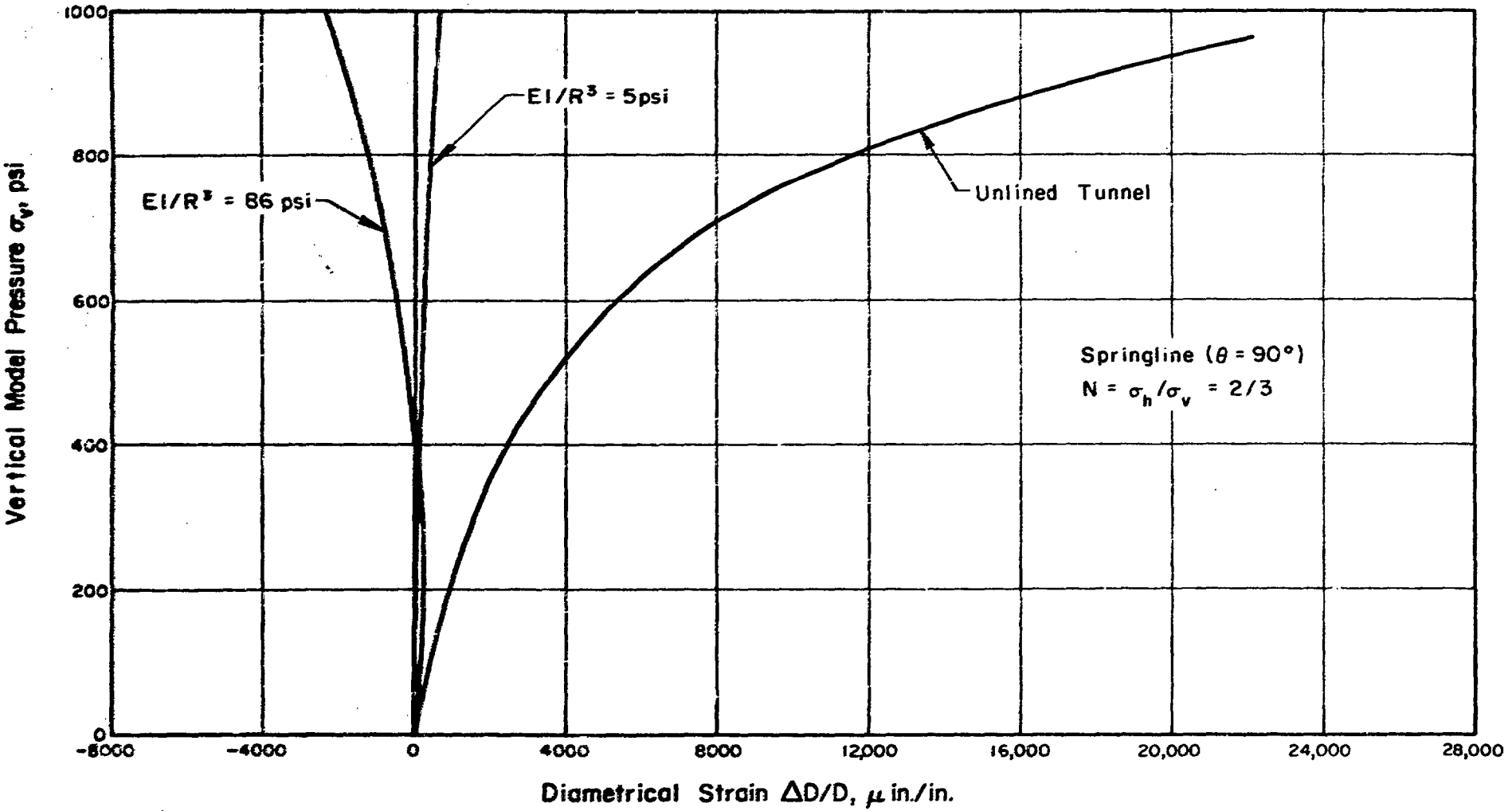

FIG. 30 COMPARISON OF DIAMETRICAL STRAINS AT SPRINGLINE FOR DIFFERENT VALUES OF LINER STIFFNESS

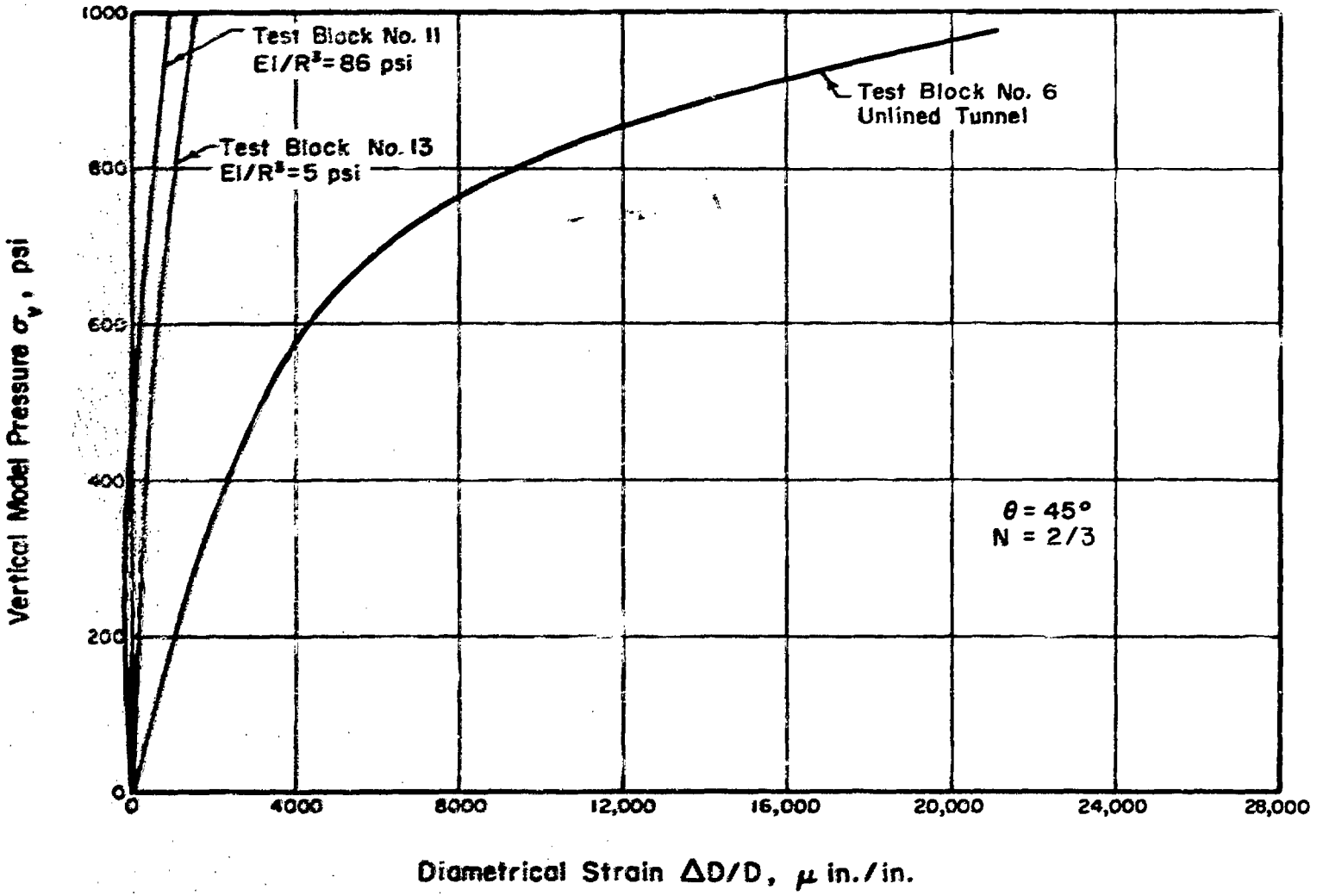

FIG. 31 COMPARISON OF DIAMETRICAL STRAINS AT $\theta = 45°$ FOR DIFFERENT VALUES OF LINER STIFFNESS

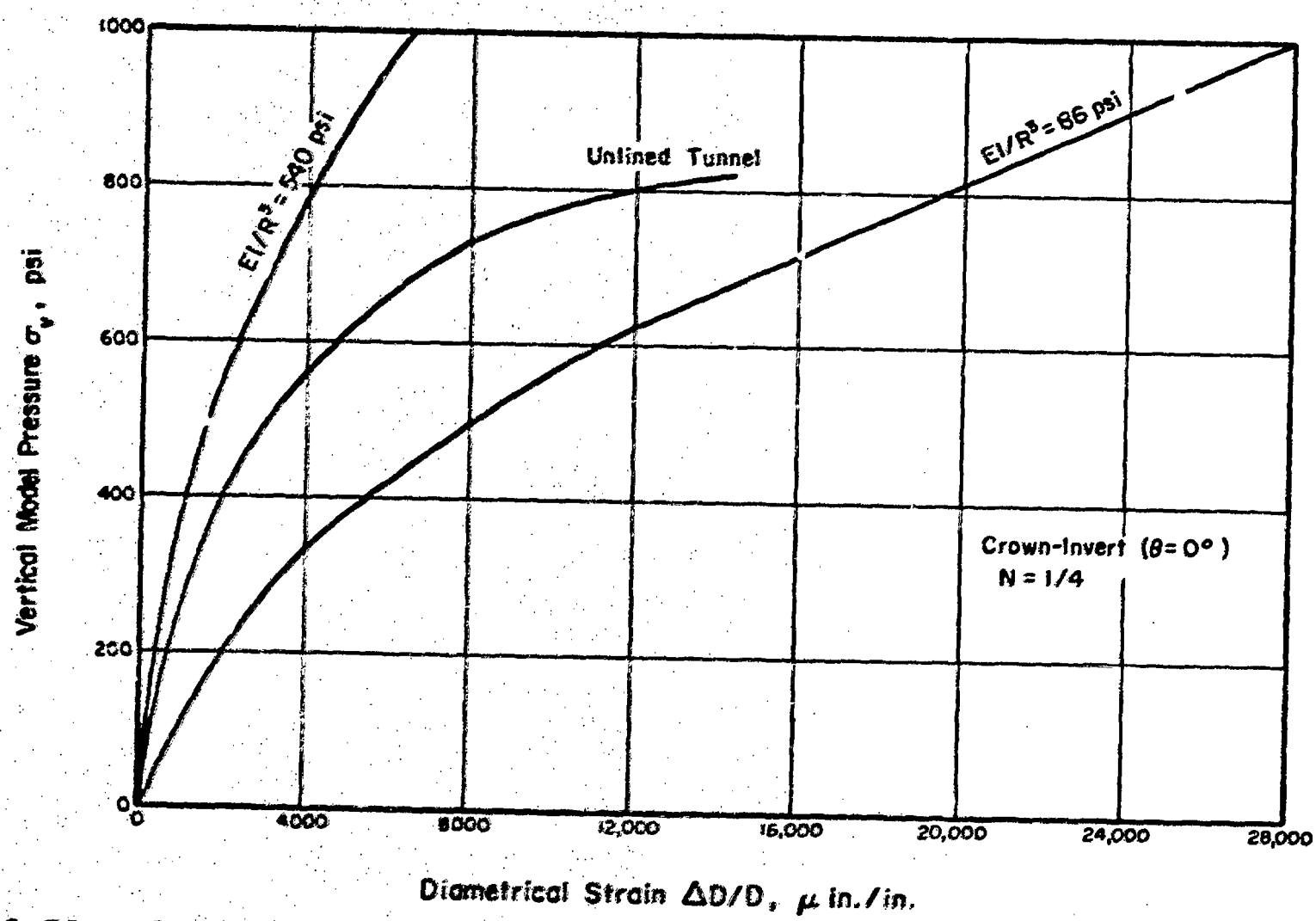

FIG. 32 COMPARISON OF DIAMETRICAL STRAINS AT CROWN-INVERT FOR DIFFERENT VALUES OF LINER STIFFNESS

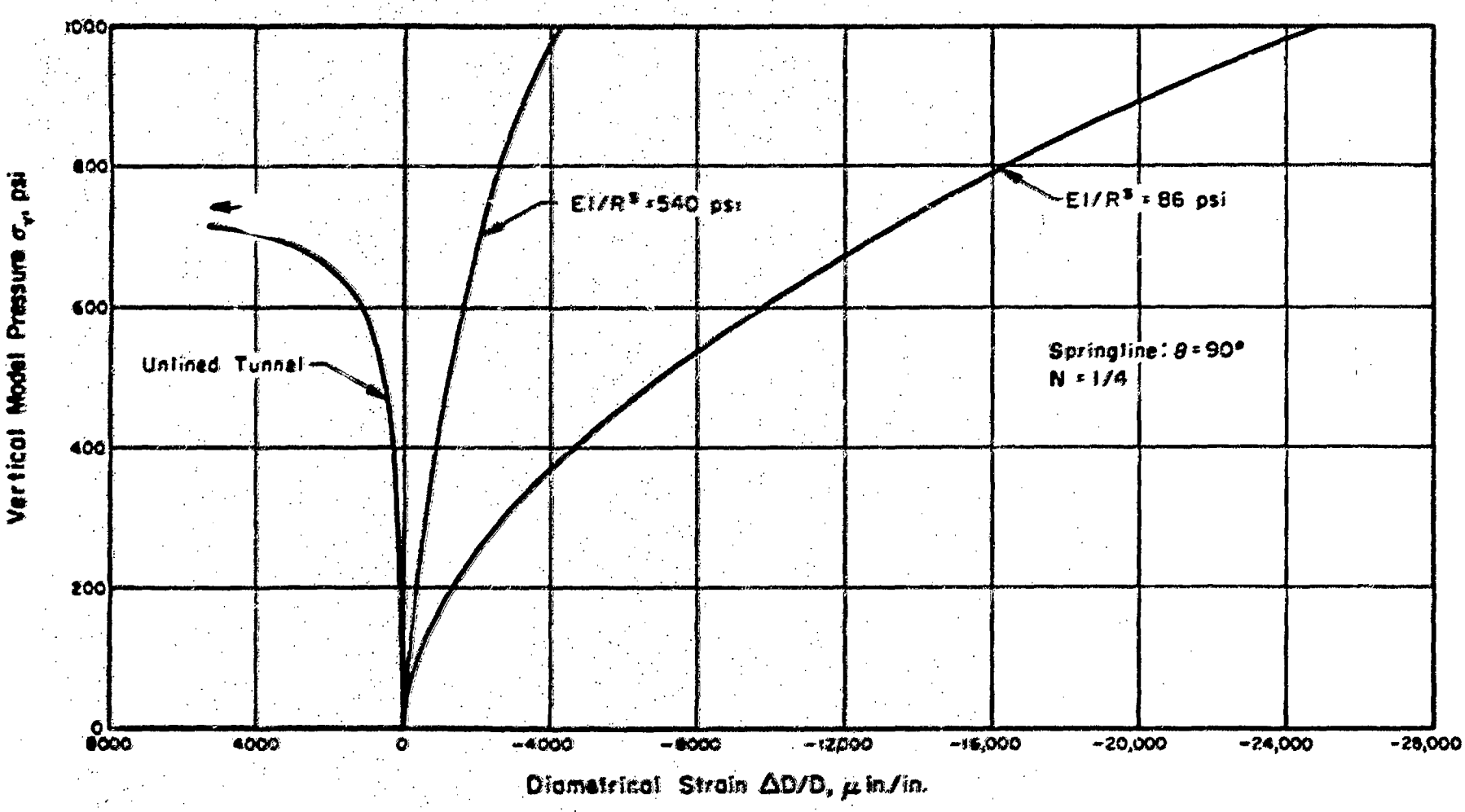

FIG. 33 COMPARISON OF DIAMETRICAL STRAINS AT SPRINGLINE FOR DIFFERENT VALUES OF LINER STIFFNESS

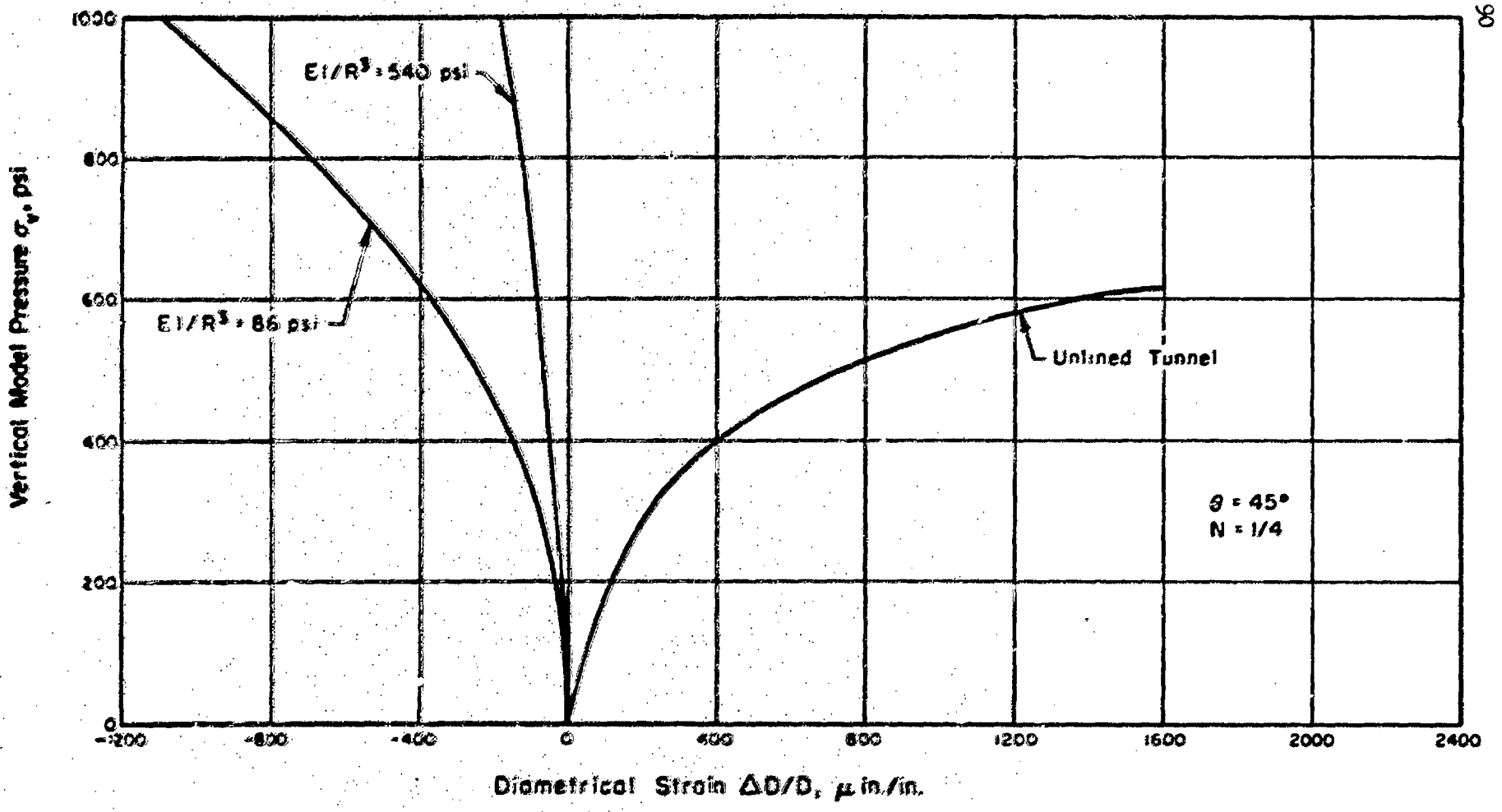

FIG. 34 COMPARISON OF DIAMETRICAL STRAIN AT θ = 45° FOR DIFFERENT VALUES OF LINER STIFFNESS

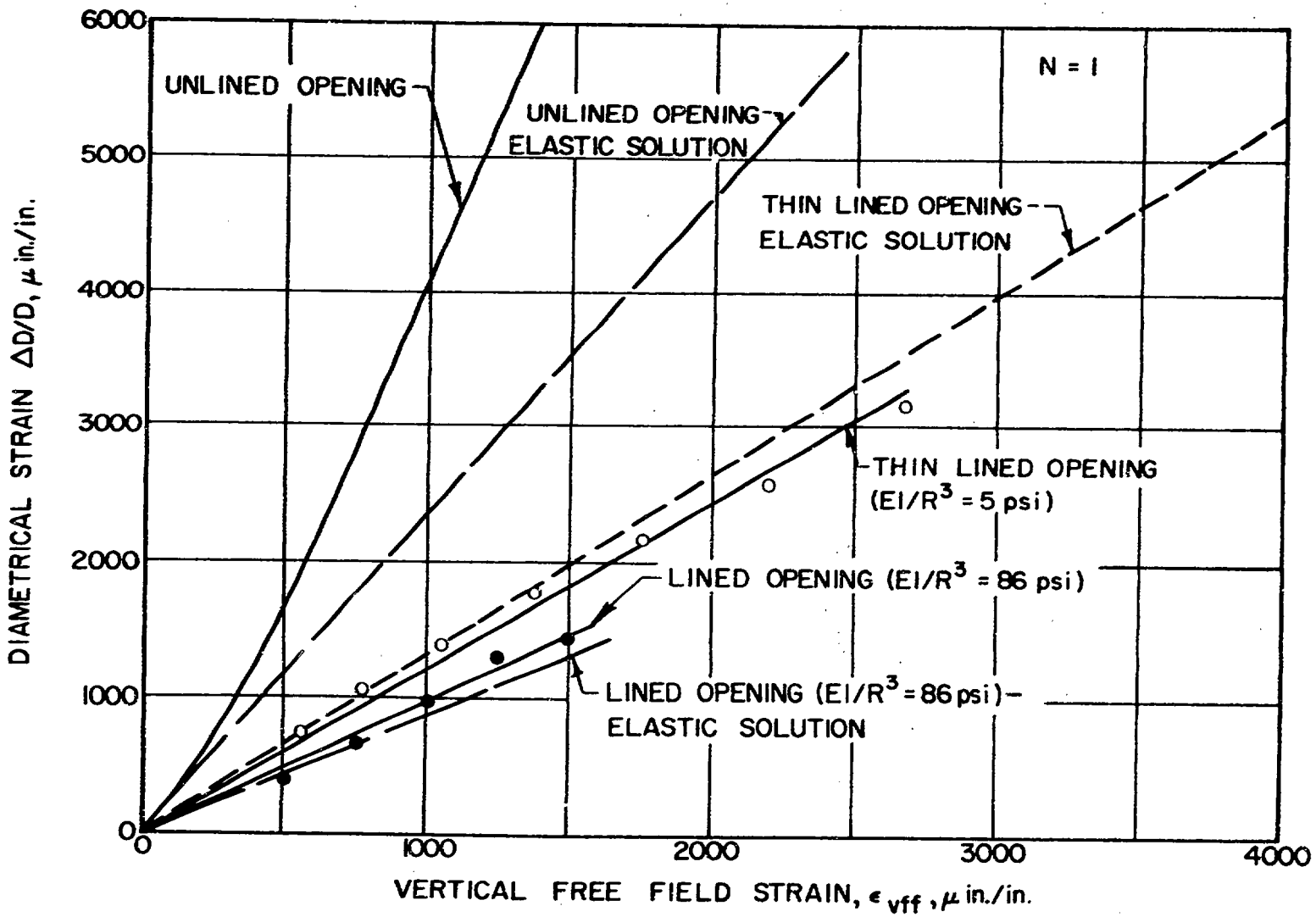

FIG. 35 DIAMETRICAL STRAIN OF LINER AS A FUNCTION OF VERTICAL FREE FIELD STRAIN ; N = 1

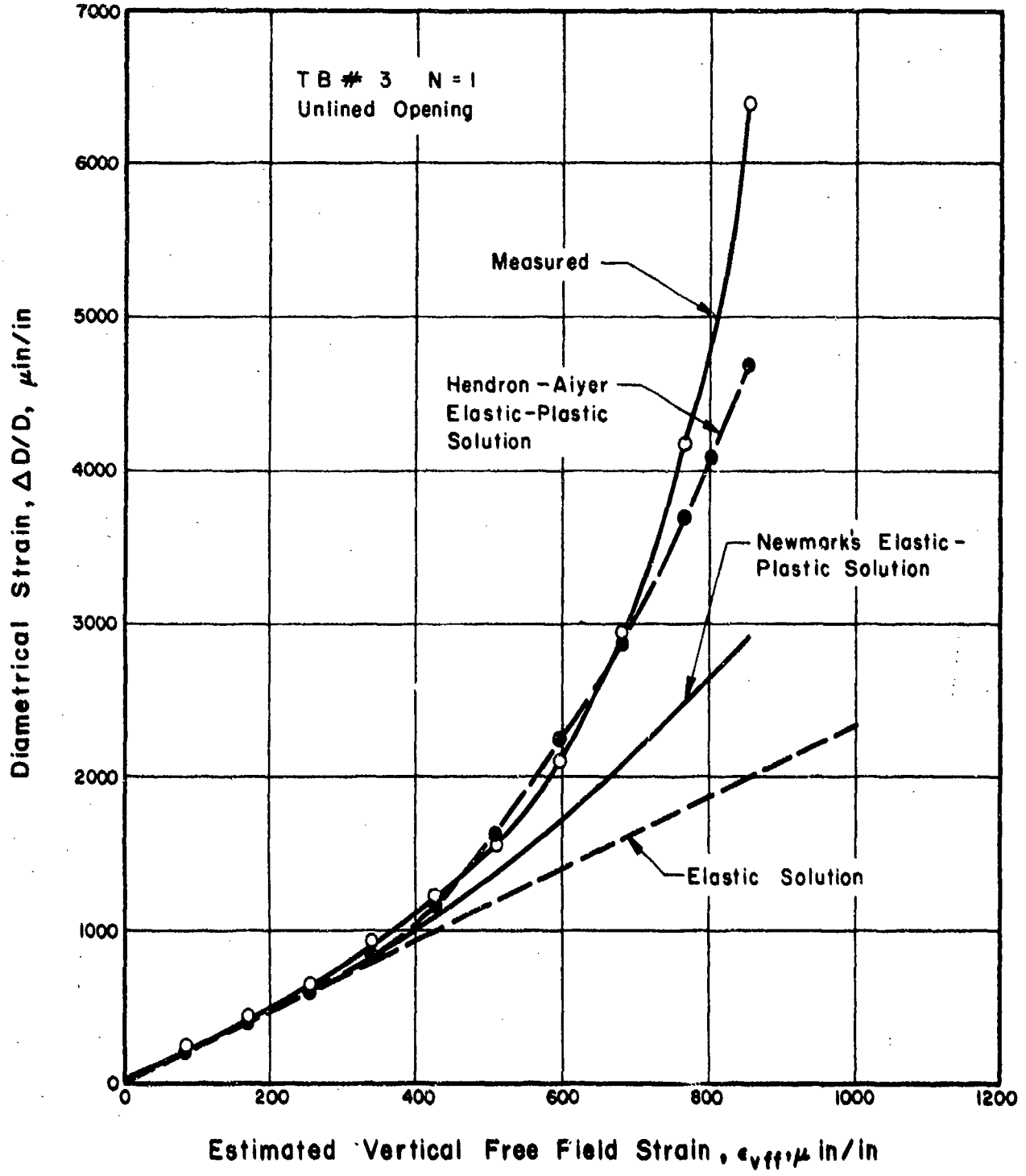

FIG. 36 DIAMETRICAL STRAIN IN AN UNLINED OPENING

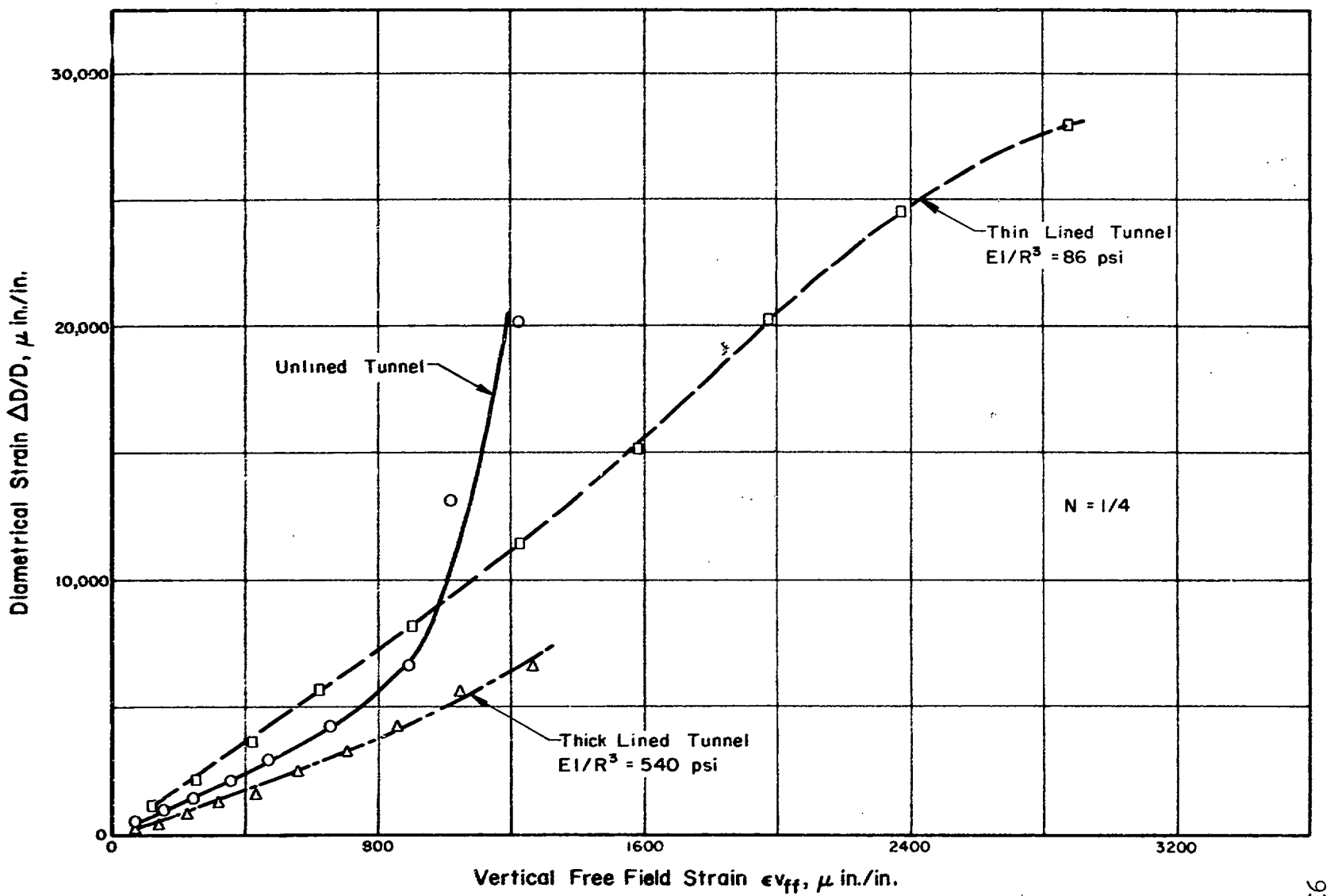

FIG. 37 DIAMETRICAL STRAIN OF LINER AT CROWN AND INVERT AS A FUNCTION OF VERTICAL FREE FIELD STRAIN N = 1/4

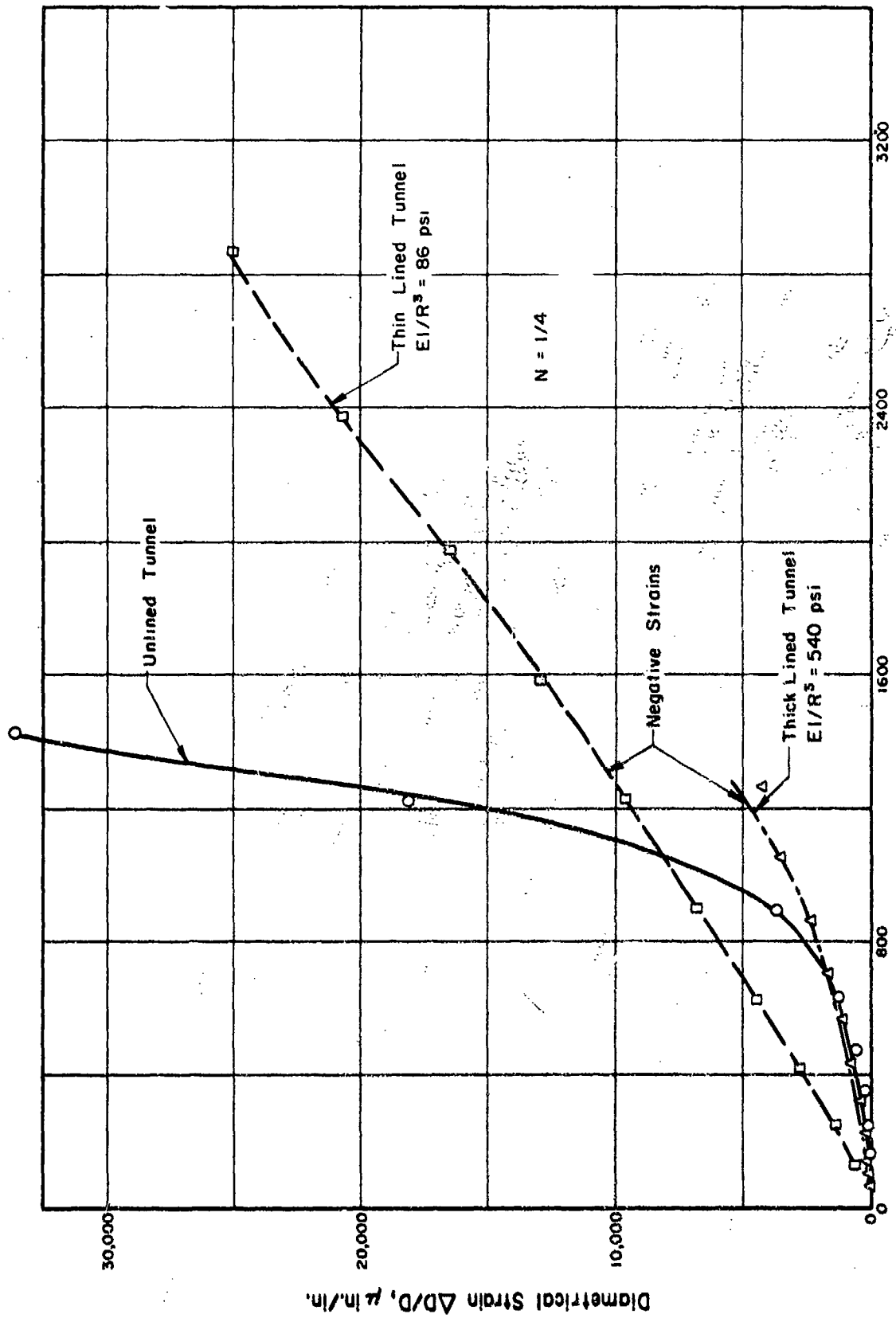

FIG. 38 DIAMETRICAL STRAIN OF LINER AT SPRINGLINE AS A FUNCTION OF VERTICAL FREE FIELD STRAIN ; N = 1/4

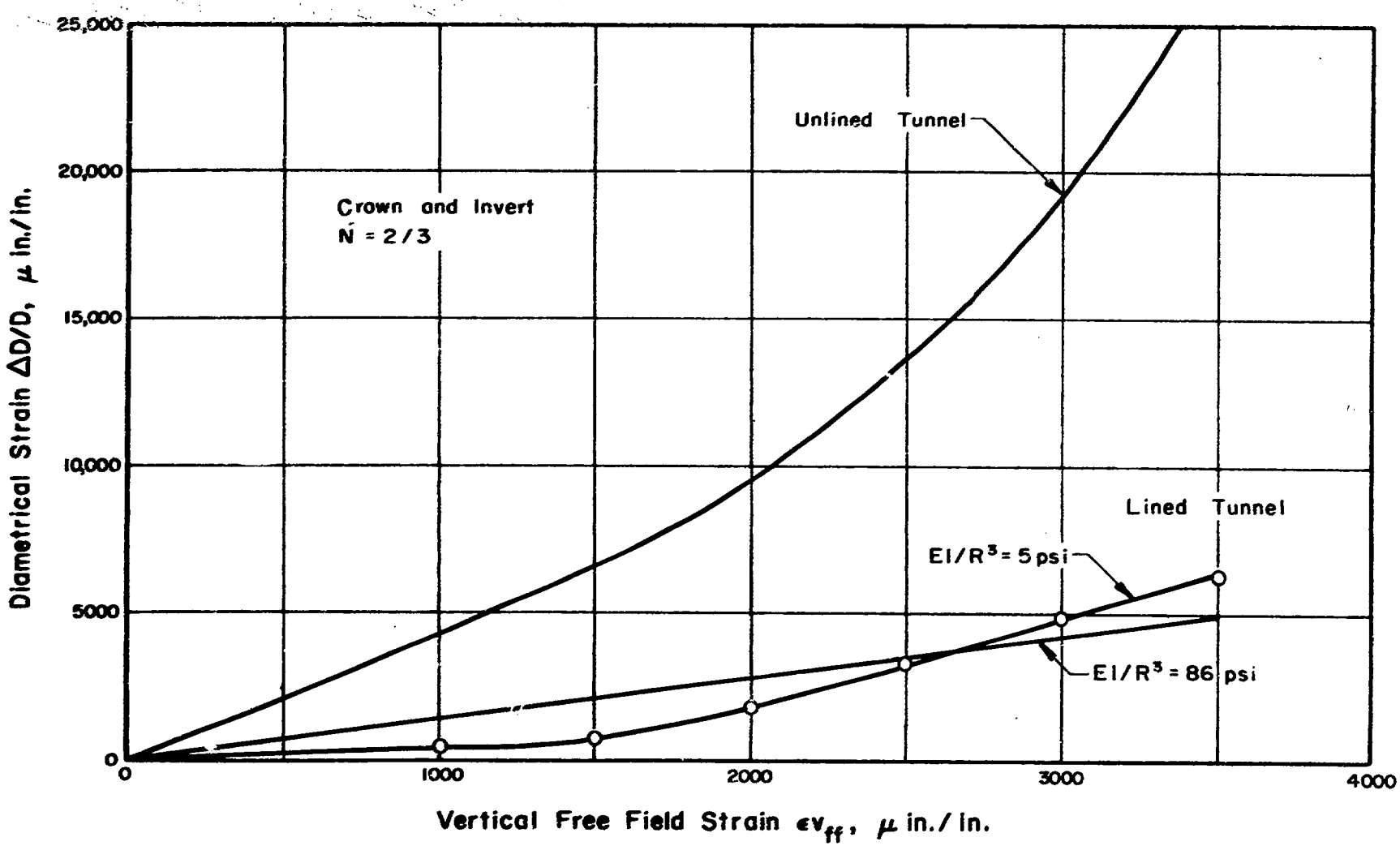

FIG. 39 DIAMETRICAL STRAIN OF LINER AT CROWN AND INVERT AS A FUNCTION OF VERTICAL FREE FIELD STRAIN: N = 2/3

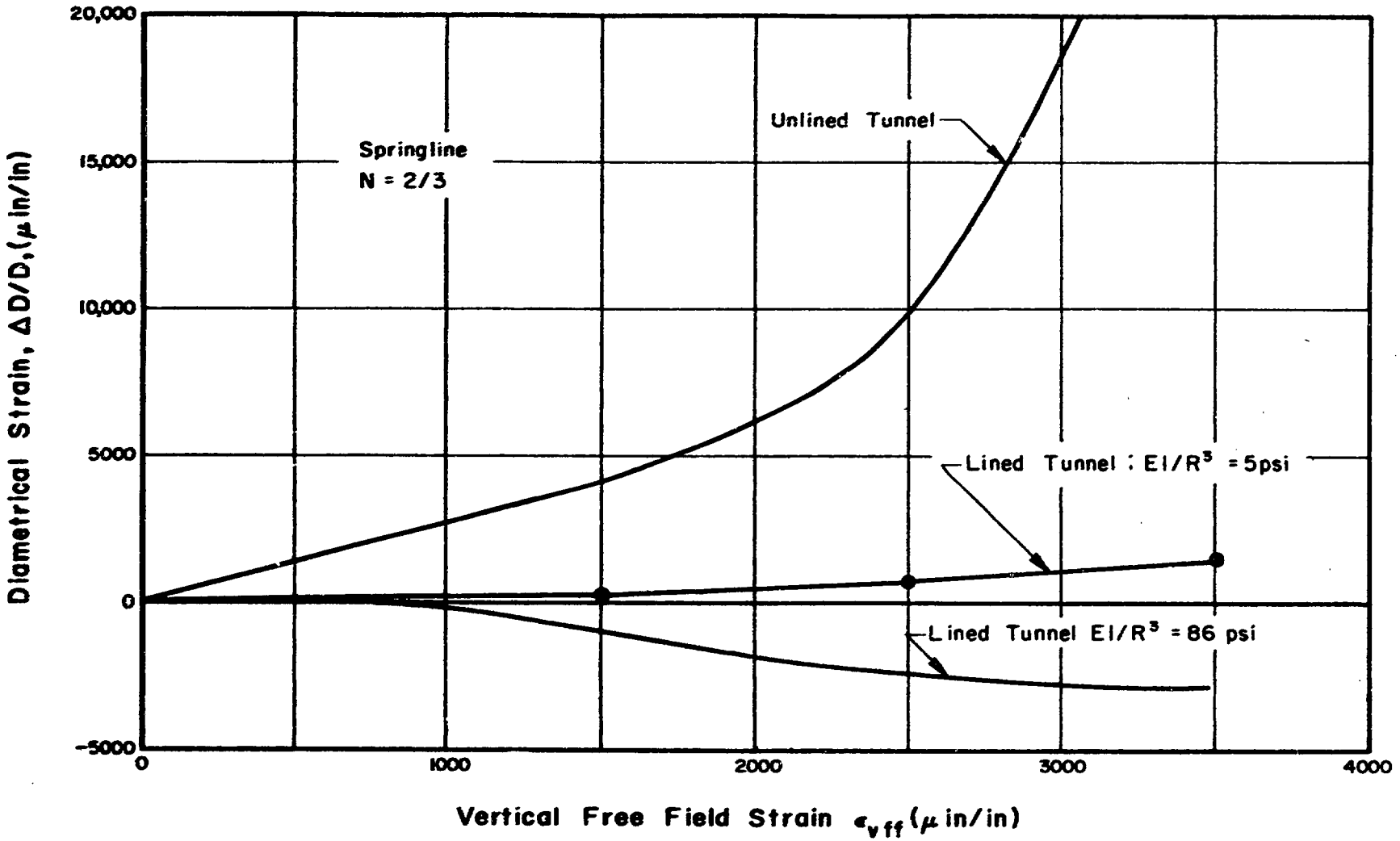

FIG. 40 DIAMETRICAL STRAIN OF LINER AT SPRINGLINE AS A FUNCTION OF VERTICAL FREE FIELD STRAIN ; N = 2/3

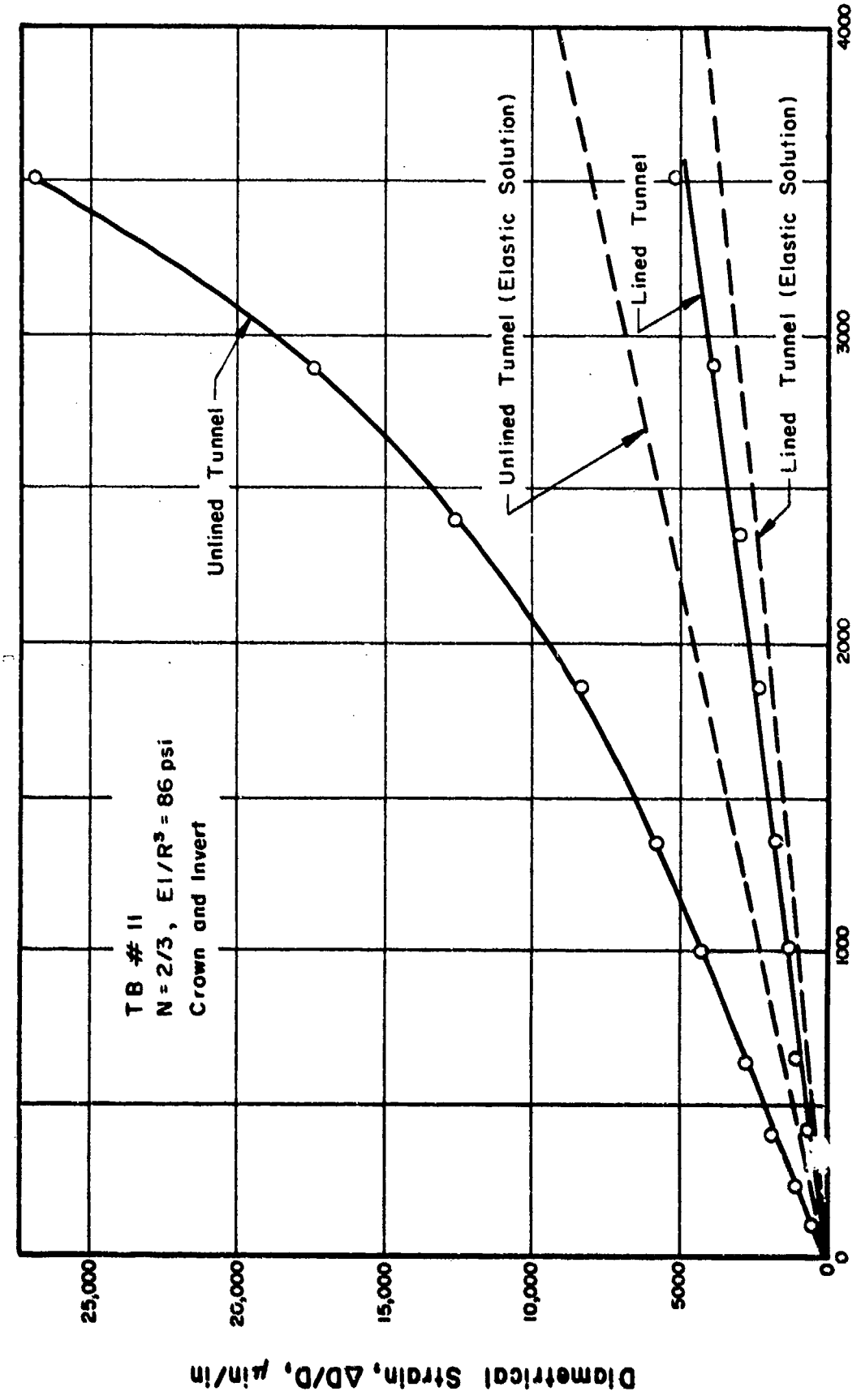

FIG. 41 DIAMETRICAL STRAIN OF LINER AS A FUNCTION OF VERTICAL FREE FIELD STRAIN

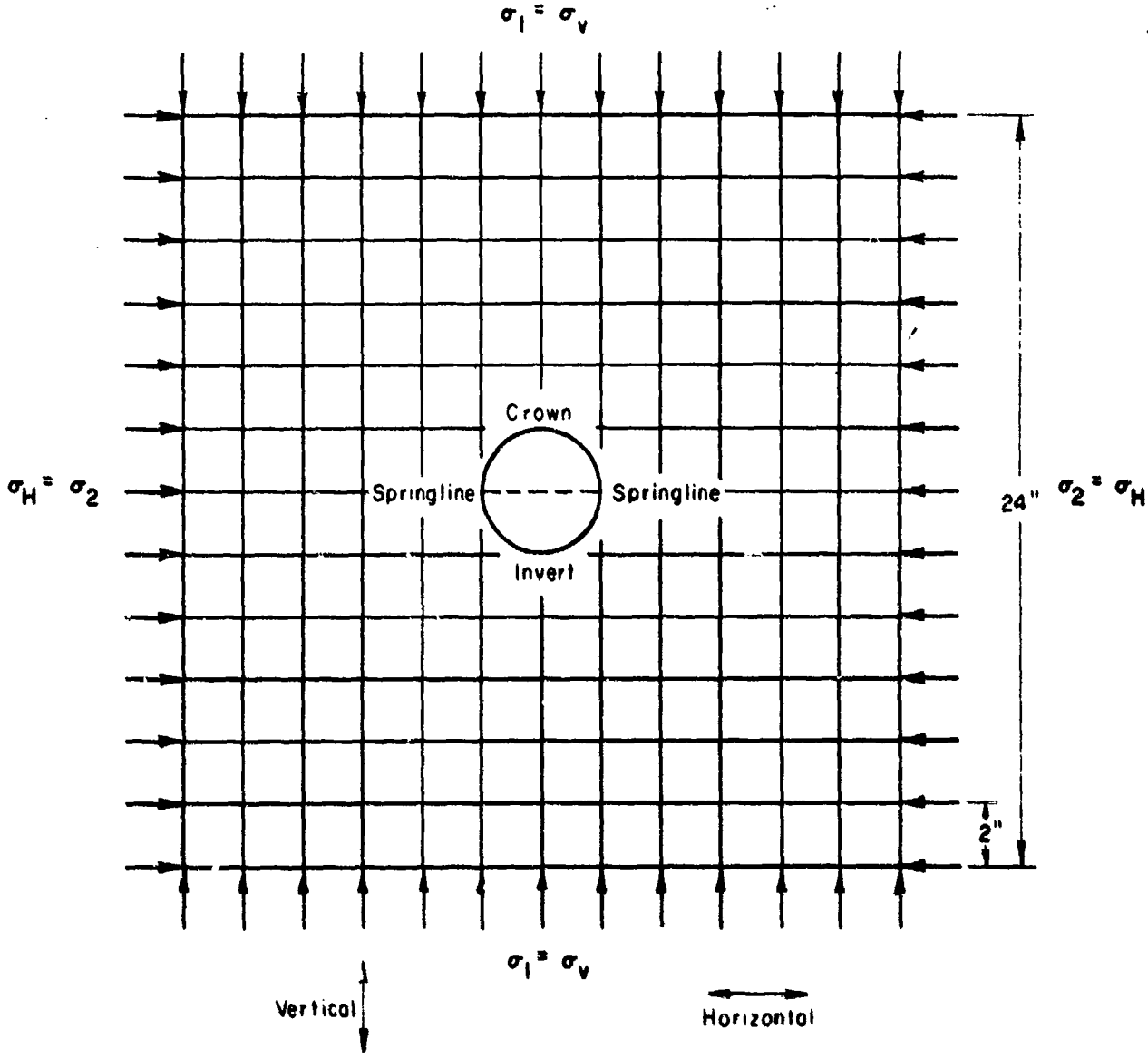

FIG. 42 JOINTED MODEL CONFIGURATION USED IN JOINT BLOCK NO. 1 AND NO. 2

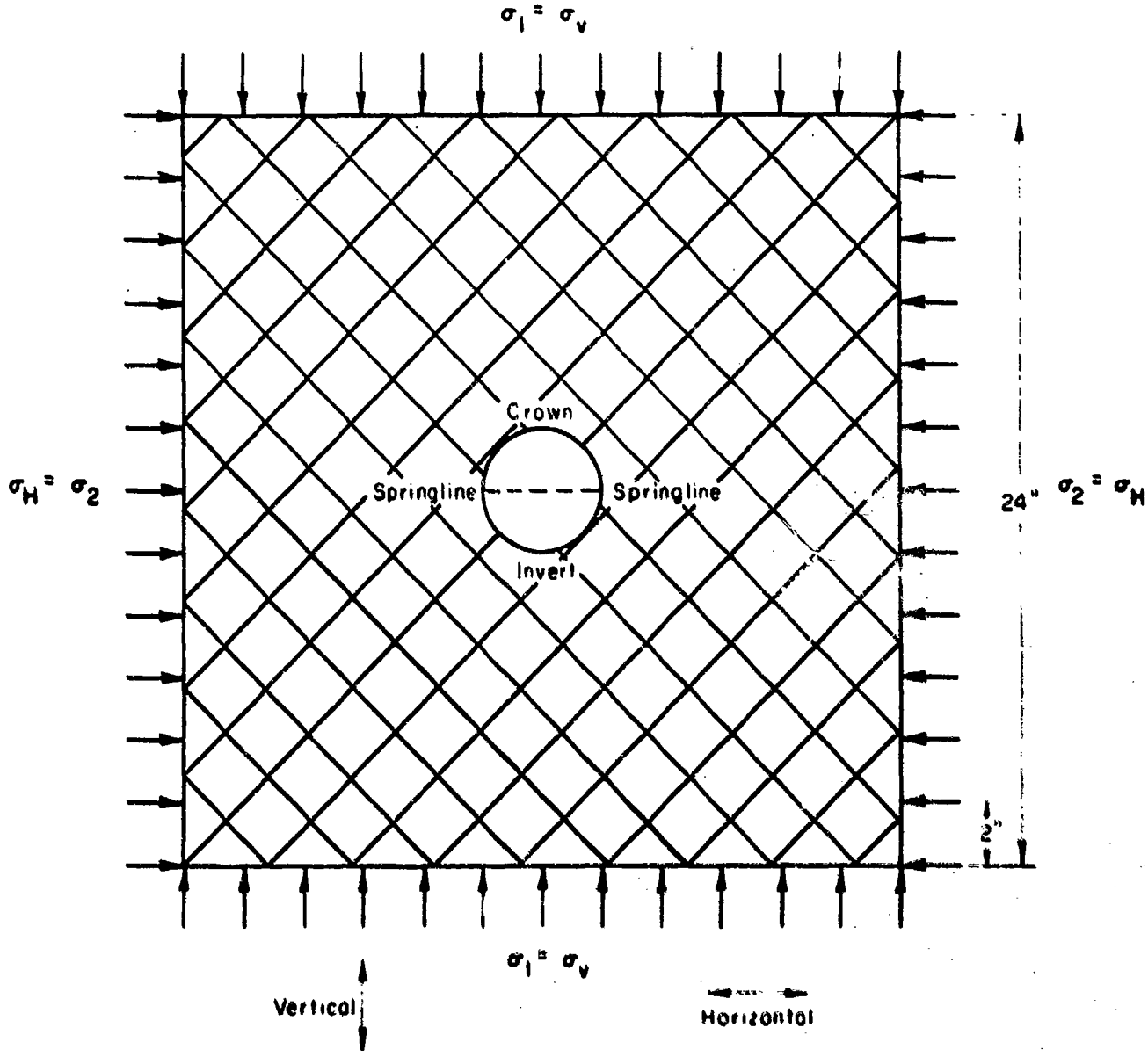

FIG. 43 JOINTED MODEL CONFIGURATION USED IN JOINT BLOCK NO. 3 AND NO. 4

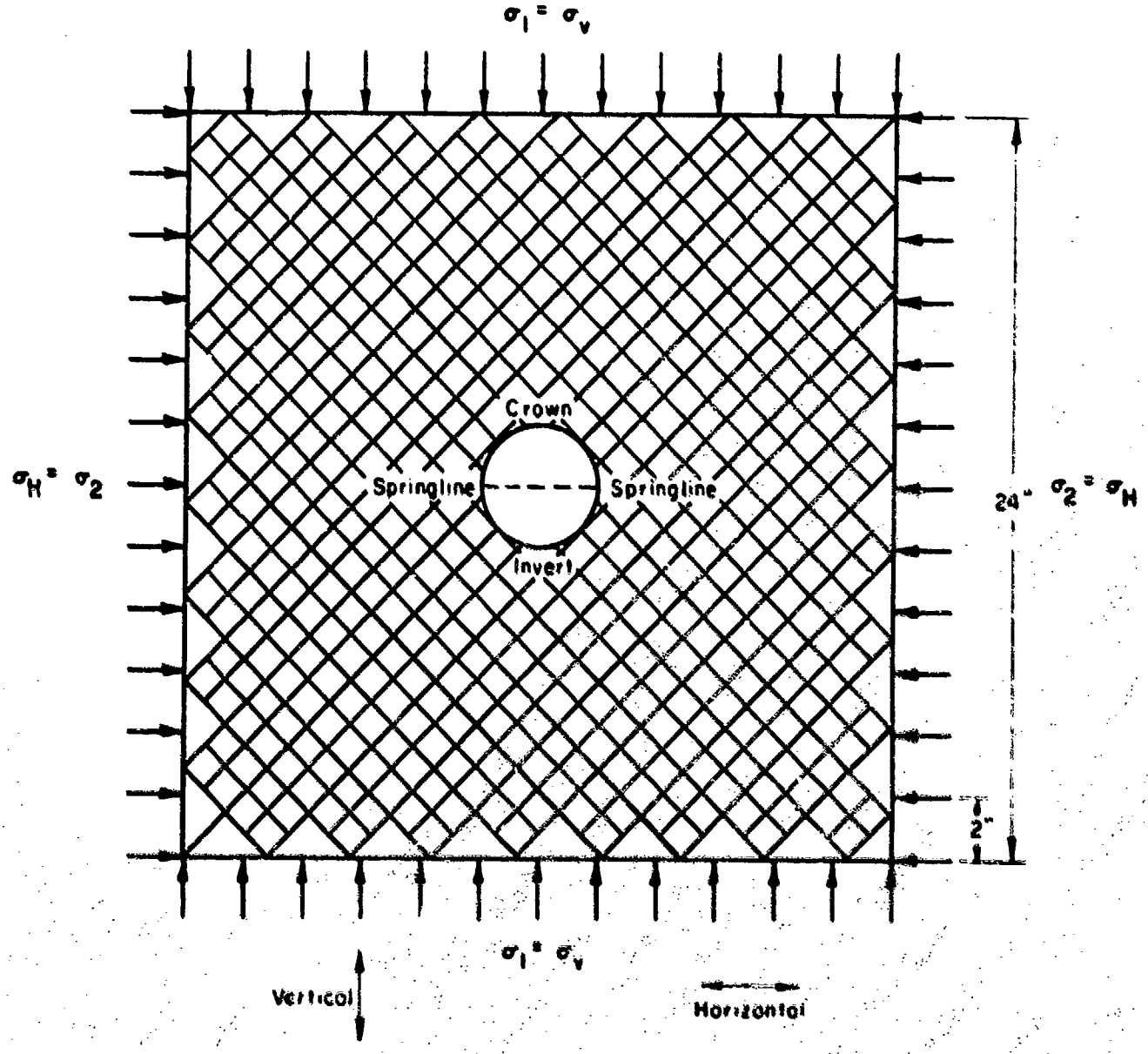

FIG. 44 JOINTED MODEL CONFIGURATION USED IN JOINT BLOCK NO. 5

Fig. 45 Compaction of 20" x 20" x 3" Block of Model Material

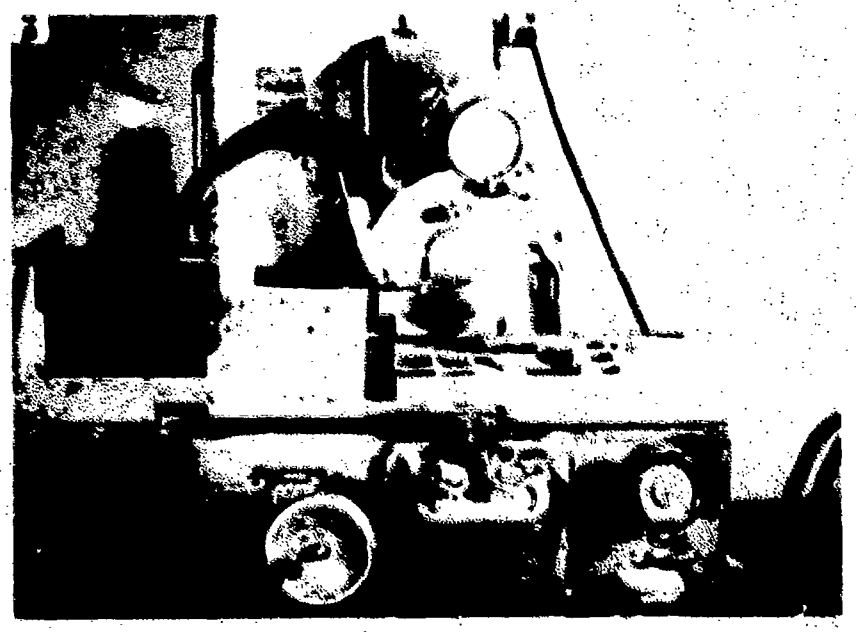

Fig. 46 Diamond Blade Saw Used to Cut Joint Blocks

Figure 47 Grain Size Distribution of Different Sands Tested

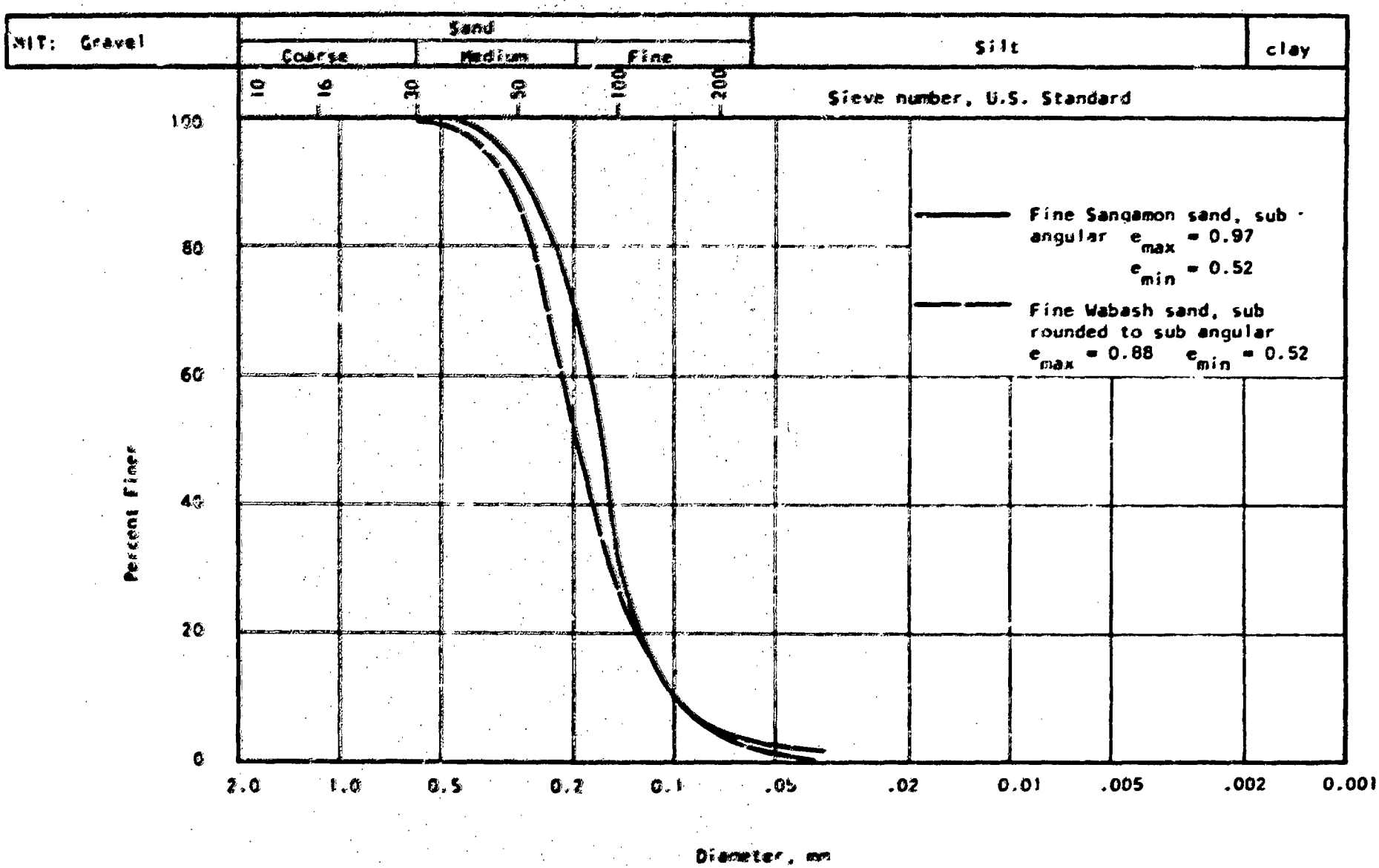

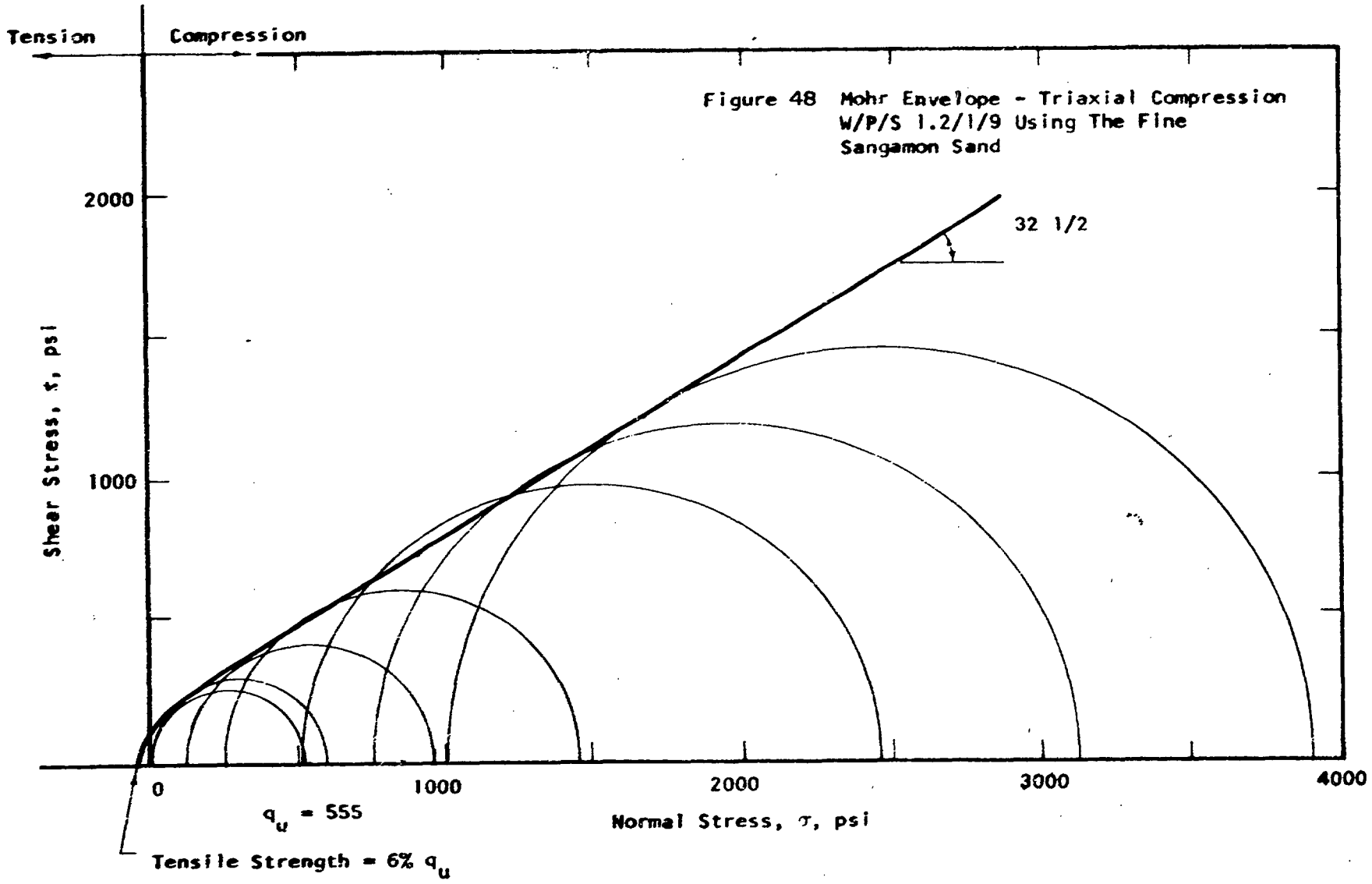

Figure 48 Mohr Envelope - Triaxial Compression W/P/S 1.2/1/9 Using The Fine Sangamon Sand

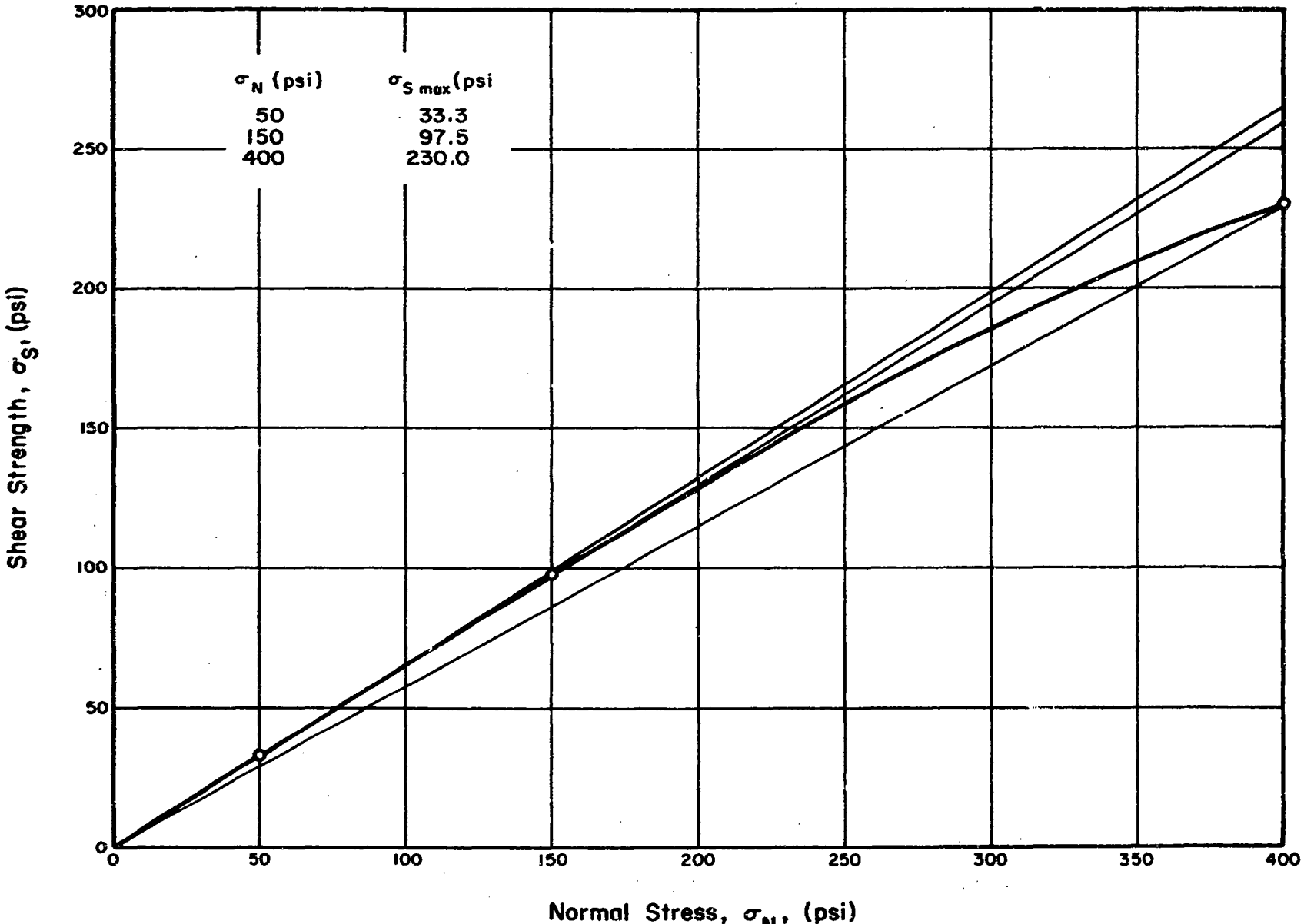

FIG. 49 RESULTS OF DIRECT SHEAR TESTS ON JOINT SURFACES OF MODEL MATERIAL

Fig. 50 Construction of Model Block on Table

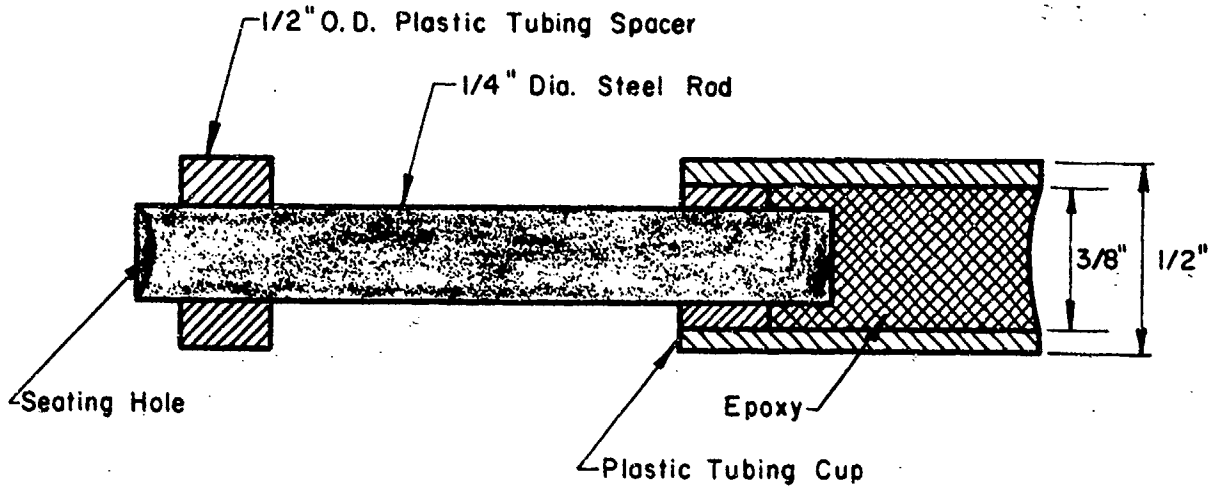

FIG. 51 DETAIL OF BURIED EXTENSOMETER

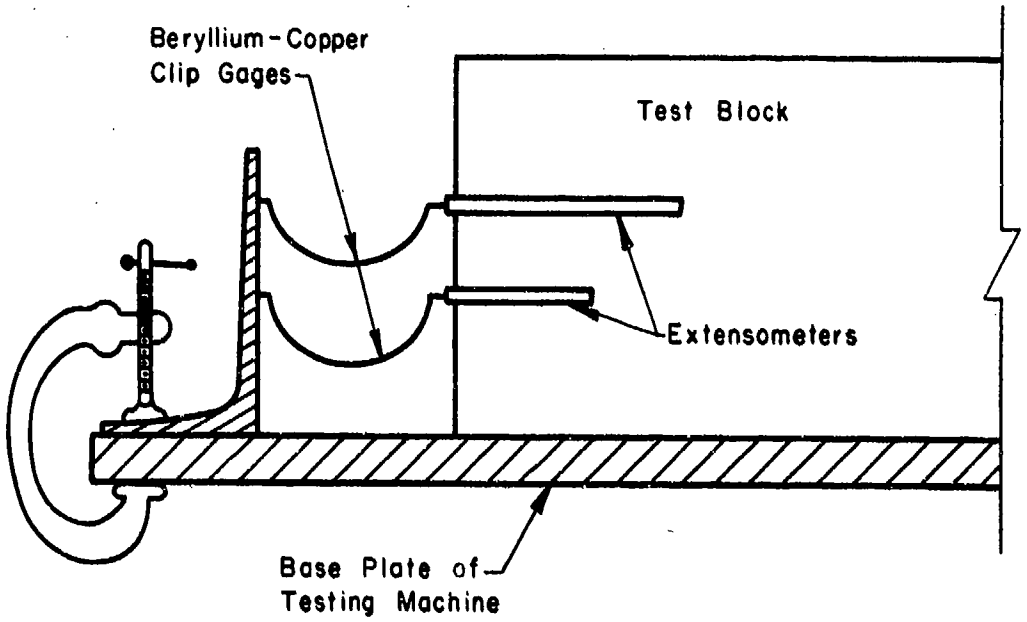

FIG. 52 DETAIL OF EXTENSOMETER MEASUREMENT SETUP

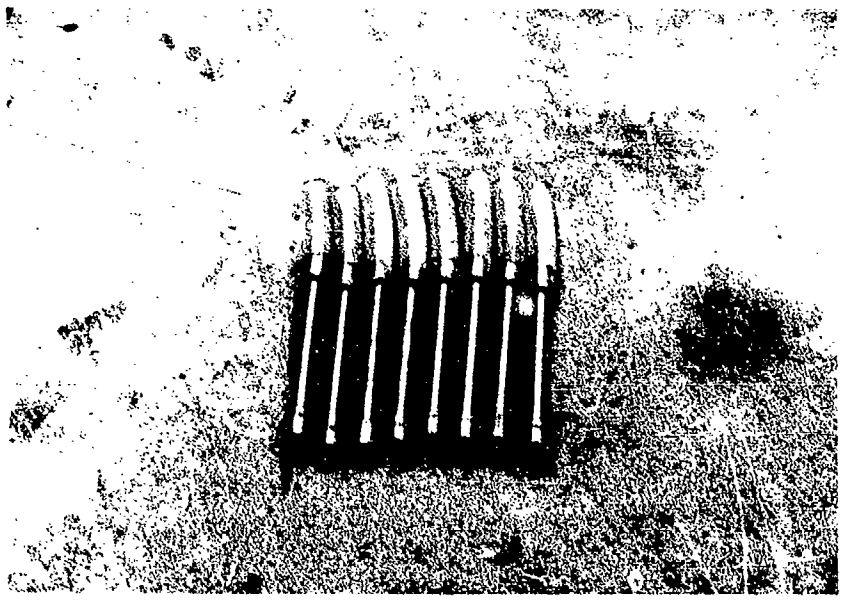

Fig. 53 Extensometers Ready for Installation In Test Block

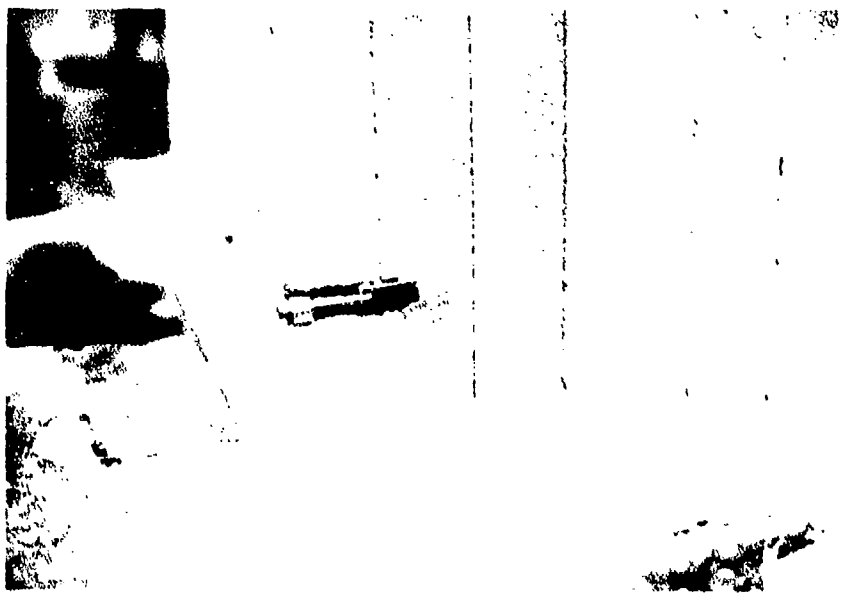

Fig. 54 Extensometer Exposed After Test

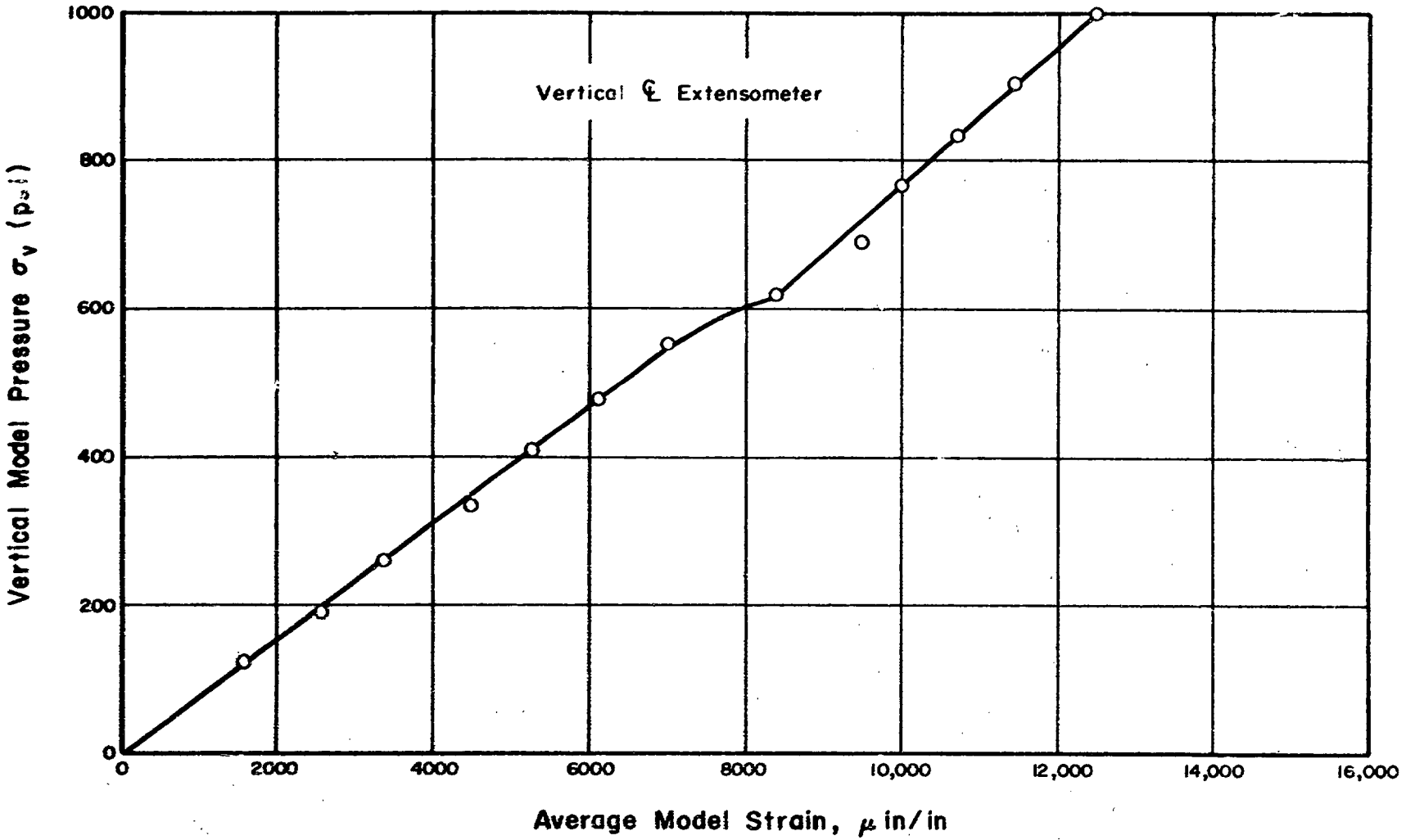

FIG. 55 AVERAGE VERTICAL STRESS—STRAIN CURVE FOR JOINT BLOCK # 1

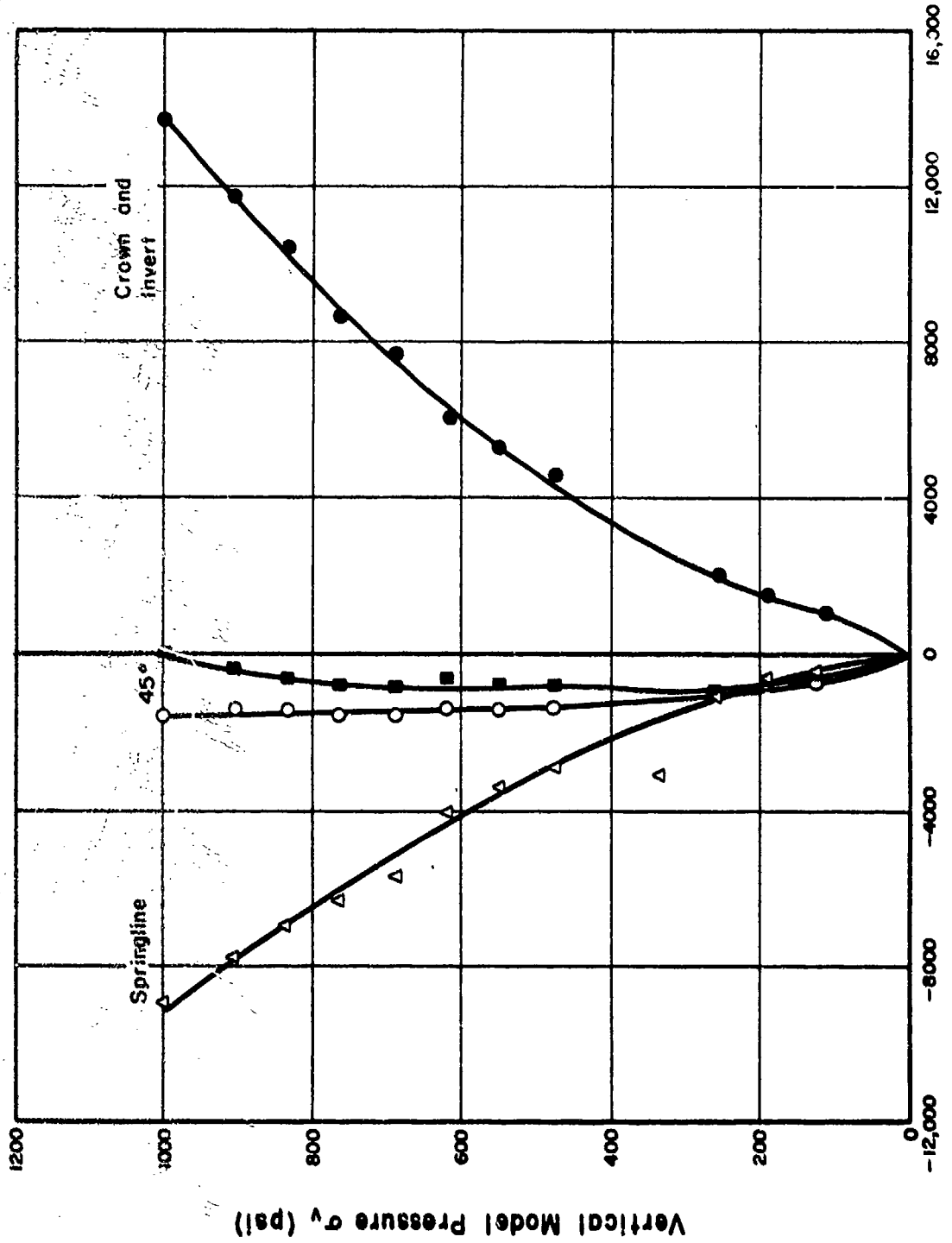

FIG. 56 DIAMETRICAL STRAIN OF LINER AS A FUNCTION OF VERTICAL MODEL PRESSURE FOR JOINT BLOCK # 1

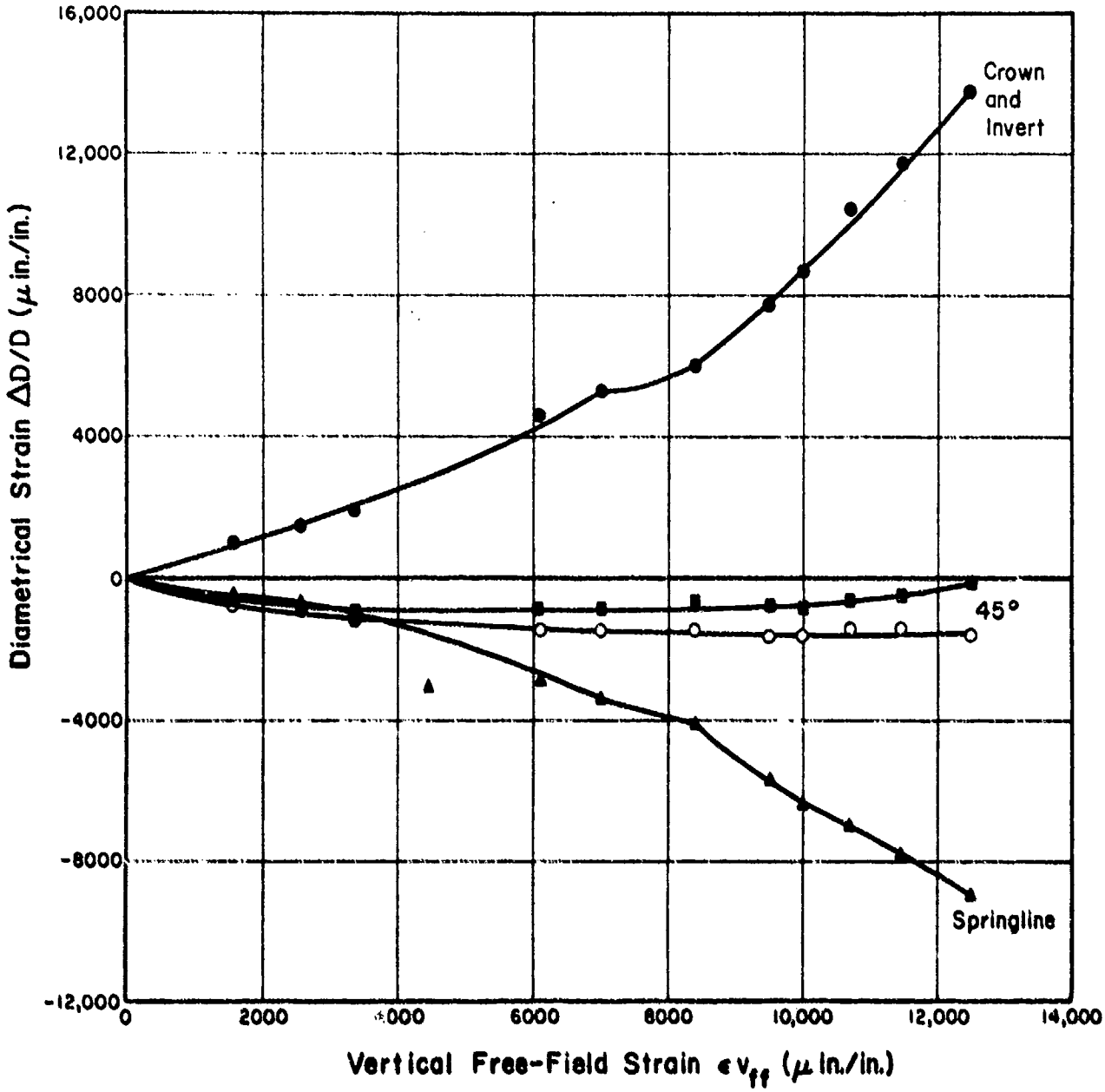

FIG. 57 DIAMETRICAL STRAIN OF LINER AS A FUNCTION OF VERTICAL FREE-FIELD STRAIN IN JOINT BLOCK # 1

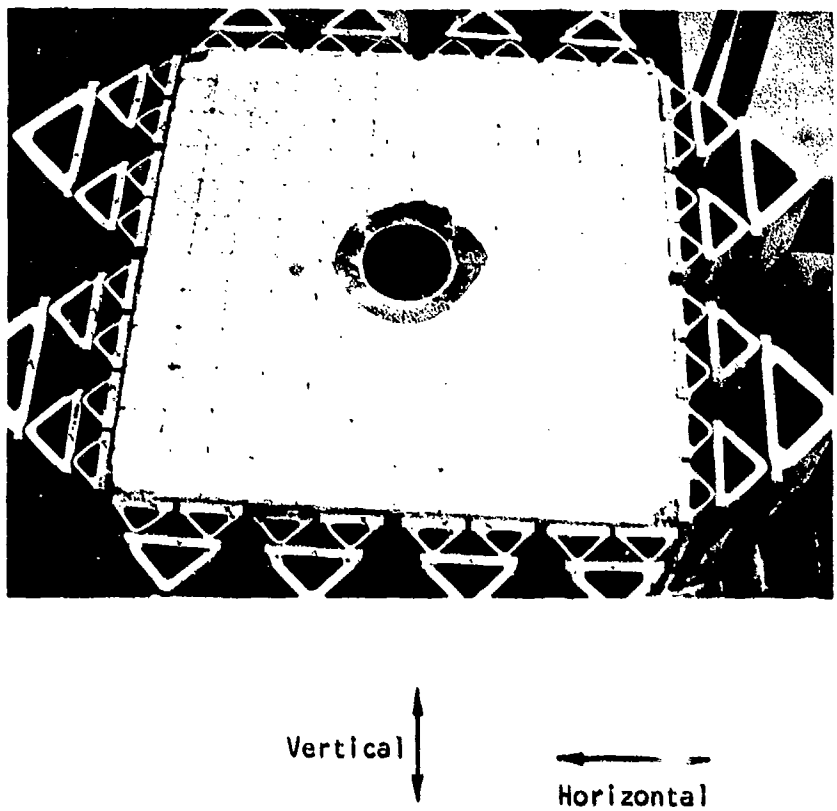

Fig. 58 Photograph of JB//2 After Test at $N = \sigma_H/\sigma_V = 2/3$

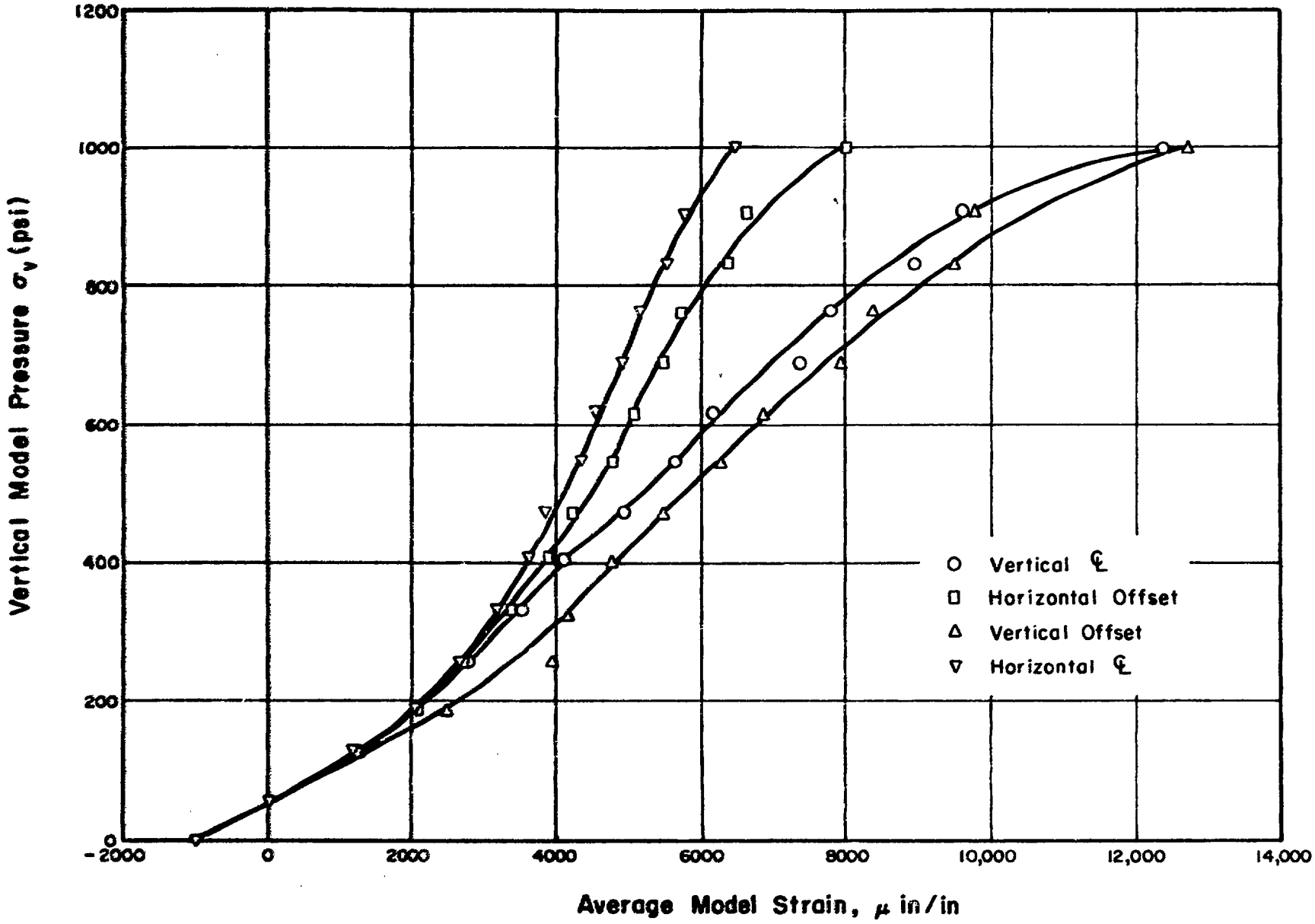

FIG. 59 AVERAGE STRESS—STRAIN CURVES FOR JOINT BLOCK # 2

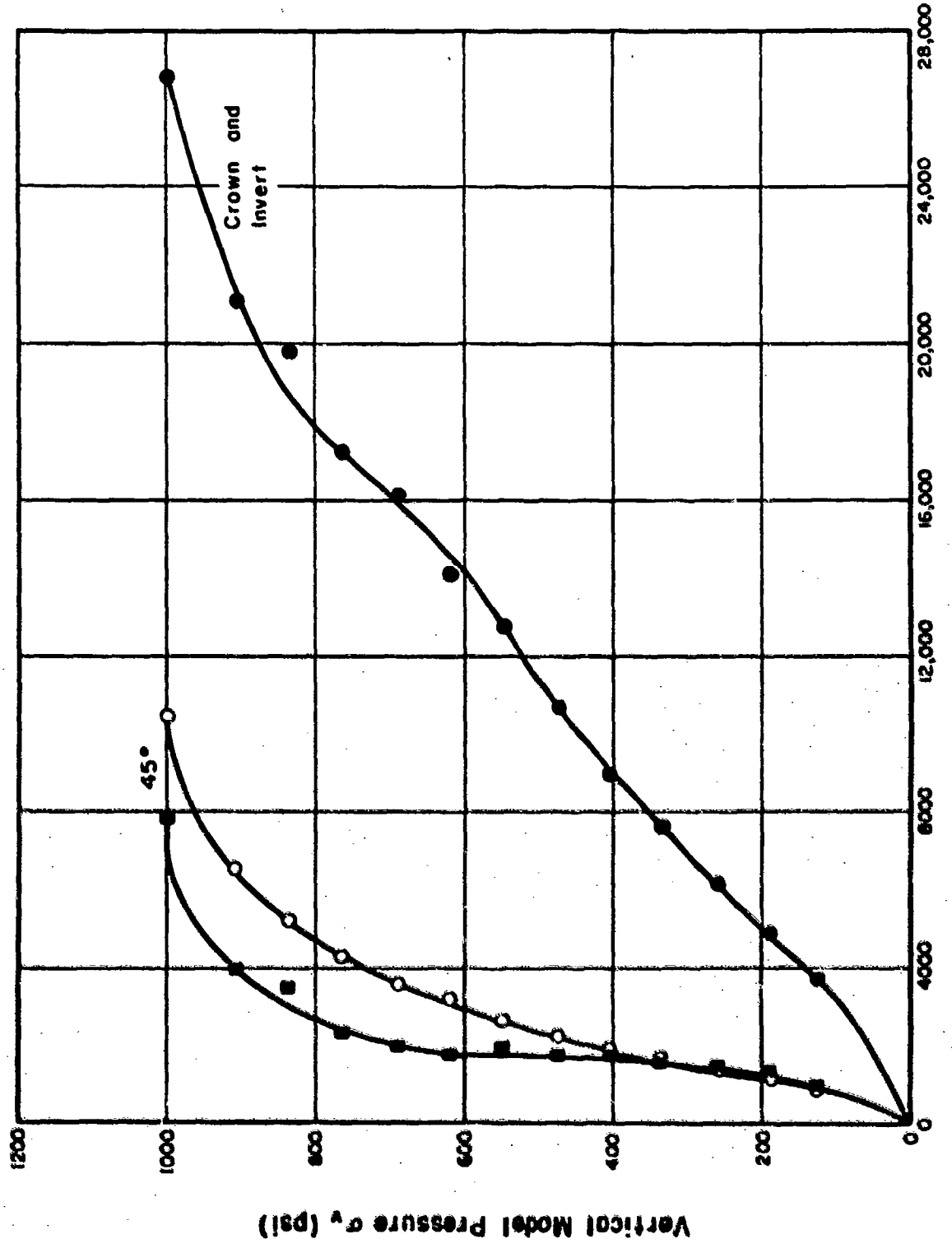

FIG. 6J DIAMETRICAL STRAIN OF LINER AS A FUNCTION OF VERTICAL MODEL PRESSURE FOR JOINT BLOCK # 2

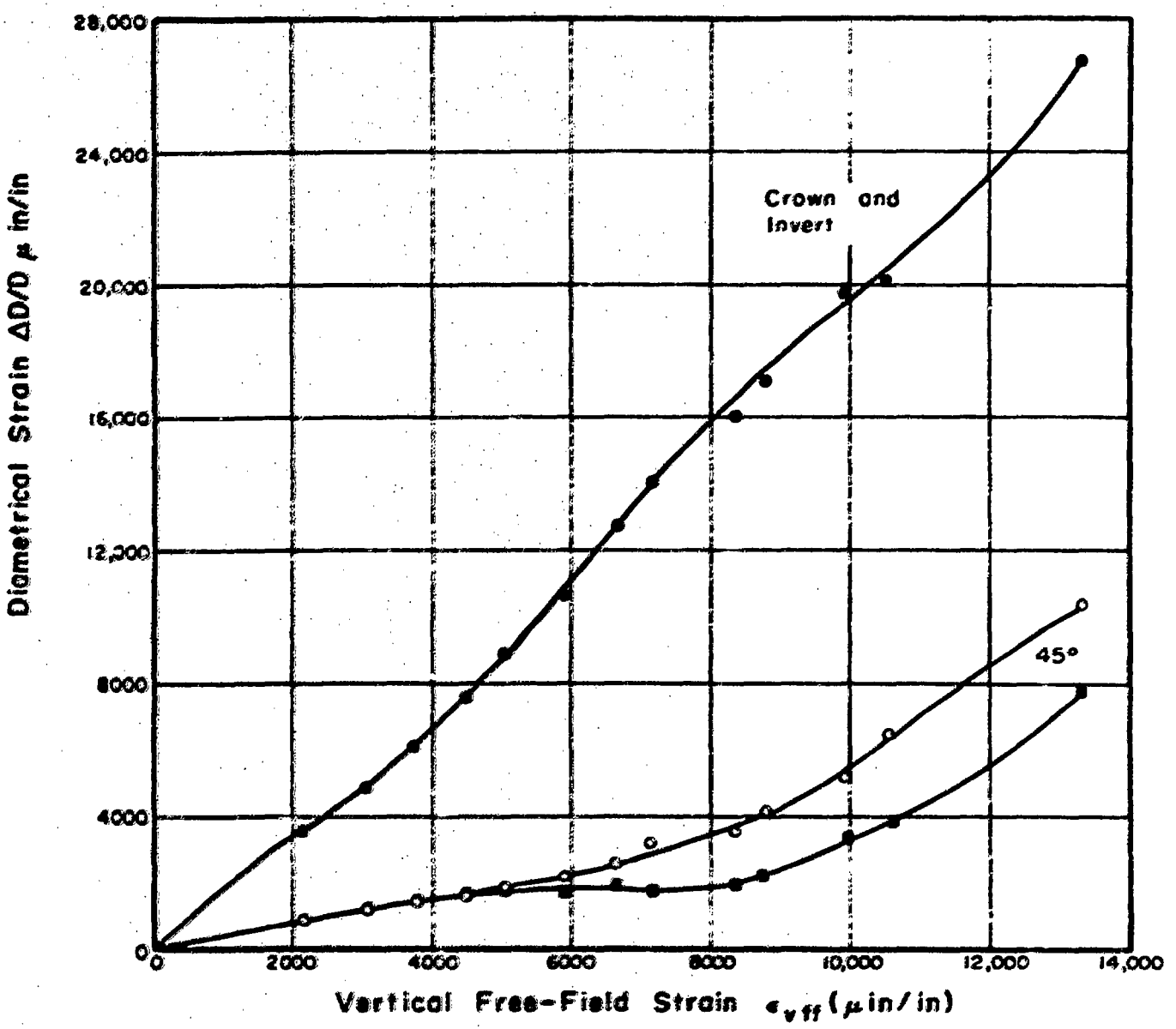

FIG. 61 DIAMETRICAL STRAIN OF LINER AS A FUNCTION OF VERTICAL FREE FIELD-STRAIN FOR JB # 2

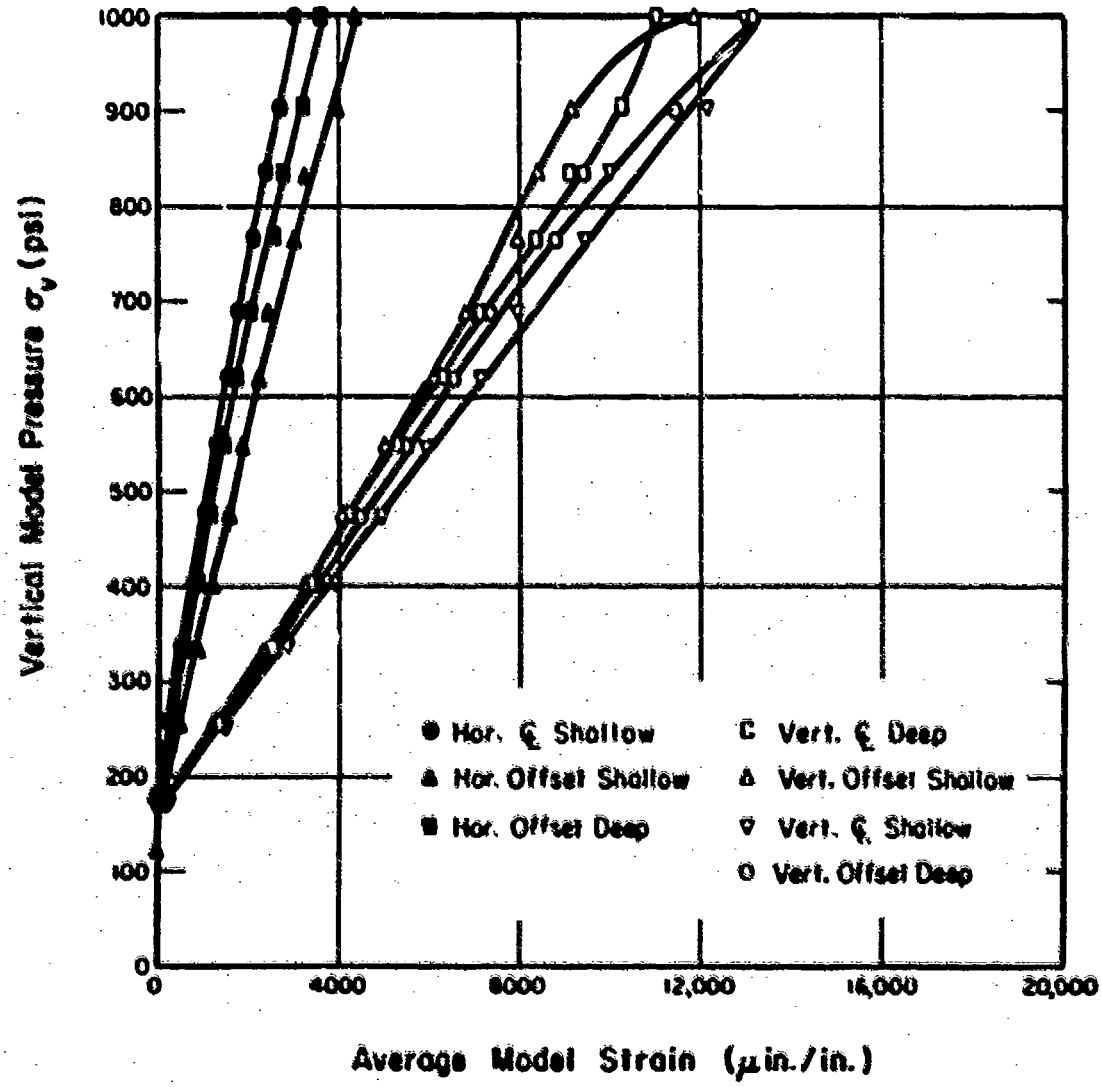

FIG. 62 AVERAGE STRESS-STRAIN CURVES FOR JOINT BLOCK NO. 3

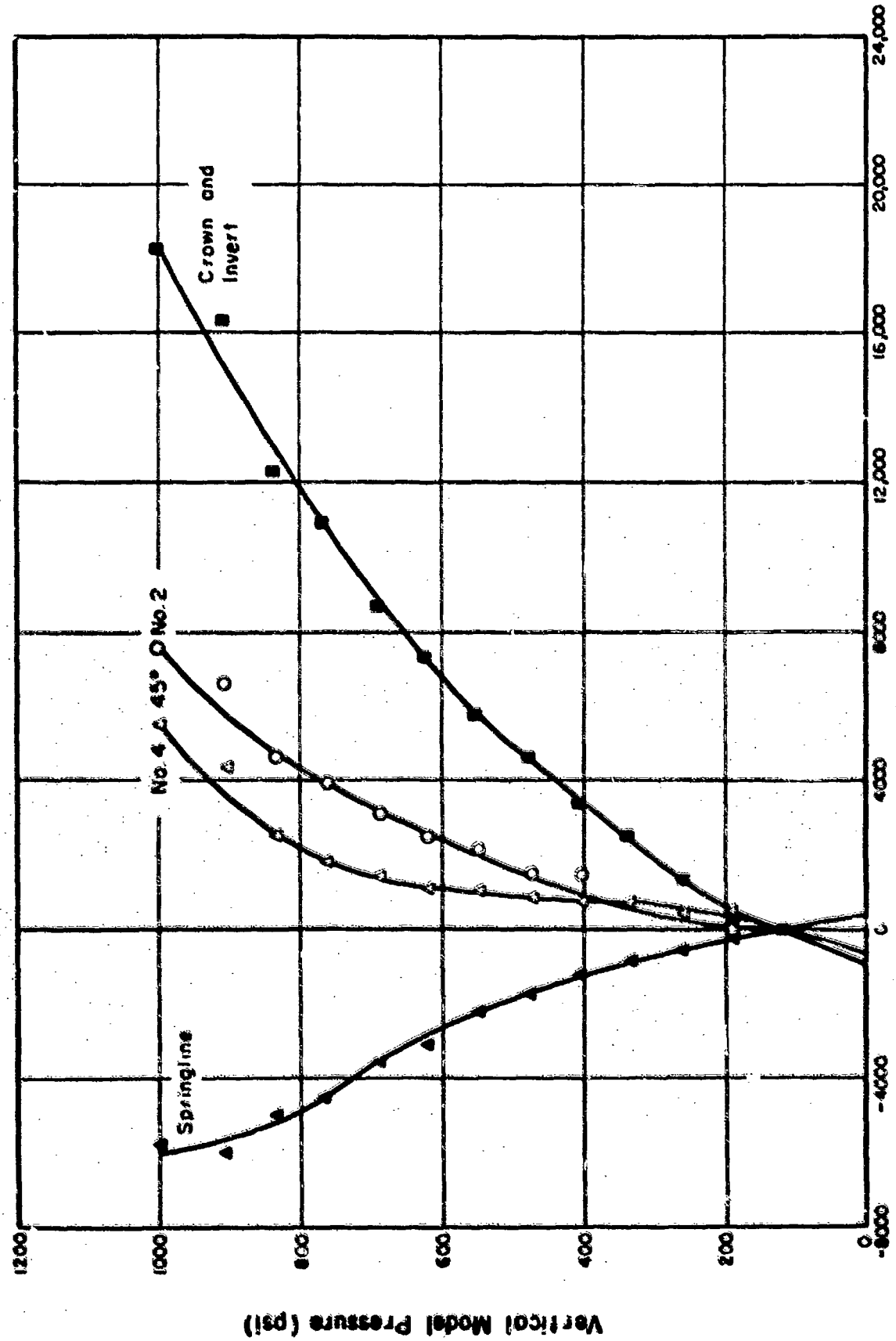

FIG. 63 DIAMETRICAL STRAIN OF LINER AS A FUNCTION OF VERTICAL MODEL PRESSURE FOR JOINT BLOCK NO. 3

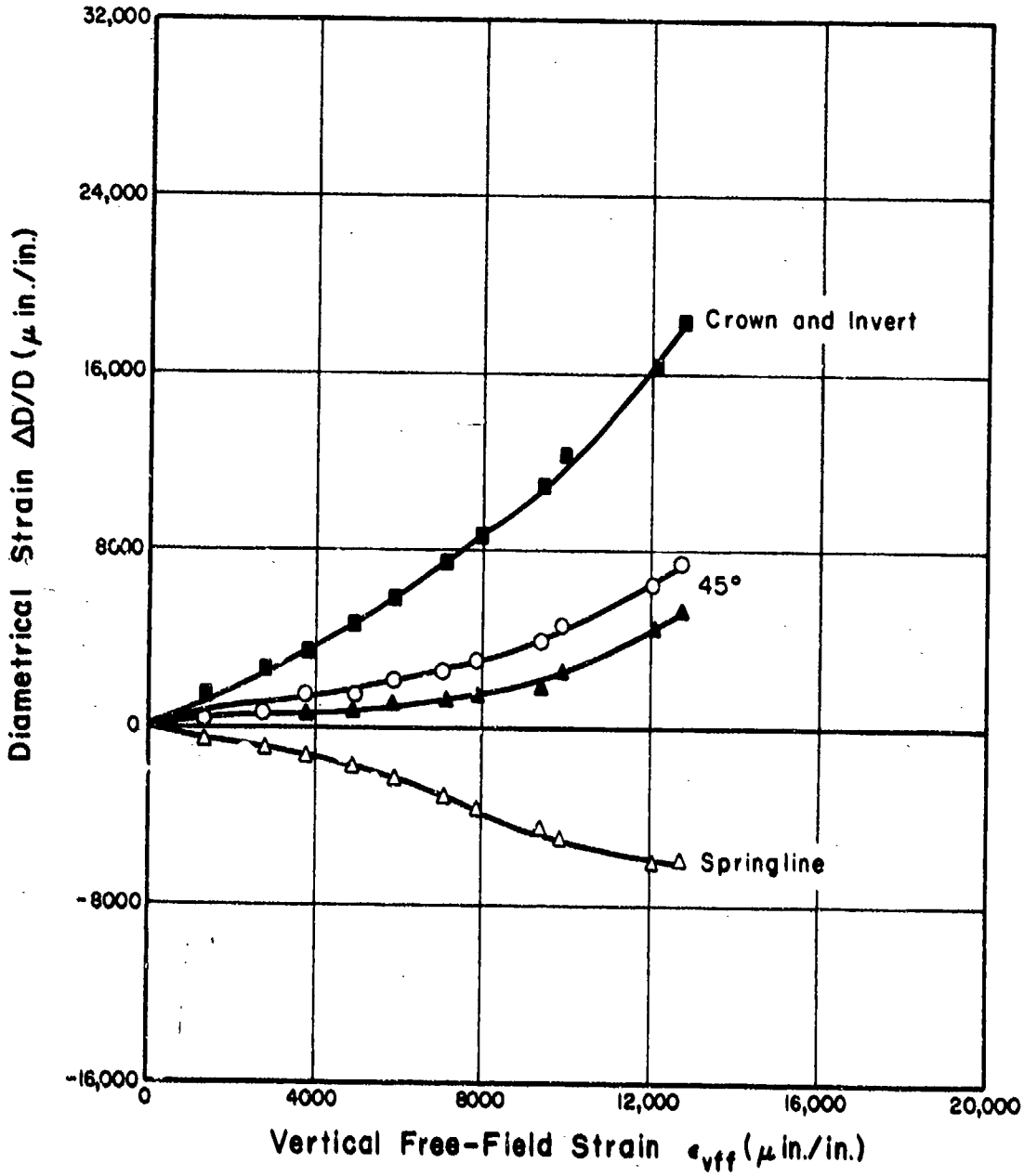

FIG. 64 DIAMETRICAL STRAIN OF LINER AS A FUNCTION OF VERTICAL FREE-FIELD STRAIN FOR JOINT BLOCK NO. 3

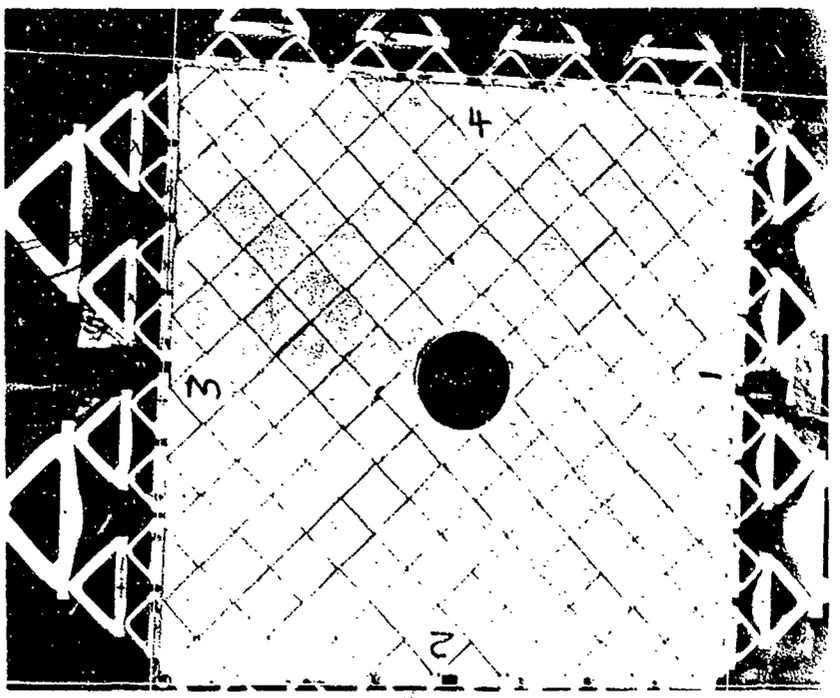

Fig. 65 Photograph of JB#4 Before Test at $N = \sigma_H/\sigma_v = 2/3$

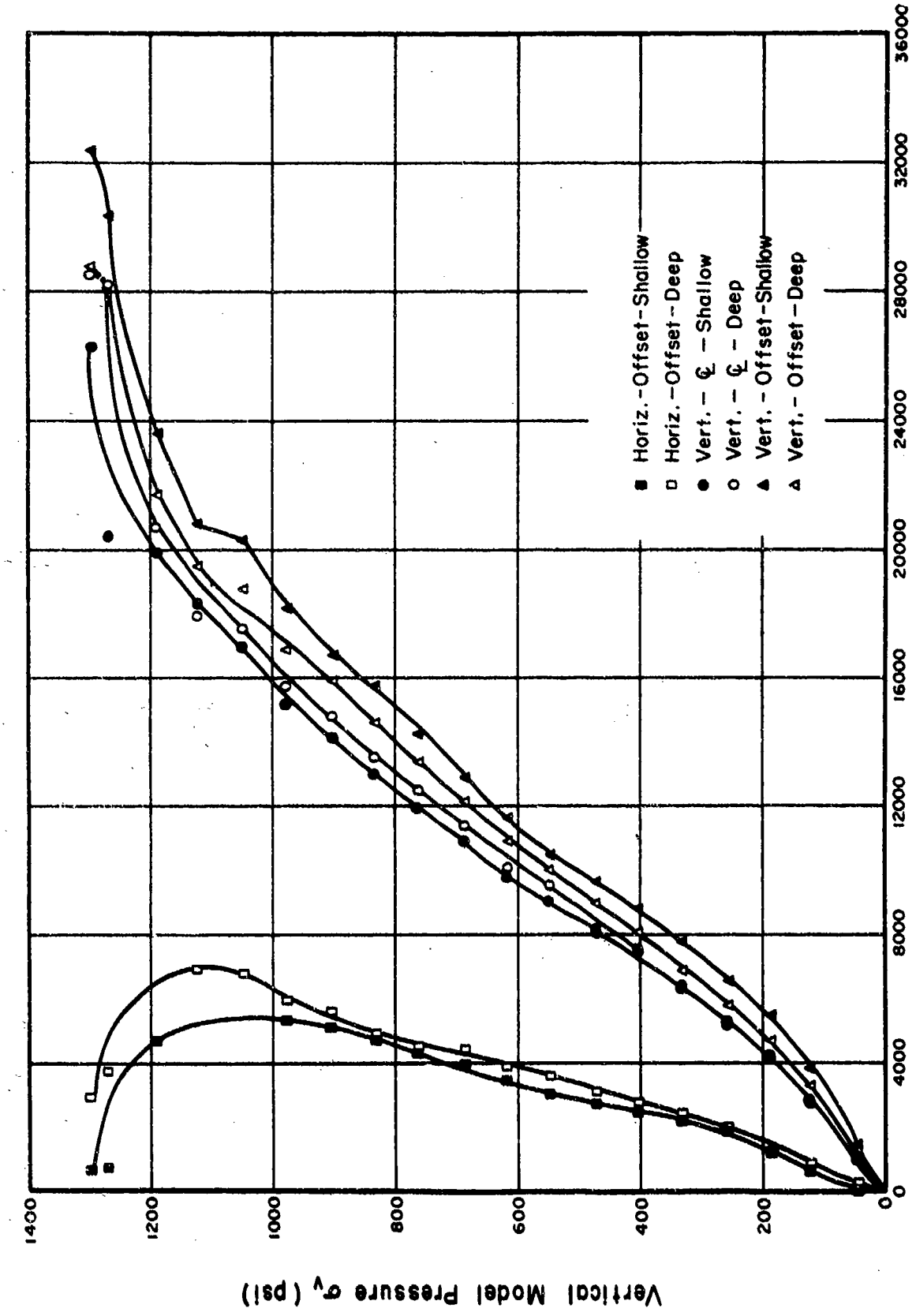

FIG. 66 AVERAGE STRESS-STRAIN CURVES FOR JOINT BLOCK #4

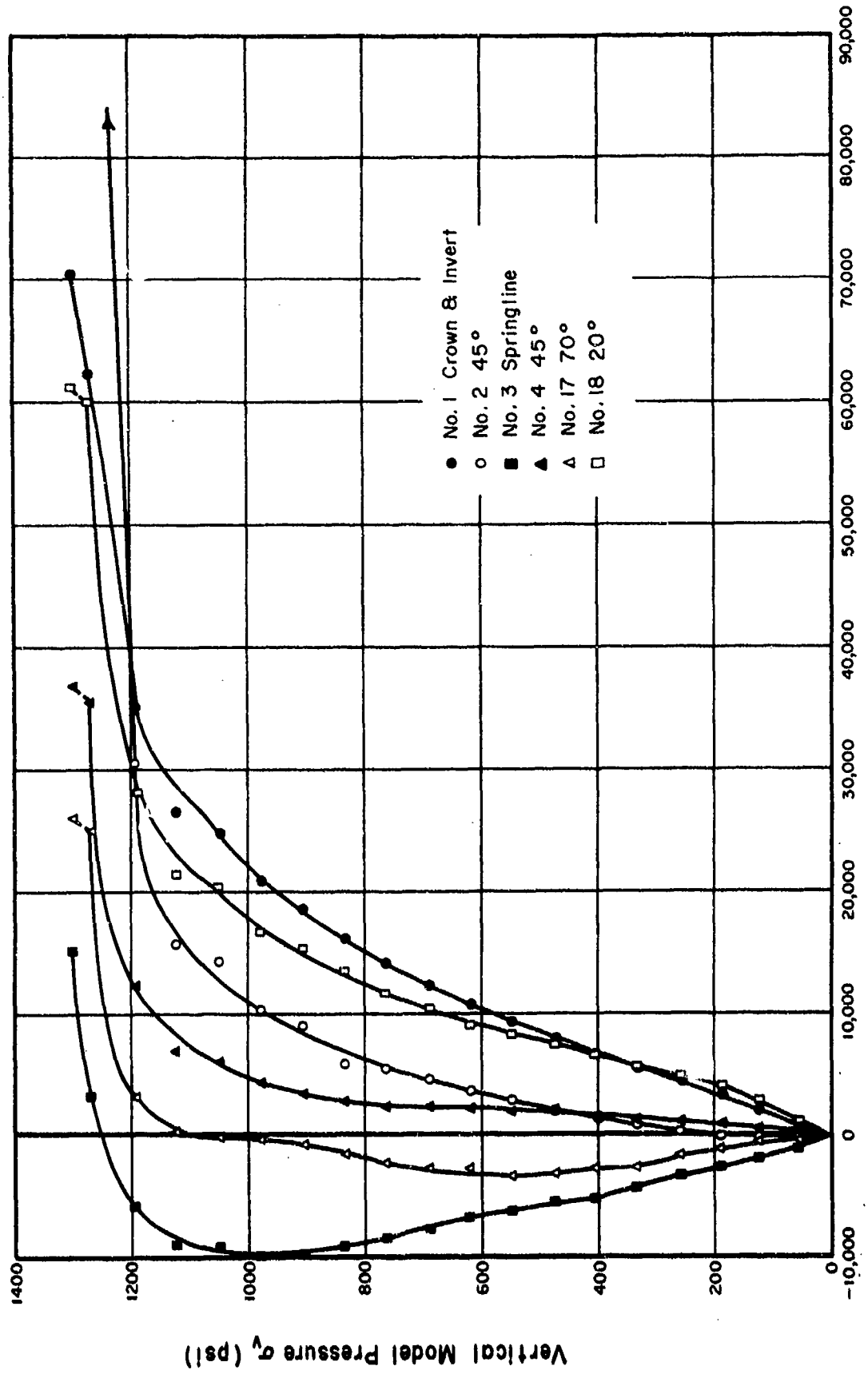

FIG. 67 DIAMETRICAL STRAINS OF LINER AS A FUNCTION OF VERTICAL MODEL PRESSURE FOR JOINT BLOCK # 4

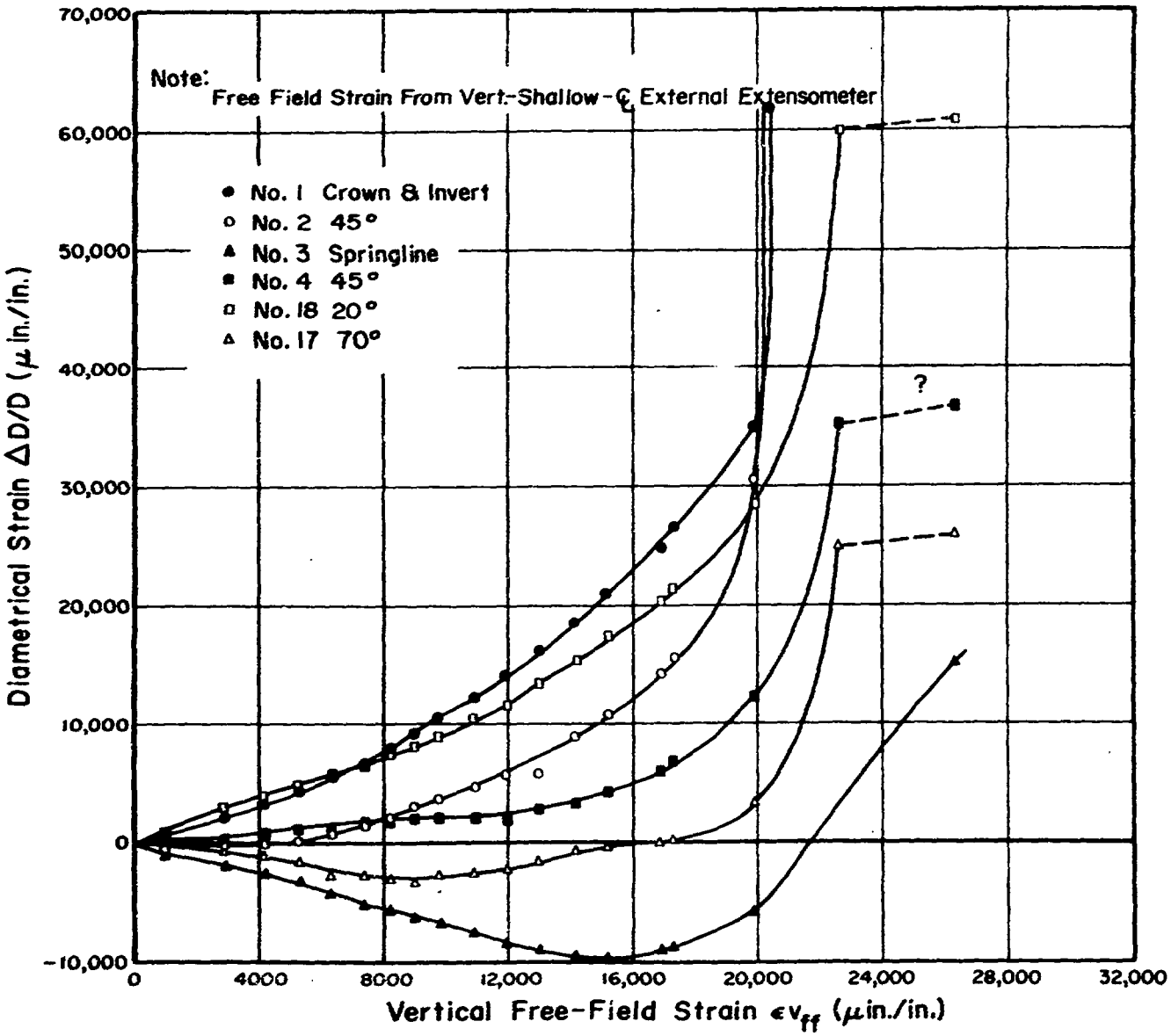

FIG. 68 DIAMETRICAL STRAIN OF LINER AS A FUNCTION OF VERTICAL FREE-FIELD STRAIN FOR JOINT BLOCK #4

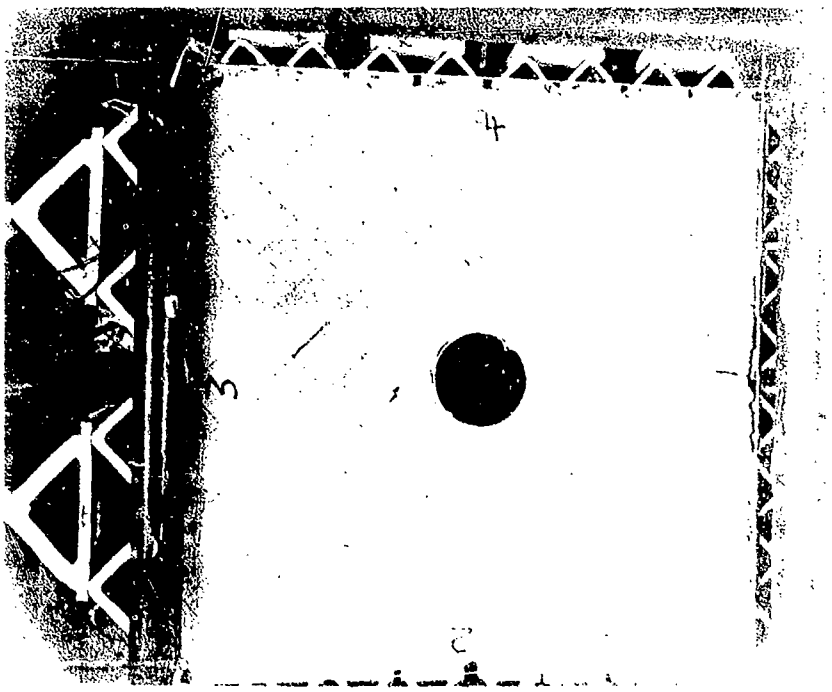

(a) View of whole model after test at N = 2/3

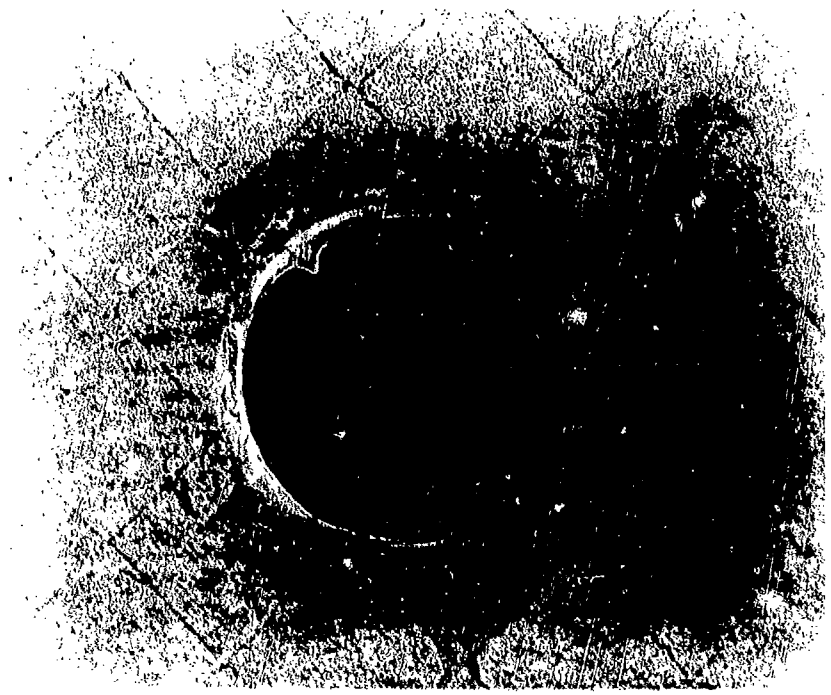

(b) Closeup of tunnel liner after test at N = 2/3

Fig. 69 Photographs of JB #4

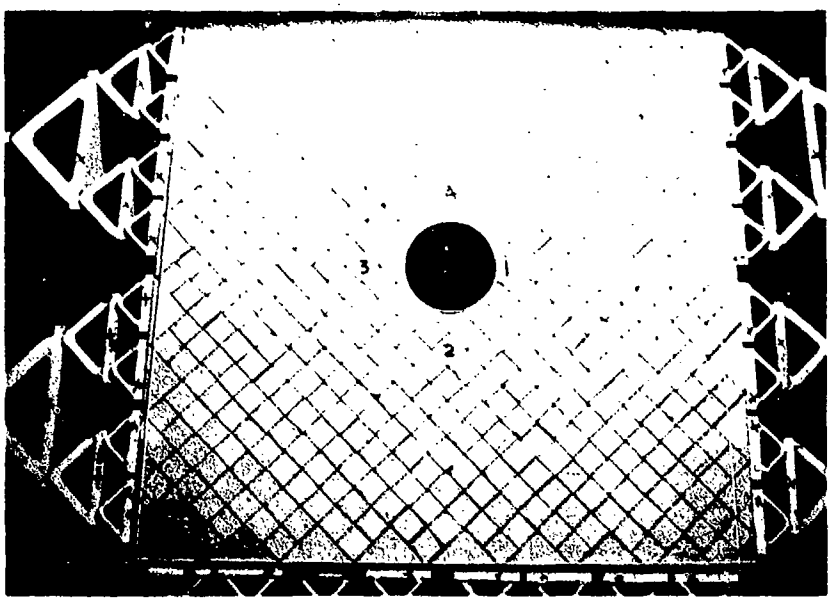

(a) Before test at $N = \sigma_H/\sigma_V = 2/3$

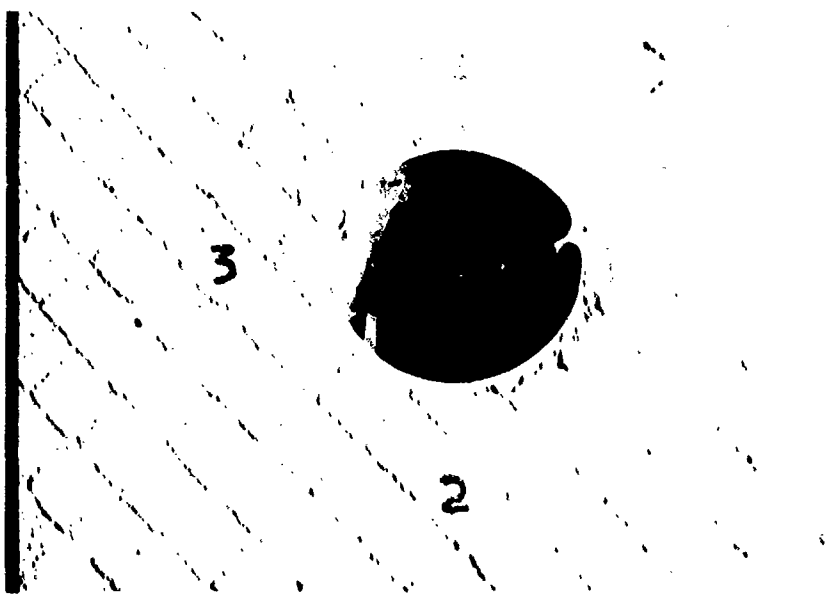

(b) After test at $N = \sigma_H/\sigma_V = 2/3$

Fig. 70 Photographs of JB#5

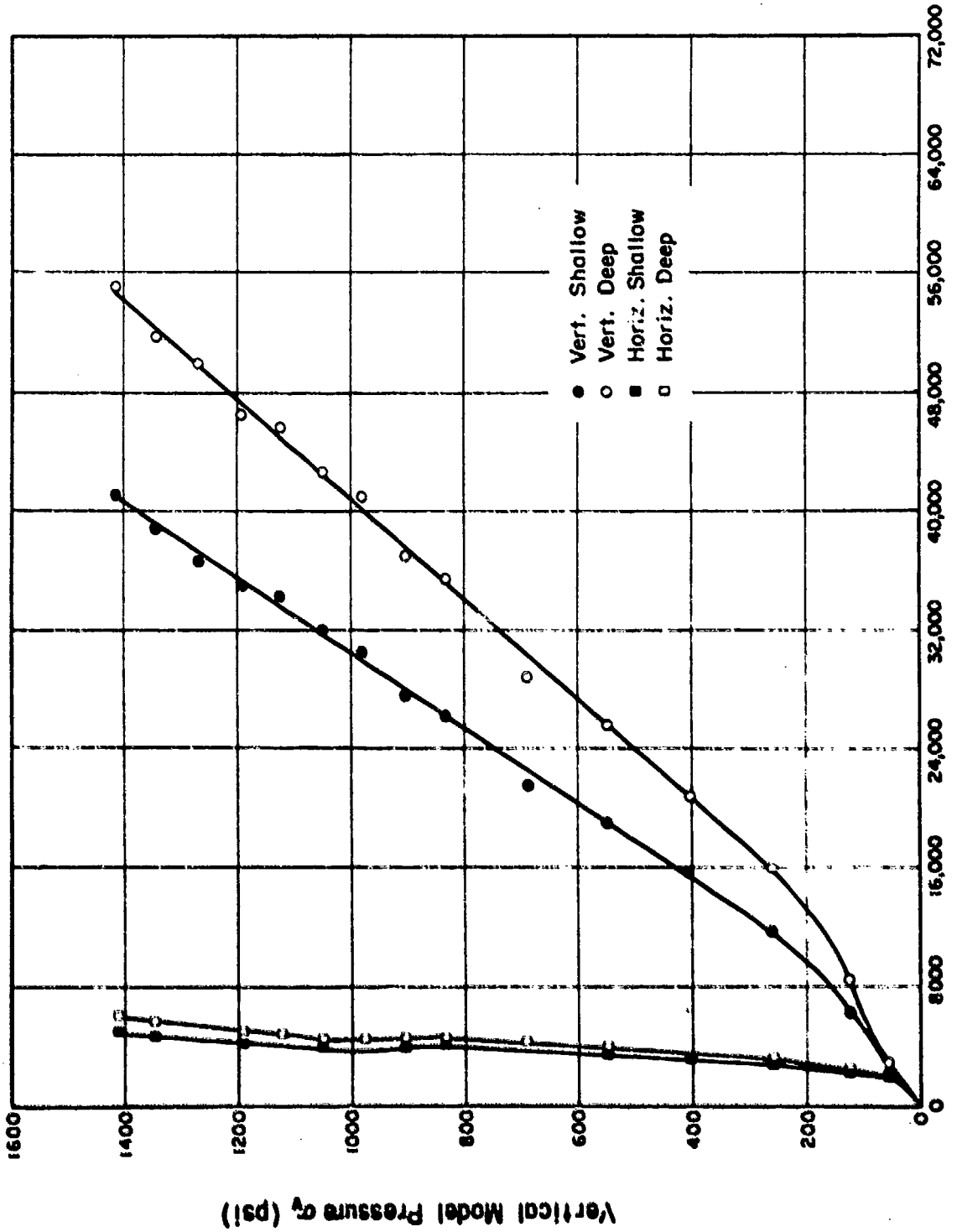

FIG. 71 AVERAGE STRESS-STRAIN CURVES IN JOINT BLOCK #5

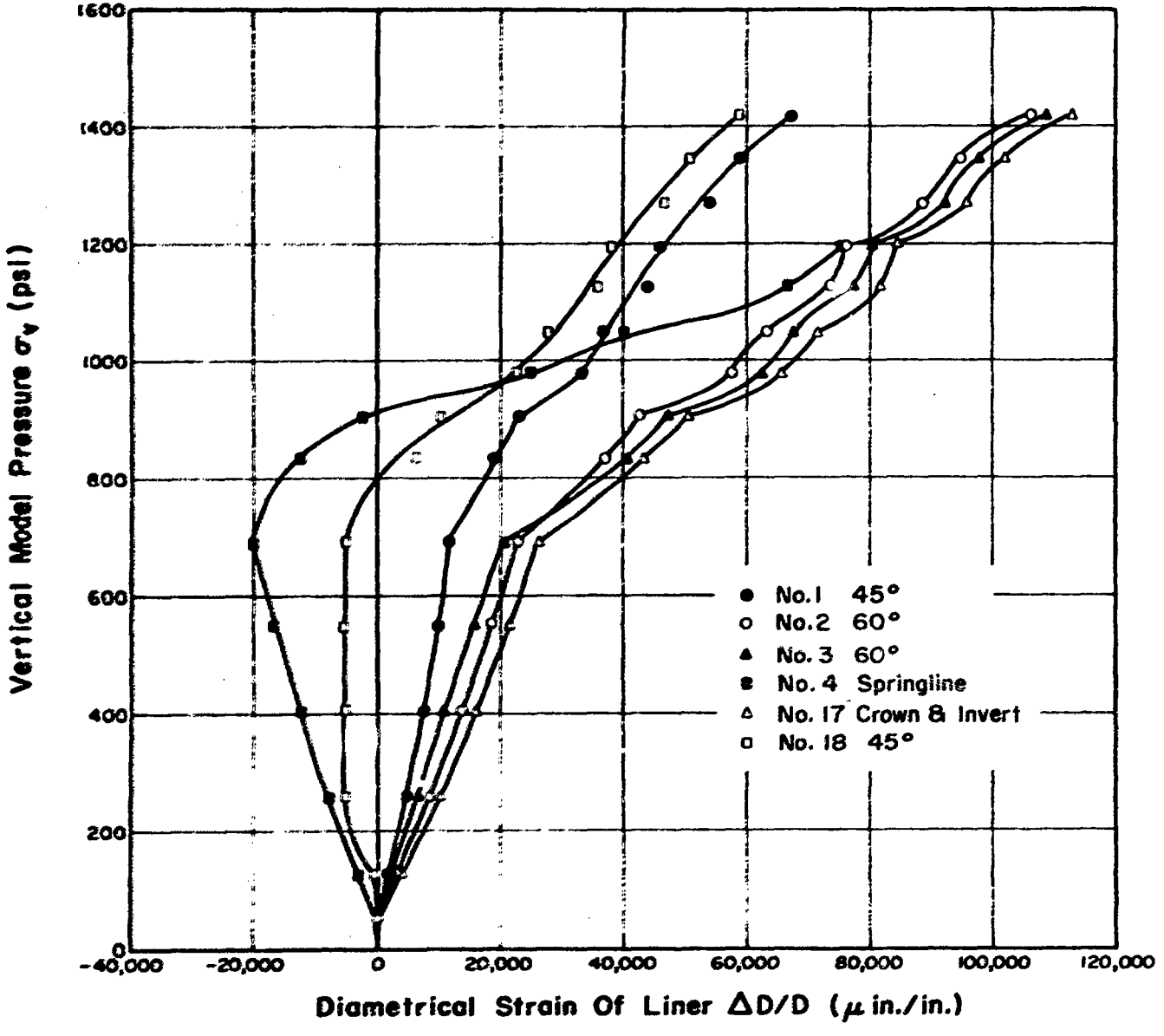

FIG. 72 DIAMETRICAL STRAIN OF LINER AS A FUNCTION OF VERTICAL MODEL PRESSURE FOR JOINT BLOCK #5

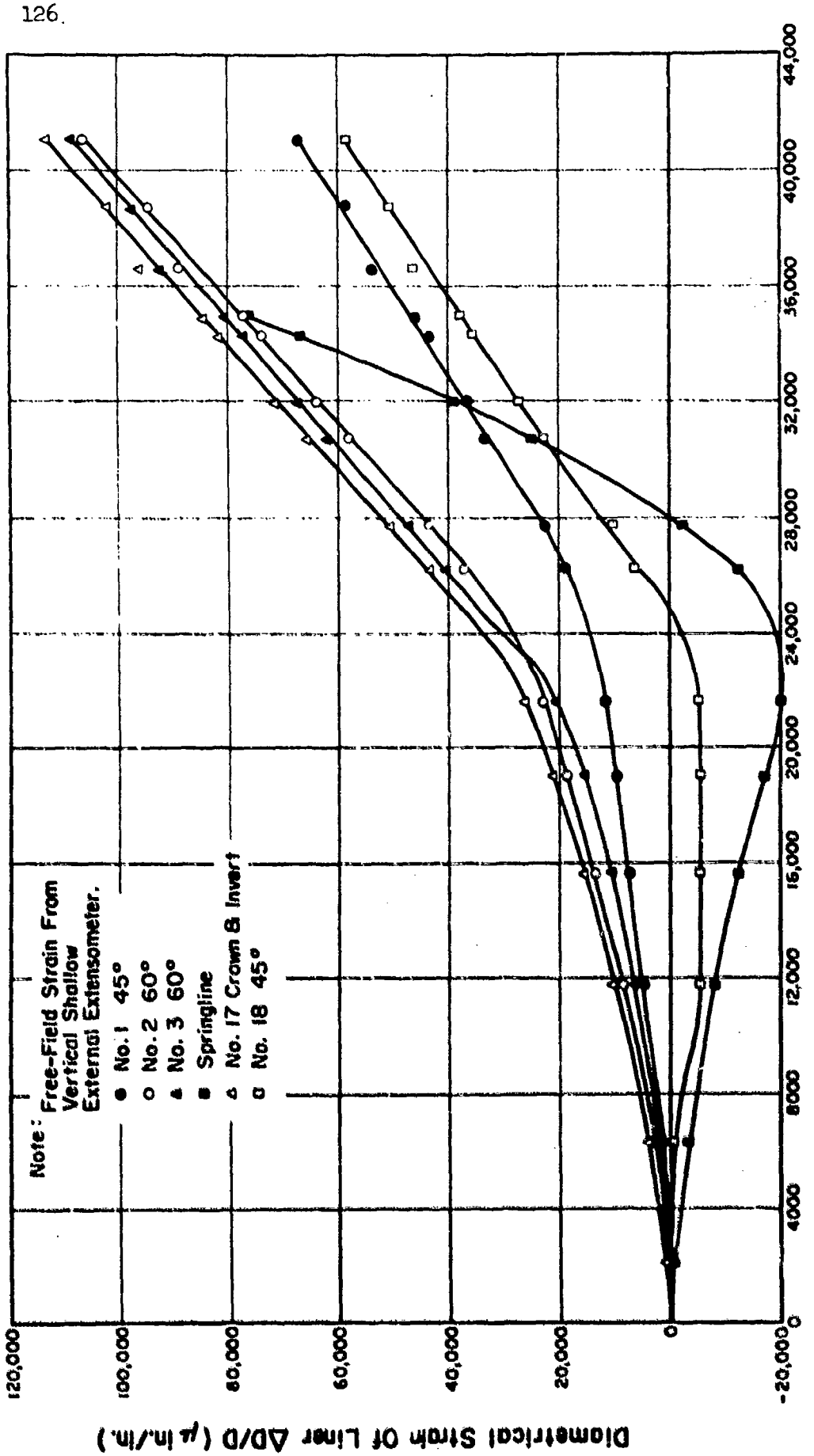

FIG. 73 DIAMETRICAL STRAIN OF LINER AS A FUNCTION OF VERTICAL FREE-FIELD STRAIN FOR JOINT BLOCK #5

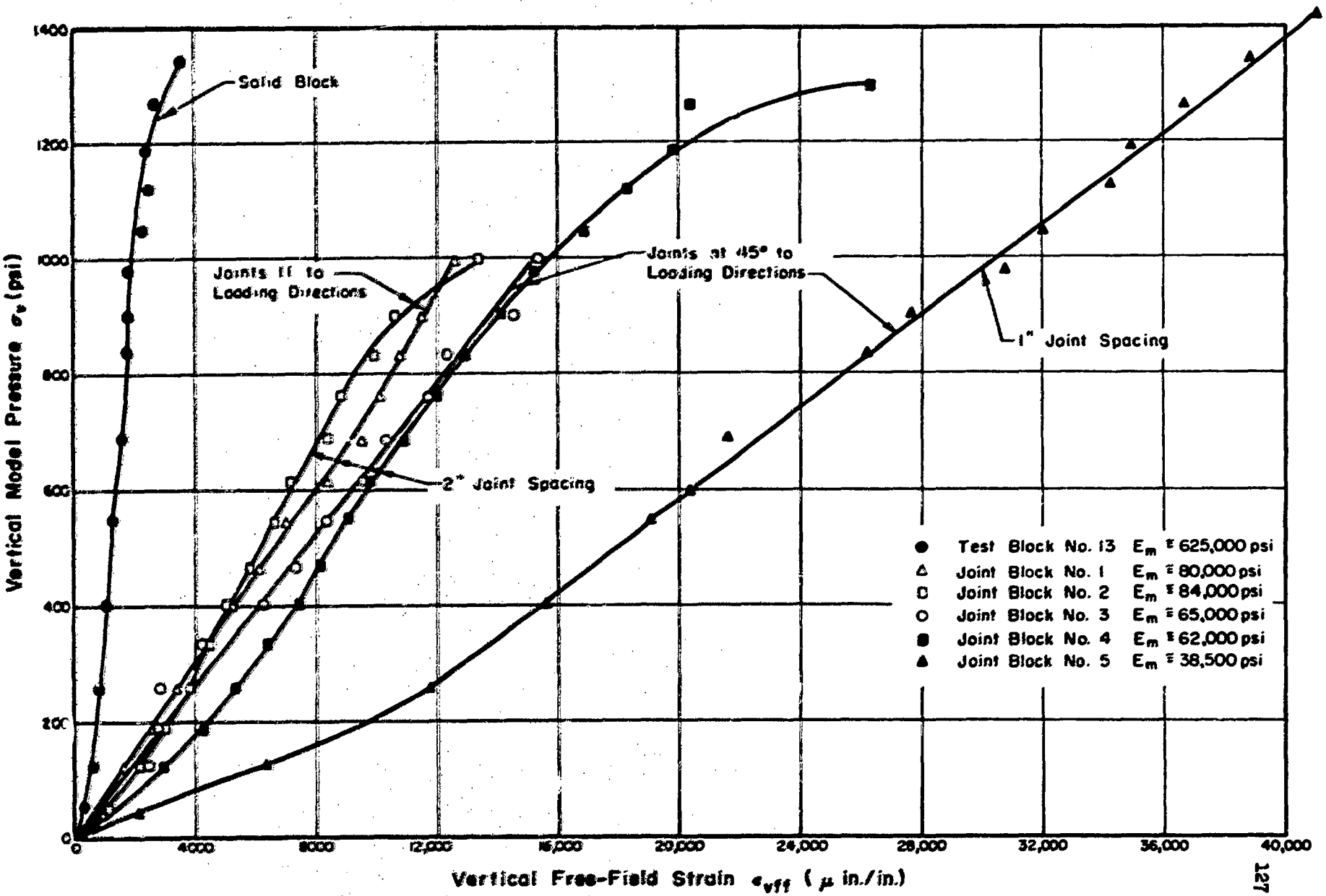

FIG. 74 VERTICAL FREE-FIELD STRESS—STRAIN CURVES FOR VARIOUS TEST BLOCKS

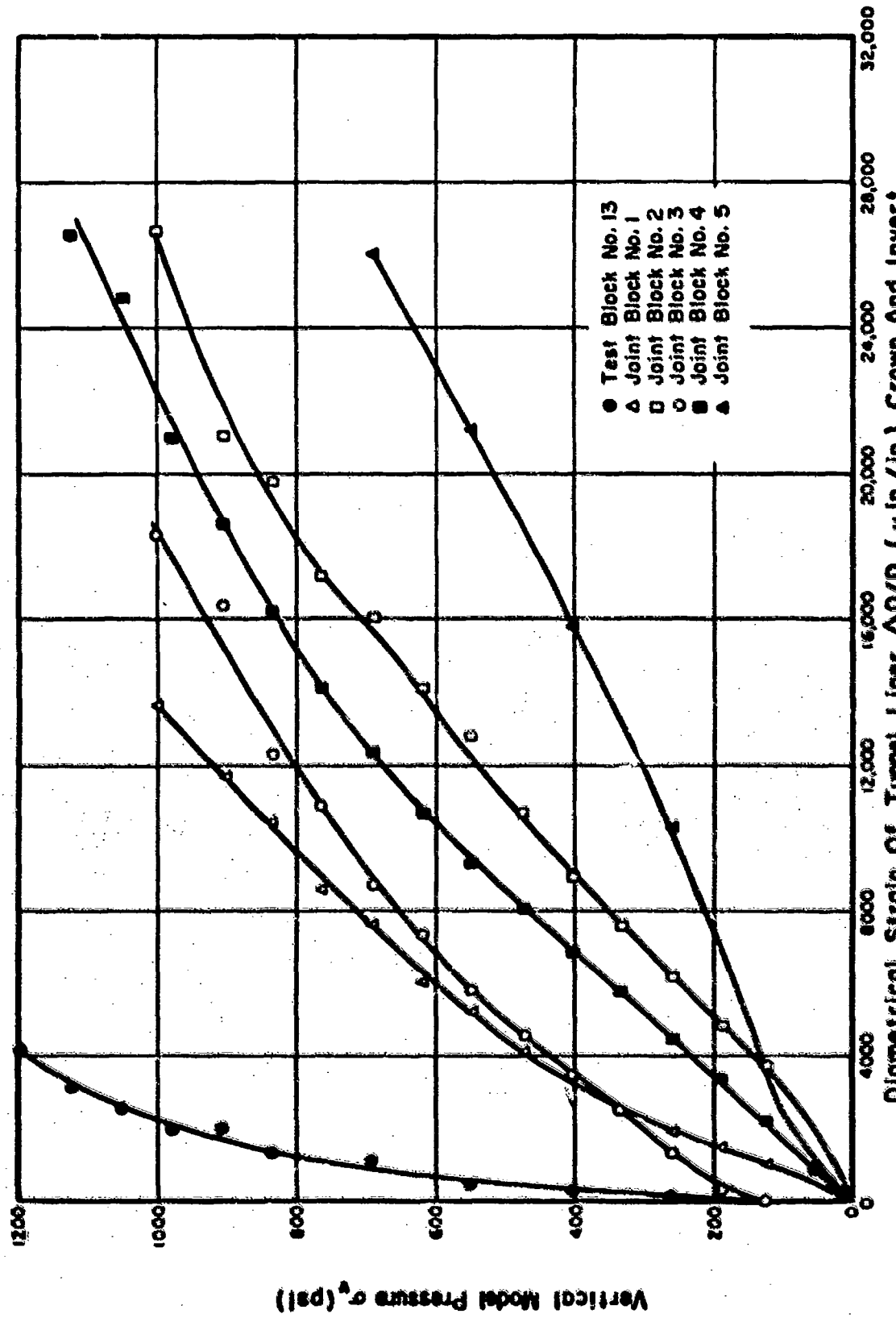

FIG. 75 DIAMETRICAL STRAIN OF LINER AT CROWN AND INVERT AS A FUNCTION OF VERTICAL MODEL PRESSURE FOR VARIOUS TEST BLOCKS

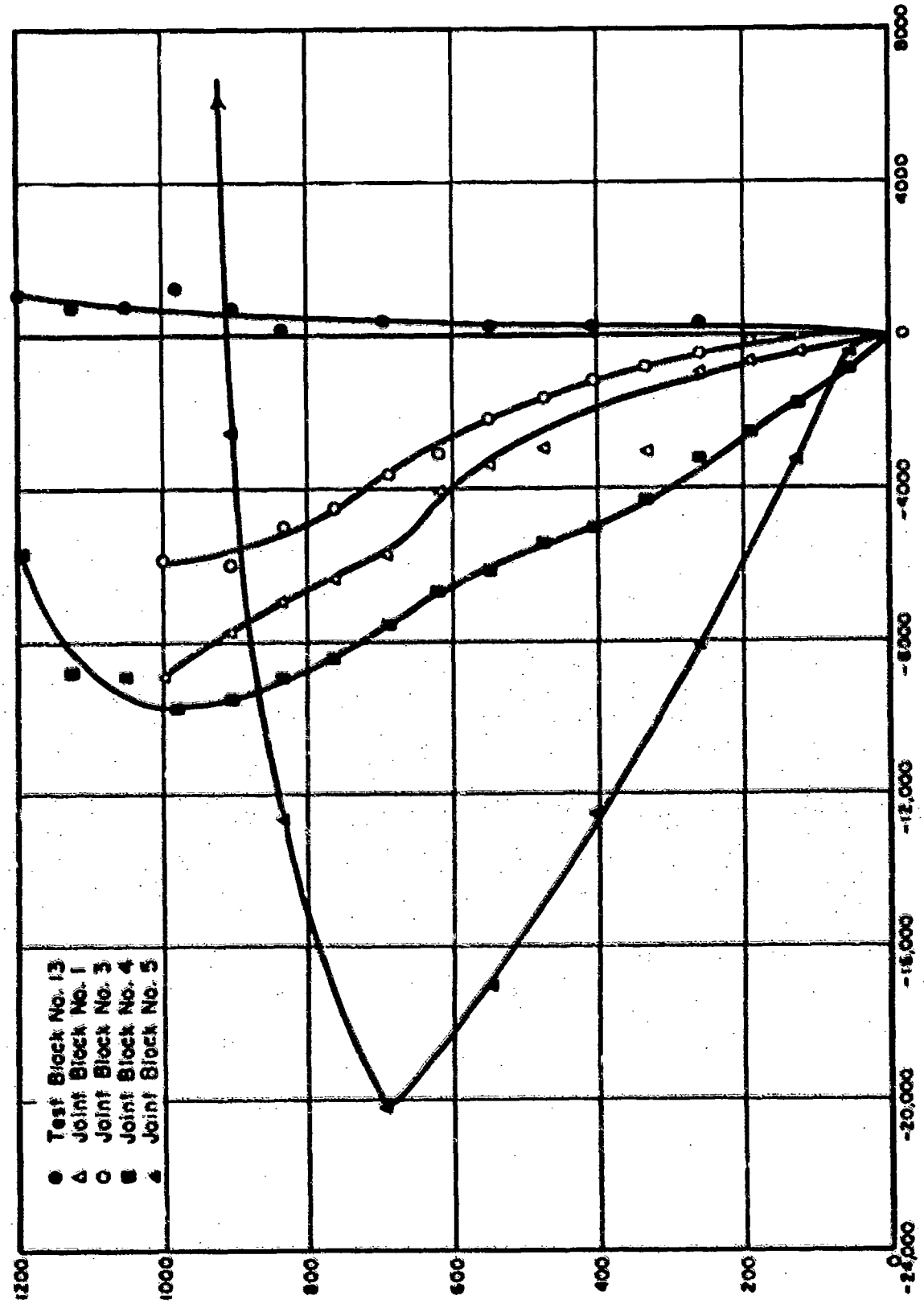

FIG. 76 DIAMETRICAL STRAIN OF LINER AT SPRINGLINE AS A FUNCTION OF VERTICAL MODEL PRESSURE FOR VARIOUS TEST BLOCKS

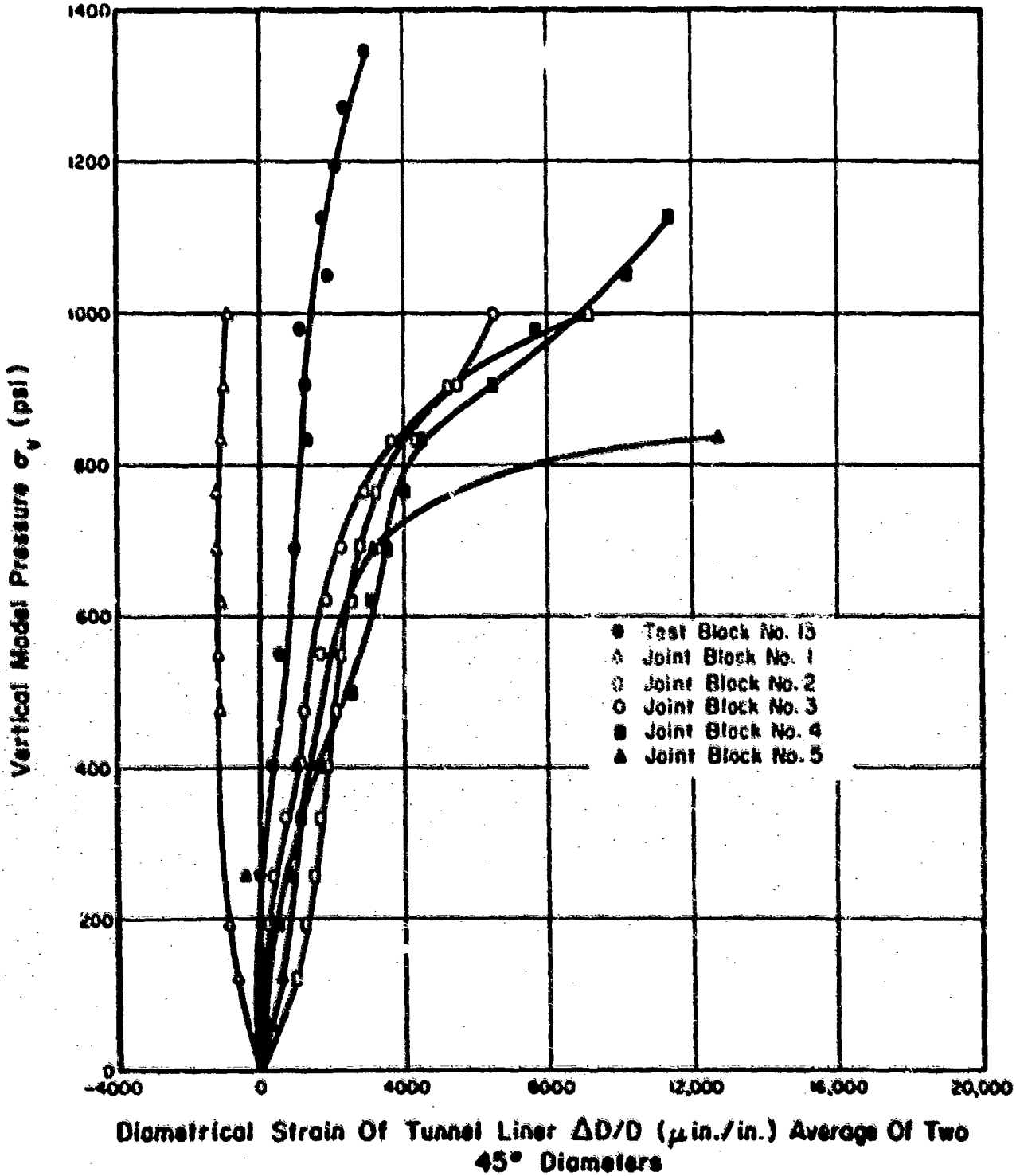

FIG. 77 AVERAGE OF TWO DIAMETRICAL STRAINS OF LINER AT 45° SECTIONS AS A FUNCTION OF THE VERTICAL MODEL PRESSURE

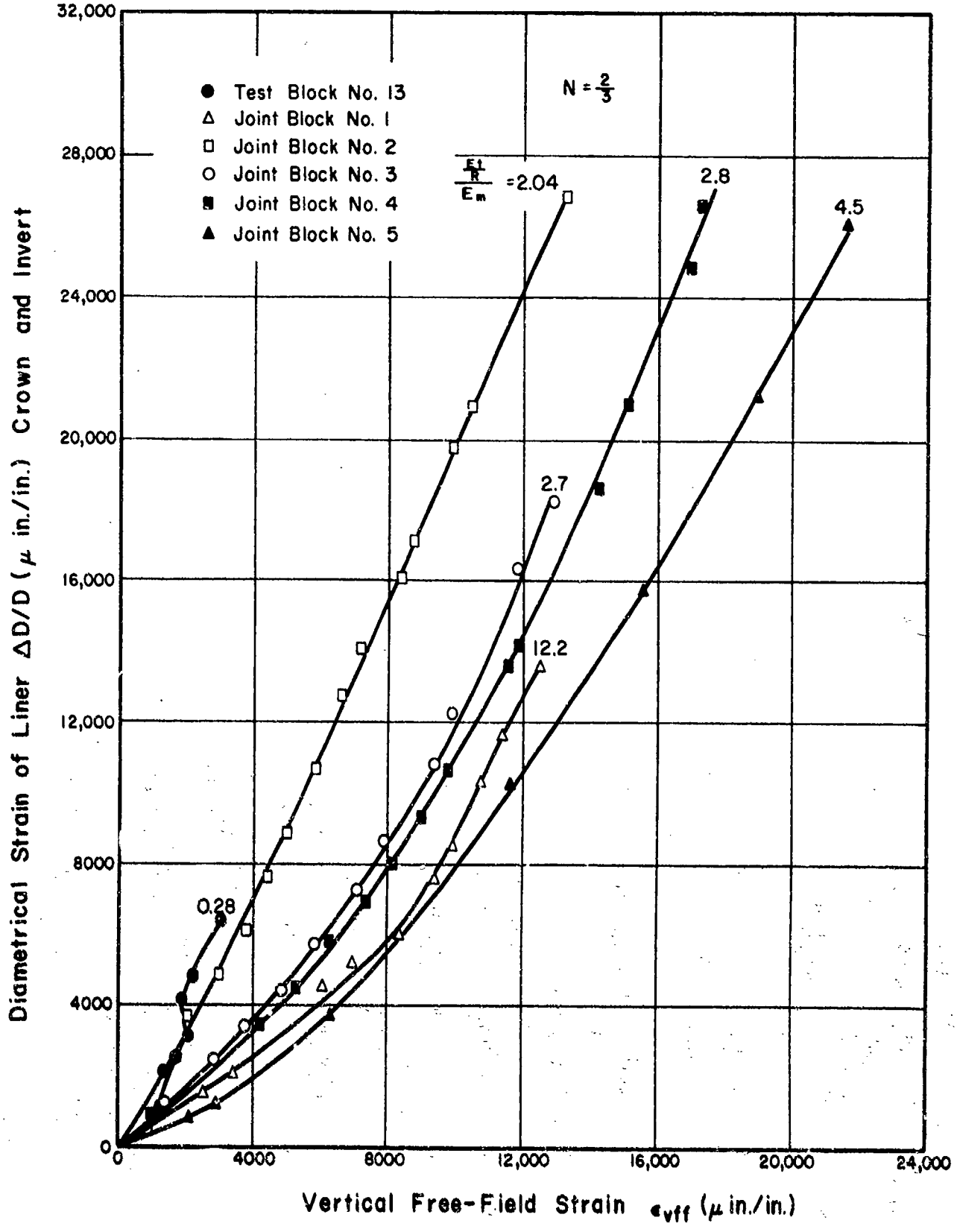

FIG. 78 DIAMETRICAL STRAIN OF LINER AT CROWN AND INVERT AS A FUNCTION OF VERTICAL FREE-FIELD STRAIN FOR VARIOUS TEST BLOCKS

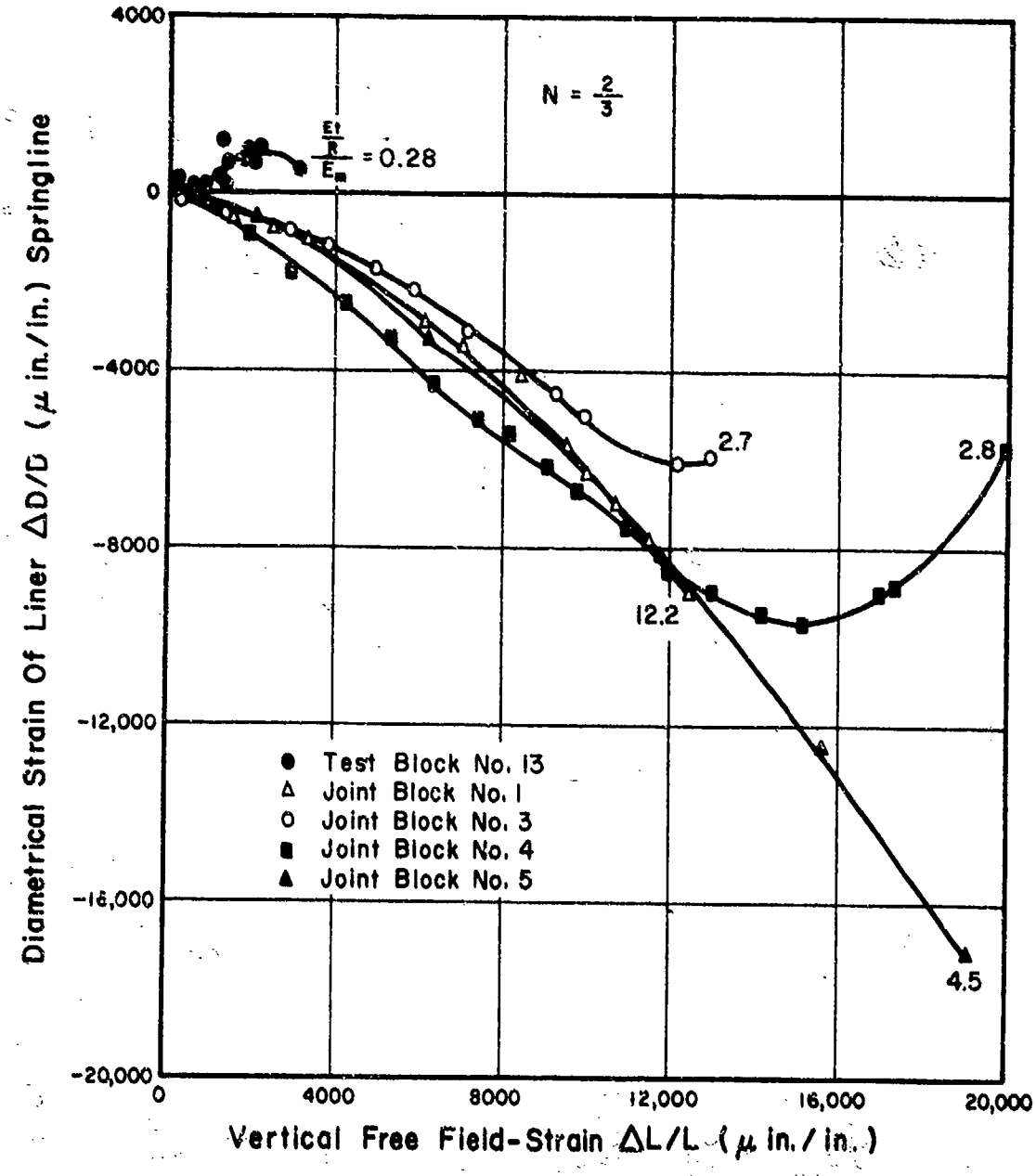

FIG. 79 DIAMETRICAL STRAIN OF LINER AT SPRINGLINE AS A FUNCTION OF VERTICAL FREE-FIELD STRAIN FOR VARIOUS TEST BLOCKS

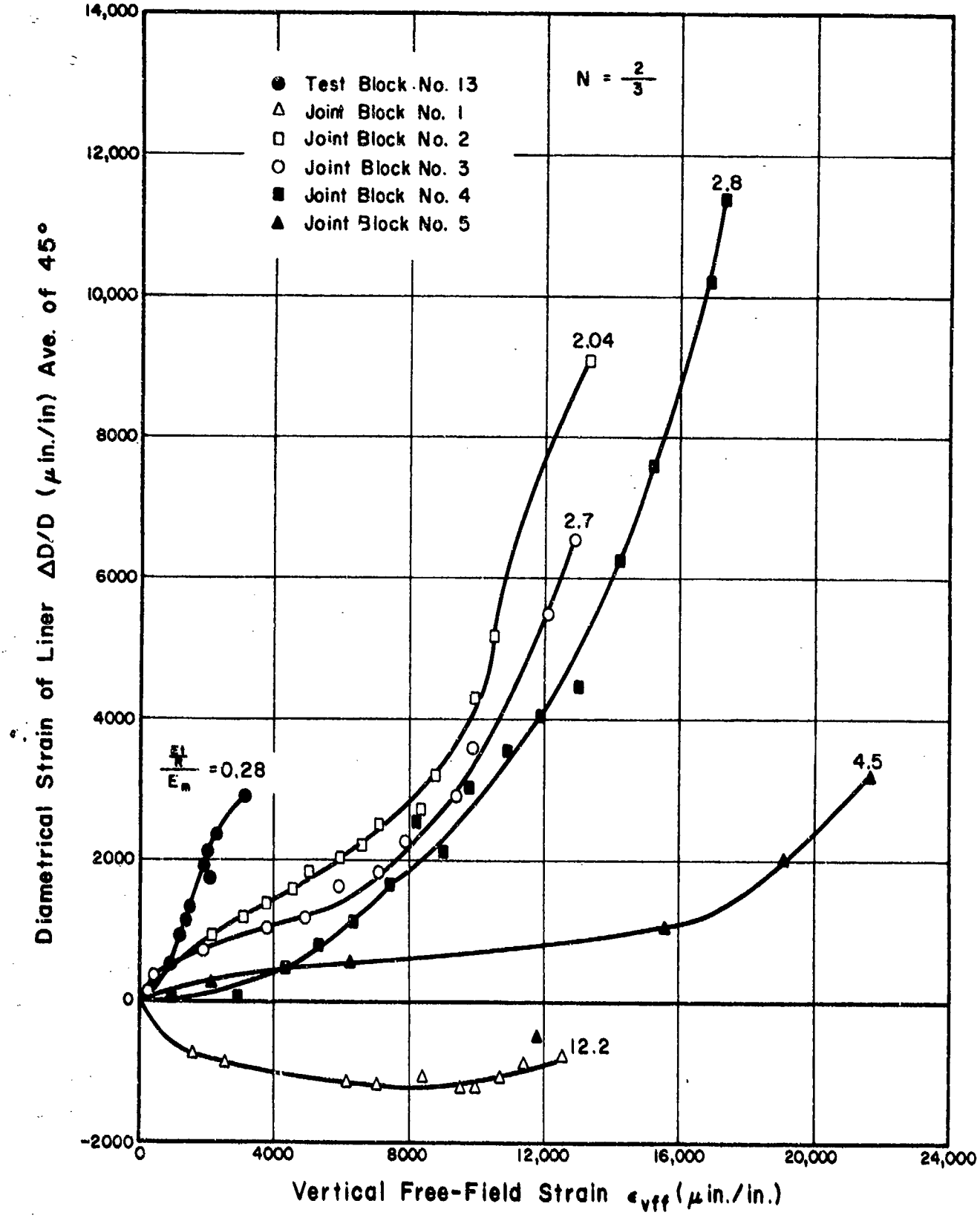

FIG. 80 AVERAGE DIAMETRICAL STRAIN OF LINER AT 45° AS A FUNCTION OF VERTICAL FREE-FIELD STRAIN FOR VARIOUS TEST BLOCKS

APPENDIX A

TESTS OF VERTICAL OPENINGS IN MODEL ROCK

by S. L. Paul and J. F. Thibeaux

A.1 Introduction

The major portion of this project has been concerned with the investigation of behavior of model rock material around openings which represent horizontal tunnels in real rock. In connection with this work two tests were performed to investigate the effectiveness of testing model rock specimens with a different opening orientation, specimen confinement, and loading arrangement from that used in the main program. In these two tests the prototype to be simulated was a vertically oriented cylindrical opening with the top of the opening at the surface. The loading applied was a static uniform hydraulic pressure on the specimen surface, to simulate a uniform surface pressure resulting from a blast loading.

In the first test the opening was unlined while in the second test a thin aluminum lining was grouted into the opening. The surface pressure applied to the cover over the opening was resisted by a steel plate which fit into the top of the openirg, and the resulting force was carried by a steel rod through the opening to a support at the bottom of the specimen.

The model rock specimen was cylindrical in shape with a diameter of 24 in. and a length of 24 in. The cylindrical opening was 4 in. in diameter along the axis and through the full length of the specimen (Fig. A.1). The hydraulic surface pressure was applied to one end of the cylindrical specimen.

A prototype opening of this type would be constructed in a rather large rock mass and the surface pressure would be applied to an area that is large relative to the area of the opening at the surface. The rock mass around the opening is thus restrained from horizontal movement. To simulate this

confinement the model rock must be restrained in the direction perpendicular to the axis of the opening. This was accomplished by grouting the specimen into a cylindrical steel container which was quite stiff relative to the model rock specimen. The container was constructed of a 24 in. long steel pipe with 24 in. inside diameter and one in. thick walls. It was further stiffened by 4 in. by 5 in. flanges around each end of the pipe section (Fig. A.1). Steel plates were bolted to the flanges over the ends of the pipe section to complete the enclosure. The effectiveness of this method of simulating the confinement will be discussed in a later section.

The size of model rock specimen and opening were chosen on the basis of the same reasoning used to make this decision in the main testing program. This reasoning is discussed in Reference (1), and depends on the distance from the opening that the free field stress is materially disturbed by the presence of the opening. This distance was chosen on the basis of theoretical solutions for stresses around a cylindrical opening based on elastic and elastic-plastic Columb-Navier material behavior. In the vertical opening orientation the free-field stresses perpendicular to the opening axis result from the Poisson effect due to the loading on the free surface. In both solutions the radial and tangential stresses approach rather closely a constant value at 5 opening radii from the side of the opening (Reference 1, p. 147). This distance corresponds to a ratio of radius of specimen to radius of opening of 6, which was chosen for these tests. The diameter of opening of 4 in. was then selected to conform to this ratio as the specimens diameter was fixed by the 24 in. diameter of the existing confining tank.

The material chosen to model the rock medium was the same one used in the main research program and is described in Reference (1). This material

was carefully designed to satisfy certain requirements of similarity between the model material and real rock. The similitude requirements for the vertically oriented opening are the same as those for the horizontal tunnel, though the relative importance of each parameter describing the two problems may be different.

The model material was not chosen to be similar to a particular rock type. The variation in properties between rock types is so great that such exactness is not justified. It was chosen, however, so that those parameters describing the model material fall in the range of values found for most rock types.

The model rock specimens were prepared by tamping the model material into molds which were circular in shape 23-1/2 in. in inside diameter and 8 in. in depth. After drying, a 4 in. hole was cored along the axis of each cylindrical block. Three blocks were bonded together to make the specimen. For testing, the specimens were grouted into the steel container to assure maximum confinement possible. The liner was grouted into the opening of the second specimen before it was placed into the container.

Surface pressure on the specimen and strains on the outer wall of the steel container were measured, to help define the boundary conditions on the top and sides of the specimen. There was some outward movement of the tank walls as well as vertical shear between the tank and model rock specimen. An estimate of these quantities is possible from the strain measurements though the added stiffness of the flanges at each end of the tank has an unknown effect on the strain measurements.

Strains were measured on the walls of the 4 in. opening and on the aluminum liner in the second test. Radial and circumferential strains were measured within the specimen by bonding gages to the top of the middle

8 in. cylindrical block before they were bonded together to make the complete specimen. The resulting measurements 8 in. below the top surface, gave the distribution of circumferential and longitudinal strain with radius from the opening. The diameter change of the lined and unlined openings was measured at 6 levels.

The test was performed by applying a hydraulic pressure in increments to the top surface of the specimen with an air-to-hydraulic booster pump. At each pressure increment the strain gages and deflection gages were read. The test in which the opening was unlined, progressed until a shear failure occurred in the model rock material at the top of the opening which forced a triangular block of material into the opening. This failure occurred at a surface pressure of 700 psi. The lined-tunnel test progressed to a surface pressure of 1000 psi when a failure in the neoprene membrane over the surface of the specimen caused a loss of pressure. The membrane was replaced and the specimen was pressurized a second time to 1200 psi when the membrane failed again. A third pressurization reached 600 psi and a fourth reached 1800 psi before the membrane failed. In a fifth pressurization, a sheet metal ring was placed around the top of the tank under the membrane to prevent the edge of the tank from damaging the membrane. The metal ring extended out from the edge of the speciman approximately 1.0 in. This test proceeded to 2500 psi at which time the O-ring between the top plate and tank flange failed. Failure of the model rock around the opening did not occur. A longitudinal buckle was observed about midheight in the liner after the fifth test, however.

In Section 2 the preparation of the test specimens and the testing arrangement will be discussed. The test results will be presented and discussed in Section 3. A summary of the results and recommendations for future studies will appear in Section 4.

A.2 Specimen Preparation and Test Arrangement

The geomechanical model used in the tests was a 24 in. diameter by 24 in. high cylinder made of a compacted plaster of paris-sand mixture. For ease of handling and instrumentation, the model was compacted in three 8 in. high x 24 in. diameter blocks. A 4-in. diameter opening was cored along the axis of each cylindrical block. Strain gages were mounted directly on the end of one block of model material. The three blocks were then joined together with epoxy to make a 24 in. long cylinder of material with a 4 in. diameter opening through the center. After assembly, the entire model was lowered into the confining tank and grouted into place. (Fig. A.1). Hydrostatic pressure was applied to the top surface of the model. There were two tests conducted: in the first the 4 in. opening was unlined; in the second the opening was lined with an aluminum tube grouted in place.

Earlier work by Heuer reported in Reference (1) showed that in order to satisfy similitude considerations, the stress-strain properties of the model material should be similar to those of the insite rock. After testing a number of materials, Heuer concluded that a compacted mixture of sand and plaster of paris would satisfy the similitude requirements. He found that the proportions by weight of water/plaster of paris/fine sangamon sand/Na_2HPO_4 should be 1.2/1.0/9.0/0.01.

This mixture was compacted in 23 1/2 in. diameter x 8 in. high molds with a pneumatic chipping hammer operating at 100 psi air pressure and equipped with a 64 sq. in. foot. The amount of compactive effort could be controlled by the amount of force applied to the chipping hammer and length of time a given area was compacted. This procedure yielded a block with an average

dry density of 1.84 gm/cc with a variation of less than 2%. Heuer achieved a density of 1.82 gm/cc using the same compaction procedure and mix proportions (Ref. 1).

After compaction, the blocks, still in the molds, were placed in the oven and dried at 105°F. The blocks were weighed periodically and the drying curves are shown in Fig. A.2. After about 200 hours in the oven, the blocks were removed and taken from the molds. Very little of the material adhered to the molds, which had been coated with oil before compaction.

In order to measure strains in the model material, SR4 electrical resistance strain gages (BLH, type A-1) were placed directly on the end of one block for each specimen following procedures developed by Heuer and described in Reference (1). The gage locations were coated with Duco cement diluted with acetone (1:1 by weight) and allowed to dry for 24 hours. The gages were then bonded on the dilute Duco cement sub-base with Eastman 910 adhesive. The location and orientation of these gages are shown in Fig. A.3 for the unlined opening test and in Fig. A.4 for the lined opening test.

In addition to strains in the material itself, the deformation of the opening walls and tank walls were measured. For both tests clip gages were used to measure diameter changes of the opening. These gages are C-shaped strips of beryllium-copper with strain gages mounted on them and calibrated to correlate strain readings with movement or closing of the C shape. The location of these gages for both tests are shown in Figs. A.3 and A.4. In addition to the clip gages, strain gages were placed directly on the wall of the opening (Fig. A.3) or on the liner (Fig. A.5). Strains on the wall of the confining vessel were measured by

four FAER rosettes placed at mid-height on the outside surface.

An attempt was made in the lined opening test to determine the effect of the epoxy joint on the A-1 gages between blocks. Some of the gages were set in 1/16 in. grooves and covered with teflon (Fig. A.4). Others were placed in a groove but with no teflon cover. To minimize the possibility of damage when the blocks were epoxied together, the leads from the strain gages were cemented with Duco cement into shallow slots leading from the gage to the opening.

After the strain gages were placed, the three blocks comprising the specimen were bonded together with a mixture of Armstrong A-35 adhesive (proportions Part B/Part A of 2/1). The epoxy was allowed to cure for three days. The opening cover plate (Fig. A.1) was placed and the entire model was lowered into the confining tank and grouted in place with Sulfaset. For the lined opening test the aluminum liner was grouted into the opening with Sulfaset before placing the specimen into the confining vessel.

A neoprene membrane was used to seal the pressure chamber from the top of the specimen. Since differential movement between the opening cover plate and the top surface of the model rock specimen was expected when pressure was applied, a 1/16-in. thick x 8 in. diameter cushion of neoprene was placed between the cover plate and neoprene membrane. The confining tank cover was bolted into place with 25 1-1/4 in. A 325 bolts.

The strain gage circuits consisted of two arm bridges for the A-1 gages, tank rosettes, and opening liner gages and four arm bridges for the clip gages. For the two arm bridges, a compensating gage was used for each gage type. This was possible because the model material could dissipate heat quickly enough to avoid significant error due to heat buildup (Ref. 1). For the unlined opening test the gages were manually switched and strains were read with a portable strain indicator. For the lined opening

test automatic switching and balancing equipment was used for all the gages except the clip gages. This equipment also had automatic printing equipment. The clip gages were read with a portable strain indicator as in the previous test.

Hydrostatic pressure was applied to the surface of the test specimen with a Haskel air to hydraulic booster pump. The air was removed from the pressure chamber before applying oil pressure.

A.3 Discussion of Experimental Results

A.3.1 Test With Unlined Opening

The unlined opening test proceeded to failure which occurred when a section of the model rock at the top of the opening sheared off and was forced into the opening at a surface pressure of 700 psi. A photograph of the failure and a drawing of the dimension of surface are shown in Fig. A.6. The failure surface intersected the opening wall about 2.25 in. below the surface and made an angle with the vertical of about 31°. This angle corresponds to the angle of internal friction reported for the model material.

Strains were measured at midheight on the wall of the confining tank to help in assessing the effects of the boundary conditions on the sides of the specimen. Figure A.7 shows the measured strains plotted against surface pressure and the corresponding stresses in the wall computed from these strains. The strains may be influenced by the presence of the flanges which are 8 in. from the gages or about 8 times the thickness of the tank wall. The strains should give at least a reasonable indication of the stresses in the tank wall.

Figure A.8 shows the average shear stress between the upper 12 in. of the confining tank wall and the model rock specimen computed from the stresses of Fig. A.7. This graph shows that the shear stress was quite small up to a surface pressure of approximately 140 psi after which it varies approximately in a linear manner reaching 135 psi at a surface pressure of 700 psi. The shear stress actually occurs between the steel wall of the tank and the Sulfaset that was used to grout the specimen into the container. Though the container wall was oiled before the specimen was placed, the shear stress is still significant;

the ratio of shear stress to surface pressure increases from about 0.05 at a surface pressure of 200 psi to 0.19 at 700 psi. The change in slope at about 150 psi surface pressure for the shear stress probably indicates that the cohesion between the tank wall specimen is broken and the shear then results from friction. Figure A.9 shows the lateral pressure exerted by the model rock specimen on the confining tank wall at midheight of the tank computed from the measured strains and plotted against surface pressure. The lateral pressure varies almost linearly with surface pressure above 200 psi and the ratio of lateral pressure to surface pressure varies from about 0.12 at a surface pressure of 250 psi to about 0.2 at 700 psi.

A significant factor in assessing the test results is the effect of the boundaries at the tank wall on the model rock behavior near the opening. The lateral movement of the wall is small. The maximum circumferential strain is about 40μ which corresponds to a radial movement of the wall on the order of 0.0005 in. This movement was much less near the bottom and top of the specimen where the tank was stiffened by the flanges. The shear between the tank wall and specimen is rather large and the distance into the model rock specimen that the influence of this shear extends is important.

The strains measured on a plane 8 in. below the top surface of the specimen are shown in Figs. A.10 to A.15. This plane corresponds to the joint between the top and middle blocks of the assembled specimen and therefore also contains the epoxy used to join the blocks. This epoxy is somewhat stiffer than the model material, but the thickness was rather small so the joint was probably not appreciably stronger than the material, and it

are tensile near the opening and decrease with increasing radius to a radius of about 4 in. and then increase again. This strain could result from an outward particle displacement for a radius greater than 4 in. as indicated by the circumferential strains.

The circumferential strains measured on each radius in Fig. A.11 are fairly consistent in that the curves are smooth, but there is a large range in magnitude of strain on the three radii. The radial strains do not have much scatter and in fact the values were so close that they were averaged where more than one gage occurred at a given radius, and it is the average that is shown in Fig. A.13 The scatter in the strain measurements was probably caused by nonhomogeniety of the specimen which allowed a nonsymmetrical deformation. The circumferential strains are more sensitive to nonsymmetrical radial deformation because they are proportional to the radial displacement while the radial strains are equal to the rate of change of the displacement which is not varying rapidly.

This discussion has been based on the assumption that the electrical strain gages give an accurate indication of the average strain over their gage length when applied within the material. In Reference (1) tests are reported in which gages are mounted on the surface and inside test cylinders which were subjected to triaxial tests. It was concluded from these tests that the strain gages do give reasonably accurate readings. The conditions under which the gages operate in these tests are somewhat different from those investigated in Reference (1), but not so different that the conclusion drawn there cannot be applied, with reservations, to these tests. In the second test of a lined opening an additional diametral set of gages was placed within the material with a different method of protecting the gages, to see

if any difference could be detected. These results will be discussed in the next section.

Errors in electrical strain gage readings within the material would occur if the gage within the material is deformed under pressure to conform to an irregular surface on which it is mounted. It is to avoid this that the gages were mounted on a base of Duco cement which forms a smooth surface for the gage and it is mounted with Eastman 910 cement under pressure to make it conform initially to the surface. This method should help to avoid the problem, but under very high normal pressure there is likely to be some deformation of the Duco cement and consequent deformation of the gage. The resulting error should always be a tensile strain, should be approximately the same for all gages within the material and should not occur for gages mounted on the surface within the opening. This phenomenon does not explain the unexpected behavior of the radial strains in Fig. A.13 however, because the shape of the curves should remain the same and have a uniform tension superimposed on them. Instead the shape is changed as would occur if the shear along the boundary of the specimen reduced the vertical stress near the wall.

Figures A.14 and A.15 show the variation of circumferential and longitudinal strains measured on the wall of the opening versus surface pressure at various depths below the surface. The divergence of the curves is of some concern since the gages with a given orientation should measure the same strain if conditions of symmetry and homogeniety exist and the model represents a mass of rock infinite in extent as desired. If the difference in strain with depth results from the shear between the model

material and the tank wall, the divergence in strain should increase with depth as the shear force builds up along the wall. This is not the case, and in fact the smallest and largest strains appear to occur at 2 in. and 4 in in the case of both the circumferential and longitudinal strains. Also, the ordering of the magnitude of the circumferential and longitudinal strains with depth is the same. This lends validity to the strain measurements and suggests that the variation in strains is due to random ariation in density of model rock material with depth.

Of particular concern is the strain condition in the failure region. A plate 0.5 in. thick was placed with a snug fit ... the opening at the top surfaces of the specimen. This plate prevented lateral movement of the wall of the opening near the surface, and may have had some effect at the 2 in. level since the circumferential strain measured there is considerably smaller than at other levels up to a surface pressure of 600 psi. The longitudinal strain is slightly less than that at the 7 in. level up to the same surface pressure. The failure of the model material occurred in shear on a surface with an angle of approximately 30° and the shear stress on this surface was approximately 300 psi at failure.

A.3.2 Test With Lined Opening

The second specimen in which the opening in the model rock material was lined with a thin aluminum tube of 0.035 in. wall thickness and 4 in. diameter was tested several times. The first pressurization proceeded to 1000 psi surface pressure when the neoprene membrane over the surface of the specimen began to leak and pressure could not be increased. The same thing occurred on the second pressurization, at 1200 psi, on the third at 600 psi, on the fourth at 1800 psi, but on the fifth trial 2500 psi surface

pressure was reached before the O-ring seal between the upper tank flange and the end plate failed. Surface pressure, strains on the confining tank, strains in the model rock material, and strains on the opening liner were measured. The model rock material did not fail even at a surface pressure of 2500 psi, but the liner buckled longitudinally on the last pressurization at about midheight. The surface of the model rock specimen was deformed permanently from its original position approximately 1/4 in. on the first pressurization and 1/2 in. by the fifth. The surface was relatively flat, indicating that slip occurred between the model material and confining tank wall. Only the complete results of the first pressurization will be presented as they are representative of the overall behavior.

Figure A.16 presents for the first pressurization the average of the strains measured at midheight on the outside surface of the confining tank wall in the circumferential, longitudinal, and 45 degree directions. If the longitudinal and circumferential directions are principal strain axes and the strain is uniform through the tank wall, the strain in the 45 degree direction should be the average of the other two. In the unlined opening test this was essentially the result, but in Fig. A.16 it is observed that the longitudinal and 45 degree strains are close together and there is considerably more scatter than in the previous test. Also, in the unlined opening test the longitudinal strain was the larger; while this is the case in the present test below 400 psi surface pressure, the circumferential strain is larger above 400 psi. This shift at 400 psi surface pressure could result from a moment applied at the flanges which caused a compressive bending strain on the outside surface of the wall of the tank which reduced the overall tension. There are two mechanisms causing bending at the flange. The upward

force of the bolts is outside the tank wall as shown in Fig. A.1 causing a moment in one direction while the bending of the tank end plates which is clamped tightly to the flanges causes bending in the other direction. The two moments may have approximately balanced one another in the first test while the latter moment dominated in the second test. This is proposed because the bolts were tightened much more in the second test as a larger surface pressure was expected.

At some pressure the bond between the Sulfaset grout and the confining tank wall must be overcome near the top of the tank, after which the shear between the two surfaces would result from friction. In Fig. A.17 and A.18 is shown the average shear stress between the upper 12 in. of the confining tank wall and the model rock specimen, and the lateral pressure exerted by the model rock specimen on the confining tank at midheight plotted against surface pressure. Both of these quantities were computed from the measured strains shown in Fig. A.16. At the maximum surface pressure of 1000 psi the average shear stress was of the order of 350 psi and the lateral pressure was about 225 psi. The ratio of lateral pressure at midheight to surface pressure was then about 0.22, and the ratio of average shear stress to surface pressure was approximately 0.35. At a surface pressure of 700 psi the ratio of lateral to surface pressure and shear stress to surface pressure was 0.21 and 0.31 respectively, while the corresponding ratios for the unlined opening test were 0.20 and 0.19. It appears that the lateral pressure ratio remained relatively constant in the two tests while the shear stress increased. The shear stress depends on the surface conditions of the confining tank wall. The tank wall was rougher in the second test because of corrosion caused by moisture in the Sulfaset in the first test.

In Fig. A.19 is shown the circumferential strains at various radii measured on a plane 8 in. below the surface vs. surface pressures. Again there is considerable variation in the strains measured on different radii, probably due to nonuniformity of the material. In Fig. A.20 the circumferential strain vs. radius is shown for a few values of surface pressure.

To determine if the strain measured was dependent upon the manner in which the strain gages were protected after being applied, three different applications over the gages were used. One set of gages was applied to the surface with no covering as in the unlined opening test, (Radius Z-Z) one set was placed in a 1/16 groove without protection, (Radius X-X) and one set was placed in a similar groove with a small piece of sheet teflon over the gage (Radius Y-Y). The first set of circumferential gages mentioned became inoperative when the lead wires were damaged during assembly of the specimen. The second two sets of gages are compared in Fig. A.20. From this comparison no consistent difference can be detected in the way in which the gages were protected.

The circumferential strains in Fig. A.20 indicate an inward particle displacement from a radius of 10 in. and less except for a reduction in displacement or slight outward movement (tensile strain) at a radius of 4 in. on two of the 3 radii. At a radius of 10 in. the circumferential strain is small and probably remains small but tensile from there to the confining tank wall where a small tensile strain was measured on the tank (Fig. A.16).

Radial strains measured on a plane 8 in. below the top surface are plotted against surface pressure in Fig. A.21 and are shown along particular radii for a few values of surface pressure in Fig. A.22. These graphs indicate a general radial tension in the specimen near the opening which becomes smaller

as radius increases until compression is measured at a radius of 4 to 5 in. At radii of 8 and 10 in. tension was measured on all but one of the radii. Thus tension dominates near the opening and near the tank wall with a narrow band of compression at a radius of approximately 5 to 7 in. This behavior is difficult to explain on the basis of what is understood about the deformation of the specimen. However, since this strain distribution was measured on three different radii, it cannot be discounted. The same three methods of gage protection discussed above for the circumferential strain was used and there is no consistent effect of gage protection on the strains measured.

In Fig. A.23 the circumferential strains measured on the opening liner are shown as they vary with surface pressure. Also shown is the computed average circumferential strain based on the change in diameter measured with the clip gages. The range in strain measured with strain gages represents a superimposed bending component in the liner after the test confirms that ovaling occurred. The average of the strains measured with strain gages represent the average strain in the liner, and give a more accurate indication of the average than the computed strain. The computed strain depends on the location of the clip guge relative to the ovaled shape and cannot average out the bending component. There is a decrease in average circumferential strain with depth as would be expected if the vertical stress is reduced by the tank wall friction. Figure A.24 is a plot of the longitudinal strains measured on the liner at various levels as it varied with surface pressure. These curves show an increase in compressive strain with surface pressure to a pressure of 300 to 500 psi after which the rate of increase is reduced. This reduction in strain rate is an actual reversal near the surface and becomes less pronounced with depth. At low pressure the shear between the cylinder and model material results in longitudinal compression in the cylinder. At the same time there is circumferential compressive strain

due to the lateral pressure from the model material, but the resulting longitudinal tensile strain in the cylinder is small as it is only due to the Poisson effect. Thus the longitudinal stress due to the shear dominates. At about 350 psi surface pressure the shear stress has reached the adhesive capacity between the materials and slip begins resulting in a reduction in the shear stress at higher pressure. The lateral pressure continues to increase and above 350 psi begins to dominate the longitudinal strain by way of the Poisson effect.

The variation of average longitudinal and circumferential stress in the liner computed from strains measured on the liner is shown in Fig. A.25. There is a general increase in longitudinal stress and a decrease in circumferential stress with depth at surface pressures greater than 100 psi. The lateral pressure exerted on the liner and the average shearing stress between the model rock and liner computed from the stresses in Fig. A.25 are shown in Fig. A.26. The unit shearing stress decreases with depth from the 2 in. to the 4 in. level and remains fairly constant from 4 in. to 12 in. The horizontal pressure increases at about the same rate to a depth of 6 in. and is somewhat less at 12 in.

In an infinite medium the lateral pressure on the liner would decrease with depth because the vertical stress near the liner would decrease due to the shear stress between the liner and rock if the liner is stiffer than the rock. It is not possible in this case to determine whether the reduction in pressure is caused by this effect or friction on the confining tank wall. Near the top of the liner little friction has accumulated so the lateral pressure calculation on the liner should be meaningful. A straight line through the points for the 4 in. depth gives a ratio of lateral to surface pressure of 0.28 (Fig. A.26). This is slightly larger than the value 0.22 which would be obtained for the ratio of lateral to surface pressure at midheight of the confining tank if a straight line is drawn through the data of Fig. A.18. For a semi-infinite linearly

elastic medium with a uniform surface pressure the ratio of lateral stress to vertical stress in the medium is equal to $\nu/(1-\nu)$ where ν is Poisson's ratio. The value of ν in unconfined compression is found to be approximately 0.17 for the model rock. This value gives a ratio of about 0.2. At the 12 in. depth and 1000 psi the ratio of lateral to surface pressure on the liner is 0.17 (Fig. A.26) and on the confining tank 0.24 (Fig. A.18). If the vertical stress is assumed to be the same at the liner and confining tank wall at this level, the lateral pressure on the liner should be less because it is less stiff than the confining tank.

The shear on the liner is fairly consistent when computed as the average from zero to 12 in., 4 to 6 in., or 6 to 12 in. It is on the order of 0.1 times the surface pressure. It is about the same as the shear stress on the confining tank below 250 psi surface pressure, and is much less than that on the confining tank at higher surface pressures.

The fifth pressurization of the lined opening specimen reached 2500 psi before pressure was lost by failure of the O-ring around the top cover. Almost all the strain gages within the specimen were no longer fucntioning, so only the strains on the outside surface of the confining tank were measured. These strains are shown in Fig. A.25 as they vary with surface pressure. The horizontal pressure exerted by the model rock specimens at midheight of the confining tank wall and shear between the upper 12 in. of tank wall and specimen are shown as they vary with surface pressure in Fig. A.28 and A.29. On the first pressurization, the average shear stress on the tank wall was slightly smaller at a given surface pressure and the lateral pressure was slightly greater than that on the fifth pressurization.

When the confining tank was disassembled after the fifth pressurization it was found that the liner had a uniform buckle at a depth below the surface of 10 in. which protruded inward approximately 1/8 in. After the fifth pressurization

the top surface of the specimen had been deformed a total of about 1/2 in. while the liner protruded above the original top of the specimen slightly less than 1/2 in. This protrusion represents the slip that had occurred between the two. The liner was deformed from the circular shape as shown in Fig. A.30 where the shape is shown at two depths below the surface after the last pressurization. There was a tendency for areas on opposite sides to flatten at both levels with a maximum deflection from the circular shape of approximately 0.01 in.

A.4 SUMMARY AND CONCLUSIONS

The confining tank was found to be stiff relative to the model rock specimen and satisfactory for providing lateral confinement. The maximum circumferential strain in the tank was of the order of 70μ and the lateral pressure on the tank wall at midheight was on the order of 0.2 times the surface pressure at a surface pressure of 1000 psi. These values are approximately those expected for an infinite half space with a uniform surface pressure. The shear stress between the model rock specimen and tank wall was found to be so large that it probably had considerable effect on the behavior of the model material around the opening. In the unlined opening test this shear was approximately 135 psi at 700 psi surface pressure and in the lined opening test it was 210 psi at 700 psi and 325 psi at 1000 psi surface pressure. The shear stress was higher in the latter test, but the ratios of lateral to surface pressure at midheight of the tank were close. The shear stress between the tank and model material could be reduced to a satisfactory level by applying sheet teflon to the tank wall before the specimen is grouted in place. It may be possible to use a layer of teflon sprayed on the tank. This would be preferable because of the thinness of the layer.

It is desirable to measure the lateral pressure and shear stress between the tank wall and model material during a test. A problem was encountered in doing this by measuring the strain at midheight of the tank wall, because of uncertainties introduced in these measurements due to moments applied to the tank flanges. Most of the uncertainty

can be eliminated by investigating the strains at midheight of the tank wall under hydrostatic pressure conditions.

Difficulty was encountered in maintaining the neoprene diaphragm over the model rock specimen because it was damaged by the top inside edge of the confining tank. This problem was overcome by placing a sheet metal ring under the diaphragm and over this top edge and extending about one in. over the outer edge of the specimen. This ring provided a rounded surface for the neoprene as the model rock specimen deformed. In the last pressurization of the lined opening test the diaphragm held and the test was terminated when the O-ring between the tank flange and lid was extruded at 2500 psi. The O-ring type of seal has been used before to a pressure of 3000 psi so this should in general not be a problem. The pressure of 3000 psi is the capacity of the confining tank.

The model rock specimen can be prepared satisfactorily in the general manner used in these tests. There is some evidence, primarily the variation in strains measured at symmetrical points, that the uniformity in density of the model material should be improved. This could be done with an automatic tamping mechanism, probably of the drop hammer type, or by devoting greater effort to maintaining uniformity in hand tamping by careful timing of the pneumatic tamping on segments of the specimen. Grouting of the specimen into the confining tank with Sulfaset was a satisfactory method of mobilizing the available confinement of the tank, and the similar procedure for placing the liner in the opening in the second test was equally satisfactory except that the grout thickness should be kept as thin as possible. In this test the thickness of grout was almost a quarter inch, and it would be possible to keep this thickness to less than one-eight in.

with care. The purpose of placing epoxy in the joint between the blocks was to assure good contact and to protect the strain gages. There is little shear stress in the joint because of symmetry so the epoxy strength is sufficient, though it may be desirable to use an epoxy with less stiffness.

The use of strain gages and clip gages to instrument the opening and opening liner appeared to perform satisfactorily but the use of strain gages within the material requires further investigation. These gages respond well, but the variation in readings at symmetrical points makes the results suspect. As mentioned earlier this variation could result from nonuniformity of the material, but it could result in some cases from unrealistic response of the strain gages due to the high normal pressure applied to them. The normal pressure alone should cause little extraneous strain response as discussed in Reference (2), but the combination of adverse effects may cause difficulties. Adequate placement and protection methods could eliminate the difficulties, however.

Any conclusions drawn from these tests concerning the behavior of the model rock in the vicinity of the opening must be drawn with the realization that the high shear stress between the model material and tank walls may have caused the specimen not to behave like an infinite half-space. This shear stress probably did not affect the failure of the material around the top of the opening in the unlined opening test, though it probably did influence the strains at the 8 in. level in the material and around the opening. It was possible, however, to determine an approximate value of lateral pressure and shear stress on the opening liner and the distribution of these quantities with depth. The shear stress on the liner depends on the materials in contact and the surface conditions of the materials.

The surface conditions were not necessarily representative of a real installation in these tests. In a prototype structure the liner would probably consist of concrete cast against rock in which case there would be a rather large resistance to slip and a friction coefficient would not be very meaningful. In further tests attention should be given to the interface conditions and an effort made to make them realistic.

Tests of the type performed can be made which will give results that will help to understand the behavior of the material around a vertical opening and the interaction of the material and the opening liner. Such tests would be very useful in furthering this understanding. A model rock specimen which contains systems of joints with various spacings and orientations can be built and grouted into the confining tank. Tests of a specimen of this type could be even more useful in understanding the behavior of real rock.

REFERENCES

1. Heuer, R. E. and Hendron, A. J., "Geomechanical Model Study of the Behavior of Underground Openings in Rock Subjected to Static Loads; Report 1, Development of Modeling Techniques," Contract Report N-69-1, U.S. Army Engineer Waterways Experiment Station, Vicksburg, Mississippi, Oct. 1969.

2. Milligan, R. V., "The Grass Hydrostatic-Pressure Effect as Related to Foil and Wire Mtrain Gages," Journal of the SESA, J. 7, N. 2, Feb. 1967.

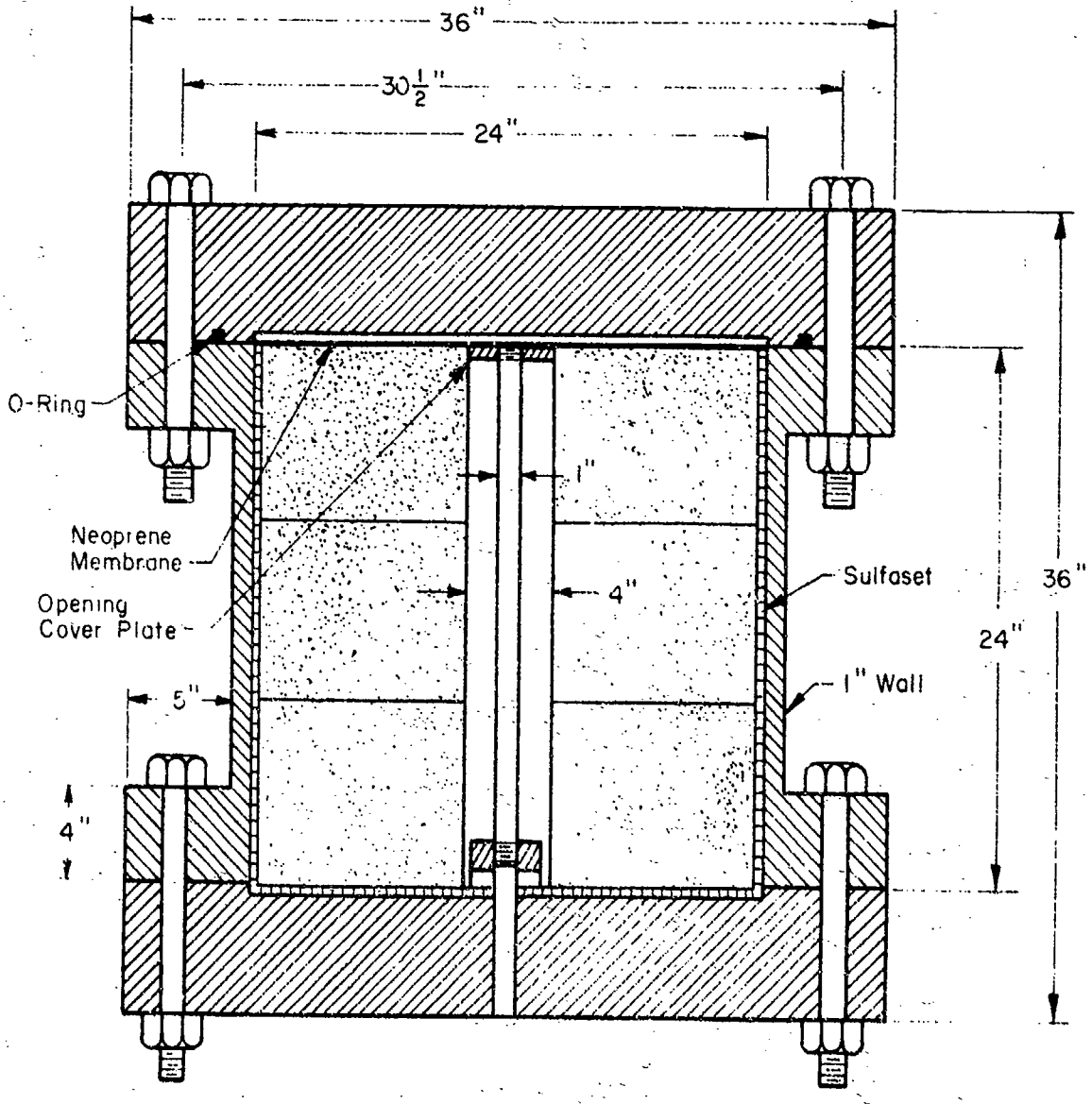

Fig. A.1 Confining Vessel

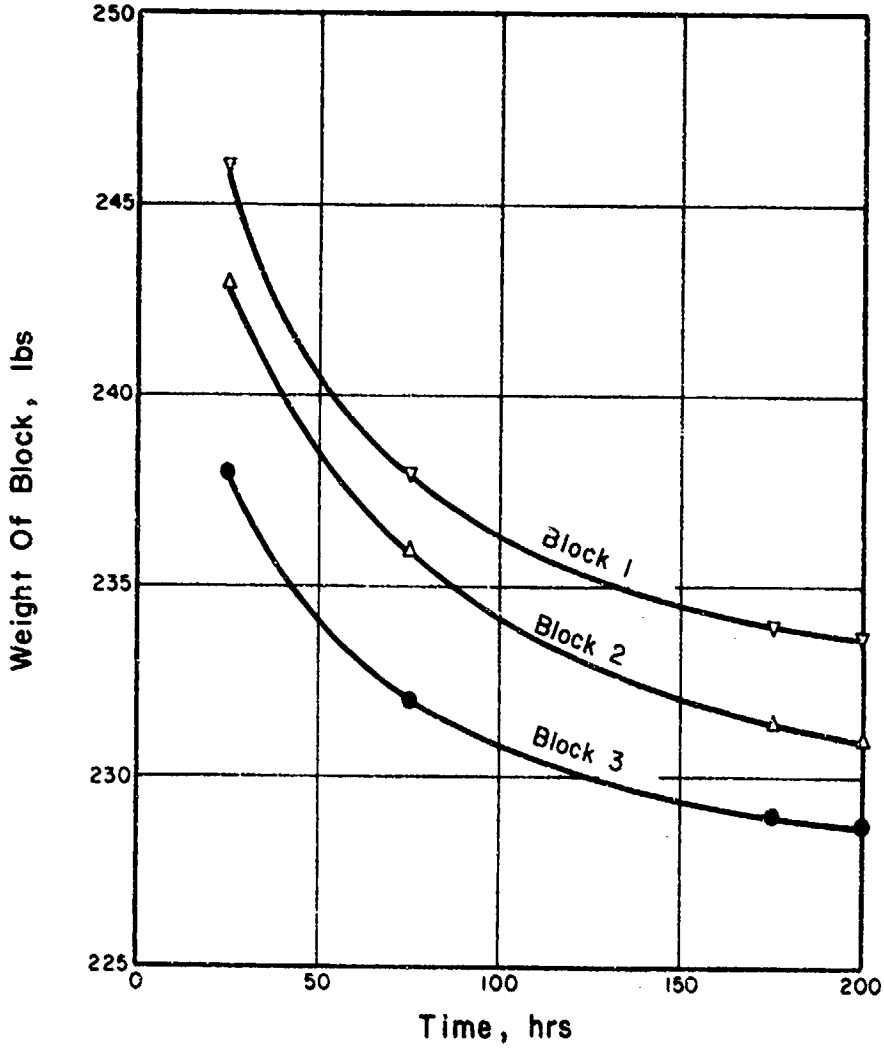

Fig. A.2 Drying curves for blocks of model rock material

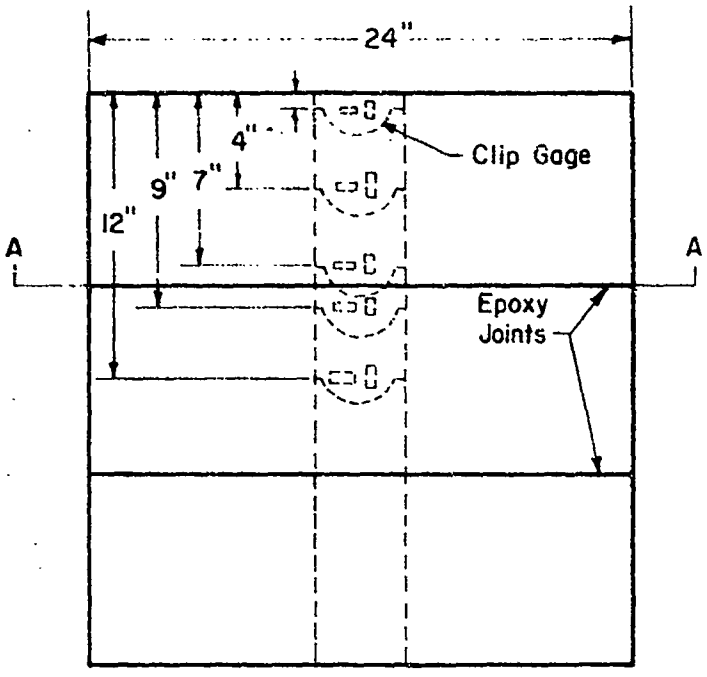

Section A—A

Circle	Radius
1	2.5 in.
2	4.0 in.
3	6.0 in.
4	8.0 in.

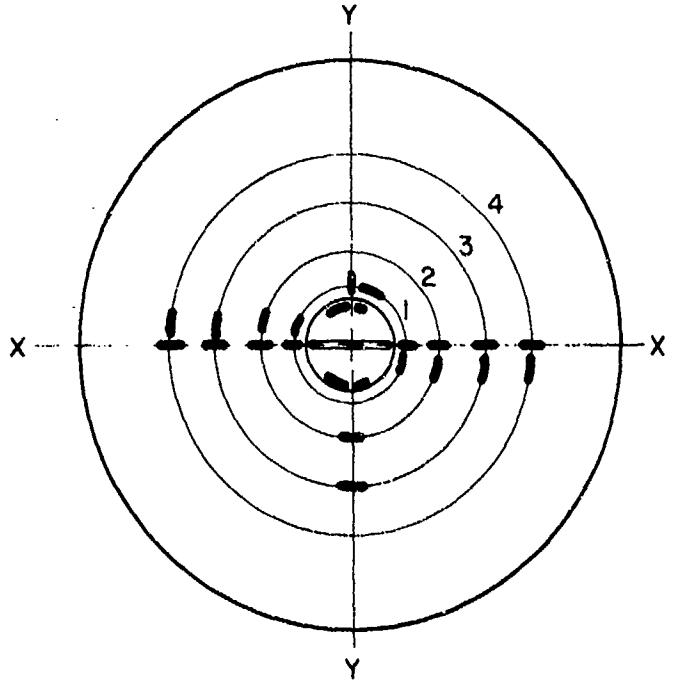

Section A—A

Fig. A.3 Gage locations in the model material for the unlined opening test

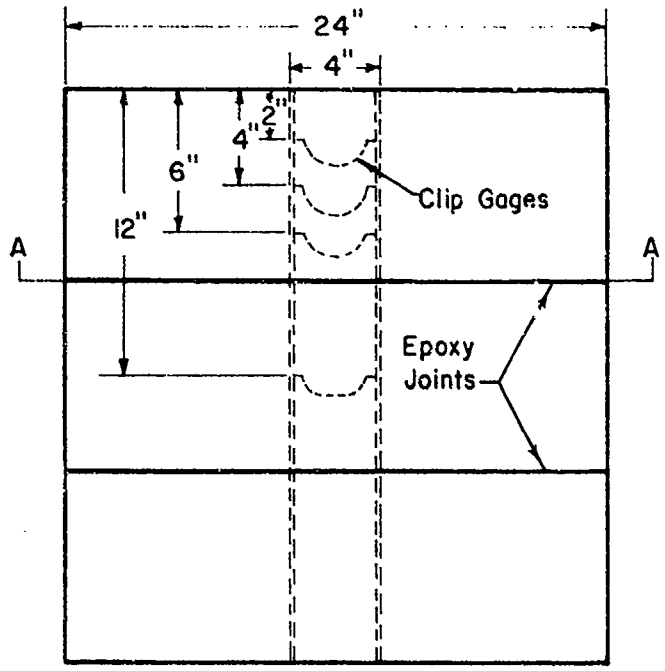

Section A–A

Circle	Radius
1	2.5 in.
2	4.0 in.
3	6.0 in.
4	8.0 in.
5	10.0 in.

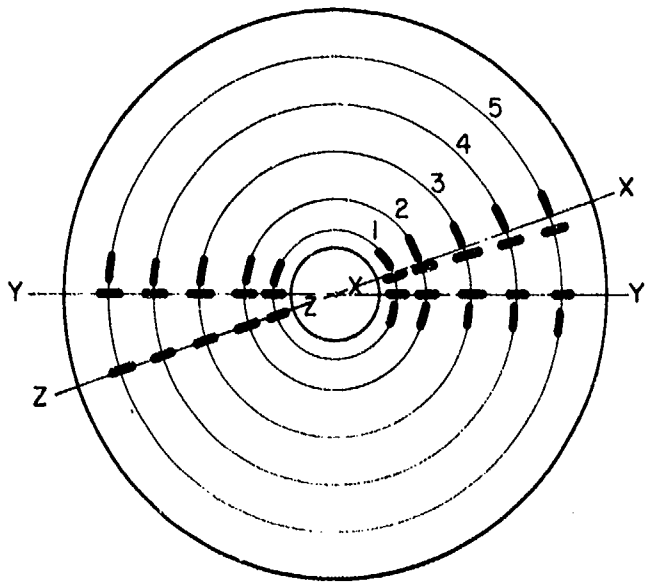

Section A–A

Note: Radial and circumferential gages adjacent to line X–X were set unprotected in 1/16 in. grooves; those adjacent to Y–Y were set in grooves and protected by a teflon sheet; the radial gages along Z–Z were not in grooves and were unprotected.

Fig. A.4 Gage locations in the model material for the lined opening test

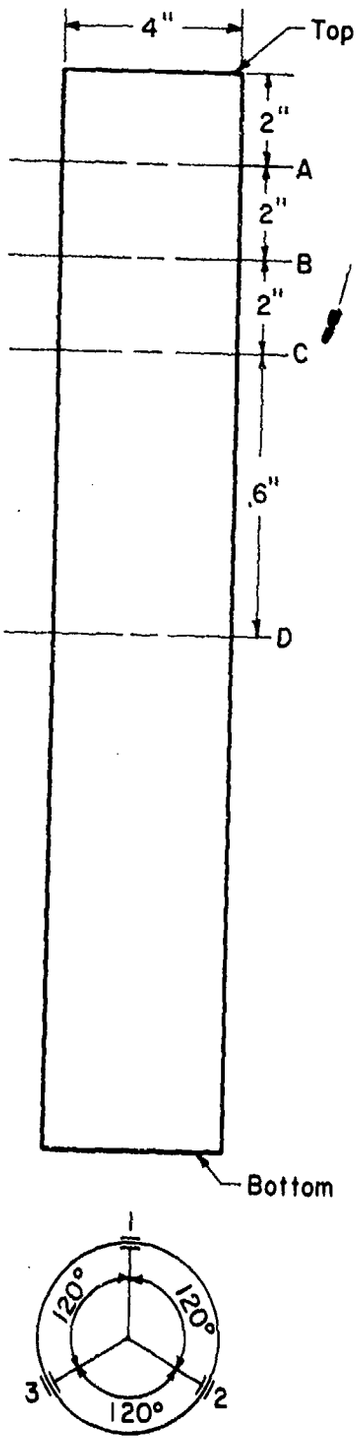

Inside surface gages - two element gages type FAET-25C-3556 with one element longitudinal and the other circumferential.

Outside surface gages - single element gages type C6-141 oriented circumferentially.

Gages were placed at levels A, B, C, and D with the same configuration.

Fig. A.5 Strain gage locations on the opening liner

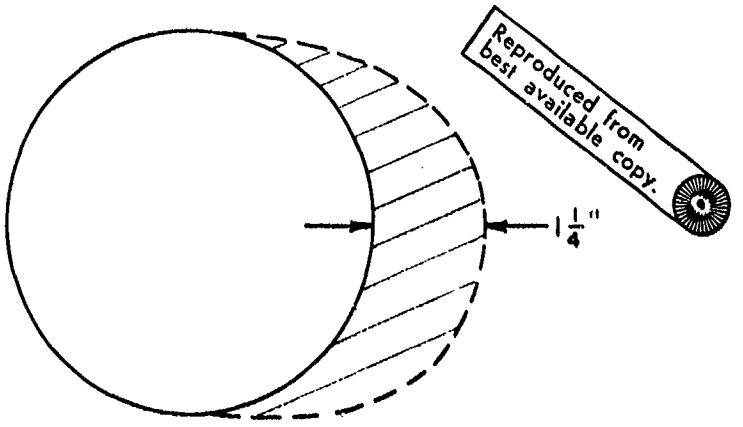

Plan View

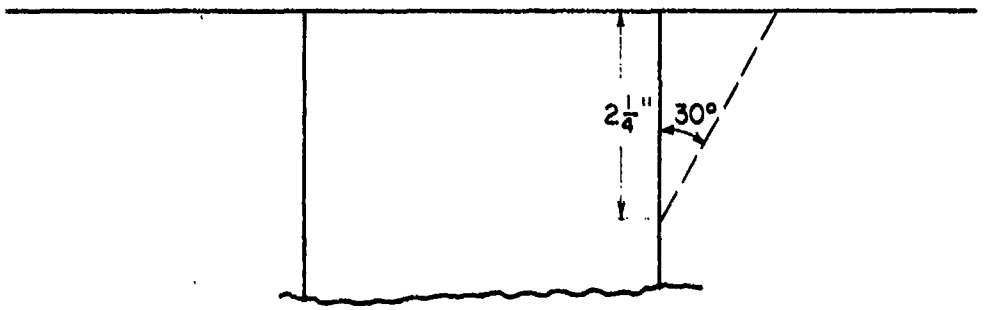

Section

Fig. A.6 Failure surface in the unlined opening test

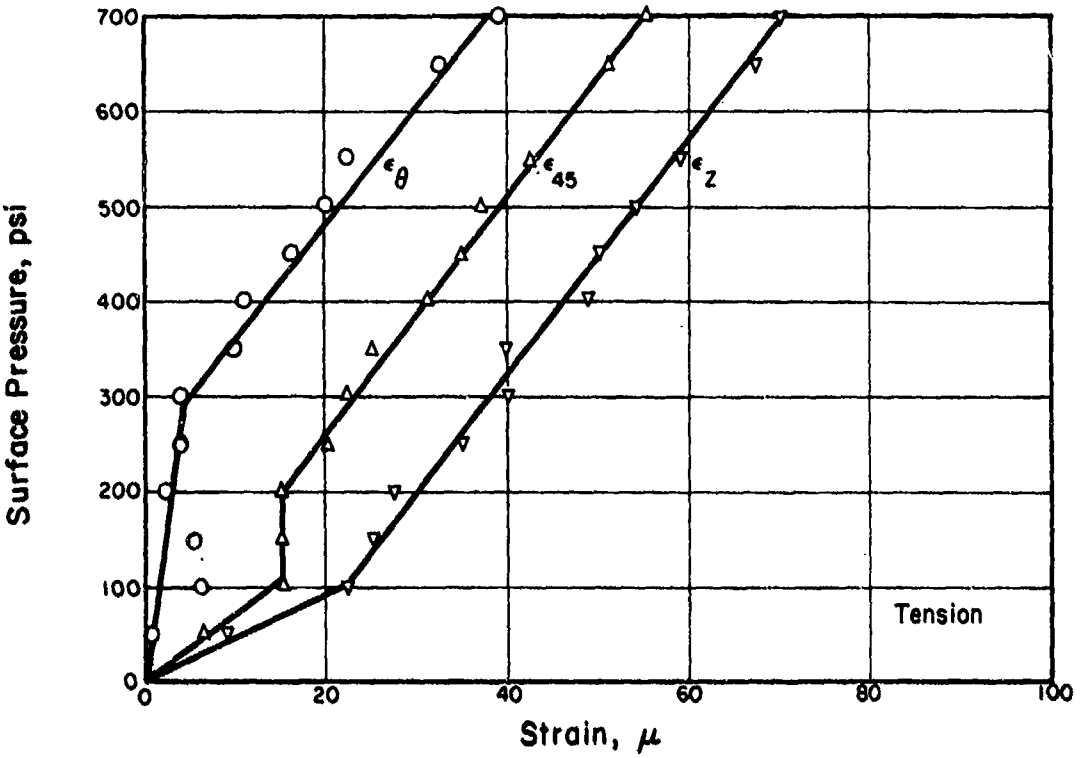

a) Strains On The Confining Tank Wall

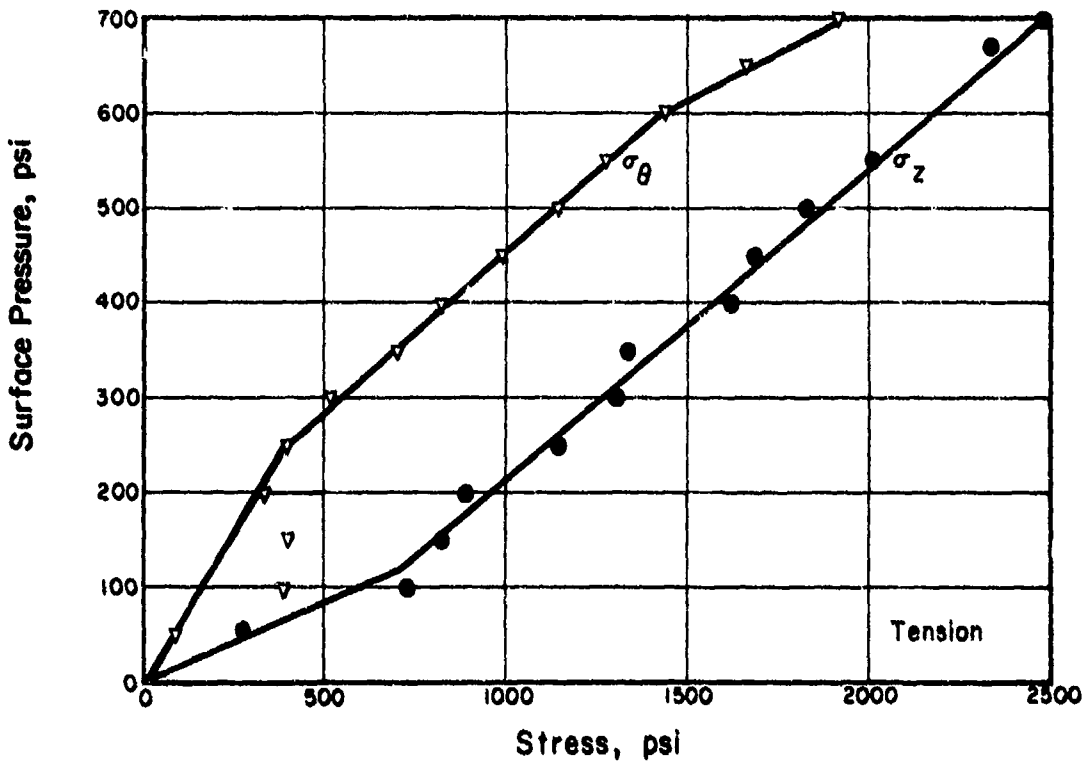

b) Stresses In The Confining Tank Wall

Fig. A.7 Strains measured on the wall of the confining vessel and the corresponding computed stresses for the unlined opening test

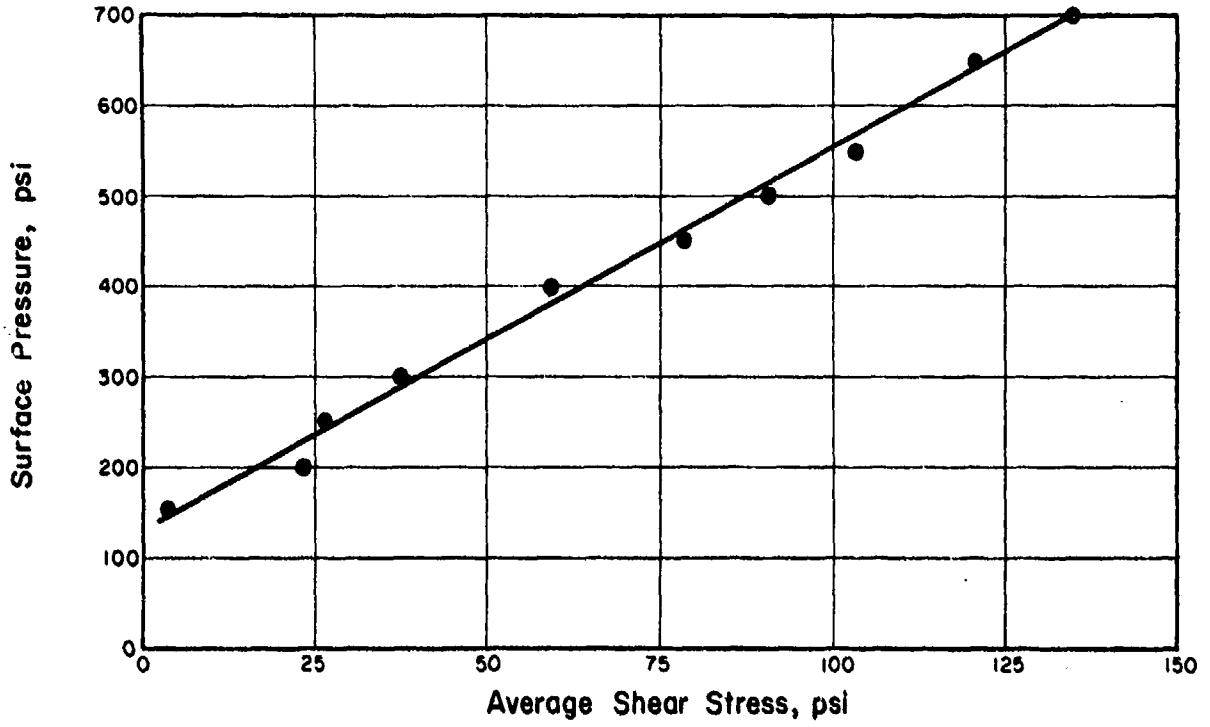

Fig. A.8 Average shear stress between the upper 12 in. of confining tank wall and specimen for the unlined opening test.

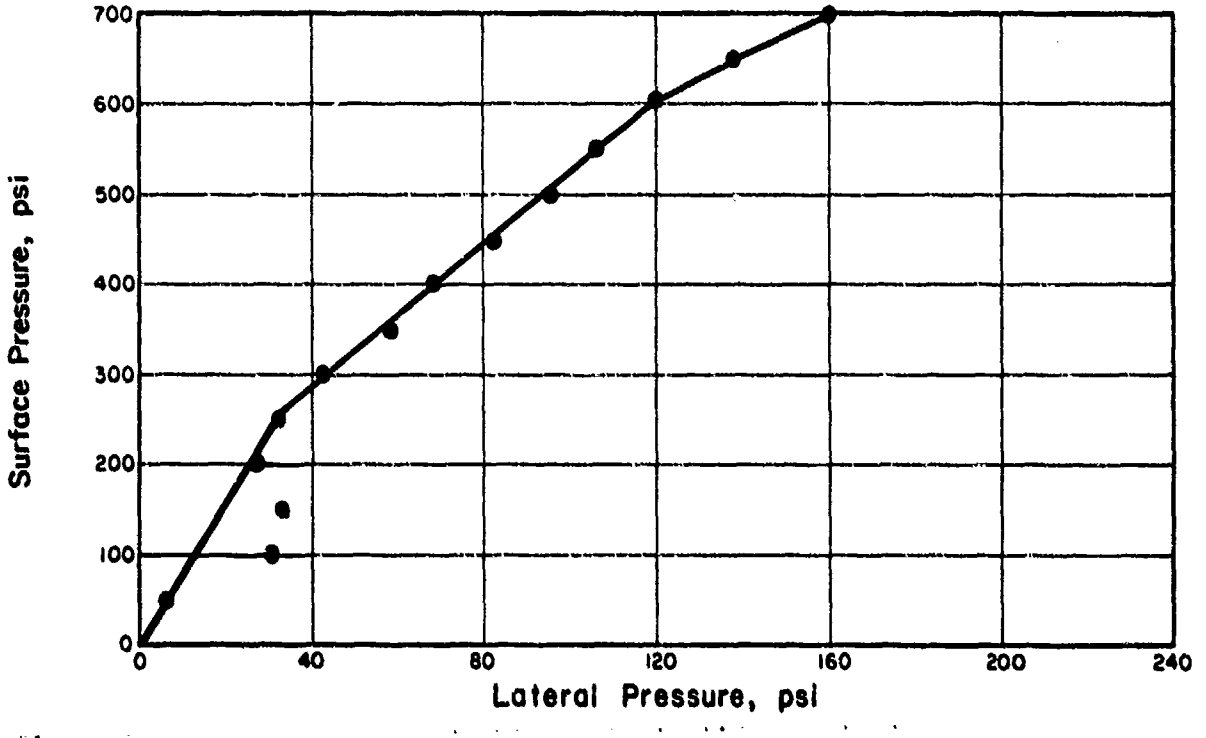

Fig. A.9 Pressure exerted by the specimen on the confining tank at midheight of the wall for the unlined opening test

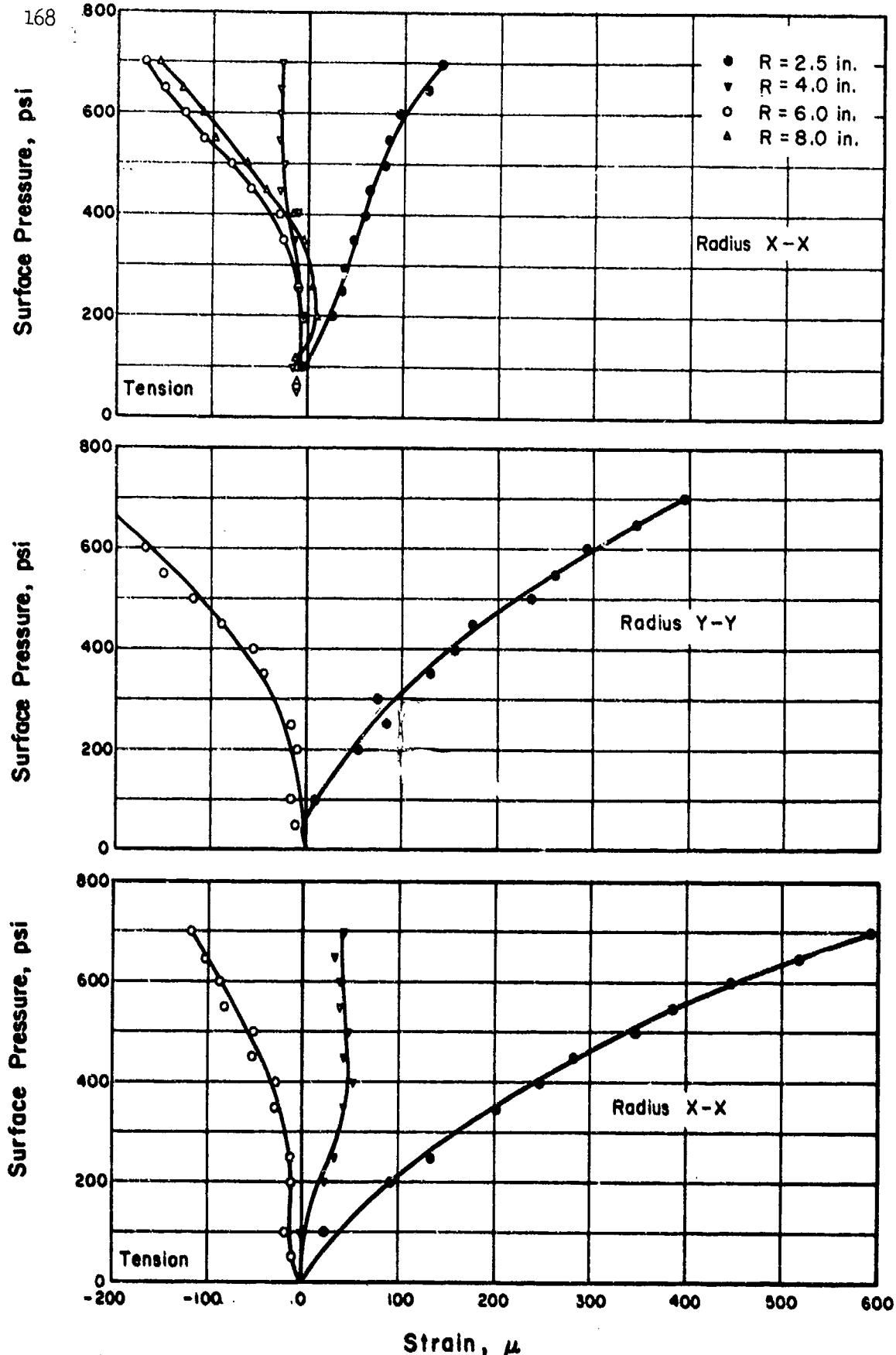

Fig. A.10 Circumferential strains measured in the specimen 8 in. below the top surface in the unlined opening test

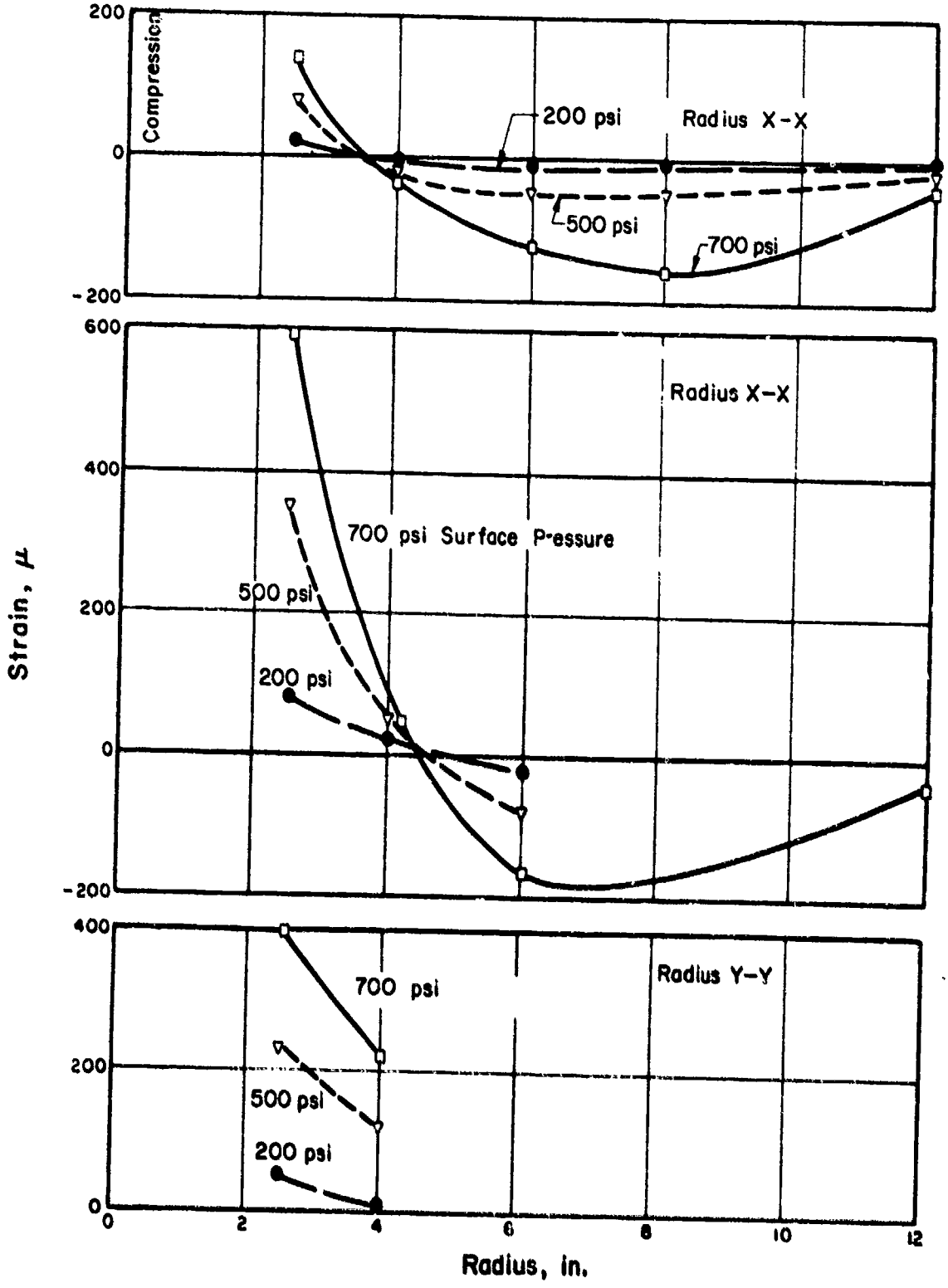

Fig. A.11 Circumferential strain vs. radial distance on a plane 8 in. below the top surface for the unlined opening test

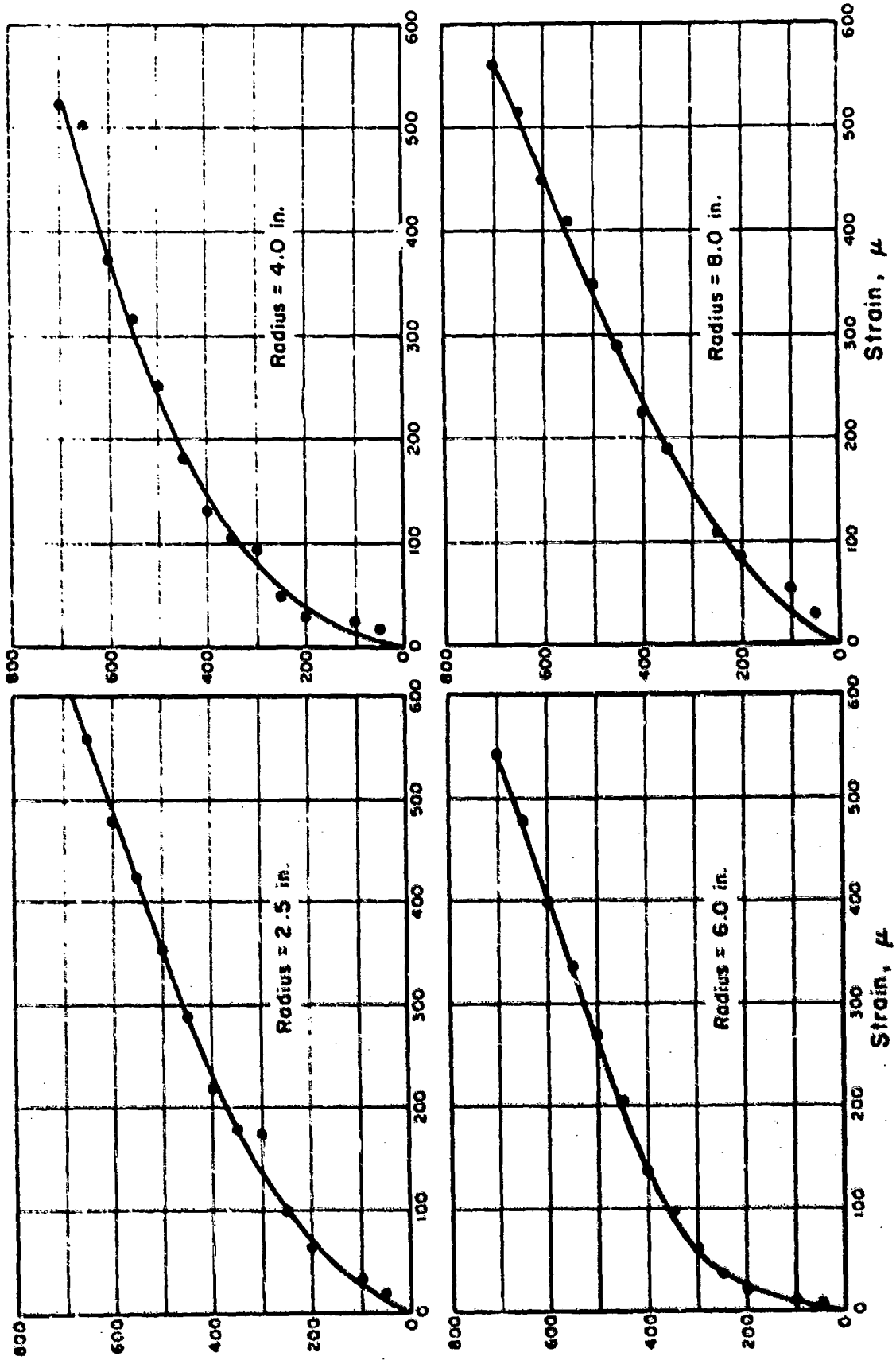

Fig. A.12 Average radial strains measured in the specimen 8 in. below the top surface in the unlined opening test.

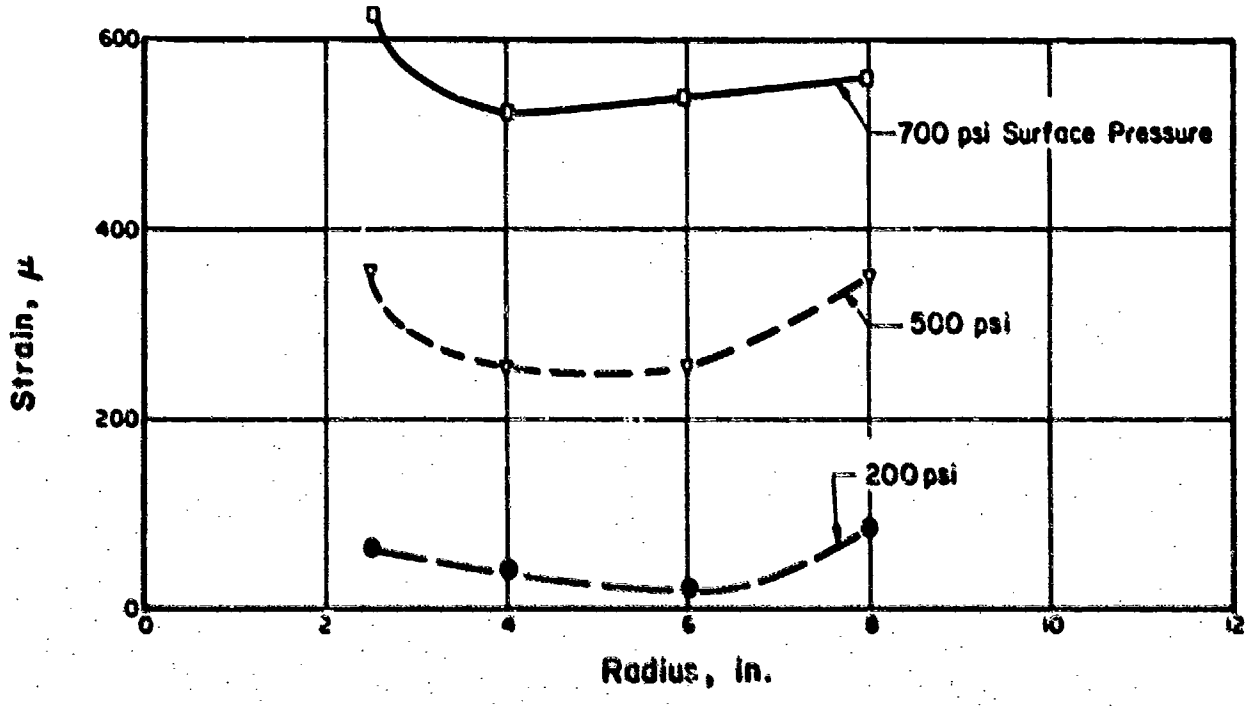

Fig. A.13 Radial strain vs. radial distance on a plane 8 in. below the surface for the unlined opening test

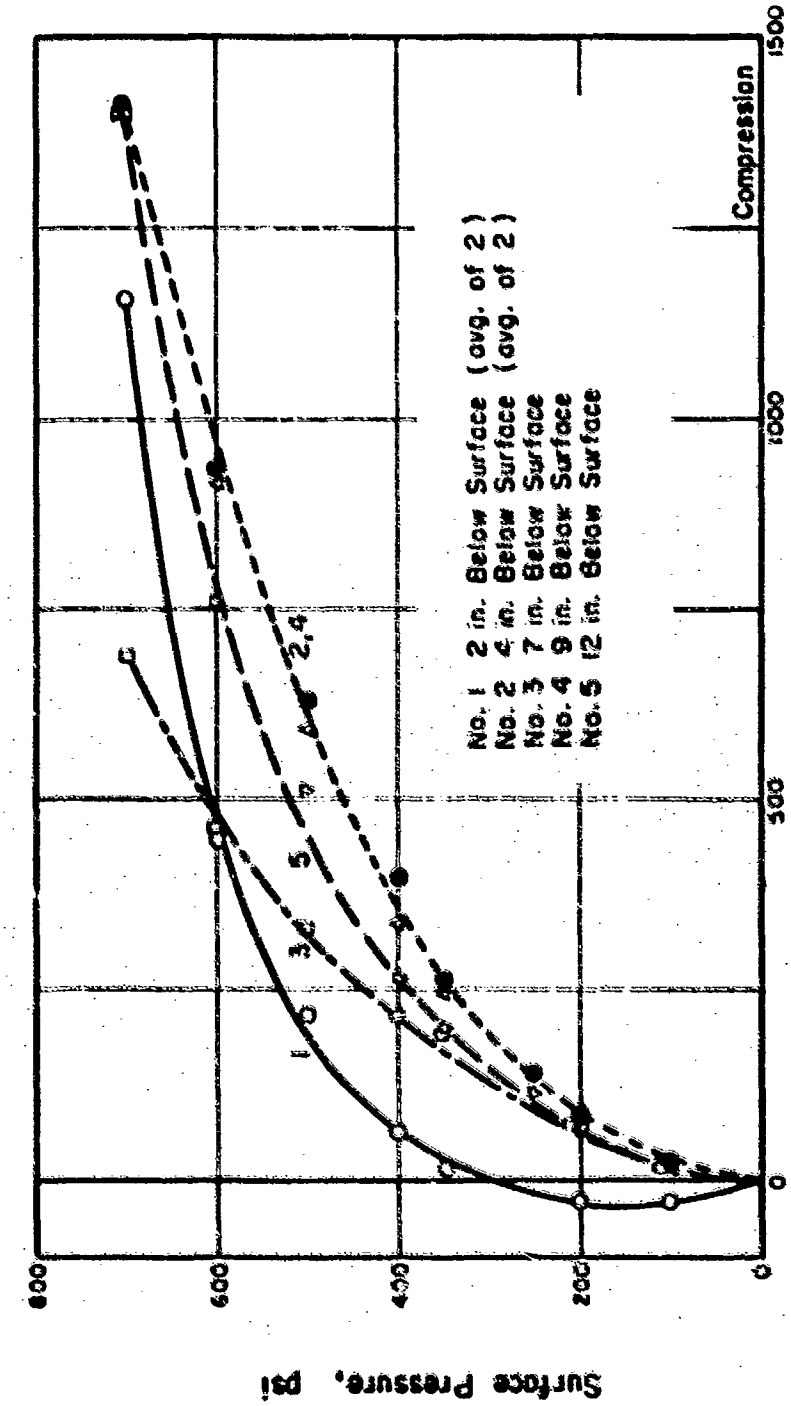

Fig. A.14 Circumferential strains measured on the inside of the opening vs. surface pressure for the unlined opening test

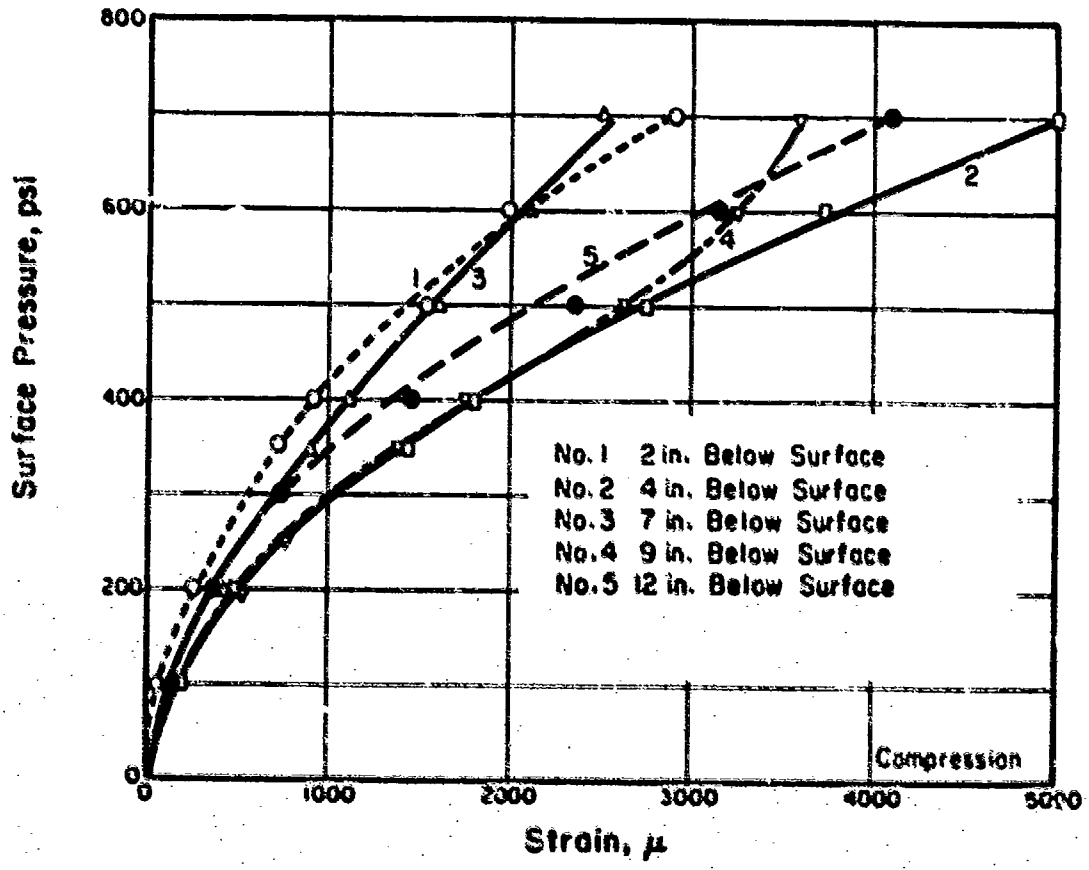

Fig. A.15 Longitudinal strains on the inside of the opening vs. surface pressure for the unlined opening test

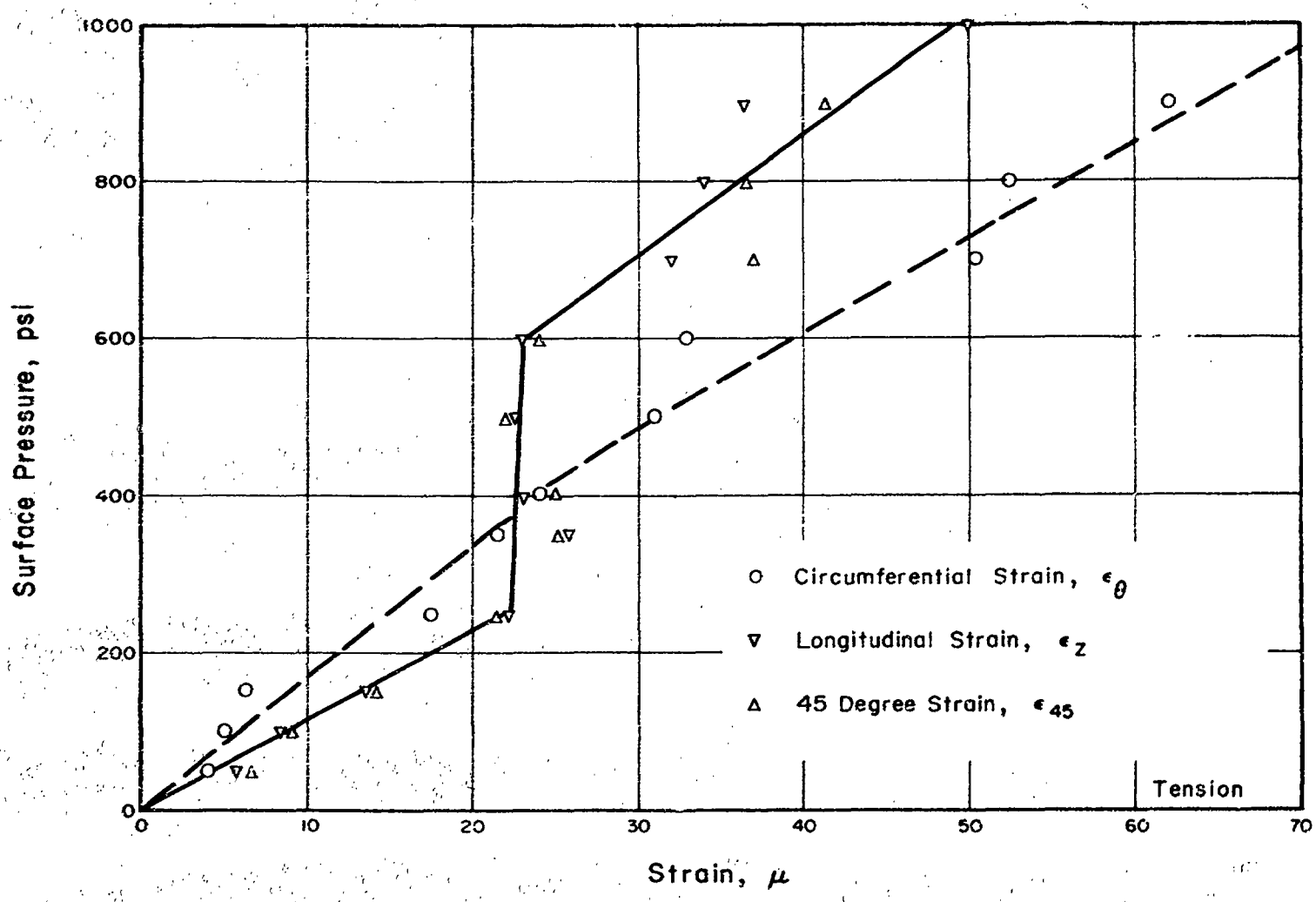

Fig. A.16 Average strains measured at midheight of the confining tank wall for the first pressurization of the lined opening test.

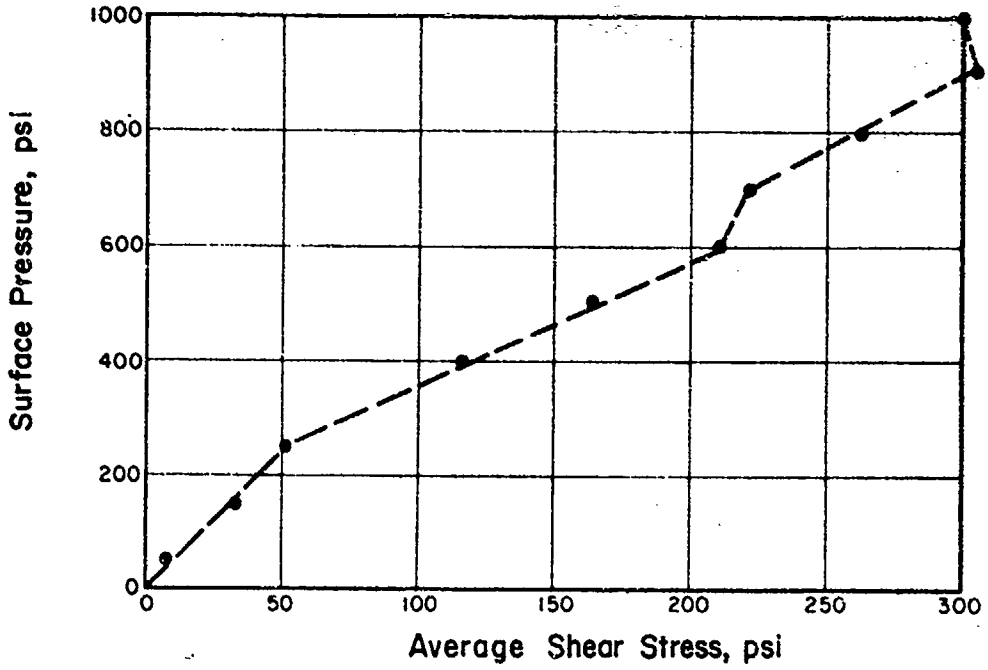

Fig. A.17 Average shear stress between the upper 12 in. of tank wall and model rock for the first pressurization of the lined opening test.

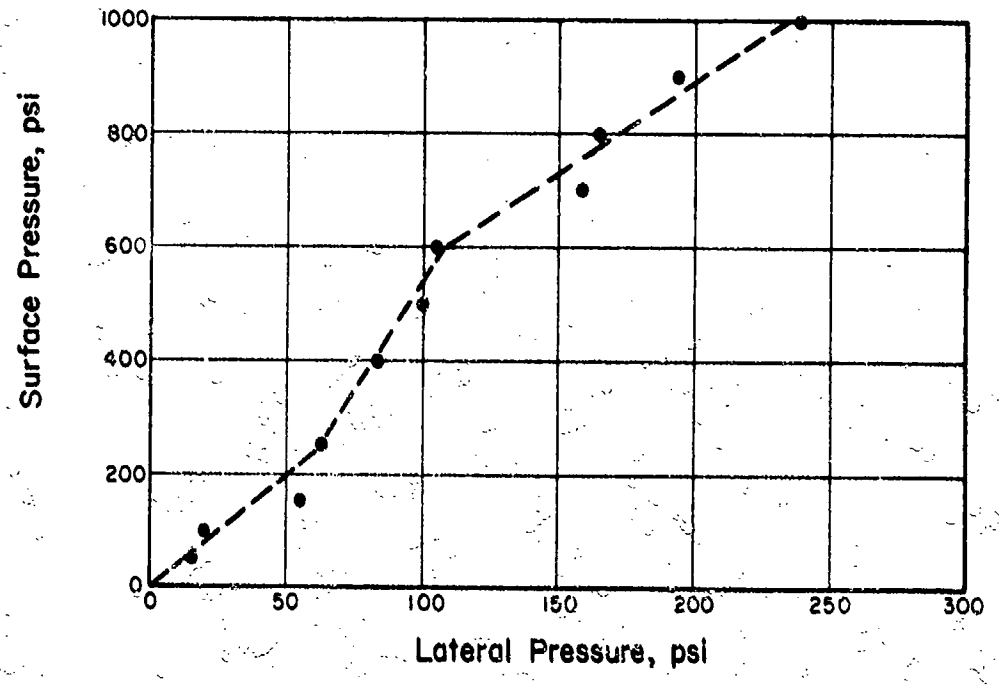

Fig. A.18 Pressure exerted by the model rock on the confining tank at midheight for the first pressurization of the lined opening test.

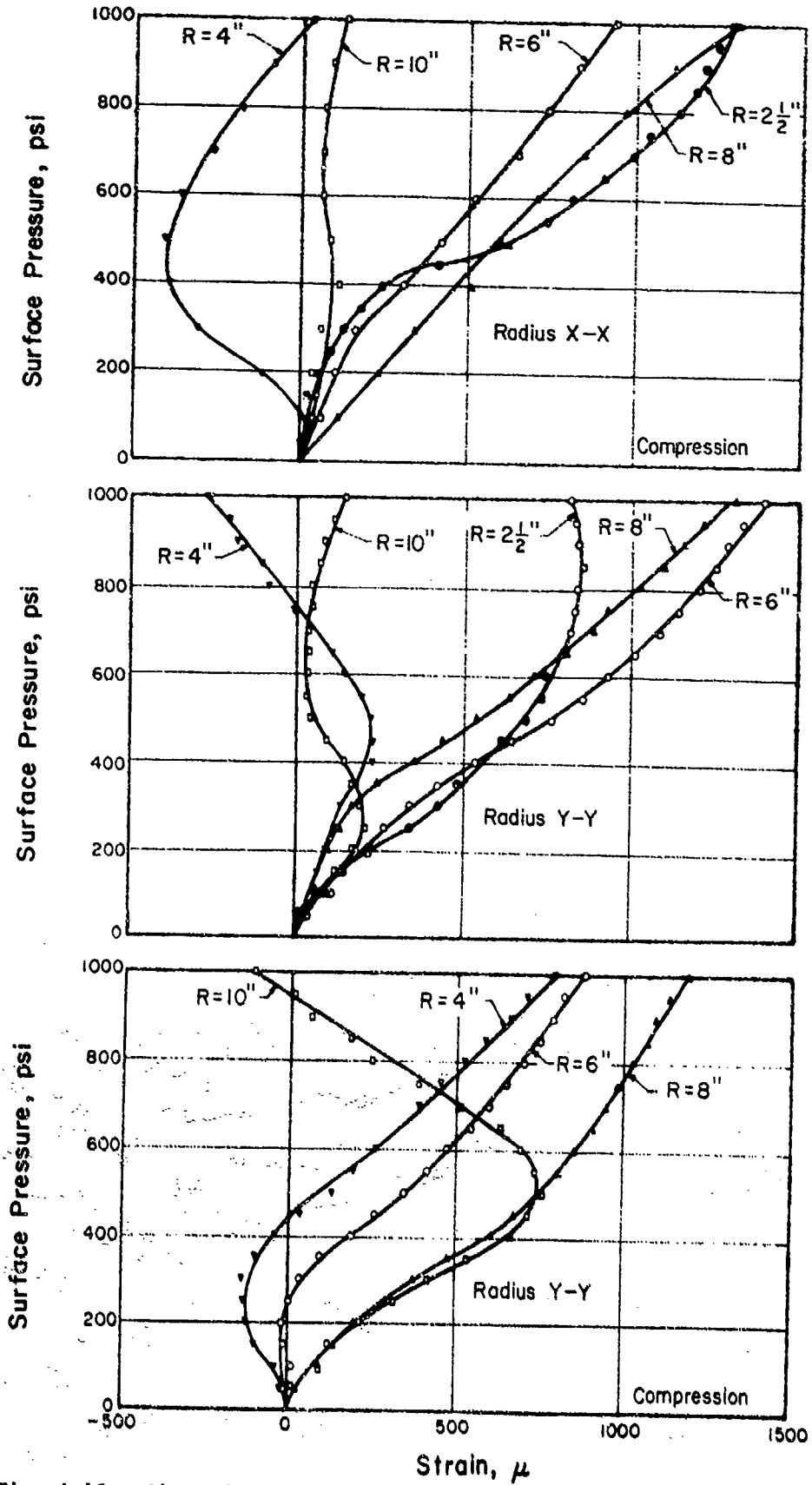

Fig. A.19 Circumferential strains measured in the specimen 8 in. below the surface during the first pressurization of the lined opening test.

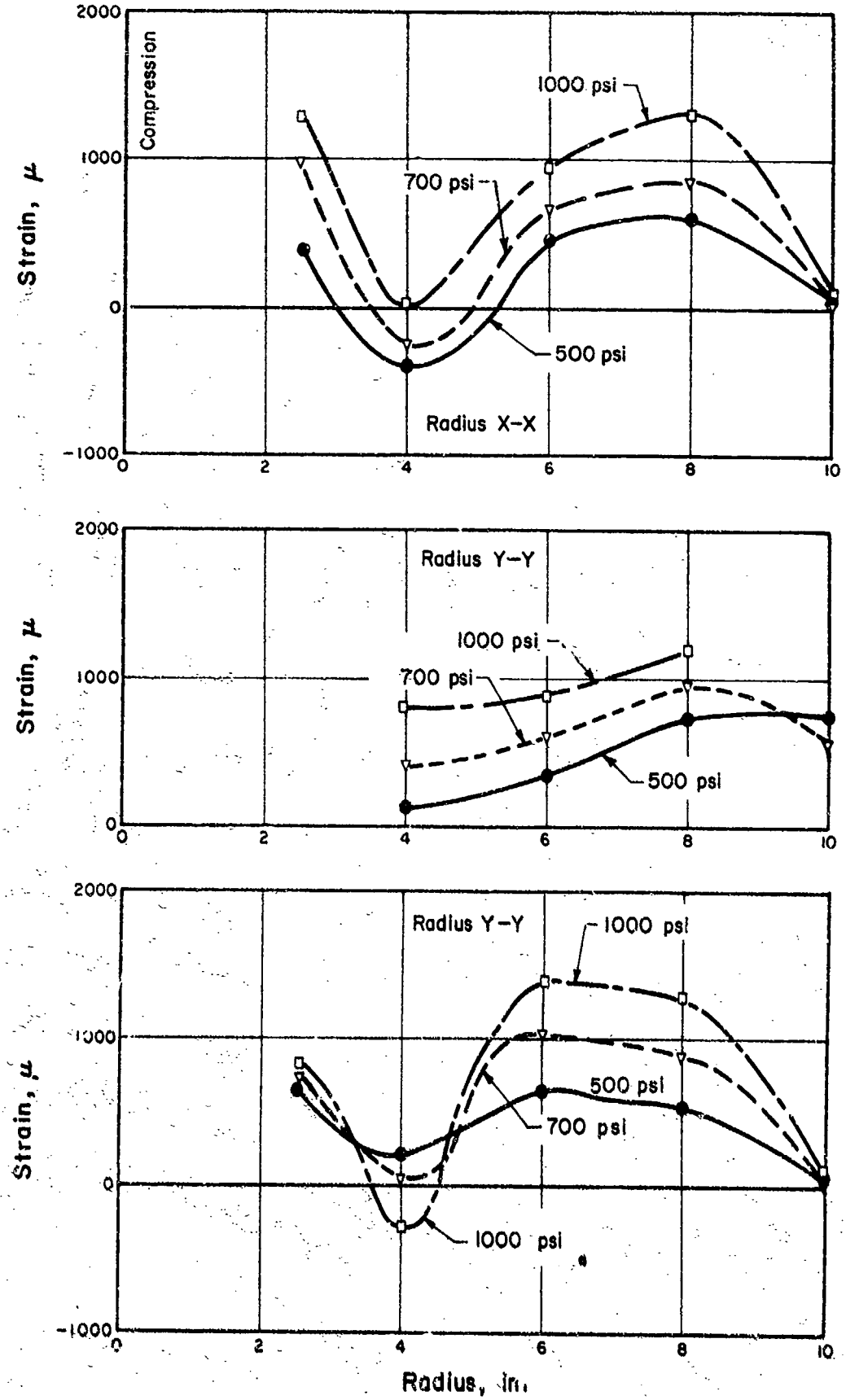

Fig. A.20 Circumferential strains vs. radius for the plane 8 in. below the surface for the first pressurization of the lined opening test.

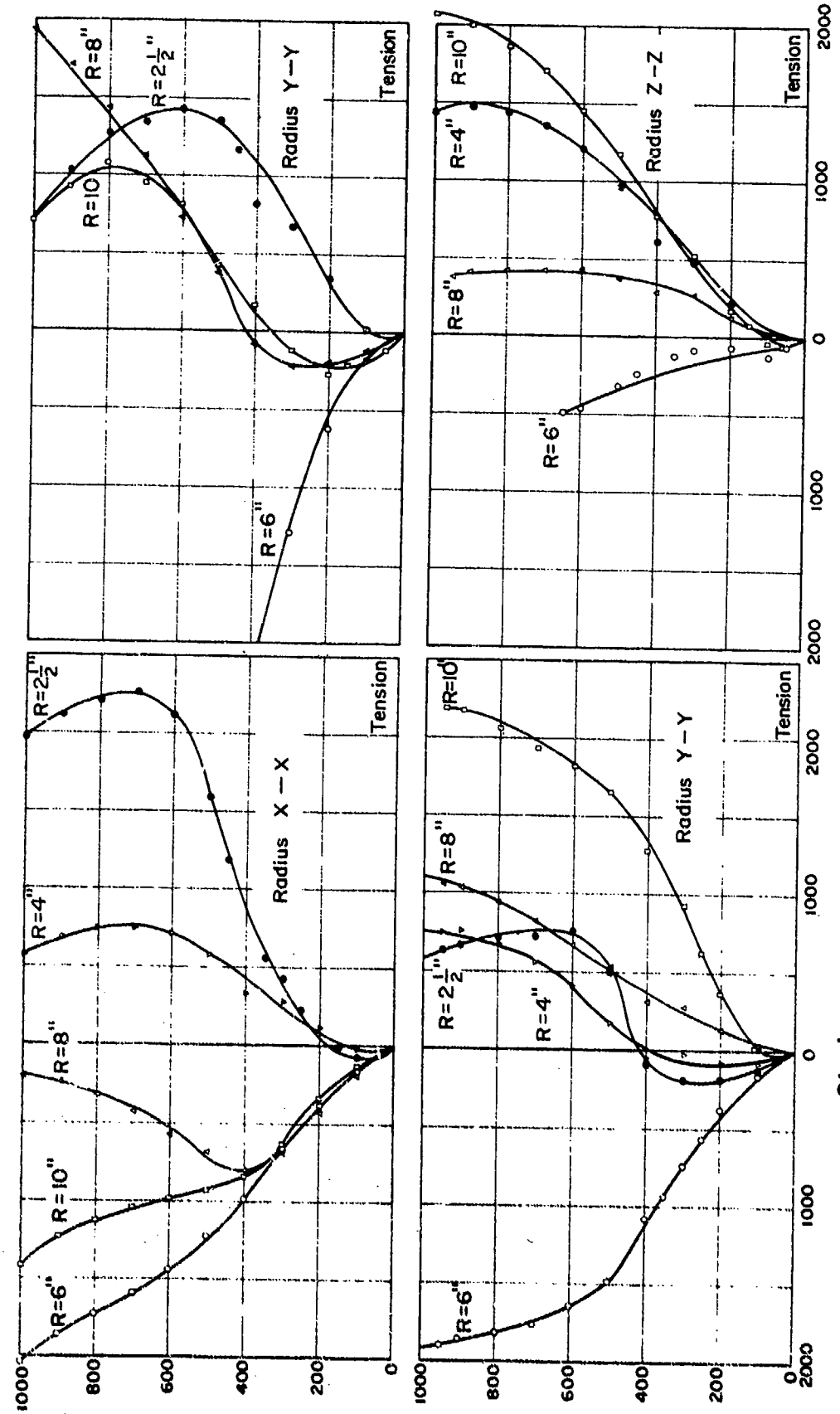

Fig. A.21 Radial strains measured in the specimen 8 in. below the surface during the first pressurization of the lined opening test.

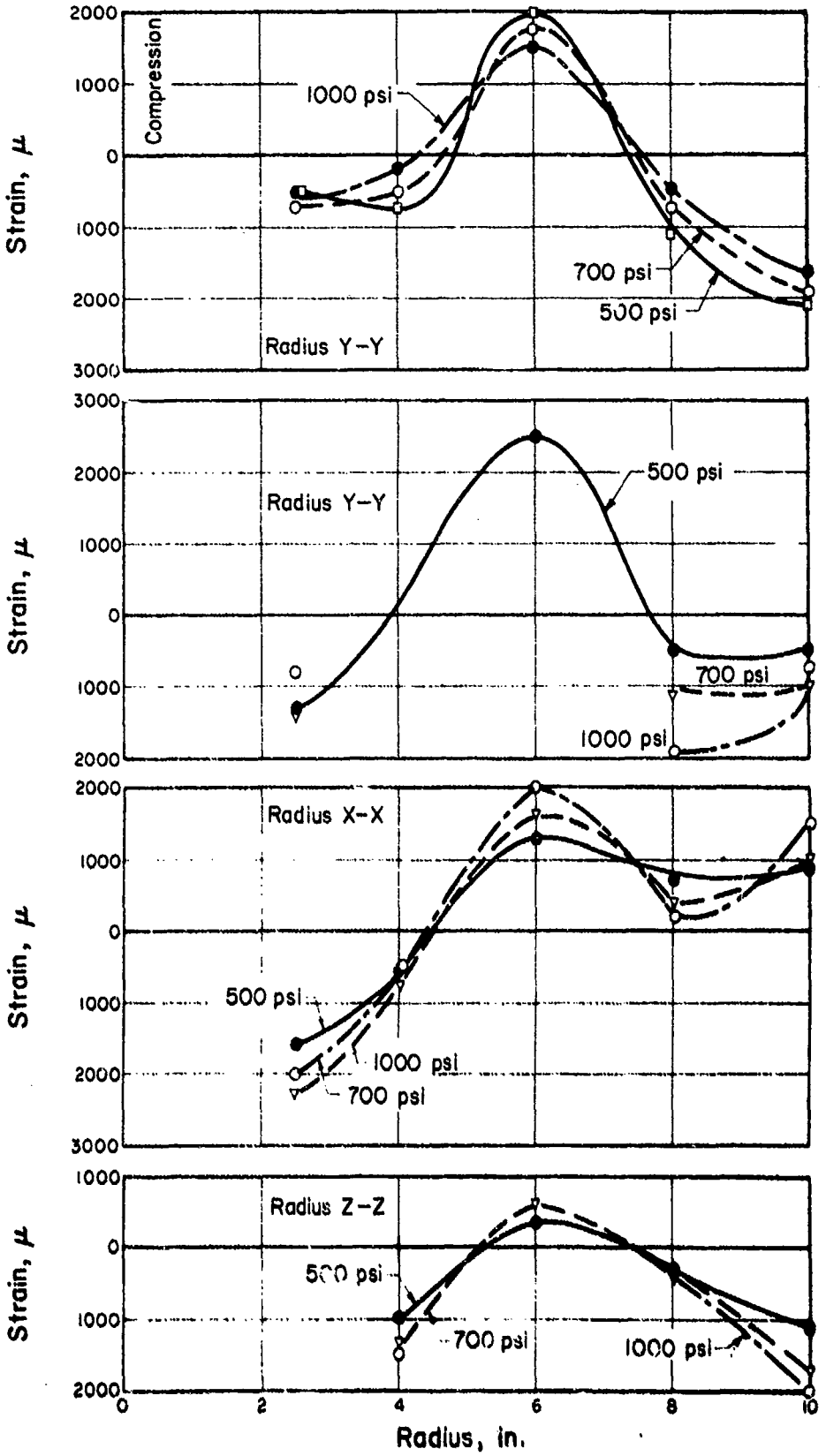

Fig. A.22 Radial strain vs. radius for the plane 8 in. below the surface in the lined opening test.

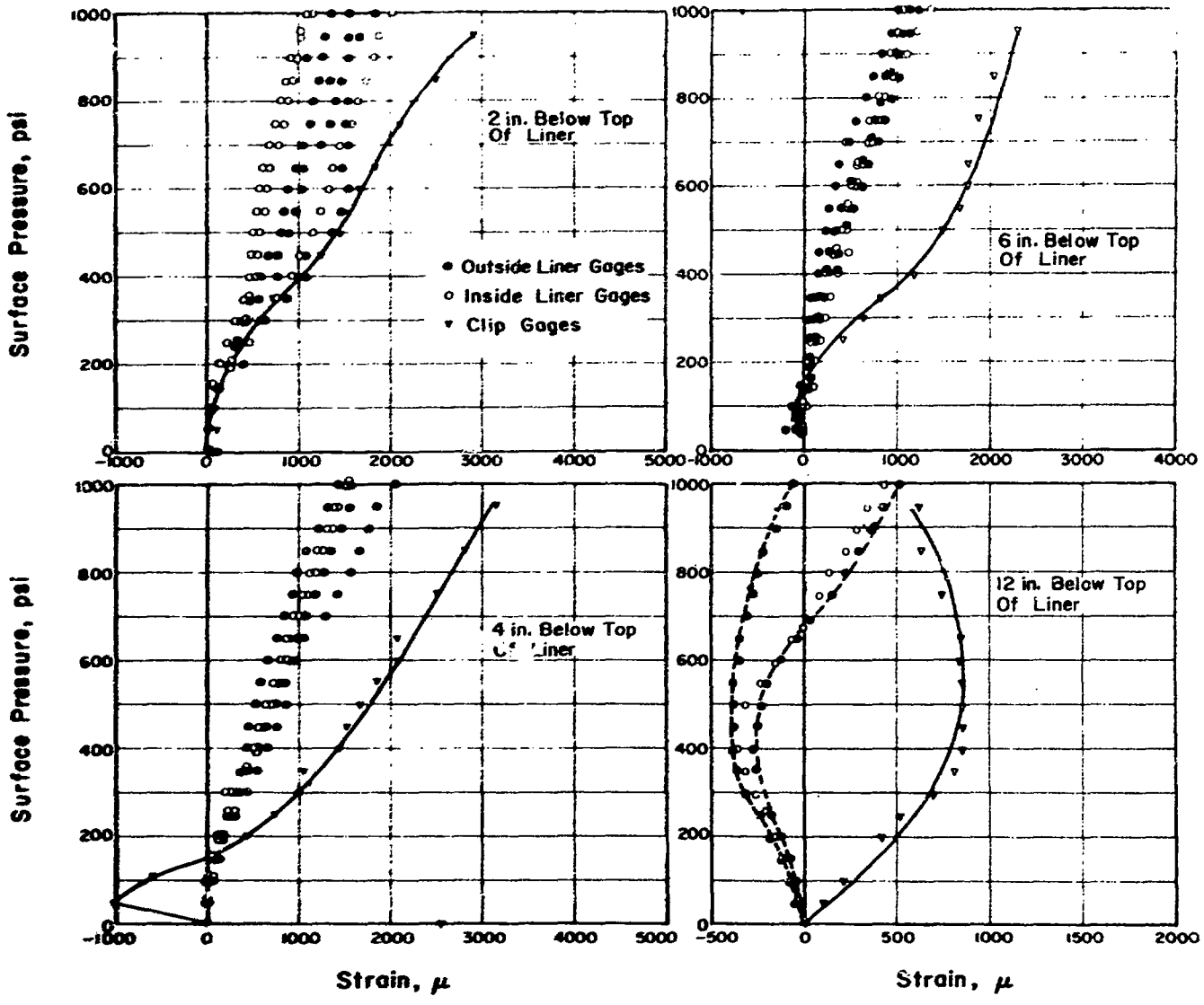

Fig. A.23 Circumferential strains measured on the opening liner vs. surface pressure for the first pressurization of the lined opening test.

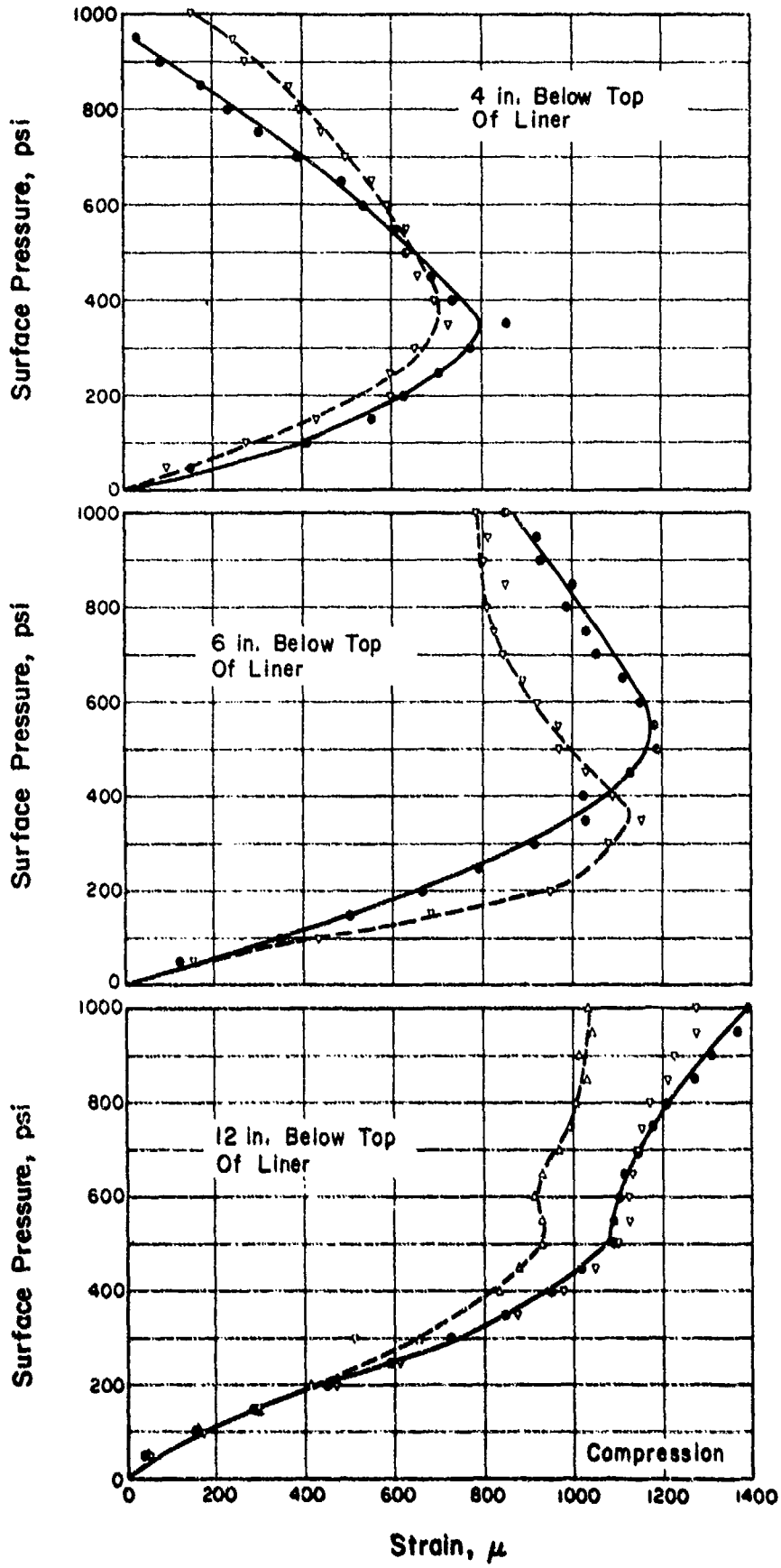

Fig. A.24 Longitudinal strains measured on the opening liner vs. surface pressure during the first pressurization of the lined opening test

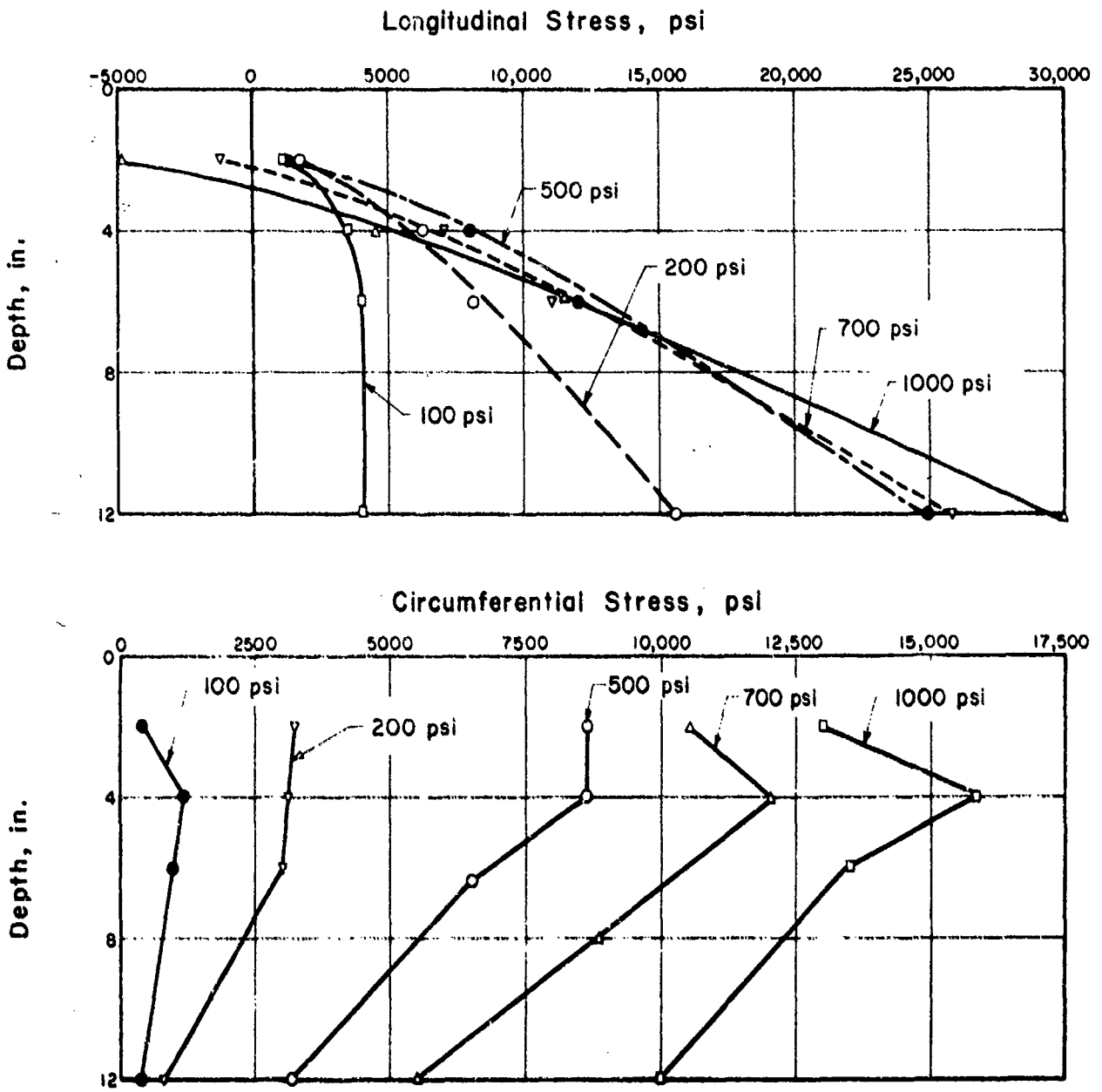

Fig. A.25 Longitudinal and circumferential stress in the liner vs. depth for the first pressurization of the lined opening test.

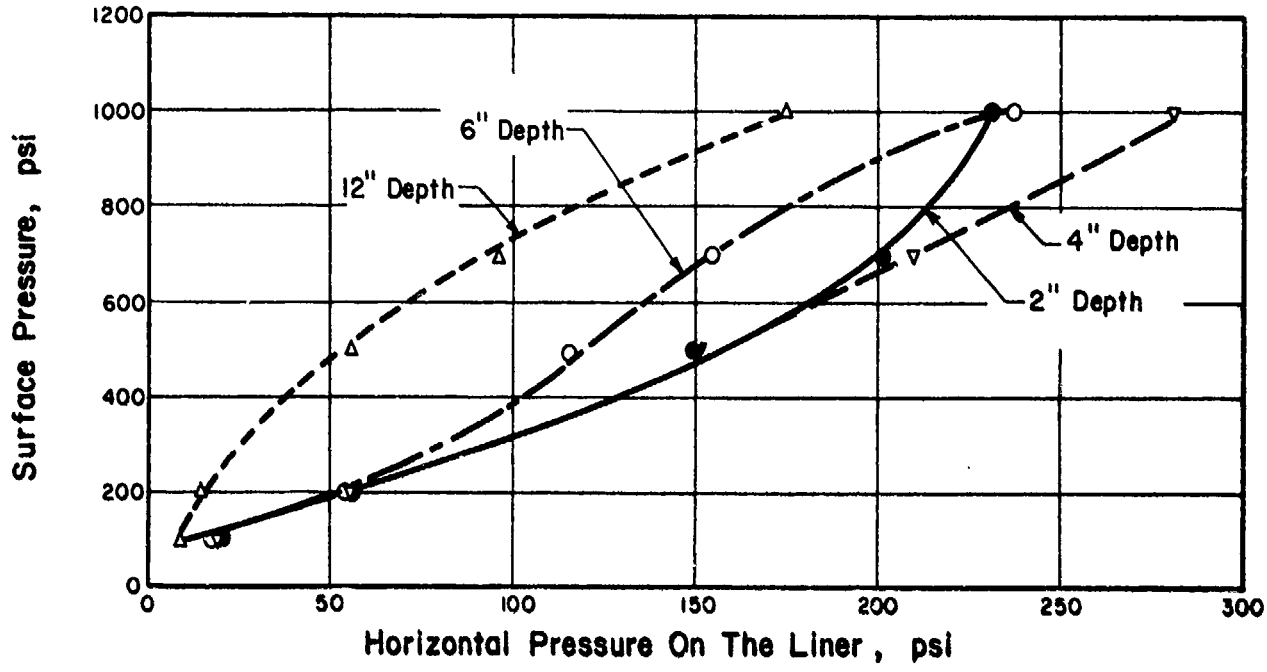

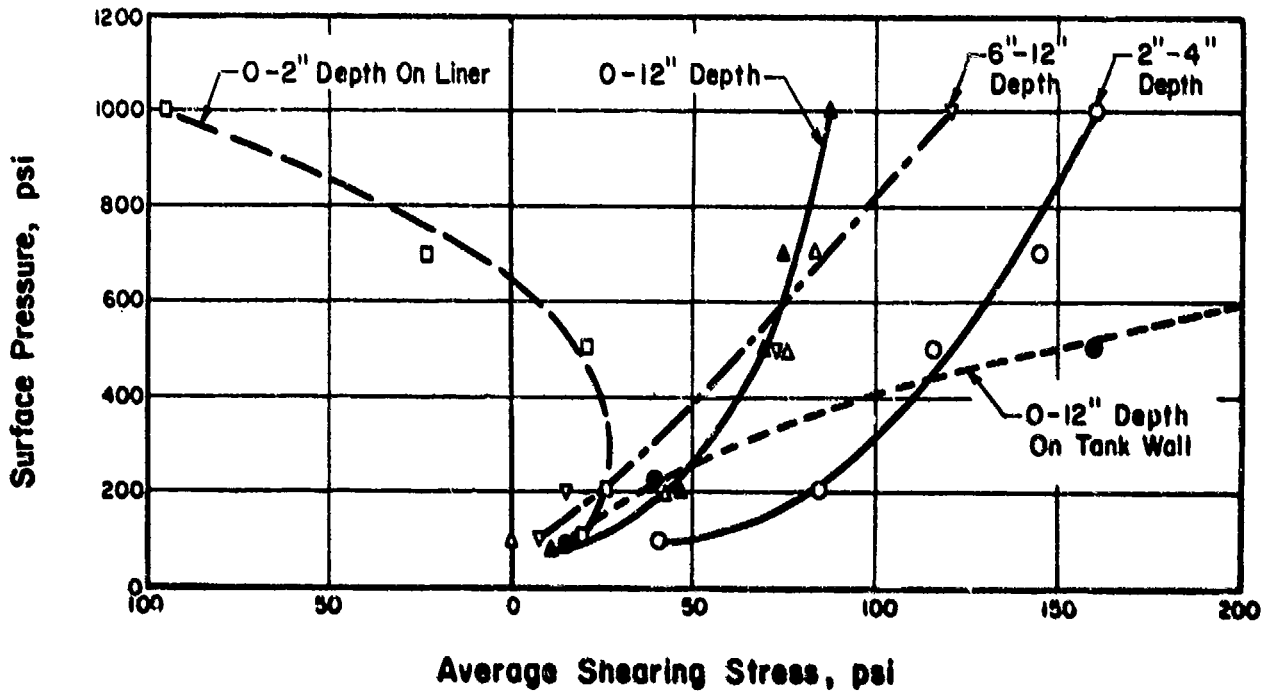

Fig. A.26 Horizontal pressure and average shearing stress on the liner vs. surface pressure during first pressurization of the lined opening test.

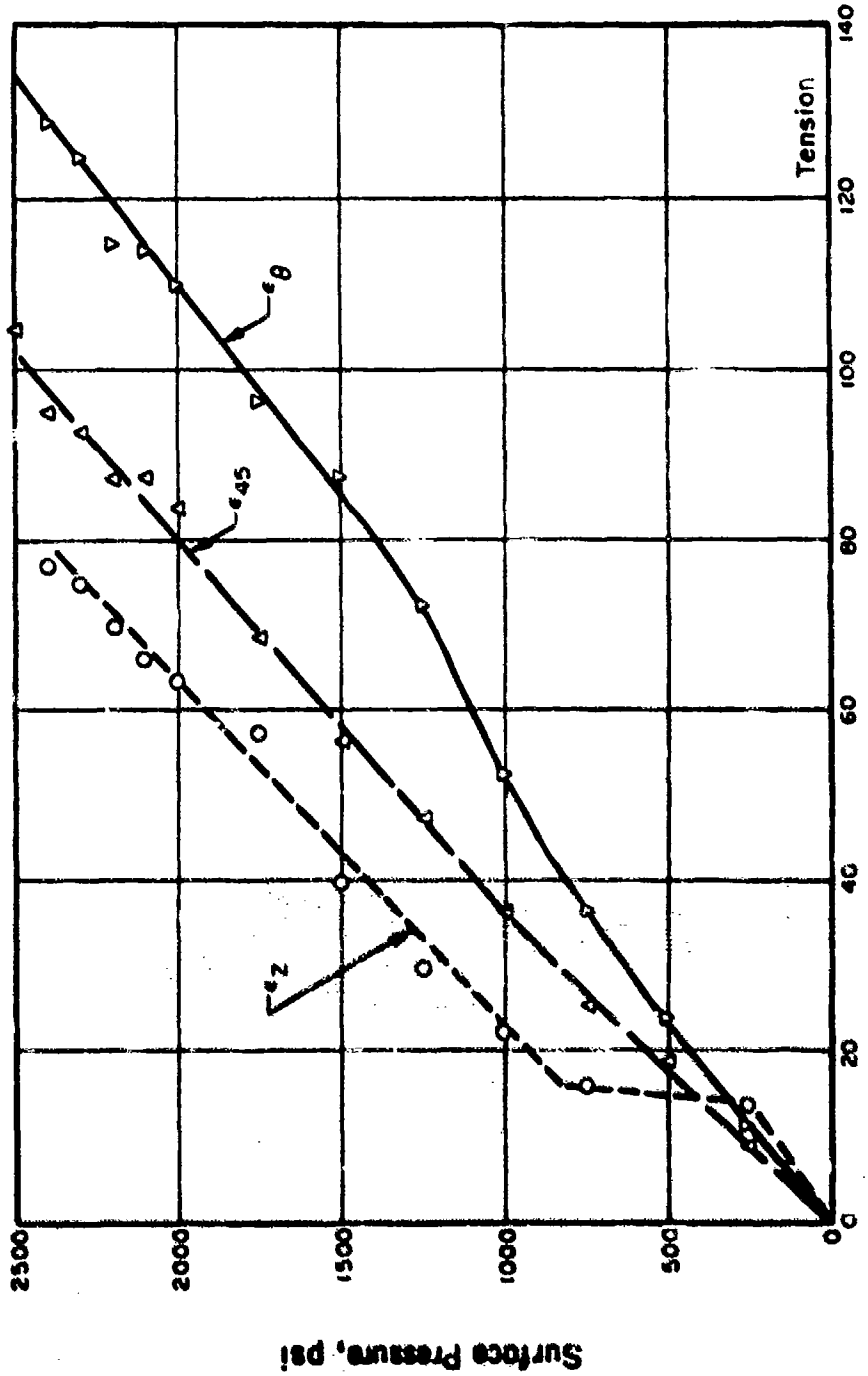

Fig. A.27 Average strains measured on the outside surface of the confining vessel during the fifth pressurization of the lined opening test.

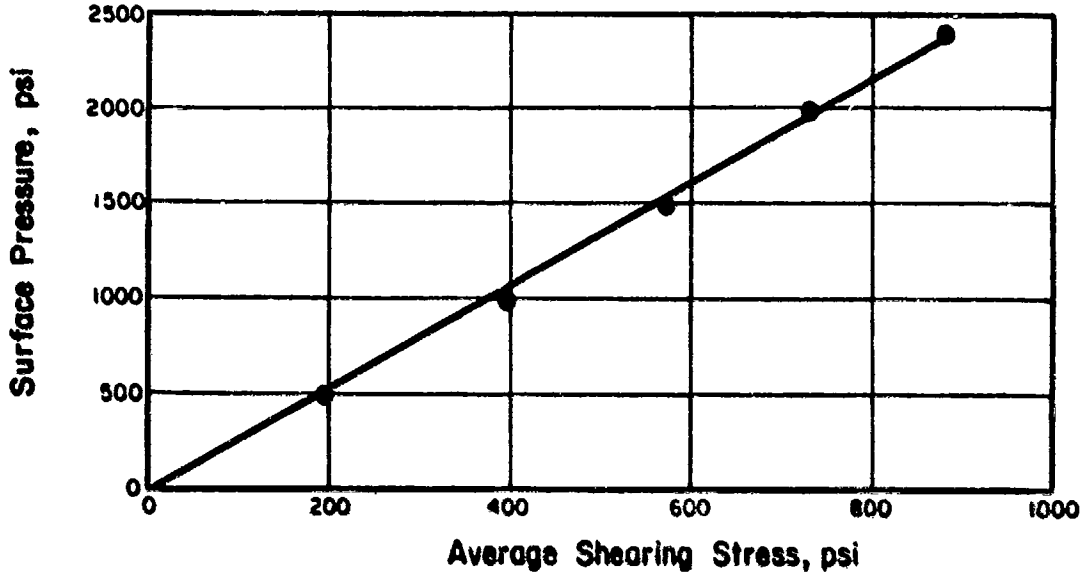

Fig. A.28 Average shear stress between the specimen and upper 12 in. of confining tank during the fifth pressurization of the lined opening test.

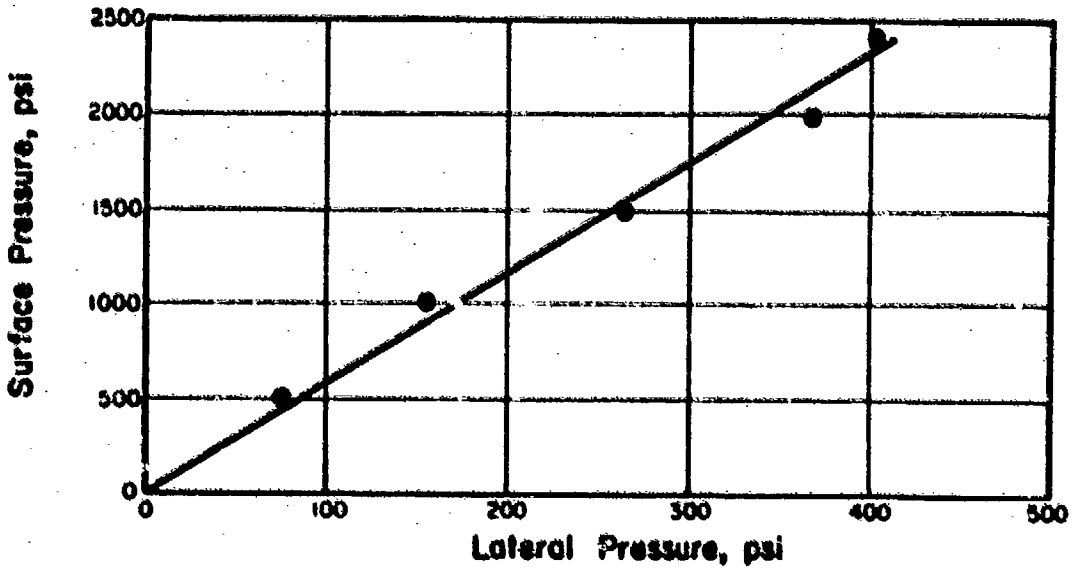

Fig. A.29 Lateral pressure at mid-height of the confining tank during the fifth pressurization of the lined opening test.

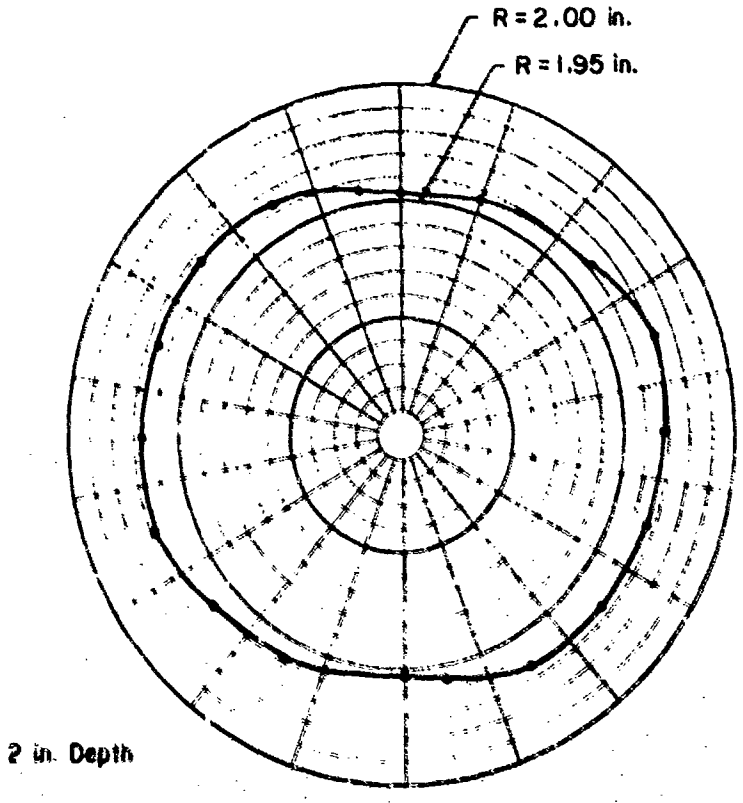

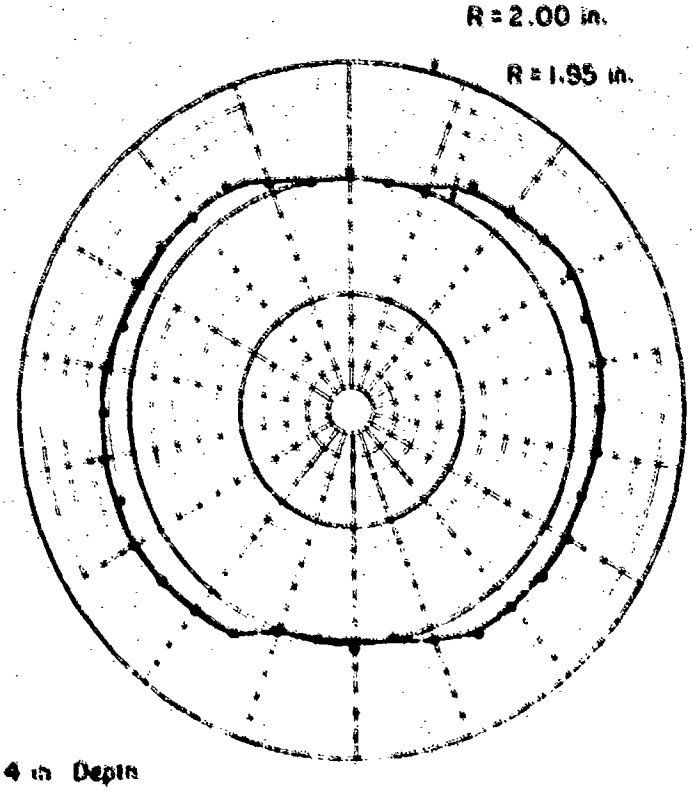

Fig. A.30 Residual deformation of the opening liner after the fifth pressurization of the lined opening test.